NUREG/CR-1846
EPRI NP-1525
GEAP-24893

BWR Refill-Reflood Program Task 4.4 — CCFL/Refill System Effects Tests (30° Sector) Experimental Task Plan

Prepared by D. G. Schumacher

Nuclear Engineering Division
General Electric Company

Prepared for
U.S. Nuclear Regulatory Commission

and
Electric Power Research Institute

and
General Electric Company

Available from

GPO Sales Program
Division of Technical Information and Document Control
U. S. Nuclear Regulatory Commission
Washington, D. C. 20555

Printed copy price: $6.50

and

National Technical Information Service
Springfield, Virginia 22161

NUREG/CR-1846
EPRI NP-1525
GEAP-24893
R2

BWR Refill-Reflood Program Task 4.4 — CCFL/Refill System Effects Tests (30° Sector) Experimental Task Plan

Manuscript Completed: December 1980
Date Published: July 1981

Prepared by
D. G. Schumacher

Nuclear Engineering Division
General Electric Company
San Jose, CA 95125

Prepared for
Division of Accident Evaluation
Office of Nuclear Regulatory Research
U.S. Nuclear Regulatory Commission
Washington, D.C. 20555
NRC FIN No. B3012

and
Electric Power Research Institute
3412 Hillview Avenue
Palo Alto, CA 94303

and
Nuclear Engineering Division
General Electric Company
San Jose, CA 95125

PREVIOUS REPORTS IN SERIES

Number	Title	Author	Date
CR-1558	BWR Refill-Reflood Program Task 4.2 - Core Spray Distribution Experimental Task Plan	T. Eckert	August 1980
CR-1707	BWR Refill - Reflood Program Task 4.2 - Core Spray Distribution Final Report	T. Eckert	September 1980
CR-1708	BWR Refill - Reflood Program Task 4.3 - Single Heated Bundle Experimental Task Plan	D. D. Jones L. L. Myers J. A. Findlay	January 1980
CR-1708 Addendum I	BWR Refill - Reflood Program Task 4.3 - Single Heated Bundle Experimental Task Plan Addendum I, Stage 3 - Separate Effects Bundle	D. D. Jones	July 1980
CR-1846	BWR Refill Reflood Program Task 4.4 CCFL/Refill System Effects Tests (30^{0} Sector) Experimental Task Plan	D. G. Schumacher	December 1980

ABSTRACT

An experimental task plan for the CCFL/Refill system effects tests (30° Sector) of the BWR Refill-Reflood program is presented. The CCFL/Refill system effects tests will provide separate effect and BWR system response data from a large-scale sector test facility (30° SSTF) for use in LOCA best-estimate model assessment. Contained in the document is a definition of: the experimental task objectives, required modification to the existing 30° SSTF, test parameters and ranges, individual test categories, measurement plan approach, and data utilization.

SUMMARY

In partial contribution to the overall objectives of the Refill/Reflood program, the Counter-Current Flow-Limiting (CCFL)/Refill System Effects tests performed in the 30° Steam Sector Test Facility (SSTF) will provide a data base for assessment of best-estimate (BE) models and identification and evaluation of controlling phenomena during the refill/reflood phase of a hypothesized boiling water reactor (BWR) loss of coolant accident (LOCA).

To provide this data base the existing SSTF, located in Lynn, Massachusetts, will be upgraded to meet the requirements of transient LOCA simulation testing, and tests will be performed to isolate key separate phenomena and to investigate BWR system refill/reflood during system blowdown from 150 psia to ambient pressure conditions.

Addressed in this Experimental Task Plan are the approach and strategy guiding the experimental task, subdivided into the following major categories:

- role and objectives,
- task approach and strategy,
- facility evaluation approach,
- facility redesign and construction approach,
- facility qualification approach,
- model assessment test approach,
- measurement plan approach,
- data utilization,
- success criteria,
- documentation, and
- schedule.

CONTENTS

TABLES

Section 1

INTRODUCTION

In partial contribution to the overall objectives of the Refill/Reflood program, the Counter-Current Flow-Limiting (CCFL)/Refill System Effects tests performed in the 30° Steam Sector Test Facility (SSTF) will provide a data base for assessment of best-estimate (BE) models and identification and evaluation of controlling phenomena during the refill/reflood phase of a hypothesized boiling water reactor (BWR) loss of coolant accident (LOCA).

To provide this data base the existing SSTF, located in Lynn, Massachusetts, will be upgraded to meet the requirements of transient LOCA simulation testing, and tests will be performed to isolate key separate phenomena and to investigate BWR system refill/reflood during system blowdown from 150 psia to ambient pressure conditions. Contained in Appendix A is a summary description of the upgraded SSTF. A more detailed description will be provided in the Facility Description Document.

Addressed in this Experimental Task Plan are the approach and strategy guiding the experimental task, subdivided into the following major categories:

- role and objectives,
- task approach and strategy,
- facility evaluation approach,
- facility redesign and construction approach,
- facility qualification approach,
- model assessment test approach,
- measurement plan approach,
- data utilization,
- success criteria,
- documentation, and
- schedule.

Section 2

ROLE IN REFILL/REFLOOD PROGRAM AND TASK OBJECTIVES

As part of the Refill/Reflood program, the 30° SSTF CCFL/Refill System Effects tests will contribute in part to the overall objectives of the R/R program as specified in the program workscope document* and listed below:

a. to develop a better understanding of the phenomena controlling the refill and reflood phases of BWR LOCAs;

b. to provide a basis for and support to the development and qualification of best-estimate BWR system thermal hydraulic codes for LOCAs; and

c. to provide a basis for assessing assumptions used in establishing BWR LOCA safety margins.

The primary role of the SSTF CCFL/Refill tests will be in providing a data base for assessment of BWR best-estimate separate effect and system models. Inherent in this task is the generation of data addressing the phenomena controlling the refill phase of BWR LOCAs and hydraulic phenomena leading to the initiation of reflood. This data base can also be utilized to address the assumptions and models currently used in the evaluation of BWR LOCA conditions.

The primary role for the SSTF CCFL/Refill task will be accomplished through the coordinated effort of three major tasks of the R/R program (i.e., Model Qualification Task, Model Development Task, and CCFL/Refill System Effects tests [30° Sector]). The Model Qualification Task will provide the link between 30° SSTF CCFL/Refill tests and the Model Development Task by specifying facility and measurement requirements, specific qualification tests, required ranges of test conditions needed for qualification of the best-estimate BWR models, and providing pretest predictions and assessment criteria using the models developed in the Model Development Task.

*BWR Refill-Reflood Program Workscope, February 12, 1979.

The objectives for the CCFL/Refill task are subdivided into three categories. The overall objectives given in Table 2-1 set overall guidelines applicable to all elements of the task. Tables 3-1 and 3-2 define facility hardware objectives and test strategy objectives derived from the overall task objectives.

The objectives are classified according to must (M) and want (W) designations. Those objectives classified as "must" are viewed as significant and must be met by the task. Those classified as "want" may be compromised if necessary.

Table 2-1
OVERALL TASK OBJECTIVES

	Objectives	Classification
a.	Provide a data base for assessment of best-estimate models.	M
b.	Identify and evaluate phenomena controlling the refilling phase of BWR LOCA.	M
c.	Evaluate emergency core cooling (ECC) mixing phenomena.	M

Section 3

TASK APPROACH AND STRATEGY

Incorporated in the SSTF CCFL/Refill task are several elements and subtasks. Listed below are the major task elements.

a. Evaluation of the existing facility adequacy with regard to BWR simulation and model qualification needs.

b. Facility redesign and modification as necessary to provide the capability to perform separate effect tests and transient blowdown refill tests (from 150 psia to ambient pressure) simulating relevant BWR phenomena.

c. Facility shakedown and qualification.

d. Test operation to provide a model assessment data base through separate effect and system tests.

e. Data evaluation with regard to overall system response and prediction.

Task Elements a through e (as well as associated subtasks) will be completed through the contribution of several groups within the General Electric Company. The Thermal Development component of Safety and Thermal Hydraulic Technology (S&THT) will provide coordination and direction of activities within GE, with overall program direction under the review and guidance of the program management group (PMG).

Figure 3-1 depicts the integration of parallel tasks and elements contributing to the CCFL/Refill task, illustrating overall task coordination.

Three tasks from the Refill/Reflood program (Model Development, Model Qualification, and CCFL/Refill Tests) are the major contributors to the program which will culminate in the qualification assessment of BWR best-estimate LOCA models. Therefore, the experimental task planning is linked to the model development and qualification tasks. Critical inputs to the experimental task planning include:

a. identification of facility and measurement requirements needed for model assessment,

b. identification of test parameters and specific test conditions needed for model assessment experiments, and

c. model qualification acceptance criteria approach.

Inputs critical to the operation of the test program include:

a. facility design evaluation assessment,

b. pretest predictions and assessment criteria, and

c. qualification judgment with regard to test results and phenomena identified.

Table 3-1

FACILITY HARDWARE OBJECTIVES

	Task Objectives	Classification
a.	Simulate initial conditions over representative BWR range	M
b.	Assure representative BWR response through refill phase of BWR LOCA by simulation of controlling BWR geometry and components	M
c.	Use existing 30° sector facility as the base facility for the 30° SSTF CCFL/Refill Tests	M
d.	Simulate BWR (ECC) injection hardware	M
e.	Simulate ECC transient flow response during LOCA simulation	M
f.	Simulate the major thermodynamic conditions driving ECC mixing phenomena	M
g.	Provide test instrumentation sufficient to supply a data base for qualification of BE models, and identification of controlling BWR refill phenomena	M
h.	Provide facility hardware features necessary to perform separate effect qualification tests	M
i.	Provide capability to simulate the time of CCFL breakdown through representative test initiation and sequencing of ECC systems and core steam injection	W
j.	Maximize the use of existing equipment	W

k.	Minimize hands-on control (integral system response)	W
l.	Simulate global real-time response (including initiation time of core reflood) by representative scaling of BWR component volumes, flow paths, initial conditions, and the sequencing of controlled inputs (ECCS and core steam injection)	W
m.	Operate from initial pressure of 150 psia to atmospheric pressure	W
n.	Minimize deviations from full-length/volume scaling basis	W
o.	Represent BWR hydraulic response during reflood phase of BWR LOCA	W
p.	Minimize existing hardware modification (e.g., bundle removal)	W

Table 3-2

TESTING STRATEGY OBJECTIVES

	Task Objectives	Priority
a.	Provide calibration/shakedown tests of as-built hardware	M
b.	Perform transient system effects tests to provide a data base for qualification of BE models	M
c.	Perform transient system effect tests to identify and evaluate phenomena controlling the refill phase of a BWR LOCA	M
d.	Perform tests to evaluate ECC mixing phenomena	M
e.	Provide separate-effects test for assessment of BE submodels	
f.	Perform tests to assess tieback to transient two-loop test apparatus (TLTA) experiments	M
g.	Provide separate effects tests for tieback to 16° sector test	W
h.	Provide tieback to adiabatic single heated-bundle tests (SHBT) (evaluate scaling basis)	W

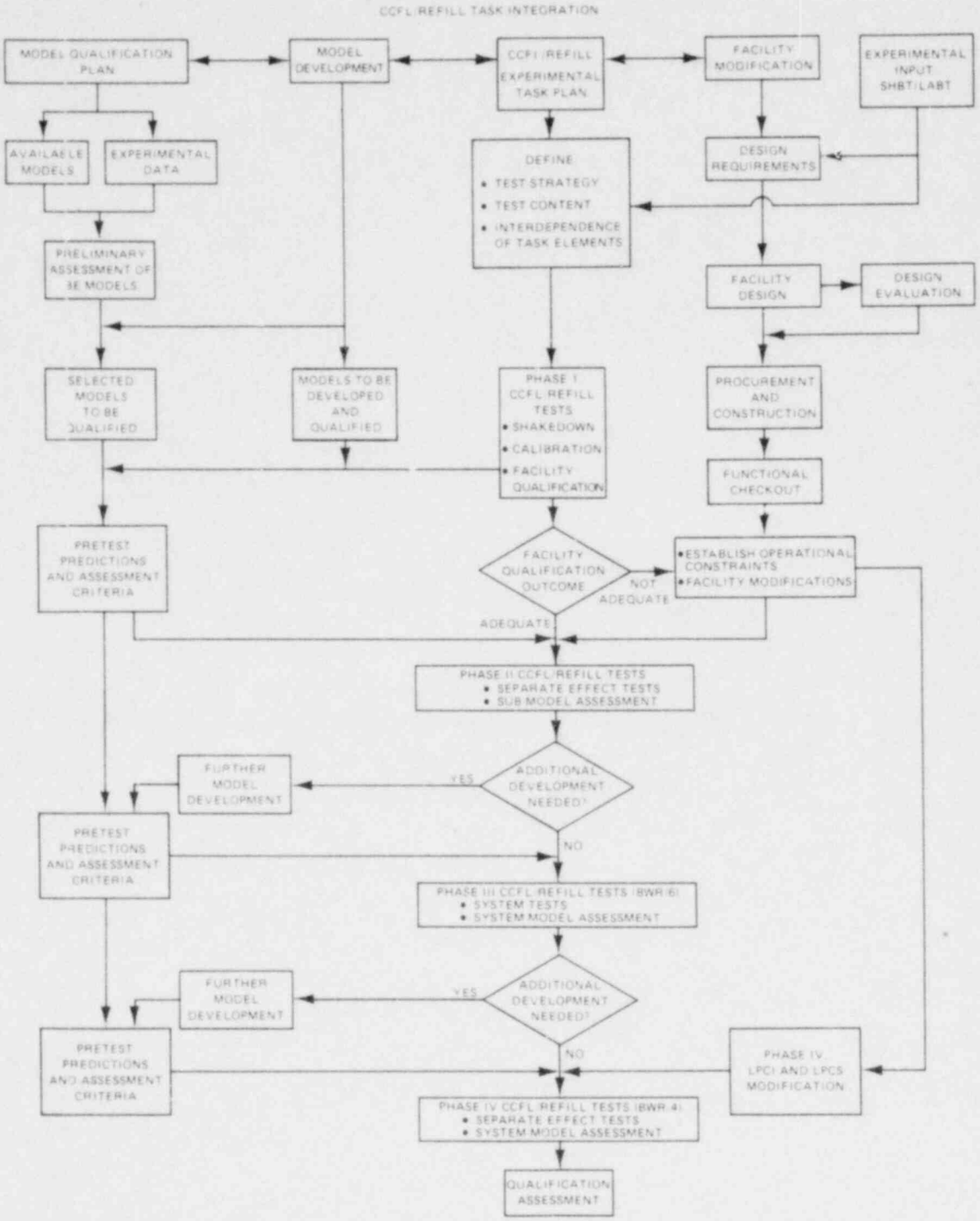

Figure 3-1. 30° SSTF/CCFL/Refill Program Strategy Diagram

3.1 FACILITY EVALUATION APPROACH

An evaluation will be made of the adequacy of the existing 30° SSTF with regard to model qualification needs and simulation characteristics essential in capturing the controlling phenomena during the refill phase of a BWR LOCA. In performing this task element, consideration will be given both to the feasibility of proposed modifications, as well as the technical payoff/penalty with regard to the BWR simulation fidelity. The primary vehicle by which facility modifications will be identified will be in facility modification/design requirement transmittals.

3.2 FACILITY REDESIGN AND CONSTRUCTION APPROACH

Included in the facility redesign are the following subtasks:

a. facility hardware design,

b. test instrumentation design,

c. process control and instrumentation design, and

d. data acquisition system (DAS)/data reduction (DR) system design.

Subtasks a. through d. will upgrade the existing SSTF to allow transient blowdown/refill test operation. Major facility hardware design tasks include:

a. Blowdown/Containment System Design; to allow BWR prototypical blowdown response and management of effluents.

b. Guide tube and lower-plenum steam injection; for separate effect testing, setting of initial conditions, and tailoring of flashing rates in those regions.

c. Guide tube and annulus water drain lines; for setting initial conditions.

d. Excess volume isolation system; to correct the SSTF test vessel volume to the scaled value for prototypical blowdown response.

e. Expanded ECCS flow capacity; to provide capability to perform tests with five scaled ECC systems low-pressure core spray (LPCS), high-pressure core spray (HPCS), and three low pressure coolant injectors (LPCIs).

f. LPCI modification to provide BWR/4 injection location.

g. Miscellaneous mechanical features to allow separate-effect tests in the SSTF.

The design basis for design tasks a through g will be drawn from the facility design requirements transmittals.

The test instrumentation design task will enhance and modify the existing SSTF measurement capability to coincide with the transient refill aspects of the CCFL/Refill test program. In particular the following new measurement capabilities will be added:

a. void fraction and fluid level measurement in the major test-section regions (i.e., upper plenum, core, bypass, annulus, guide tubes, lower plenum);

b. temperature profile measurements in the upper plenum, bypass, lower plenum, and selected fuel bundles;

c. temperature measurements at controlling CCFL locations (selected upper tieplates and side-entry orifices);

d. blowdown mass flow measurement;

e. mass flow measurements associated with new system inputs (i.e., guide tube and lower-plenum steam injection), and

f. internals differential pressure chain relating pressure of major components.

A significant effort in process instrumentation and control design will be necessary to provide the operational control required in performing the transient CCFL/refill tests. Primary control functions include:

a. transient programmed control of ECCS injection rate, with capability to simulate operator override of the ECCS injection function;

b. transient programmed control of core steam-injection;

c. pressure control of excess vessel volume;

d. transient control of guide tube and lower-plenum steam injection;

e. injected steam superheat control, and

f. overall test operation sequencing device to control the transition from initial steady-state conditions to LOCA simulation during transient tests.

The SSTF data acquisition/data reduction system will be upgraded to accommodate the measurement and data processing requirements of the CCFL/refill system effects tests. To accommodate the required CCFL/refill instrumentation, the data acquisition system (DAS) input channel capacity will be increased to approximately 400 channels. A corresponding data acquisition software effort will be required to access the additional data channels.

The nature of the transient phenomena studied in the CCFL/refill tests will require data processing in addition to the existing data reduction capability. Inherent in this data reduction software upgrade will be conversion to RTE IV software to facilitate added data processing capability and improve DAS utilization efficiency.

The data reduction software modifications will be guided by the following three objectives:

a. expand data reduction capability to perform instrument/data accuracy checks to streamline data verification,

b. expand data reduction capability to address the key phenomena inherent in transient blowdown/refill tests, and

c. provide special calculations and data format consistent with model qualification needs.

Specifics with regard to the above objectives will be developed as part of the DAS/DR design subtask and documented in the Facility Description Document.

3.2.1 Design Assessment

Three reviews will be conducted during the facility design period addressing facility modification conceptual design, measurement system preliminary design, and facility final design. The review meetings will occur within the periods specified in the schedule of Section 5. The purpose of the meetings is to assure design congruence with the program objectives and to obtain PMG concurrence.

3.2.2 Facility Procurement and Construction

Early procurement and construction of long-lead-time items will be initiated as necessary prior to final approvals to expedite the schedule.

All new test equipment will be functionally verified prior to testing to ensure proper operation and corrections/completions rectified as necessary. During the construction phase, equipment verifications/inspections will be performed.

3.3 FACILITY QUALIFICATION APPROACH

The purpose of the facility qualification is to ensure that the experimental facility is capable of achieving and measuring those BWR representative conditions

deemed appropriate for separate-effect and transient LOCA simulation tests. Qualification of the modified SSTF will be accomplished by consolidation of the four elements listed below:

a. GE/PMG review and approval of the SSTF modification design;

b. equipment inspections and verifications performed during facility construction;

c. facility calibration, shakedown, and tieback tests; and

d. facility evaluation with regard to design compromises and the sensitivity of dependent phenomena, including comparisons with predicted BWR response.

After completion of facility construction and functional checkout of the equipment, the initial phase (Phase I) of the CCFL/Refill test series will begin.

Phase I (facility qualification) tests will address facility operational characteristics and capabilities relative to design requirements and will perform facility/equipment calibrations. The outcome of the Phase I tests will be an assessment of the facilities operational capabilities with respect to the facility objectives. As a result of the Phase I tests, minor modifications to the facility will be performed as necessary to correct facility shortcomings.

The following categories of shakedown/calibration tests will be performed in the Phase I series:

a. instrument verification and calibrations,

b. mechanical equipment performance checks,

c. control systems performance tests,

d. support-system performance tests (i.e., excess volume system, blowdown/suppression system),

e. test section calibrations,

f. initial conditions control tests,

g. overall system performance tests, and

h. phenomena simulation qualification tests.

Details with regard to the sequencing and content of the shakedown/calibration tests will be defined in the subsequent shakedown test plan prepared as an addendum to the experimental task plan for review and approval by the PMG prior to phenomena simulation qualification tests.

The overall results of the qualification tests together with an assessment of facility adequacy will be documented in a report to the PMG.

3.4 TEST APPROACH

After successful completion of facility qualification (Phase I) experiments, model assessment tests will be conducted. The model assessment tests will follow a building block approach in which the breadth of model application will be increased in each of three subsequent test phases. Pretest predictions using the best-estimate models will be provided for selected tests prior to each test phase, thus providing a basis for model assessment according to the assessment criteria developed in the model qualification task. If, in the course of the model assessment tests, model deficiencies are identified, further development of the best-estimate models will be conducted as necessary to improve the BE model capabilities.

3.4.1 Test Categories

Phase II tests will provide a data base by which BE submodels will be assessed through separate-effect (SE) tests conducted over a representative range of BWR conditions. The Phase II test series will include the following categories of separate-effect tests:

SE 1. Multiple bundle CCFL at upper tieplate (UTP) and side-entry orifices (including bottom of bypass leakage paths)

SE 2. Combined bundle and bypass CCFL

SE 3. Upper-plenum mixing/CCFL breakdown

SE 4. Bypass/channel wall heat transfer

SE 5. LPCI-induced bypass mixing and steam condensation

SE 6. Jet pump/core steam flow split

SE 7. Simple blowdown tests

Phase III tests will provide a data base for assessment of BE system model by conducting transient LOCA simulation tests over a representative range of BWR conditions. In this test phase the adequacy of the BE system LOCA model (composed of BE submodels substantiated in Phase II) will be assessed by comparison of pretest predictions to the data base, according to the methodology of the assessment criteria developed in the model qualification task. All Phase III tests will be conducted with BWR/6 simulation of core-spray header geometry and LPCI location. The following test categories define system response (SR) variations which will be addressed in the Phase III tests:

SR 1. Initial mass in scaled regions

SR 2. Break area variations

SR 3. ECCS combinations

SR 4. ECCS temperature

SR 5. Core-steam generation transient variations

Consideration will also be given to variation in radial core stream profile if sensitivity studies and separate-effect upper plenum mixing tests (Phase II) suggest sensitivity to that parameter.

Additionally, tieback tests to SHB and TLTA will be conducted in the Phase III test series to assess SSTF system response relative to single-bundle results and identify the extent of multidimensional effects.

Phase IV tests will extend the range of the data base to include separate-effect and transient-system response tests with LPCI location and LPCS lower header geometry representative of BWR/4 configuration. The data base thus generated will allow extended application (EA) assessment of the BE global model capabilities by comparison to pretest predictions through the assessment criteria developed in the model qualification task. The following categories of tests will be addressed in the Phase IV test phase.

EA 1. Separate-effect upper-plenum mixing with BWR/4 LPCS

EA 2. Separate-effect lower-plenum mixing with BWR/4 LPCI location

EA 3. Transient system response tests with variation in:

  a. ECCS temperature

  b. blowdown restriction size

Redirection of the test content and strategy may be required during the testing period as the results of previous tests are evaluated. Under such conditions the test categories and system variations identified in this document will be reassessed in light of the current test results and additions/substitutions/deletions made to the test content as deemed appropriate. Such test content changes will be proposed by GE to the PMG for approval prior to implementation. Resultant schedule delays because of negotiation/approvals period or additional test requirements will be reflected in a revised task schedule.

3.4.2 Test Parameters

The following parameters will be varied in the CCFL/Refill test series:

a. Test Vessel Pressure

The influence of vessel pressure on ECCS mixing and CCFL breakdown will be addressed by variation of test vessel pressure within the range of ambient pressure to 150 psia* in separate-effect tests. The data collected in this manner will provide steady-state information at discrete pressure points over the pressure range of the transient LOCA simulation tests, thus aiding interpretation of the transient results and providing a data base for model assessment.

b. Break Size

To address the effect of break area on test vessel depressurization and overall system blowdown/refill response, the break size will be varied in BWR/6 and BWR/4 transient tests over the range of full BWR/6 design basis accident (DBA) to 0.45 BWR/6 DBA (corresponding to 0.93 and 0.42 BWR/4 DBA, respectively). The range so chosen covers a representative large-break spectrum.

c. Core Steam Injection Rate and Transient Input

The influence of the steady-state magnitude of injected core steam on CCFL, CCFL breakdown, and upper-plenum mixing will be addressed in separate-effect tests by variation in core-steam flow over the approximate range of 0 to 70,000 lbm/hr. This steam-flow range corresponds to the maximum range in core steam at 150 psia based on core decay heat, shored heat, and flashing. Performing steady-state tests with core-steam injection rates within this specified range will provide data for BE submodel assessment and aid in interpretation of transient LOCA simulation tests.

*150 psi is the design limit of the existing SSTF pressure vessel.

d. Radial Core-Steam Profile

Sensitivity studies will be performed to assess the impact of variation in radial core-steam profile on upper-plenum draining and resultant system refill response. Two radial steam profiles may be utilized in separate-effect, upper-plenum mixing tests, if deemed appropriate by the outcome of the sensitivity studies. The two profiles to be tested are not yet finalized; however, the basis for selection is to bound the estimated steam profile over the expected range of conditions for the transient LOCA simulation.

If separate-effect upper-plenum mixing tests show high sensitivity to core-steam profile variations, both profiles may also be utilized in the transient LOCA-simulation tests.

e. Guide Tube and Lower-Plenum Steam Flow Rate

To assess the dependence of total core liquid drainage on guide tube and lower plenum steam injection, the injection rates will be varied within the range of expected transient conditions in separate effect CCFL and upper plenum mixing tests. The data thus obtained will aid interpretation of transient test results and contribute to the data base available for BE submodel assessment. The range in steam-injection rates estimated by existing analytical tools are given below:

Guide Tube Steam Injection- - - - - - - - - - - - 0 to 30,000 lbm/k

Bypass Steam Injection- - - - - - - - - - - - - - 0 to 21,000 lbm/hr
(injected through guide tube)

Lower-Plenum Steam Injection- - - - - - - - - - - 0 to 48,000 lbm/hr

f. ECCS Flow Rate, Temperature, and Combinations

Separate-Effect Tests

ECCS flow, temperature, and system combinations will be varied as parameters in separate-effect CCFL, upper-plenum mixing, and bypass mixing/heat transfer tests conducted under steady pressure conditions. This will assess the impact of ECCS flow rate, temperature, and combination of systems in operation on localized thermodynamic conditions and resultant liquid drainage paths. The range in ECCS parameters is given below:

ECCS temperature → ambient to ~175°F

ECCS flow → scaled design flow at 150 psia to scaled runout flow

ECCS Combinations → various systems in operation composed of:

LPCS
HPCS
LPCI (one to three pumps in operation)

Transient System Tests

During transient LOCA simulation tests, the ECCS liquid temperature will be varied within the expected range of suppression pool temperatures during the refill phase of the simulated LOCA transient. The data thus obtained will assess the sensitivity of the transient system response to the injected ECCS temperature and address the impact of constant ECCS temperature (throughout each transient LOCA simulation test) on the overall system response. The range of ECCS temperature will be from 95 to 145°F.

During transient LOCA simulation tests the ECCS combinations corresponding to the following LOCA failure modes will be tested:

1. HPCS failure, in which three LPCIs and the LPCS remain operational.

2. LPCS failure, in which two LPCIs and the HPCS remain operational.

3. LPCI diesel generator failure in which one LPCI, the HPCS, and the LPCS remain operational.

4. All ECCS operational (i.e., three LPCIs, HPCS, and LPCS).

ECCS Combinations 1 through 4 will be tested in Phase III tests as a representative sample covering the spectrum of BWR/6 ECCS combinations.

ECCS Combination 1 will be tested in Phase IV tests because only the LPCS and LPCI systems of the BWR/4 reactor will be simulated in the SSTF.

Because the SSTF maximum vessel pressure (150 psig) is outside the design range of the BWR/4 HPCI system (1135 to 165 psia), the BWR/4 HPCI will not be simulated in the SSTF. Scoping studies of the contribution of the HPCI system (from potential system runout at pressures between 150 and 100 psia) to the total integrated ECC injection over the test transient show the HPCI contribution to be quite small (less than 3% of the initial ECCS injection).

Means will be provided to override any of the ECC systems during a test to simulate reactor operator intervention.

The automatic depressurization system (ADS) will not be simulated because of the insignificant effect on vessel depressurization over the SSTF break-size spectrum.

g. ECCS Configuration

To assess the impact of ECC configurations (other than BWR/6 prototypical) on the transient refill performance, tests will be conducted with an LPCS lower header, nozzles, and jet-pump LPCI (both typical of BWR/4 design).

h. Initial Fluid Inventory

To assess the effect of lower-plenum fluid level on the steam flow split between the core and jet pump, the fluid level will be varied as a parameter in separate-effect, lower-plenum steam-flow split tests. The range in fluid levels tested will be from the bottom of the lower plenum (to allow assessment of single-phase steam-flow split, representing conditions in which the bottom of the jet pump is not submerged) to approximately six inches below the top of the lower plenum (upper limit of fluid-level control system), in which the bottom of the jet pump is submerged and influencing the steam-flow split.

The influence of initial upper-plenum fluid level on upper-plenum mixing and CCFL breakdown will be addressed through variation of the initial fluid level in separate-effect upper-plenum mixing/CCFL breakdown tests. The data thus generated will expand the model assessment data base and aid in the interpretation of transient test results. The initial fluid levels tested will include the limiting conditions of the upper plenum filled with 2Ø mixture and the upper plenum initially filled with single-phase steam. Additionally, two intermediate initial two-phase levels will be tested to further address initial level effects.

In the transient LOCA simulation tests, the initial liquid mass in the major scaled regions — core, bypass, upper plenum, guide tubes, annulus, and lower plenum — will be adjusted to prescribed values determined from best-estimate analytical predictions of the BWR mass distribution at 150 psia in the LOCA transient. The initial mass inventories for one LOCA condition will be varied to assess the sensitivity of the transient refill response to variation in the initial component inventories. It is expected that a typical range of ±30 percent will be sufficient to cover the range of uncertainties in the methods. Sensitivity studies will be utilized to provide a basis for the variation.

3.4.3 Test Matrix

A detailed test matrix for the CCFL/Refill system effects has not yet been finalized. The values of individual test parameters and the detailed strategy by which the matrix will be organized is currently under development. Sensitivity studies will be utilized to provide a basis for final parameter selection and range.

Presented in Table 3-3 is a preliminary test matrix identifying the key parameters and approximate number of tests currently under consideration. It is anticipated that a detailed matrix patterned after the parameter variations and number of tests identified in Table 3-3 would require approximately an eight-month period for test operation after completion of facility shakedown and qualification.

Table 3-3

PRELIMINARY TEST MATRIX

Test Phase/Category[a]	Test Parameters[b]	Approximate No. of Tests
II/SE1	A,C	15
II/SE2	A,C,E	11
II/SE3	A,C,E,F	14
II/SE4	A,C,F	7
II/SE5	A,E,F	6
II/SE6	E,H	9
II/SE7	B,H	7
III/SR1	H	3
III/SR2	B	3
III/SR3	F	4
III/SR4	F	4
III/SR5	C	3
IV/EA1	A,C,E,F	14
IV/EA2	A,E,F,H	8
IV/EA3	B,F	6

[a]See Subsection 3.4.1 for description of test categories.
[b]See Subsection 3.4.2 for description of test parameters.

Detailed test matrices will be prepared as addenda to the experimental task plan for the review and approval of the PMG prior to the individual test phases.

3.5 MEASUREMENT PLAN APPROACH

The overall objective for the test measurements made in the CCFL/Refill System Effects test is to provide a measurement network in the SSTF adequate to identify and evaluate the phenomena controlling the system behavior during the

separate-effect and transient LOCA simulation tests performed in the SSTF. The strategy utilized in developing the measurement plan reconciles measurement desires with facility and schedule constraints by adapting a measurement approach consistent with the "system effects" nature of the test. Under such an approach the measurement system is biased toward global measurements within the test system rather than a high concentration of detailed localized measurements. Following this strategy a measurement approach consistent with the data utilization needs and measurement implementation constraints has been developed utilizing proven measurement techniques.

3.5.1 Measurement Categories

To address the overall measurement objective, the following preliminary set of test measurement categories are currently planned for the SSTF:

a. Mass and Energy Input and Discharge from the Test Vessel, including:

   1. ECCS inputs (LPCI, LPCS, HPCS);
   2. injected steam inputs to steam dome, core, guide tube/bypass, and lower plenum;
   3. vessel steam discharge;
   4. vessel blowdown mass discharge; and
   5. lower-plenum liquid discharge.

b. Mass History and Fluid Levels in Internal Test Section Regions, including:

   1. upper plenum at three radial locations;
   2. annulus;
   3. minimum of six fuel bundles of the core sector;
   4. bypass at three radial locations;
   5. one jet pump; and
   6. lower plenum at three locations.

c. Internal Flows through the Following Paths:

   1. liquid downflow through a minimum of six fuel bundles;
   2. vapor updraft indication through three standpipes; and
   3. reverse flow through each jet pump.

d. Internal Pressure and Differential Pressure Strings, including:

1. vessel pressure;
2. differential pressure across three standpipes;
3. upper-plenum pressure;
4. upper-plenum axial pressure differential at three radial locations;
5. bypass axial pressure differential at four radial locations;
6. bypass radial pressure distribution string at one axial location;
7. annulus differential pressure;
8. differential pressure across one jet pump;
9. core support plate differential pressure;
10. lower-plenum pressure
11. lower-plenum axial differential pressure at three locations;
12. axial differential pressure across selected guide tubes;
13. differential pressure between selected guide tubes and the lower plenum; and
14. differential pressure across the excess volume diaphragm.

e. System Temperature, includin :

1. temperature of all liquid and vapor inputs and discharges;
2. temperature above six and below all 58 upper tieplates;
3. axial temperature string in six bundles;
4. jet pump fluid temperature;
5. fluid temperature above and below selected side-entry orifices;
6. upper-plenum temperature profile;
7. lower-plenum temperature profile;
8. bypass temperature profile; and
9. miscellaneous surface temperatures within the test vessel.

Flow splits between the bypass, core, and jet pump of the SSTF will be simulated and assessed per the following discussion:

The flow splits from the lower plenum to the core region in a BWR are shown in Figure 3-2. Of the total flow from the lower plenum during a BWR LOCA, only about half goes up the core region, with the remaining half out of the jet pump. Most of the flow to the core region enters through the SEOs mounted in the fuel-support casting at the bundle inlet (i.e., Flow Path 1). This flow path accounts for approximately 98 percent of the core flow. The remaining 2 percent or less is leakage flow from around the fuel support casting and fuel support plate (i.e., Flow Paths 5 to 7). Downstream of the bundle-inlet orifice are three leakage flow paths — lower tieplate holes (Flow Path 2), finger springs (Flow Path 3), and leakage around the lower tieplate and fuel support casting (Flow Path 4). These leakage paths will allow approximately 10 percent of the flow through the SEOs, i.e., Path 1, to leak into the bypass region; the remaining 90 percent enters the fuel-core region.

Prototypical BWR hardware is used in the SSTF wherever practical so that the important leakage paths will be identical. Actual fuel-support castings, lower tieplates, and fuel channels are used so that Flow Paths 1, 2, 3, 4, and 6 are accurately reproduced. Flow Path 5 is mocked up in SSTF core-support plate with small holes. The extremely small leakage flow at 7 is not mocked up. The total leakage through these paths (5 through 7), however, represents less than 1 percent of the leakage flow.

Flow split in the SSTF will be derived from measurements of the jet-pump flow, local liquid mass accumulation, and from pressure measurements across the SEOs in the instrumented fuel bundles. Leakage from the bundles to the bypass region, which accounts for about 10 percent of the SEO flow, will be estimated from the pressure-drop instrumentation along the instrumented fuel bundles and within the core bypass. The less than 2 percent leakage flow corresponding to Flow Paths 5 and 6 will be derived from pressure-drop measurements across the core-support plate.

It should be noted that, as shown by previous BWR LOCA tests in the TLTA, the flow rates emanating from the lower plenum are generally very low and are counter-current. State-of-the-art measurement schemes have not proven useful for direct measurement of flow rate. On the other hand, inventory measurements in the

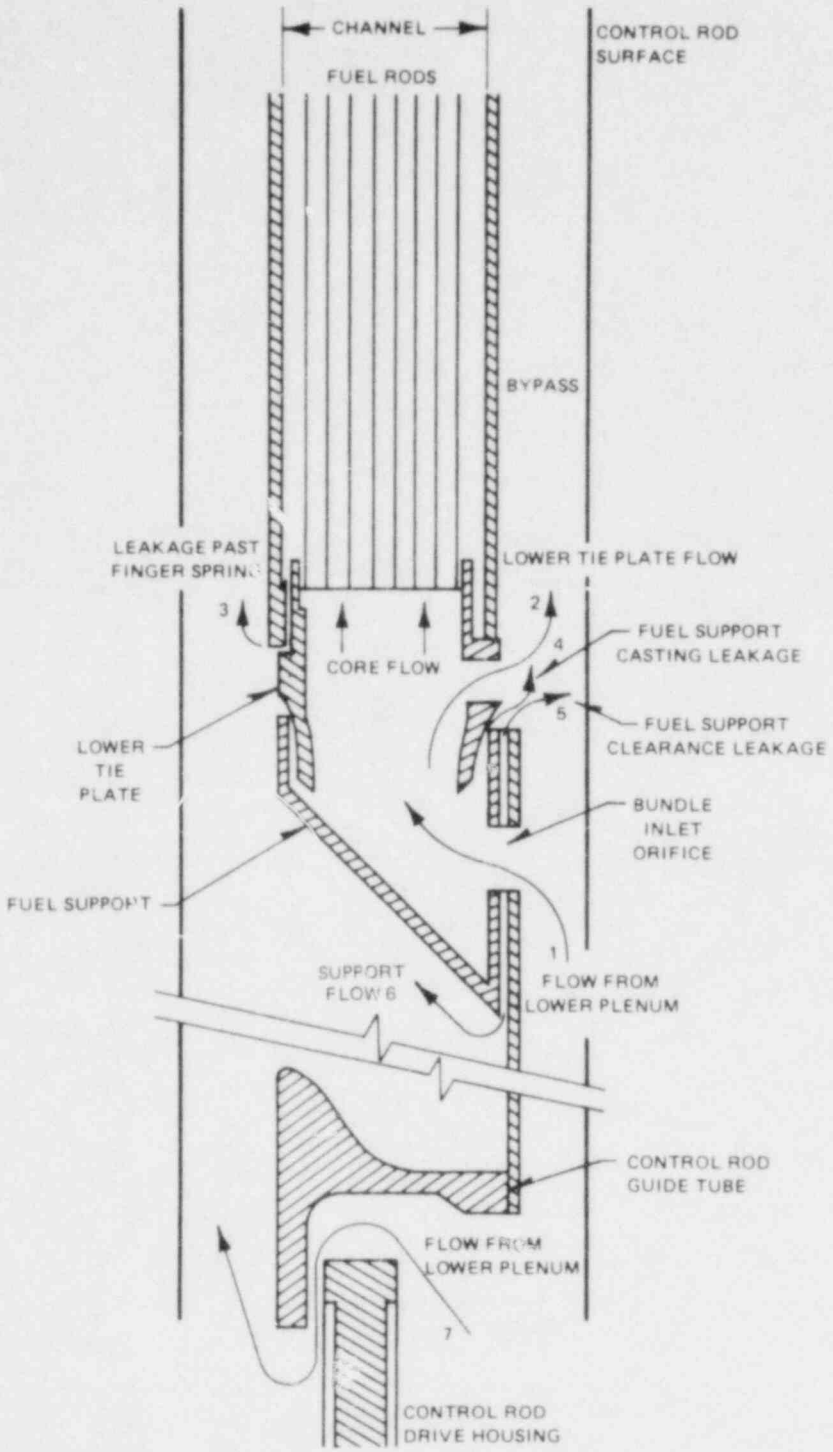

Figure 3-2. Core Leakage Paths

various regions, such as lower plenum, bypass, guide tube, etc., have proved highly successful in providing data for code and for phenomena assessment. The SSTF measurement plan is expected to provide similar quality data to meet the program objectives.

The details of the SSTF measurement system are under development. A detailed measurement list based on the measurement categories cited in this document will be provided in the facility description document.

3.5.2 Instrument Utilization

Table 3-4 identifies the primary elements and sensing devices planned to provide the measurement functions identified in the previous section. The instruments chosen rely on proven measurement techniques found successful by GE in similar applications.

3.5.3 Measurement Verification Approach

Verification of experimental measurements will be accomplished through the combination of pretest instrument verification and calibrations, coupled with on-line instrument checks, comparisons, and adjustments throughout the testing periods.

During the shakedown/calibration portion of the Phase I test period, the facility instrument will be verified with regard to correct installation and patching, functional operation, and consistency. The accuracy of the measurements will be further verified through direct calibration of pressure transducers, thermocouple reference junctions, and weir-tube flow elements, as well as energy and mass balance tests conducted under simplified conditions to demonstrate the overall measurement accuracy of the system.

Measurement verification will be an integral part of the subsequent test series. Prior to each testing interval, the test instruments will be checked in place under ambient and hot conditions with respect to consistency and established reference standards, and adjusted as necessary. As a part of the baseline data reduction package, the test measurements will be further verified through mass and energy balance checks and test-section pressure-string balances for each test. At the end of each test interval, the instruments will again be checked under simplified conditions with respect to consistency and established reference standard to detect instrument shifts or failures during the test.

Table 3-4

INSTRUMENT UTILIZATION

Measurement Category*	Primary Element	Sensing Device
a1 - a5	Orifice Plate, Annubar	P, ΔP, TC
b		ΔP, TC, CP
c1	Weir Tube	ΔP
c2	Oririce	T, P, ΔP
c3	Annubar	T, P, ΔP
d1,d2,d3		P
d2,f4,d5,d6,d7,d8,d9,d11,d12,d13,d14		ΔP
e		TC

P - Pressure Transducer
ΔP - Differential Pressure Transducer
CP - Conductivity Probe
TC - Thermocouple

*See Subsection 3.5 1.

As necessary, additional tests will be conducted at the end of major test series to repeat test cases in which failure of critical instruments was detected by the measurement verification plan. Such repeat tests, when jeopardizing cost or schedule, will be contingent on PMG decision following determination of schedule and cost impact.

3.6 DATA UTILIZATION

The primary usage of the data obtained in the SSTF CCFL/Refill tests will be in the qualification of test-estimate models. In fulfilling that objective the controlling phenomena and detailed results observed in the tests will be compared to predictions made with the available best-estimate models. The methodology of the comparison between the prediction and the test data will be defined by the model qualification acceptance criteria developed under the model qualification task of the refill/reflood program.

Controlling phenomena identified in the test series which are not simulated in the best-estimate models will be used to direct further model development efforts as necessary.

3.7 SUCCESS CRITERIA

The success criteria for the experimental program are subdivided into two categories of assessment, addressing: (a) test control capability, and (b) phenomena simulation capability.

3.7.1 Test Control Capability

Various independent parameters will be controlled during separate-effect and system tests to simulate BWR boundary conditions derived from empirical studies, analytical predictions, or BWR system-design requirements. The accuracy with which these parameters are controlled could significantly affect the resulting test phenomena. To avoid misleading or erroneous test results the control accuracy of selected key input parameters will be tested in the Phase I shakedown/calibration tests and assessed according to the criteria given below:

a. Initial Mass in Test-Section Regions

The adjustment range and control stability in setting the initial mass in the following test-section regions will be compared to limits specified in the scaling evaluation section of the Facility Description Document:

1. upper plenum,
2. bypass,
3. fuel bundles,
4. annulus,
5. guide tubes, and
6. lower plenum.

Both the range and stability will be determined under 150 psia pretest conditions using the test instrumentation. The acceptance limits specified in the Facility Description Document will define the required range in controlled mass for each region 1 through 6, and the maximum mass fluctuation when controlling to a specific mass value.

The initial mass control capability will be judged successful if the measured range and stability fall within the acceptance limits.

b. ECCS Mass Flow Transients

The mass flow-control accuracy for each ECCS System [LPCS, HPCS, LPCI (one through three systems)] will be compared to allowable deviation limits superimposed on the ECCS flow characteristics specified in the SSTF loop requirements. The mass flow response limits will be specified in the format of maximum and minimum allowable mass flow for each ECC system as a function of vessel pressure, thus creating an acceptance envelope for the control response of each ECC system.

The acceptance envelope for the control systems will be specified in the Facility Description Document.

The ECCS flow-control systems will be judged successful if the measured ECCS mass-flow transients (using test instrumentation) fall within the acceptance envelope under test vessel depressurization representative of that expected in transient blowdown tests.

c. ECCS Temperature Control

The range and stability of the ECCS spray temperature will be tested and compared to limits specified in the scaling evaluation section of the Facility Description Document. The acceptance limits will define the range in ECCS temperature required and the maximum allowable temperature variation when controlling to a specific temperature. The ECCS temperature control system will be judged successful if the spray temperatures at the ECCS injection location (immediately upstream of LPCS and HPCS headers and LPCI injection line) equals or exceeds the required range and meets the fluctuation limits.

d. Core-Steam Transient

The control accuracy of the transient steam flow injected into the adiabatic fuel bundles of the SSTF will be compared to acceptance limits specified in the scaling evaluation section of the Facility Description Document. The acceptance limits will define an envelope of acceptable steam flows over the range of the independent variable of the steam-injection input function.

The core-steam control system will be judged successful if the measured steam injection transient falls within the acceptance envelope under vessel depressurization conditions representative of that expected in transient blowdown tests.

e. Injected Steam Superheat Control

The capability of the steam desuperheat system will be compared to acceptance limits specified in the scaling evaluation section of the Facility Description Document. The acceptance limits will define the maximum allowable superheat as a function of test-vessel pressure over the range of ambient to 150 psig for each steam-injection system.

Success of the steam-injection system will be gauged on the ability to maintain the steam superheat (measured at the upper tieplates of the fuel bundles) within the acceptance limits under vessel depressurization conditions representative of that expected in transient blowdown tests.

3.7.2 Phenomena Simulation

During the hypothesized LOCA several phenomena induced by the interaction and separate effects of ECCS injection and reactor steam generation are expected to play roles of varying importance to BWR refill. Of those phenomena the following three are selected for assessment of facility simulation adequacy:

a. upper tieplate CCFL,

b. global side-entry orifice CCFL, and

c. bypass hydraulic drainage.

Phenomena a. through c. have been investigated by GE in single-channel and/or small-scale test facilities. Extrapolation of these test results to the SSTF, however, involves some uncertainty because of potential local phenomena which cannot be readily measured in the SSTF. Assessment of the phenomena simulation can be made, however, by comparing separate-effect test results to global predictions of the relevant phenomena using current methods and appropriate acceptance bands. By this method controlling phenomena can be verified without detailed local information.

The acceptance limits for the three phenomena will be specified in the Shakedown Test Plan.

The purpose of the phenomena simulation tests is to demonstrate that the characteristic response of the selected phenomena exists in the SSTF under controlled test conditions, thus assuring representative BWR response in the subsequent transient LOCA simulation tests. The acceptance limits to be developed for the simulation assessment will consider both the prediction uncertainty and the degree of accuracy needed to discern the characteristic response of the phenomena in the SSTF. It is anticipated that broad acceptance bands will be necessary to compensate for local uncertainties, yet be adequate to address the characteristic response.

3.7.2.1 Upper Tieplate CCFL. The total CCFL drainage from the 58 fuel bundles of the SSTF core will be compared to the predicted CCFL drainage at four separate total core-steam flow rates. During this test the SSTF bypass will be isolated so that ECCS liquid can drain only through the fuel bundles.

The phenomena simulation will be judged successful if the test results fall within the acceptance band of allowable drainage versus injected steam flow, or if deviations can be shown to be due to multidimensional effects.

3.7.2.2 Global Side-Entry Orifice CCFL. The total SEO CCFL drainage from the 58 fuel bundles of the SSTF core array will be compared to predicted CCFL drainage at four separate lower-plenum steam-flow rates. To perform these tests the two jet pumps of the SSTF will be blocked to prevent steam or water flow through those paths.

The phenomena simulation will be judged successful if the test results fall within the acceptance band of allowable drainage versus injected steam flow, or if deviations can be shown to be due to multidimensional effects.

3.7.2.3 Bypass Hydraulic Drainage. The hydraulic drainage characteristics of the SSTF bypass will be compared to the predicted performance under ambient temperature and pressure conditions by measuring the total bypass drainage at five steady-state bypass water levels covering the entire range of the SSTF bypass.

Phenomena simulation success will be achieved if the measured drainage falls within the acceptance band of drainage versus bypass fluid level, or if deviations can be shown to be due to multidimensional effects.

3.7.3 Acceptance Limits for Phenomena Comparisons

The acceptance limits for the phenomena comparisons of the previous section will be developed as part of the model qualification task.

Section 4

DOCUMENTATION

The following documents will be submitted to the PMG during the experimental program according to the schedule provided in Section 5:

a. facility description document, defining the configuration of the modified SSTF including instrumentation, DAS, scaling rationale, and compromises;

b. shakedown test plan, defining the shakedown test matrix for the Phase I shakedown/calibration tests, published as an addendum to the experimental task plan;

c. CCFL/Refill test plans defining the test matrices for the Phase II Separate-Effect Tests, Phase III BWR/6 System Tests, and Phase IV BWR/4 ECCS configuration tests, published as addenda to the experimental task plan;

d. data reports following each of the major test periods; and

e. topical report.

Section 5

SCHEDULE

Figure 5-1 defines the sequence and timing of key events in the CCFL/Refill task. Items marked with an asterisk identify intermediate milestones.

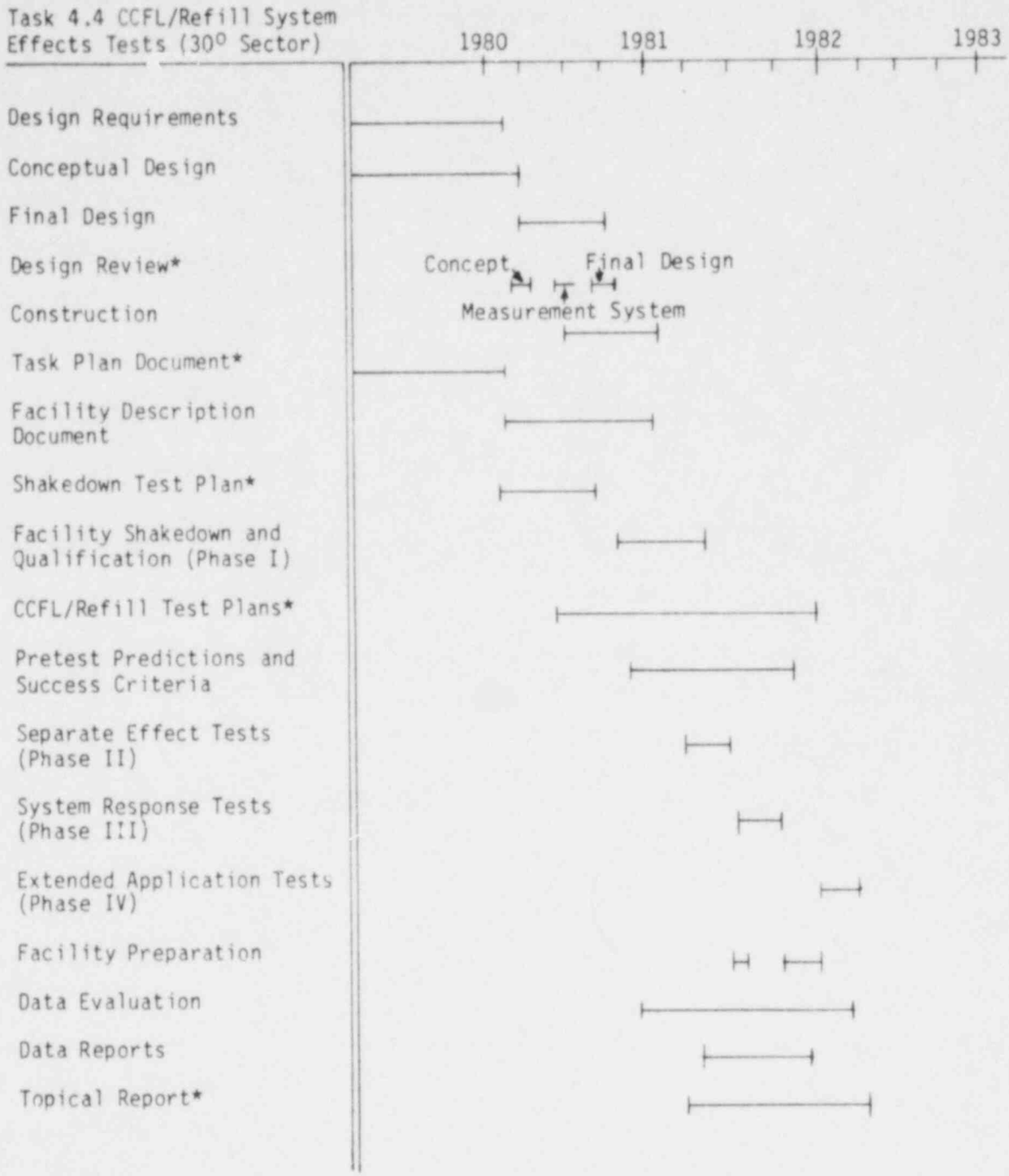

*Intermediate milestones

Figure 5-1. Schedule

Appendix A

FACILITY SUMMARY DESCRIPTION

A-1. SUMMARY FACILITY DESCRIPTION

The 30° Steam Sector Test Facility (SSTF) is located at GE's gas turbine/jet engine installation in Lynn, Massachusetts. Facility construction was initiated in 1977, with core-spray distribution tests initiated in 1979. As part of the CCFL/Refill System Effects task, the existing SSTF will be upgraded to perform transient LOCA simulation tests. The existing SSTF configuration is depicted in Figures A-1 and A-2. Following is a summary description of the upgraded SSTF categorized in terms of the 30° sector internals, pressure vessel, facility services, and vapor injection simulation.

As a result of design evaluation and review, deviations from the summary description presented herein may occur as required. The facility description document will define the final form of the upgraded facility configuration.

A-1.1 30° SECTOR INTERNALS

The 30° sector internals provide accurate representation of the reference BWR/6-218 (624 bundle) reactor through the use of prototypical hardware and geometry. The upper plenum is a full-scale mockup of a 30° sector of the reference upper plenum with accurate simulation of geometric shape and shroud head curvature and height. Standpipes simulating the steam separators extend up from the shroud head. The upper and lower core-spray spargers are full-scale mockups of 30° sectors of the reference BWR/6-218 HPCS and LPCS spargers with regard to size, curvature, location, and nozzles. An LPCS lower header representative of BWR/4,5 design can also be installed in the upper plenum to simulate earlier core-spray designs. The core region simulation includes both mock fuel bundles and bypass region. The core region is full-scale in cross section but is approximately five feet shorter than the BWR reference because of overall facility height limitations. Fifty-eight (58) mock fuel bundles are included in the 30° sector — 42 complete bundles, and 16 partial bundles with removable cover plates and baffles to simulate the 30° boundary within the partial bundle. The bundles utilize

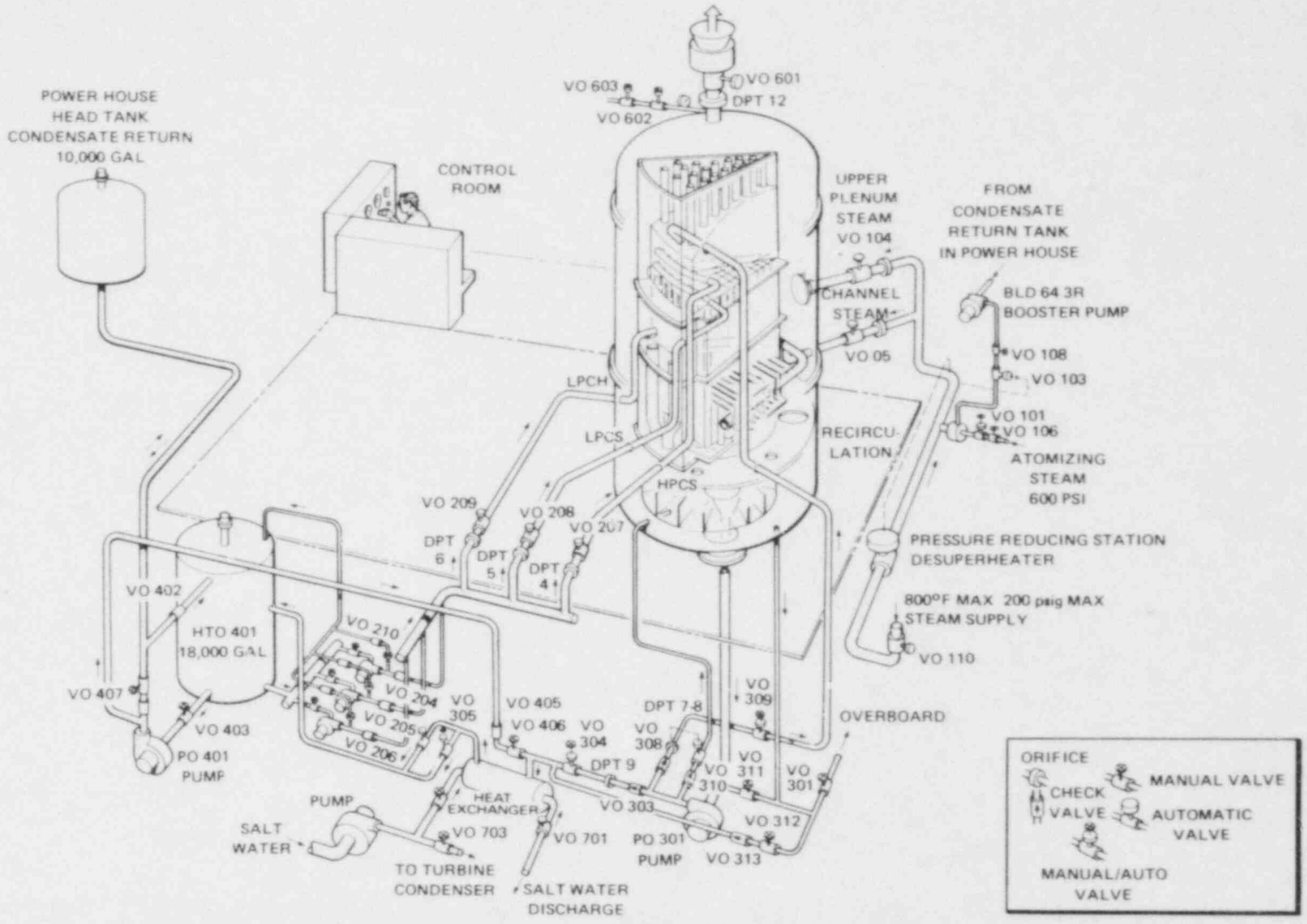

Figure A-1. 30° Steam Sector Test Facility

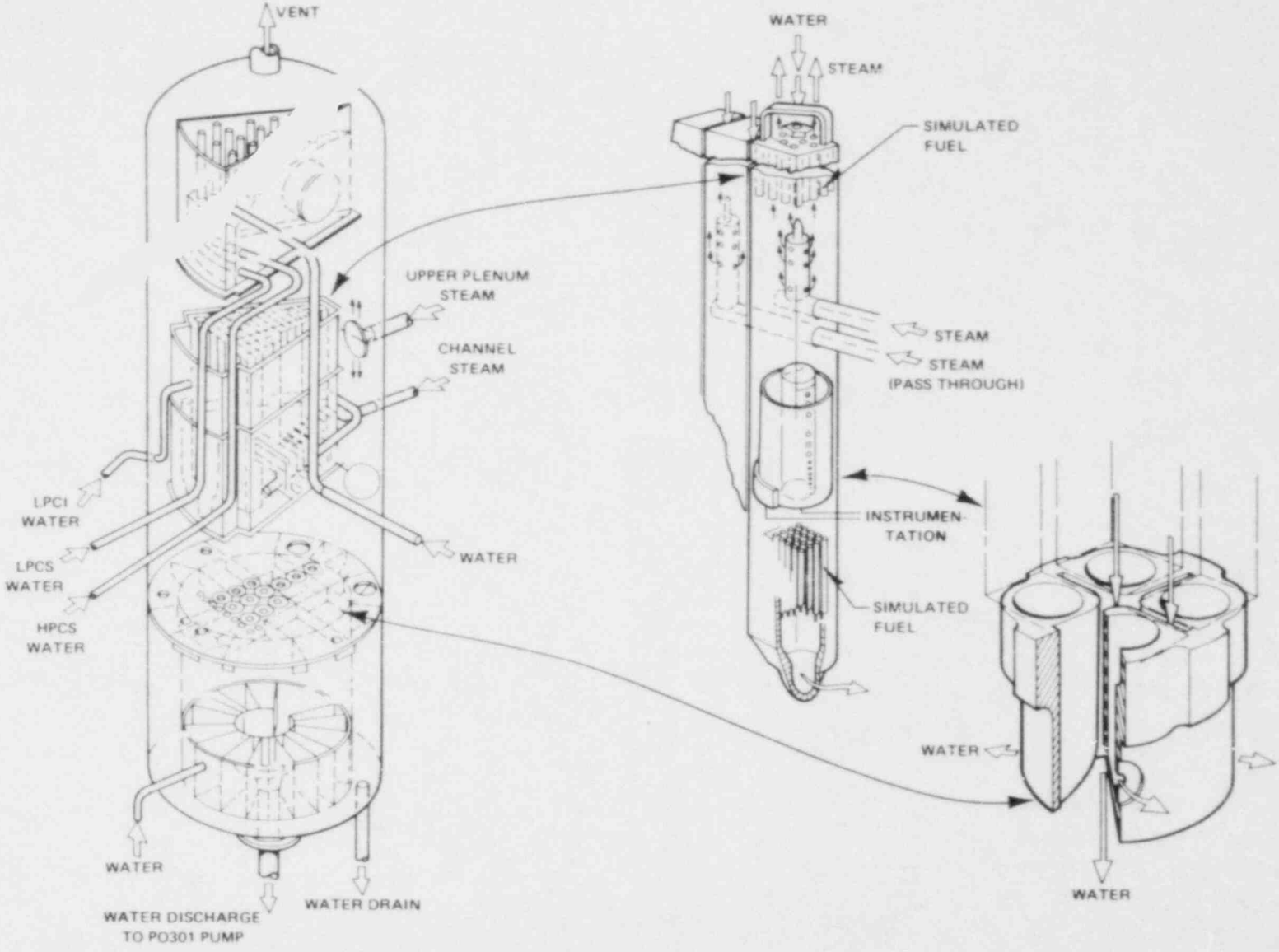

Figure A-2. 30° Steam Sector Test Section

production version hardware for channel, channel fasteners and spacer, upper tieplate, lower tieplate, and finger springs. Simulated fuel rods are included in both the upper and lower tieplate regions. Upper fuel-rod simulation includes production version expansion springs, end pins, locking tab washers, hexagon nuts, and one fuel-rod spacer. A steam injection tube is provided in each bundle below the upper rods to deliver the channel steam from the steam distribution manifold located outside the 30° shroud wall. A weir-tube measuring device is provided in selected bundles above the lower rods to measure the liquid flow. The bypass region flow area is simulated and includes dummy control rods mounted on production version fuel-support castings. Leakage and flow path simulation between bundle, bypass, upper plenum, lower plenum, and guide tube are assured by using production-version hardware in conjunction with accurate representations of the top fuel guide and core plate. Twelve (12) volume-scaled guide-tube regions are provided (one for each of the 12 centrally located side-entry fuel supports). The lower-plenum volume represents the scaled volume of the reference lower-plenum region outside the guide tubes.

Two jet pumps scaled on the basis of BWR equivalent single-phase flow resistance connect the lower plenum to the annulus. The jet-pump lengths are scaled to compensate for the foreshortened core. The annulus region is scaled on a volumetric basis with regard to the reference BWR/6-218.

LPCI injection lines pass through the annulus to inject ECC flow into the core shroud for BWR/6 LPCI injection simulation. By modification to the internals LPCI piping, ECC liquid can also be injected into the top of the jet pumps to simulate BWR/4 LPCI injection.

A blowdown pipe connected to the outer wall of the annulus simulates the BWR recirculation line outlet and (under transient LOCA simulation tests) directs the blowdown mixture past a flow-restricting nozzle (simulating the reactor break area) to the blowdown suppression tank.

A volumetrically scaled steam dome region completes the BWR simulation. The steam dome is formed by partitioning the volume between the test section internals and the excess volume* of the pressure vessel.

---

*Vessel-free volume in excess of the BWR-scaled value.

A-1.2 PRESSURE VESSEL

The SSTF pressure vessel (14-ft. inside diameter and 27-ft. inside height) serves as a pressure envelope for the 30° sector internals. The vessel is designed with numerous nozzles and penetrations to permit attaching the various process lines which service the internals and to provide routing for the various instrumentation lines and cables. The vessel is surrounded by service platforms and walkways and is serviced by a traveling overhead crane.

A-1.3 FACILITY SERVICES

The SSTF is located in the central region of an existing turbine hall, to which the necessary process equipment and loop hardware have been installed to provide the required services to the facility. A steam supply of 130,000 lbm/hr at 150 psia and 388°F is available.

Water is supplied to the facility from a 10,000-gallon condensate tank and retained in an 18,000-gallon supply tank which is part of the ECCS water supply and recirculation loop. The temperature of the water in the tank can be controlled by recirculating through a 500-gpm heat-exchanger loop. Water from the lower plenum of the test section can be pumped back to the supply tank via a single-pass heat-exchanger unit, recirculated to the top of the upper plenum, or circulated through the LPCI systems to accommodate both separate-effect and transient-test operation needs. The ECCS supply system provides flow representative of the reference BWR/6-218 reactor. The system consists of three 600-gpm pumps connected in parallel and one 2400-gpm booster pump to provide up to 2400 gpm at 150 psia to the 10-in. main ECCS header. This main header in turn supplies a 6-in. HPCS line with up to 533 gpm and an 8-in. LPCI line with up to 1333 gpm. A secondary water drainage system provides drainage capability for the guide tube and annulus regions of the test section for control of initial mass inventory during transient tests.

A vessel blowdown system consisting of a blowdown line (with removable flow restricting nozzle), quick-opening valve, flash tank, and suppression/containment tank manages the blowdown effluents during transient LOCA simulation tests.

Onsite data acquisition/data reduction is provided by a Hewlett Packard processor with 400-channel input signal capacity (see Subsections 3.2 and 3.5 for further discussion of the data acquisition/measurement system).

A-1.4 VAPOR INJECTION SIMULATION

A batic steam injection is provided in the core, guide tubes, and lower plenum of the test section to simulate/augment liquid flashing and bundle steam generation during separate-effect and t[illegible]sient LOCA simulation tests, and to set initial void and mass distribution conditions representative of that predicted for the reference reactor at the initiation of the tests. Control of the injected steam flow will be by automatic systems capable of providing steady-state injection rates or programmed injection transients.

Appendix B

UPPER-PLENUM SEGMENT TEST

B-1. ABSTRACT

An exploratory investigation of the effects of subcooled ECC injection on the CCFL phenomena in a segment representation of the BWR upper plenum was conducted in the Upper Plenum Test Series. Test results indicated that breakdown of the CCFL phenomena could be achieved over a range of test conditions. It was found that previous single-bundle observations of CCFL breakdown when net subcooling is achieved represent a conservative bounding limit for the breakdown observed in these three-dimensional studies. The mixing phenomena and CCFL breakdown were found to be influenced by variation in the following parameters:

a. core radial steam profile,

b. core spray flow rate,

c. core spray header elevation, and

d. initial upper-plenum two-phase level.

B-2. INTRODUCTION

Current BWR-LOCA licensing models account for the effects of counter-current flow-limiting (CCFL) phenomena at the top of the fuel bundles with the simplified assumption that only saturated liquid enters the fuel bundles throughout the LOCA transient. However, it has been demonstrated in single-bundle experiments that when the emergency coolant injection into the upper plenum is sufficient to produce net subcooling, then subcooled liquid enters the top of the fuel bundle. The condensation in the bundle then results in a reduction of steam flow through the CCFL restriction, and, through positive feedback, elimination or "breakdown" of CCFL controlling the liquid drainage results. This produces a rapid transfer of the liquid from the upper plenum to the lower plenum. These CCFL breakdown phenomena would significantly reduce the predicted time to reflood and cool the core. Therefore, the present program was initiated to further study these phenomena in a configuration more representative of a three-dimensional BWR

upper plenum. To address the effect of subcooled core-spray injection in breaking down the CCFL condition, a 16° sector facility was built as a separate-effect test of the mixing phenomena. In particular the following topics were discussed:

a. evaluate the saturated CCFL characteristics of the 16° facility,

b. evaluate the CCFL breakdown characteristics for a typical BWR upper plenum with subcooled injection through peripheral header/nozzles, and

c. evaluate the effect of vertical position of the injection nozzles (i.e., upper vs. lower header) on the CCFL breakdown characteristics of the test apparatus.

Contained in this appendix is a description of the 16° experimental facility and a compilation of the important results of experiments addressing BWR upper-plenum mixing.

B-3. TEST FACILITY DESCRIPTION

The test apparatus is a low-pressure, 16.5-degree radial segment (of reduced radius) representation of the BWR/6 upper plenum, referred to as the 16° Upper Plenum Facility. Figure B-1 displays the major components of the test apparatus in an exploded pictorial format. The test facility is comprised of the following elements:

a. Steam/water, adiabatic, atmospheric pressure test loop

b. Segment test section

   1. 16.5-degree segment

   2. test section radius ap[illegible] 5 feet

   3. full upper-plenum height with curved dome and simulated standpipes

   4. actual tieplates and shortened fuel bundles

   5. 13 zones for steam introduction and water collecti[illegible]

c. Minicomputer data acquisition system

The steam supply for the test facility is a 6000-lb/hr, 150-psi boiler.

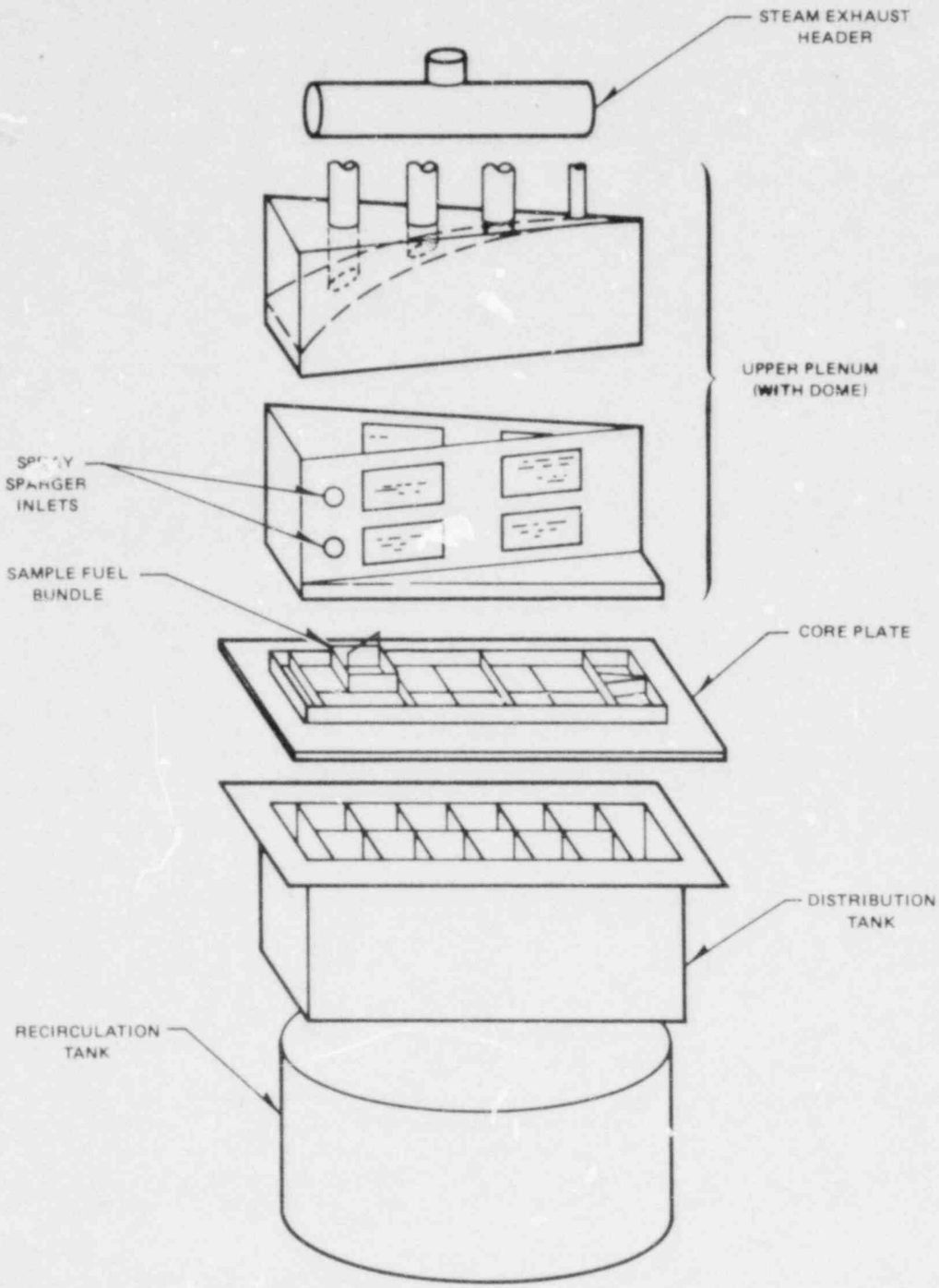

Figure B-1. Major Test Apparatus Components

B-3.1 TEST SECTION DESCRIPTION

The 16° upper plenum facility has the following characteristics and capabilities:

a. BWR/6-218, 624 standard plant to serve as reference for upper plenum simulation;

b. test-segment size determined so that the existing 6000-lbm/hr boiler supplies flow to the simulated core on a full-scale mass flux basis as determined from bundle vaporization;

c. variable core-spray distribution through nozzle reaiming;

d. ECC water-flow capacity equivalent to either LPCS or HPCS operating in reference reactor case;

e. capability for variation of LPCS and HPCS header orientation;

f. capability for variation of spray-flow rate;

g. capability for variation of spray subcooling; and

h. capability for varying steam-flow rate by valve adjustment and radial distribution by steam-orifice replacement.

To provide a representative upper-plenum geometry based on the BWR/6 plant design and within the limitations of the existing steam facilities, the following scaling basis was used:

a. Core Area - To maintain the vapor volumetric flux through the core segment equal to the reference reactor flux, using existing steam facilities, the scaled core area follows the ratio of the maximum available steam flow to the calculated reactor steam flow from bundle vaporization.

$$\text{CORE AREA} = \left[\frac{\text{Available Steam Flow}}{\text{Reactor Steam Flow}}\right] \text{Reactor Core Area}$$

$$\frac{6077}{395{,}527 \text{ lbm/hr}} (22458.3 \text{ in.}^2) = 345 \text{ in.}^2$$

b. Test Section Geometry - The upper-plenum segment is an approximately five-foot-long triangular-shaped section with an included angle of 16.5°. This geometry provides the scaled-core area defined above with an included angle large enough to allow multiple spray nozzle injection points and limit the extent of geometry-imposed wall effects on the mixing phenomena.

c. Fuel-Bundle Area - The fuel-bundle area is full-scale relative to the reference reactor.

d. Bypass Region - The bypass region is blocked (assumed flooded) and therefore nonparticipating.

e. Steam Dome and Standpipe Heights - Full-scale height to preserve real time refilling rates of these regions.

B-3.2 TEST LOOP DESCRIPTION

The test loop supporting the 16° test apparatus is a low-pressure (30 psia maximum), steam/water system (see Figures B-2 and B-3). The primary capabilities and capacities of the loop are listed below:

a. 6000-lb/hr steam capacity,

b. 100-gpm water pumping capacity,

c. 5000-gallon water supply storage capacity,

d. variable steam flow,

e. variable core-spray flow, and

f. variable core-spray temperature.

The test loop-design uses deionized water and allows for the recycling of this water to the test section and/or to the steam boiler.

B-3.3 TEST INSTRUMENTATION DESCRIPTION

The measurement capabilities of the upper plenum segment facility are as follows:

a. core spray flow, temperature, and upstream pressure;

b. total inlet steam flow, temperature, and pressure at the measurement station;

c. total discharge steam flow, temperature, and pressure;

d. liquid mass drainage and temperature from each of the 13 core regions;

e. upper-plenum pressure;

f. collapsed level of two-phase mixture at three radial locations in the upper plenum;

g. vertical temperature profile at three radial locations in the upper plenum;

h. temperature measurement above and below each tieplate; and

i. absolute pressure inside the two peripheral distribution chambers.

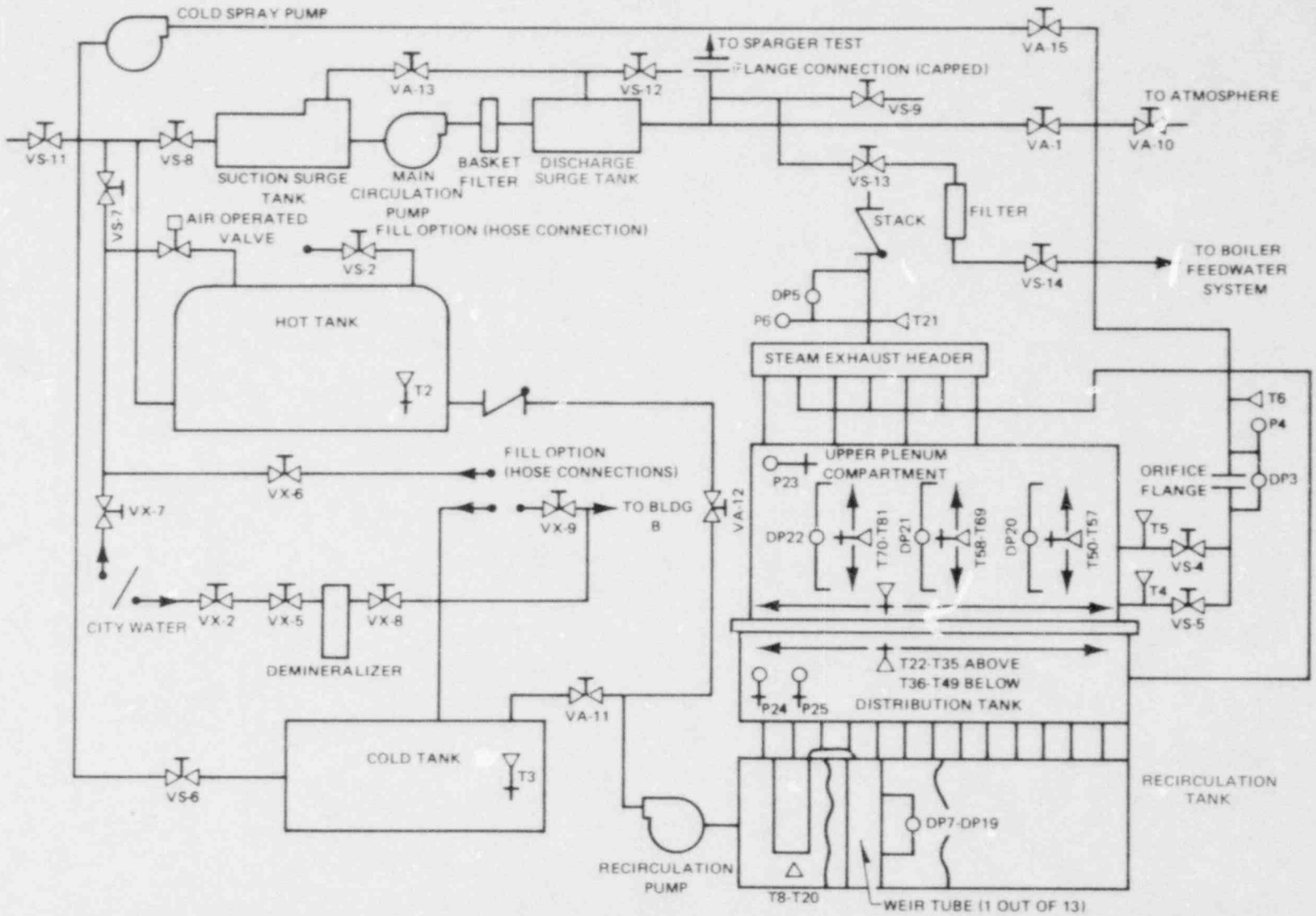

Figure B-2. Water System Piping and Instrumentation

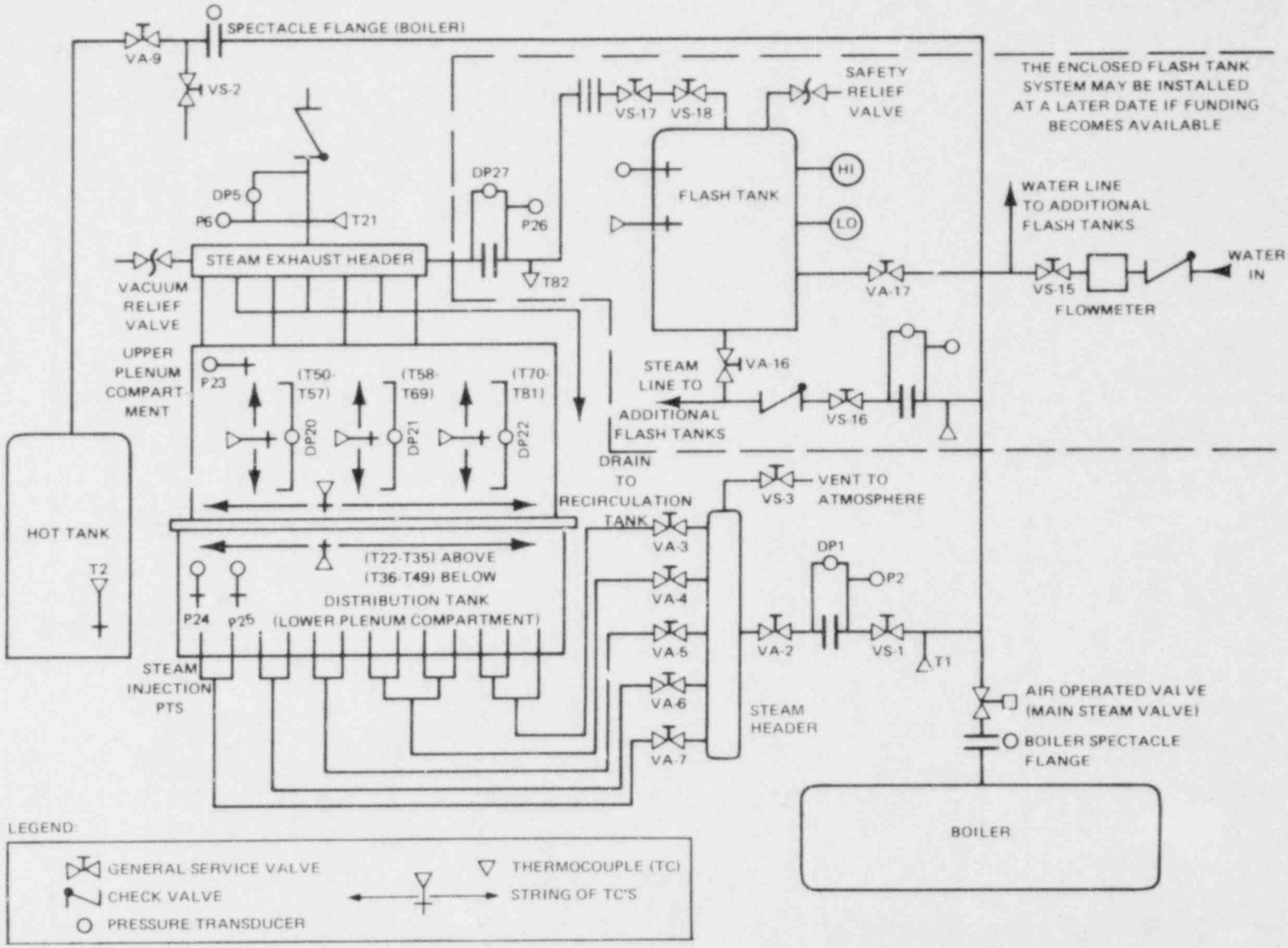

Figure B-3. Steam System Piping and Instrumentation

Measurement accuracies are as specified below:

Liquid flow rates (weir tube, orifice)	(±6%, ±4%)
Steam flow rates	±6%
Pressure	±3%
Temperature	±3%
Upper plenum collapsed liquid level	±7%

The location and general designation of the upper plenum segment test instrumentation is shown in Figures B-2 and B-3. The basic instruments and their uses are listed below (and further defined in Table B-1):

a. Thermocouples - Measurement of fluid temperature around the test loop for diagnostic and control purposes and temperature distribution in the upper-plenum test section.

b. Differential Pressure Transducers - Measurement of steam and water flow rates through orifices and pressure drops across regions of the test section.

c. Absolute Pressure Transducers - Measurement of pressure conditions in the steam system and upper plenum region.

d. Pitot Tubes - Measurement of steam flow leaving the upper plenum test section.

e. Weir Tubes - Measurement of water drainage from each of the 13 collection chambers.

All the instruments were checked and/or calibrated prior to the beginning of testing.

B-3.4 DATA ACQUISITION SYSTEM DESCRIPTION

The data acquisition system for the upper-plenum segment test program is a minicomputer-based system of the following elements and configuration:

a. Hardware Block Diagram - The ECCS data acquisition and display computer system consists of the components shown in Figure B-4. The processor is a Hewlett Packard 21MX, with ROM-implemented microcode which simulates the earlier HP-2100 series instruction set. 32K 16-bit words of semiconductor memory with memory protect are available. Dual DMA channels provide fast data transfer capability between core and peripherals (MUX, DISK, MAG TAPES).

Table B-1

INSTRUMENTATION DESIGNATION

Instrument Type	Manufacturer (Model Type)	Units	Full-Scale Range	Instrument Accuracy	Measurement Accuracy
Absolute pressure transducers	BLH (DHF)	psia	50	±0.125 psia	±0.375 psia
Differential pressure transducers	BLH (HLD)	inches of H_2O	±100	±0.25 in.	±0.67 in.
Absolute pressure transducer	BLH (DHF)	psia	200	±0.5 psia	±1.5 psia
Thermocouples	Type K chromel/alumel	°F	+32° to +2300°F	±2°F	±5.5°F
Thermocouples	Type J iron/constantan	°F	+32° to +1400°F	±4°	±7.3°F
Reference junction	acromag 343 - Type J	°F		±0.2°F	±4.2°F
Spray-flow orifice		GPM		±2%	±2%
Pitot tube	annubar Model 71	GPM	18-390 GPM	±1.55%	1.88%
Steam-flow orifice		lbm/hr		±2.33%	±2.33%
Computer multiplexer	Hewlett Packard			±0.33%	
Weir tubes	GE design	lbm/h	2500-20,000 lbm/hr		±6%

b. Peripherals - The major purpose of each peripheral is described below:

1. Process Peripherals

- Two 2313 High-Speed Multiplexers and A/D Converters: utilized to read analog signals from thermocouples and other loop instrumentation to core.
- 16-Relay Output Card: which can be utilized to send signals from the computer to the process.

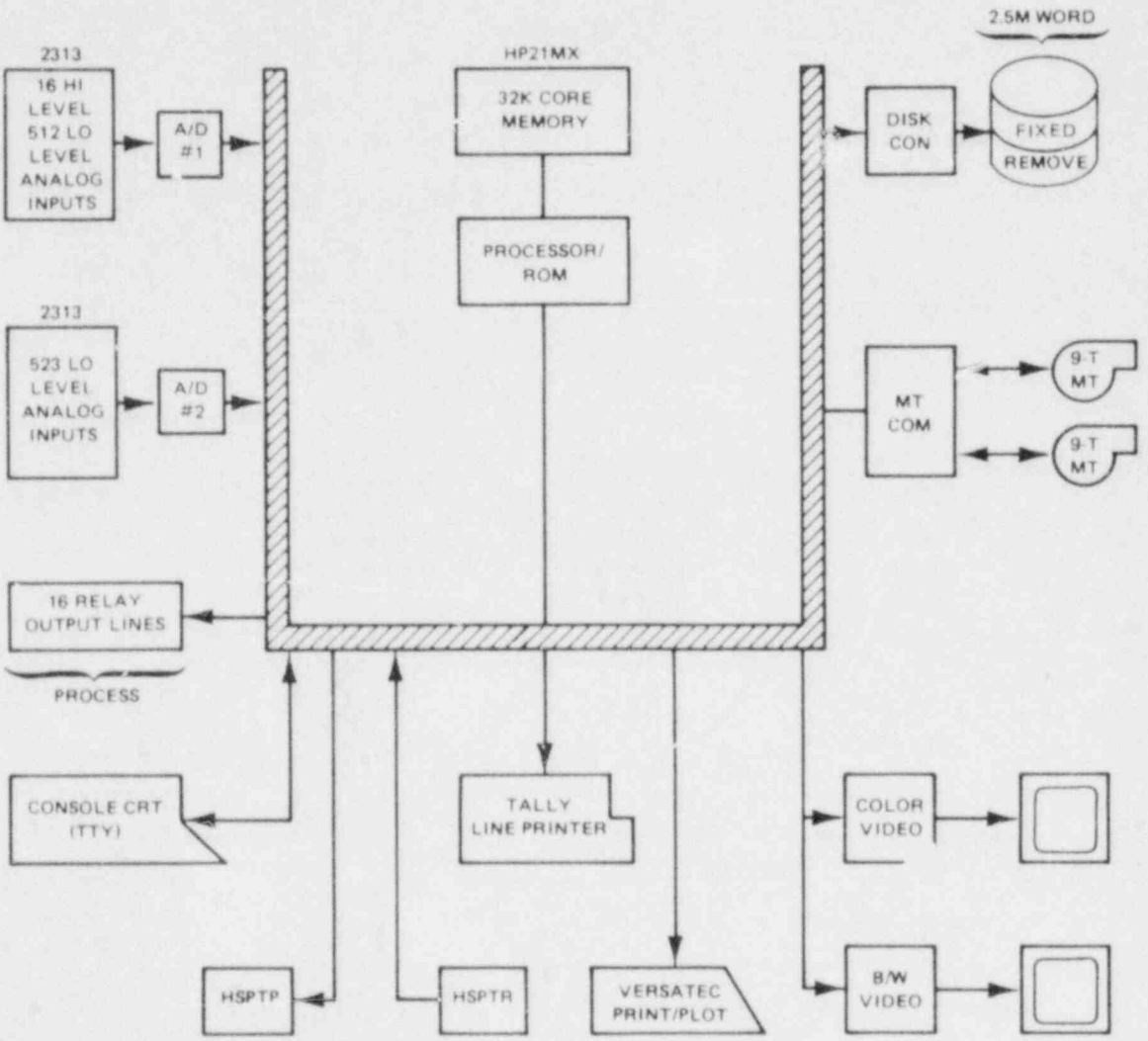

Figure B-4. DAS System Schematic

2. Business Peripherals

- Dual-Disc Subsystem: maintains program logic in absolute, relocatable, and source format. Maintains disc data tables and files required by the programs. Provides scratch bulk memory as needed.

- Dual Transport Nine-Track Magnetic Tapes: utilized as the primary data storage medium during data acquisition. Provides industry-standard data storage medium for test data transfer to batch computer (H-6000). Provides a "disc dump" backup medium.

- Color CRT: displays three variable versus time plots of three types of variables. The fourth quadrant of the screen maintains an ASCII parameter legend.

- Versatec Printer Plotter: provides an on-line "strip-chart" trend for up to 10 selected variables during data acquisition. The offline usage will be for tape data "playback display" and for generating plots.

- TALLY Line Printer: provides a fast input device capable of printing alarms, logs, and run parameters during data acquisition. Provides offline device for data reduction printing requirements. Provides a program preparation device for printing code listings, load maps, and file libraries.

- High-Speed Paper Tape Reader: provides a fast input device for loading diagnostics, source files, free-standing offline programs, and DOS or BCS System bootstrap paper tapes.

- High-Speed Paper Tape Punch: provides program preparation punch device requirement for any interim BCS program development.

- Console CRT: provides a "system TTY" console required by DOS and BCS. Provides the primary vehicle for test operator input requests for log printing and data display variables.

B-4. TEST PARAMETERS AND PROCEDURES

The 16° upper-plenum test facility was designed so that several test parameters could be varied and their effect on the CCFL phenomena investigated. These parameters can be divided into two groups: core-spray and steam-flow variables, and variation in core-spray header elevation (i.e., LPCS (lower header) and HPCS (upper header)).

The core-spray and steam-flow variables were set prior to each test run in addition to being monitored and recorded throughout the run. Three core-spray flow rates were used; 100, 83, and 75 gpm. The 100-gpm flow rate is a scaled parameter which corresponds to BWR HPCS and LPCS runout flow conditions. The 83-gpm flow rate is also a scaled parameter and corresponds to the BWR rated LPCS flow condition. Similarly, the 75-gpm flow rate is scaled from the BWR HPCS rated flow condition.

In addition to flow rate, the core-spray temperature was also an independent variable. For a saturated CCFL test, the spray temperature was typically maintained in the range of 205 to 212°F. For a subcooled CCFL test, the spray temperature was adjusted to a value between ambient and 150°F.

The source of steam for the upper plenum test was a 6000 lbm/hr boiler, which delivered slightly superheated (2°F to 4°F beyond the test apparatus saturation condition) steam to the test apparatus. For the saturated CCFL tests, the steam-flow rate was adjusted to a specific value between 4000 and 6000 lbm/hr. The nominal value of steam flow for a subcooled CCFL test was 6000 lbm/hr.

The upper-plenum test series was composed of spray distribution, saturated CCFL, subcooled CCFL, and steam-profile tests. The following paragraphs summarize the procedures followed in each test category.

B-4.1 SPRAY DISTRIBUTION TEST

Core-spray distribution tests were conducted in an air upper-plenum environment for calibration of the actual spray pattern provided by the core-spray configuration for both upper and lower spargers. No steam injection was used in these tests. Core-spray water from the cold reservoir was circulated through the test section at a rate of 83 or 75 gpm. Drainage rate data for each of the bundles were then recorded for a period of three minutes. Table B-2 defines the nozzle aimings and estimated flows splits.

B-4.2 SATURATED CCFL TESTS

The objective of the saturated CCFL tests was to determine the CCFL characteristics of the test section. For these tests the spray water, which was maintained at approximate saturation conditions, was injected into the upper plenum via the lower header. The spray flow rate was then adjusted until a steady-state, two-phase mixture level was observed in the test section. After data were recorded at these conditions, the test was repeated at a different nominal steam flow rate. Thus, data points for a CCFL response curve were generated.

Table B-2

CORE SPRAY DATA

Core Spray Configuration	Location 1	Location 2	Location 3
Lower Header	3/4 in. O.E.[1]/-48°	1 in. O.E./-20°	3/4 in. O.E./-48°
Upper Header	3/4 in. O.E./-64°	1 in. O.E./-32°	3/4 in. O.E./-64°

Estimated Flow Splits

(100 gpm total spray flow)

Core Spray Configuration	Location 1 (gpm)	Location 2 (gpm)	Location 3 (gpm)
RCS LH	30	40	30
RCS UH	31	38	31

B-4.3 SUBCOOLED CCFL TEST

The majority of tests performed during the test series were of this type. The desired nominal conditions for steam and spray flows were determined from the test matrix. Typically, the desired spray temperature was achieved by mixing saturated water gradually into the cold-water reservoir. For the test run, the steam flow was brought up to 6000 lbm/hr and a two-phase mixture established in the test section by introducing saturated water (205 to 212°F) through the core-spray system at the desired flow rate. After the test section was filled and more or less steady conditions had been achieved, the computer and video tape equipment were brought on line and data recording started. At this point, the saturated water was valved off and the cold-spray water at the preset temperature valved in. The spray flow rate was then adjusted as quickly as possible to the desired nominal flow rate. Throughout the rest of the test run, usually three to five minutes, periodic adjustments were made to maintain the test conditions at the desired values. If, after initiation of subcooled spray, the level of the two-phase mixture in the test section dropped and the upper plenum eventually drained, breakdown was achieved. If the test section did not drain within three to five minutes, the run was ended and preparations made for the next set of test conditions.

B-4.4 STEAM PROFILE TEST

Two separate steam profiles were used in the test series. The first profile tested had radial steam flow proportional to the core radial power in the reference reactor. The second steam profile was based on conservatively biased computer models of the individual bundle steaming rates. The major difference between the two profiles is that the latter has a higher steaming rate in the peripheral bundles. Both profiles were used in the test series to determine the sensitivity of the subcooled CCFL breakdown response to variations in the steam profile.

B-5. TEST RESULTS

B-5.1 STEAM PROFILE MEASUREMENT

Following the procedures described in Section B-4 for a steam profile test, the two steam profiles used in the test series were experimentally verified. The steam-flux profiles normalized to the average bundle flux of the test apparatus are shown in Figures B-5 and B-6. The total steam flow through the test section is the same for both profiles. However, for the profile shown in Figure B-6, the orifice area in the two peripheral rows of bundles was adjusted to increase the steam flow through these regions. The result was an increase in steam flux of approximately 27 percent in the first peripheral row and 11 percent in the second peripheral row. Consequently, the steam flux for the inner bundles was reduced and thus produced a flatter steam profile relative to that shown in Figure B-5.

The steam profile of Figure B-5 will be referred to as the Low Peripheral Flux Steam Profile in subsequent sections of this appendix. The steam profile of Figure B-6 will be referred to as the Medium Peripheral Flux Steam Profile. This profile was patterned after conservative computer model predictions of bundle steaming rates.

B-5.2 CORE SPRAY DISTRIBUTION

Measurements of the core-spray distribution of the test apparatus with an air upper-plenum environment revealed a relatively good match between this configuration of the test apparatus and typical BWR/6 full-scale data extrapolated to the 16°-sector facility (see Figure B-7). Only in the second peripheral row of bundles is there significant difference between the BWR/6 extrapolation and the test results.

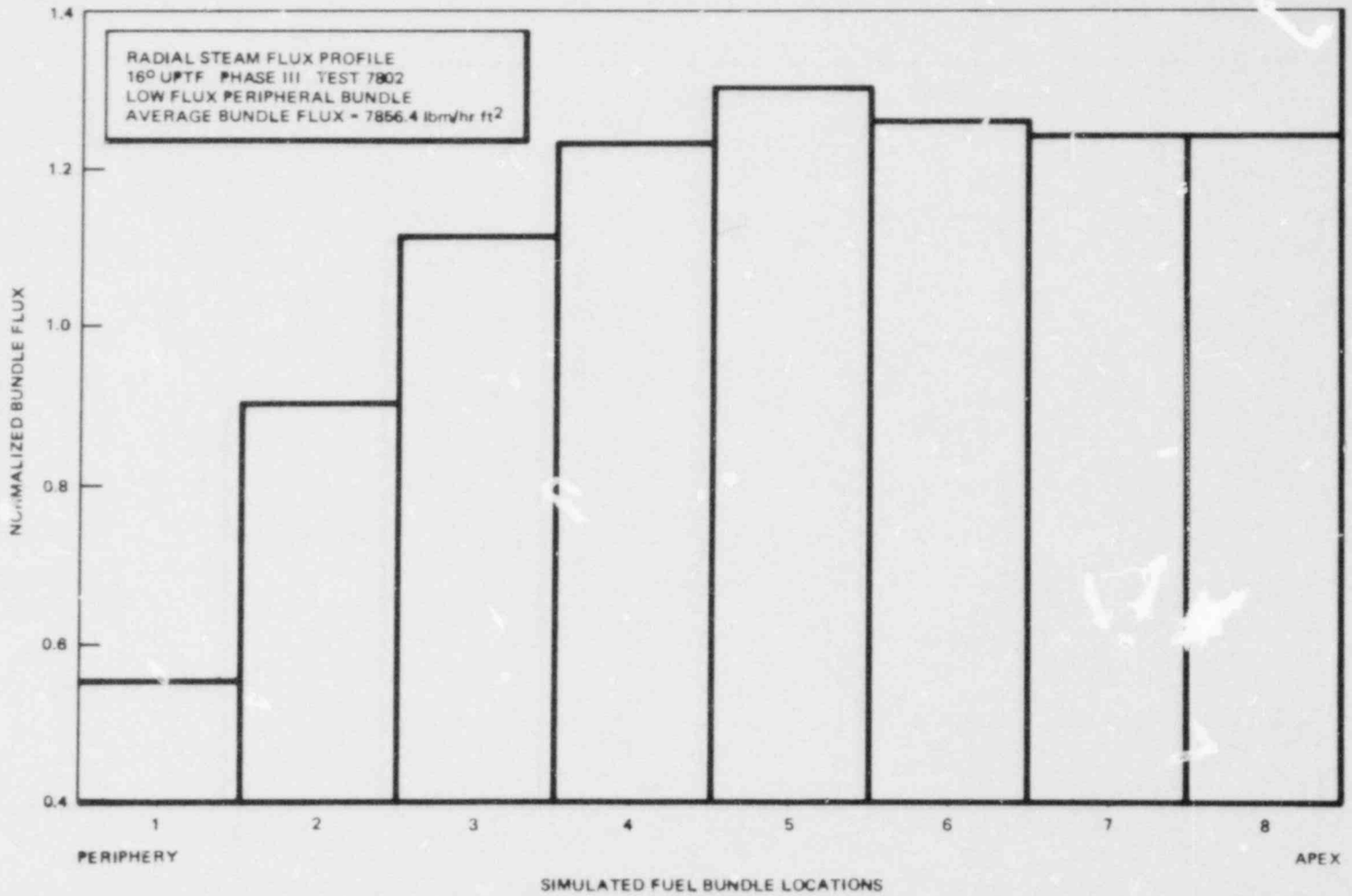

Figure B-5. Low Peripheral Flux Steam Profile

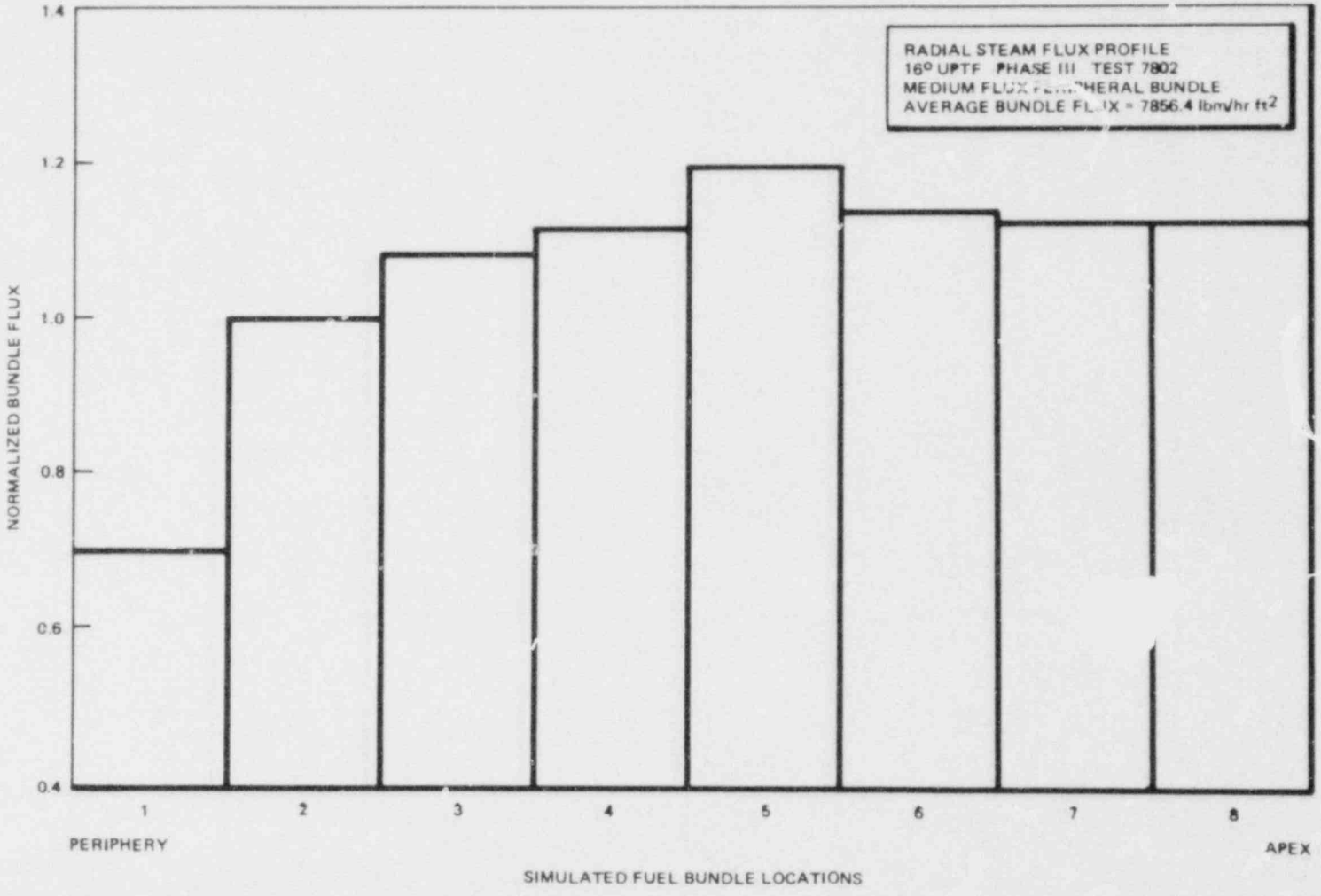

Figure B-6. Medium Peripheral Flux Steam Profile

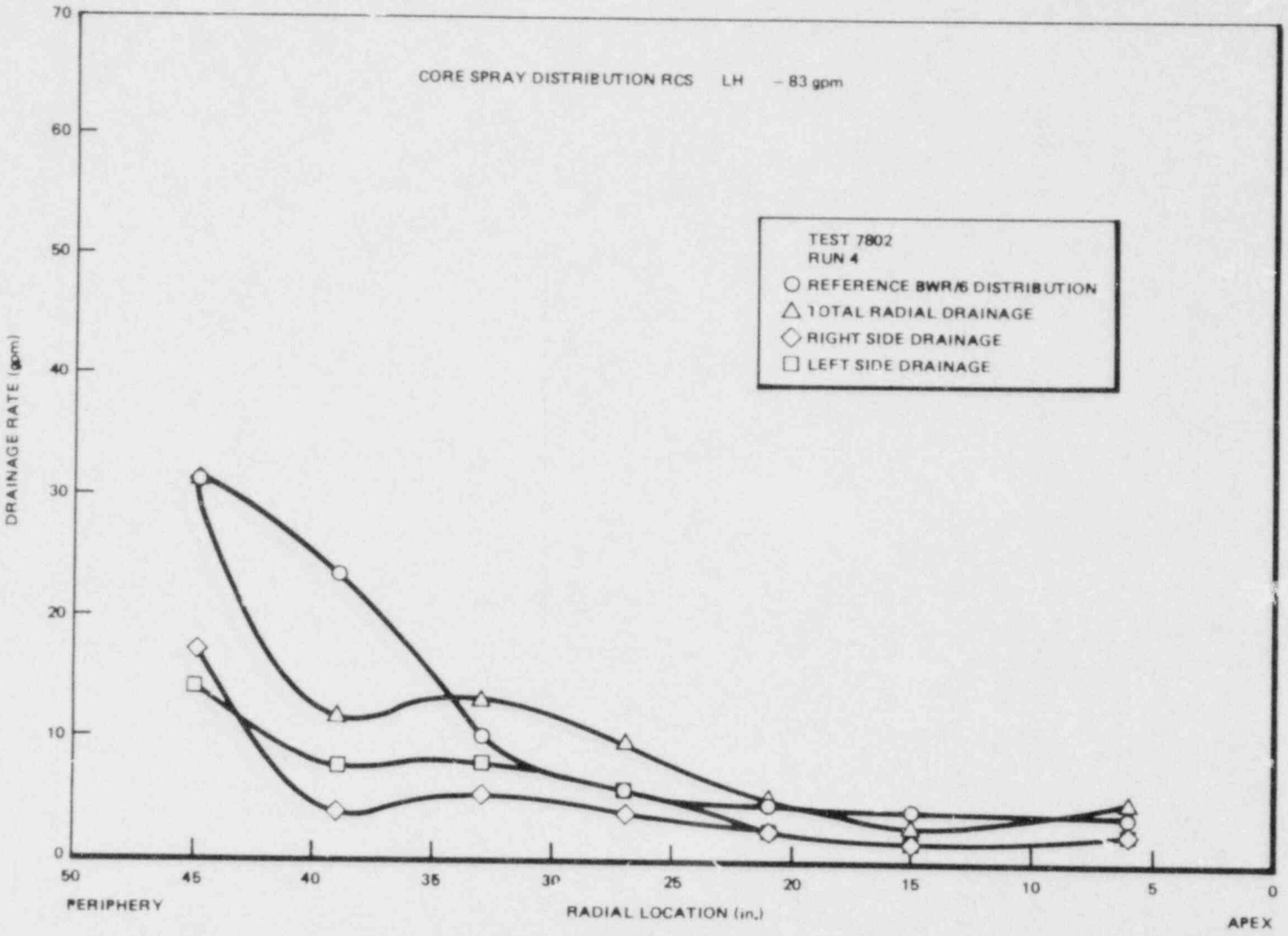

Figure B-7. 16% Spray Distribution Relative to Reference BWR/6

B-5.3 SATURATED CCFL RESULTS

Figure B-8 displays the measured upper-plenum drainage (square symbols) at steam flows ranging from 4000 to 6000 lbm/hr. For each of the five steam flow rates, the core-spray injection rate (triangular symbols) into the test section was adjusted to match the liquid volume discharged from the upper plenum, so that a steady two-phase level was observed in the upper plenum. Performing the experiments in this manner provided a redundant measurement of liquid discharge from the test apparatus. As displayed in Figure B-8, the spray injection and drainage measurements appear to diverge at higher steam flow. To some extent this is to be expected because a portion of the injected spray becomes entrained at the higher steam flows and is blown out of the upper plenum through the standpipes. However, there is also some uncertainty as to the accuracy of the drainage measurements at high steam flows because of small and occasional spurts of steam into the weir-tube elements which measured the drainage flow. The triangular symbols therefore define a conservative upper bound on the drainage measurement uncertainty. Tabulations of the CCFL drainage from each of the simulated bundles of the test apparatus are contained in Section B-9.

Figure B-9 displays the CCFL data from each of the individual fuel bundles of the test apparatus. Bundle Location 1 is at the core periphery and encompasses two complete fuel-bundle simulations and two "steam-box" simulations of fractional bundles. Bundle Location 2 is located one row radially inward from the periphery and encompasses two complete fuel-bundle simulations. Regions 3 through 6 are comprised of pairs of partial fuel-bundle simulations located radially inward. Region 7, located at the apex of the test apparatus, is composed of two extremely small partial bundle simulations and one "steam-box" simulation of fractional bundles. Figure B-10 displays the bundle locations in plane view. A best-fit line through the scatter of the data (with slope equal to 1) produces a correlation constant of 0.621 $ft^{\frac{1}{4}}$ in the Modified Wallis form of the CCFL correlation. At vapor flux parameter values between 0.25 $ft^{\frac{1}{4}}$ and 0.375 $ft.^{\frac{1}{4}}$, the liquid flux tends to diverge from the 0.621 line. This trend, which is observed in the peripheral bundles (Region 1), appears to be due to momentum effects from the peripheral core-spray nozzles.

The data from Core Region 7 are not recorded in Figure B-9 because the bundle flow area and consequent CCFL drainage are so small that they are outside the range of the drainage instrumentation.

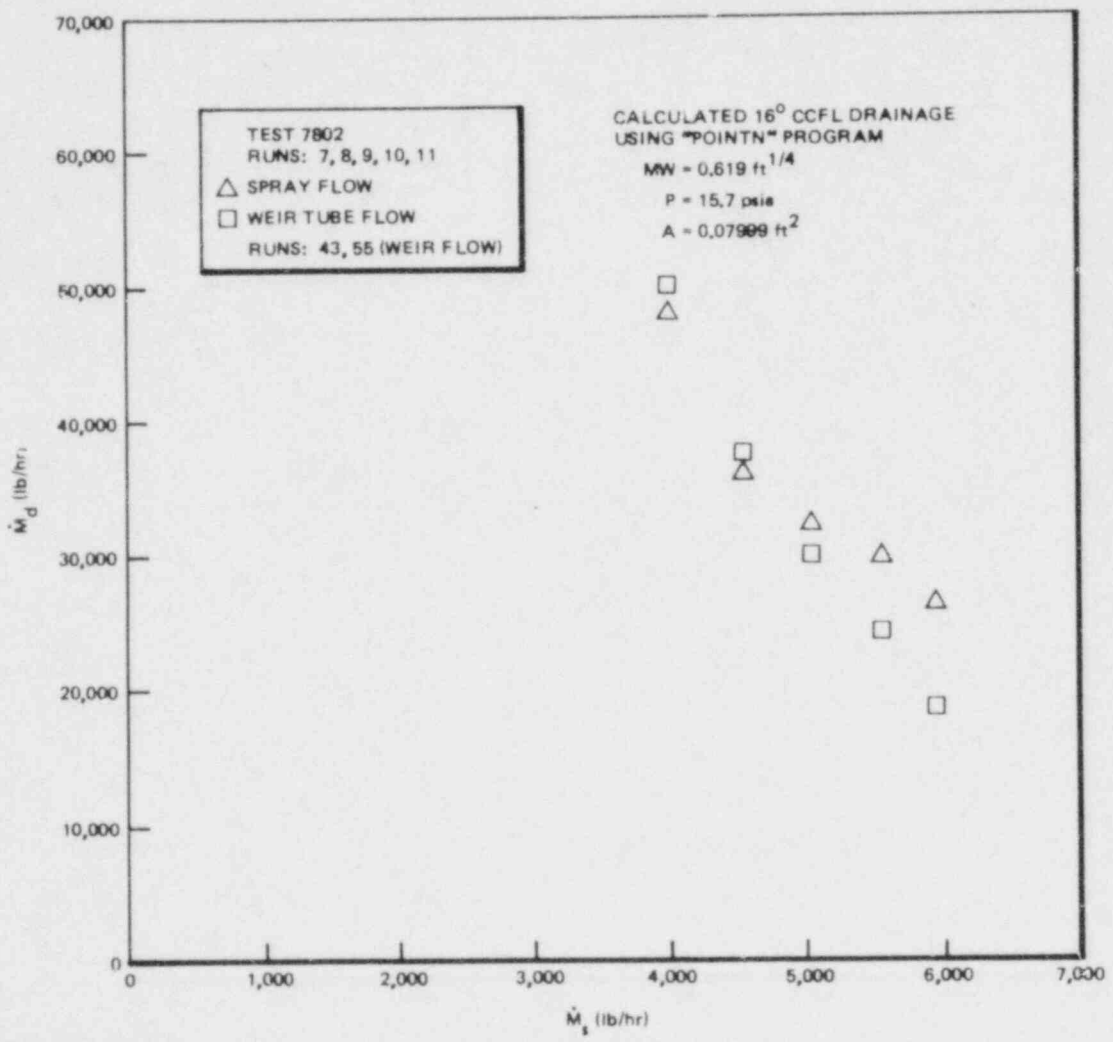

Figure B-8. Overall Upper-Plenum Drainage

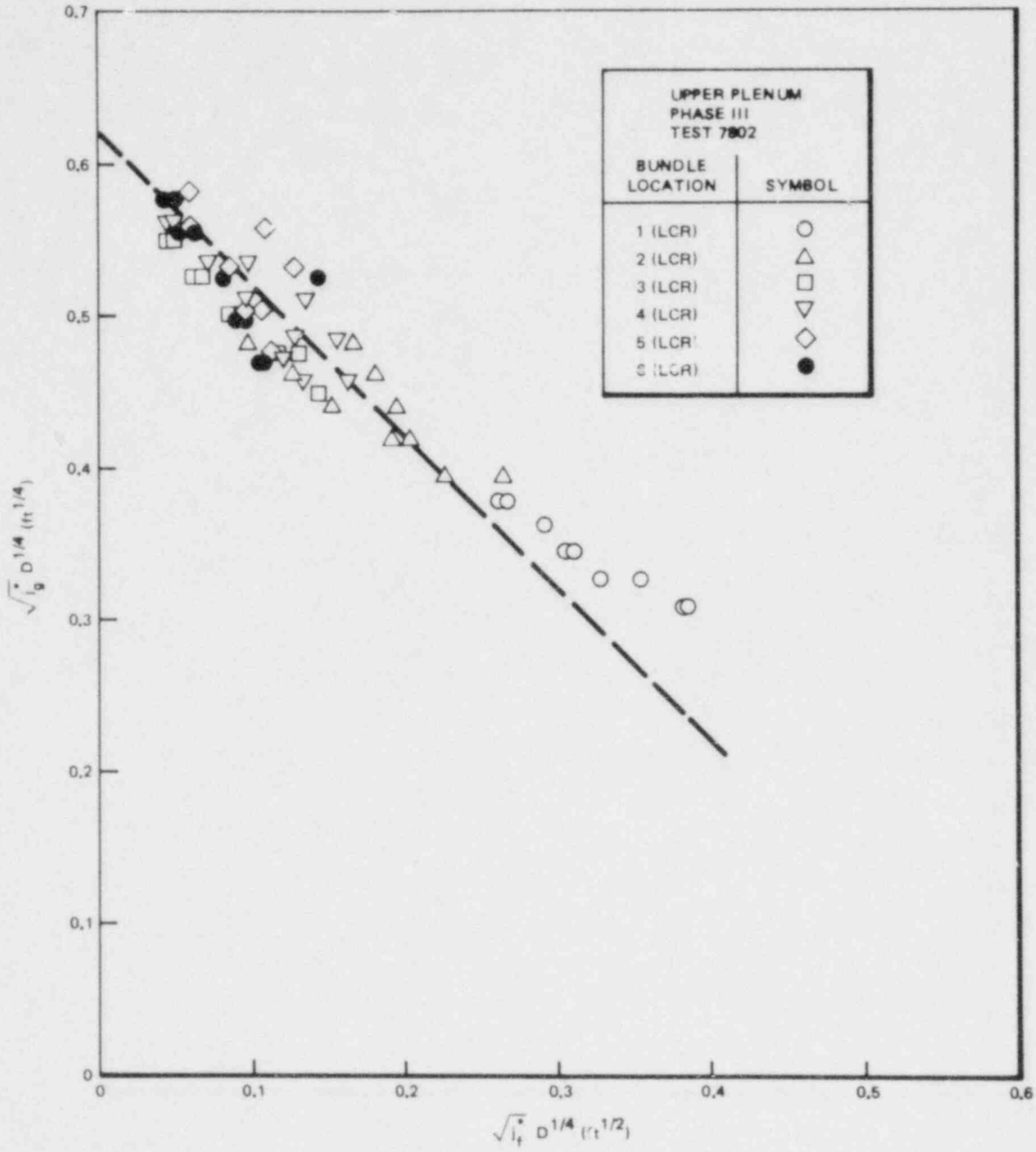

Figure B-9. Individual Bundle CCFL

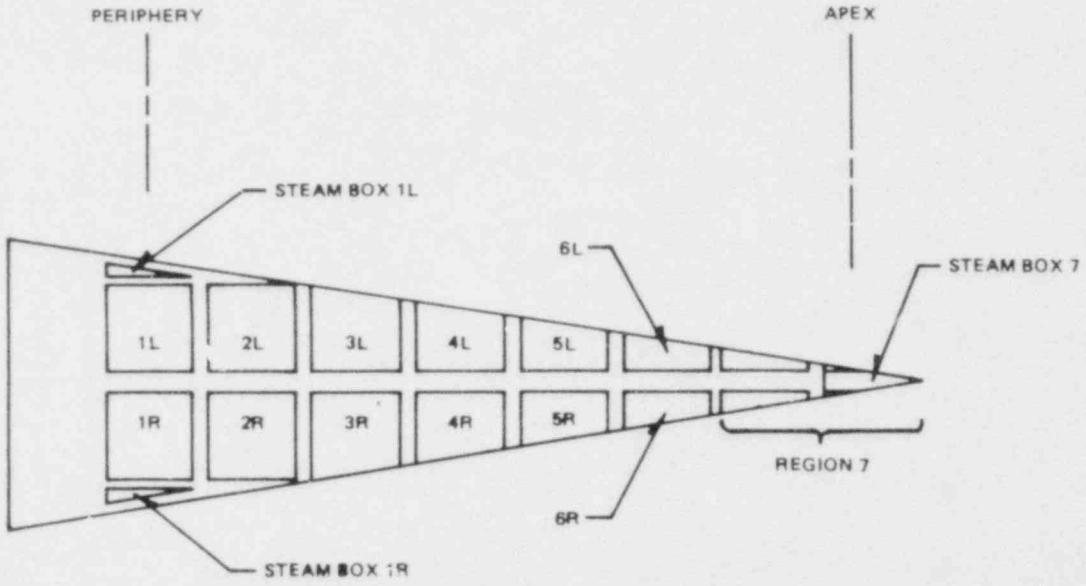

Figure B-10. Fuel Bundle Locations

B-5.4 SUBCOOLED CCFL BREAKDOWN RESULTS

B-5.4.1 Regular Core Spray with Low Peripheral Flux Profile

The regular core-spray (RCS) configuration simulates the BWR core-spray design and thus provides core-spray distribution capability representative of the BWR. This configuration provides tieback information to preliminary 16° upper-plenum experiments using an alternate core-spray configuration similar to the RCS configuration.

B-5.4.1.1 Lower Header. As seen in preliminary experiments with an alternate core-spray configuration (see Section B-7), radial mixing of the subcooled core-spray water increases with core-spray flow rate. The effect of this phenomenon is an increase in the spray-water/upper-plenum mixing efficiency such that a smaller proportion of subcooled core-spray water is available to preferentially cool the core periphery and promote subcooled breakdown in the low-power peripheral bundles. Consequently, higher core-spray flow rates require lower values of the condensing factor "C" (i.e., lower ratio of core-steam energy to spray-condensing energy). See nomenclature section. This trend is most pronounced at the CCFL breakdown limit (cross-hatched region of Figure B-11).

With the RCS configuration on the lower header, CCFL breakdown was achieved for test conditions without net upper-plenum subcooling at "C" values up to 1.41 and spray temperatures up to 130°F. Figure B-12 displays the overall results of the lower header RCS experiments in terms of spray temperature and breakdown time.

The effect of core-spray flow rate on CCFL breakdown time is readily apparent from Figure B-12. At low spray temperatures (approximately 100°F and less) breakdown time is roughly independent of spray flow rate (for the two flows tested). However, as the spray temperature is increased, breakdown is accomplished more quickly (for a given temperature) at the higher spray flow. This effect seems primarily due to the increase in spray-cooling capacity resulting from an increase in spray flow for given spray temperature and steam flow. Consequently, the increased available cooling more quickly cools the upper plenum mixture.

It is unclear which of the last two data points (125°F, 129°F) of the 100-gpm case represents the true trend of the data at temperatures above 120°F. The reason for the discontinuity in the data trend is not clear, but it indicates instability of the breakdown phenomena at temperatures close to the CCFL breakdown/no-breakdown limit.

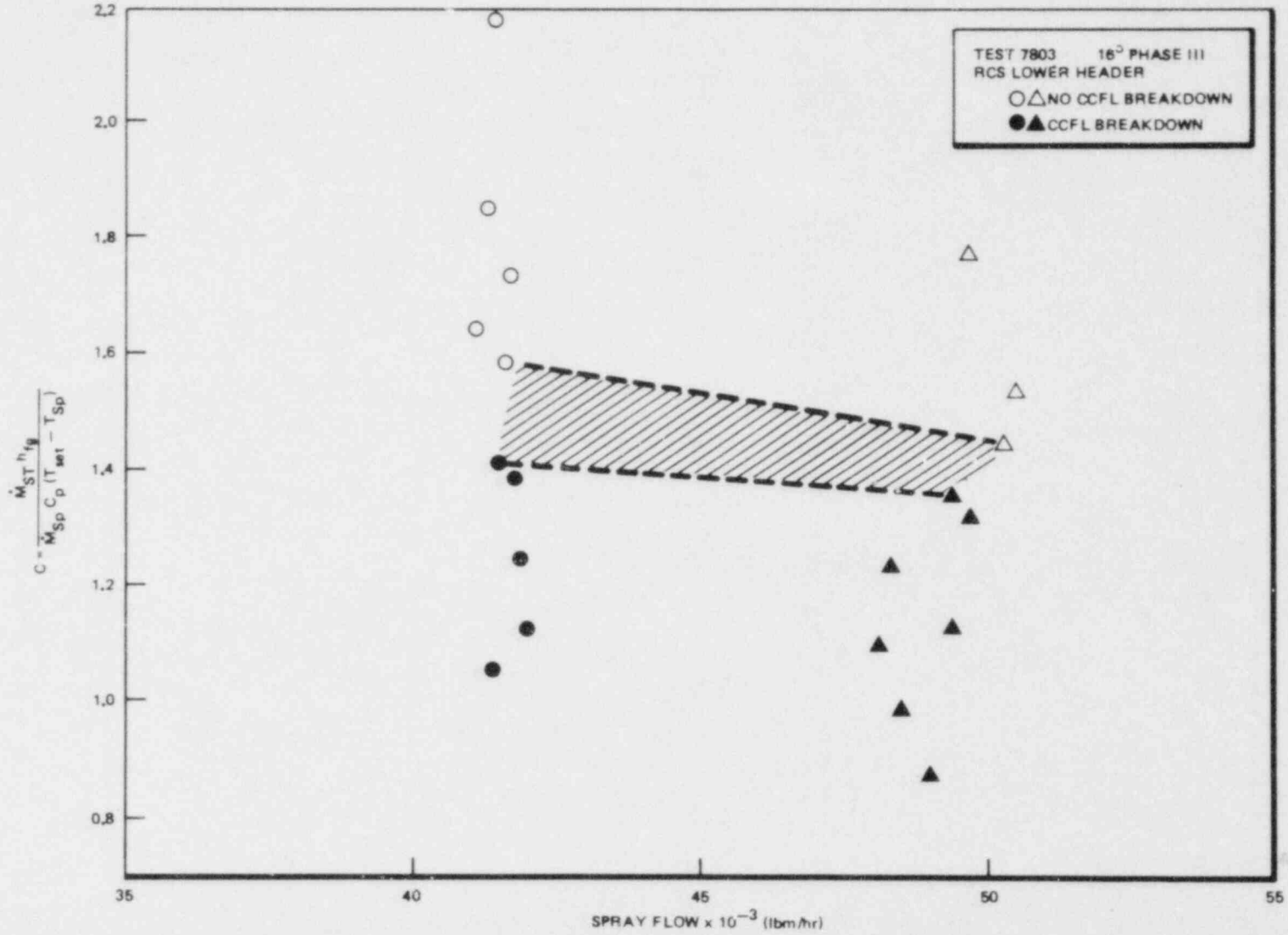

Figure B-11. Effect of Core-Spray Flow Rate on Breakdown "C" Value

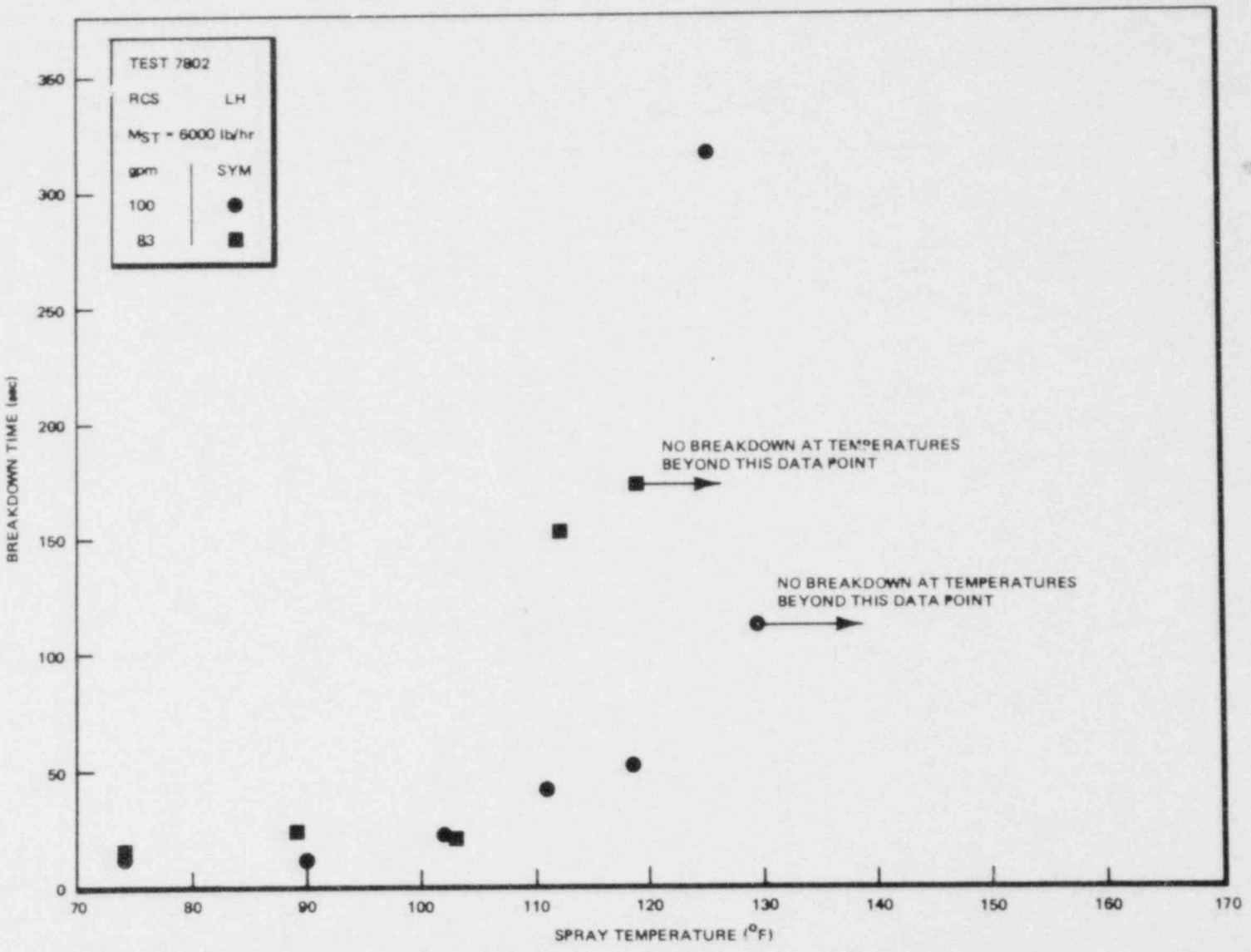

Figure B-12. Lower Header RCS Breakdown Time vs. Spray Temperature

The core-spray nozzles and associated nozzle flow rates of the RCS configuration induce CCFL breakdown by gross subcooling of the fluid above the low-power peripheral fuel bundles. Figure B-13 displays the approximate temperature zones in the upper plenum at the time that the first tieplate temperature becomes subcooled.*

Although subcooling was observed in much of the upper plenum, the major subcooling was observed close to the periphery. Both thermocouple measurements and visual observation of subcooled liquid water above the peripheral bundles confirmed major subcooling in the periphery.

As might be expected from the temperature zones of Figure B-13, CCFL breakdown was accomplished only in the peripheral bundles of the test apparatus for the vast majority of CCFL breakdown cases observed. Only in one case (maximum subcooling $C < 1.0$) did breakdown propagate radially inward beyond the peripheral bundles.

For cases in which the CCFL phenomenon was not broken down in a sustained manner, intermittent CCFL breakdown was often observed in one or both of the peripheral fuel bundles. Although the spray subcooling was then not adequate to continuously subcool the periphery, local peripheral cooling briefly subcooled one tieplate, broke down CCFL, and increased bundle drainage. Saturated water from the remainder of the upper plenum then replenished the subcooled pool and reestablished the CCFL phenomena. Although the overall drainage from the test section under these conditions was in excess of saturated CCFL downflow, the time-averaged drainage was not adequate to drain the upper plenum. Figure B-14 demonstrates the intermittent CCFL breakdown phenomena as indicated by subcooled tieplate temperature spikes.

B-5.4.1.2 Upper Header with Low-Peripheral Flux Profile. To gauge the effect of core-spray-header elevation on the CCFL breakdown phenomena, the RCS configuration was also tested on the upper core-spray header of the test apparatus. Although the phenomena observed were very similar to those seen when operating on the lower header, upper-header operation proved somewhat less effective at breaking down the CCFL phenomena. For both 100-gpm and 75-gpm core-spray flow rates, lower "C"

*The indicated temperature zones are intended as a visual aid. They were derived from visual test observations and test section thermocouple measurements. The actual boundaries of the zones are not well defined by the data and are subject to individual interpretation. Zero numerical values in Figure B-13 indicate no measurement at that elevation.

RCS-LOWER HEADER
TEST 7802
RUN NO. 21

VERTICAL TEMPERATURE ARRAY

LOC. (in.)	PERIPHERY	CENTR	APEX
62.3	0.	0.	212.2
56.3	0.	214.3	210.8
50.3	0.	156.5*	213.5
40.5	0.	212.3	214.5
36.3	0.	211.7	214.3
32.1	213.8	0.	0.
32.0	0.	210.0	214.3
29.6	213.8	0.	0.
27.8	0.	211.0	214.5
27.1	213.7	0.	0.
23.6	213.0	0.	0.
21.4	0.	211.7	215.2
20.1	213.0	0.	0.
16.0	203.0	0.	0.
15.0	0.	212.3	215.0
13.5	210.3	0.	0.
11.0	211.3	0.	0
10.8	0.	212.7	215.7
8.5	209.3	0.	0.
6.5	0.	212.0	215.6
6.0	210.0	0.	0.

NUMERICAL VALUE (°F)

*FAULTY THERMOCOUPLE

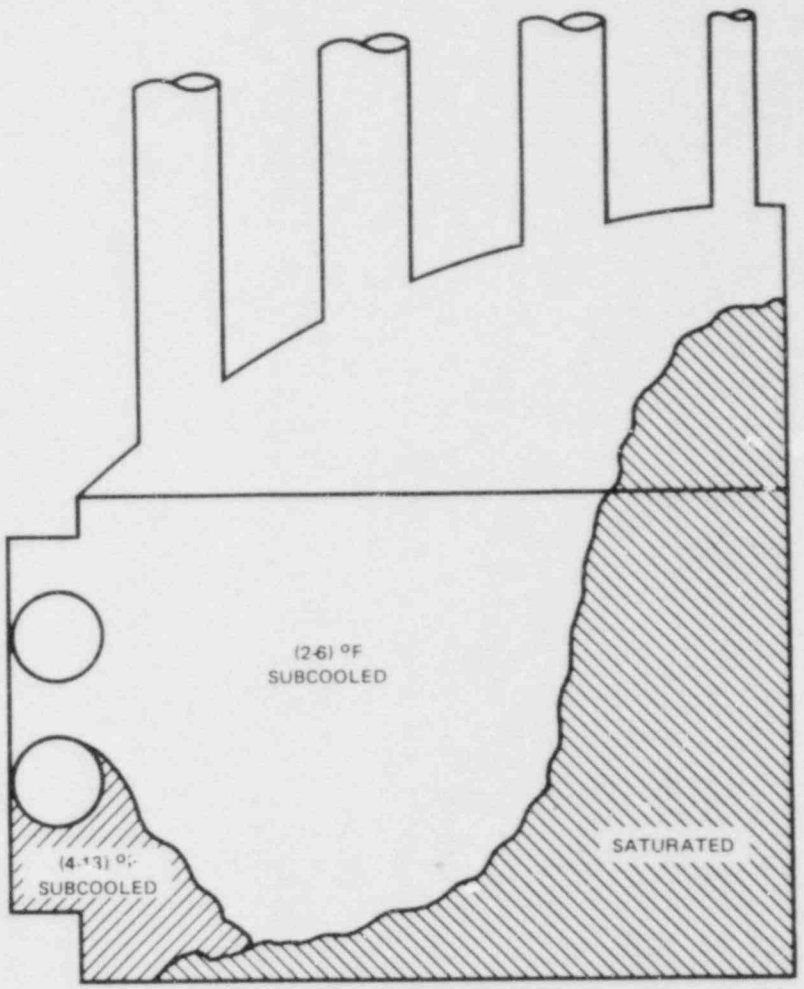

APPROXIMATE TEMPERATURE ZONES

Figure B-13. Upper-Plenum Temperature Distribution

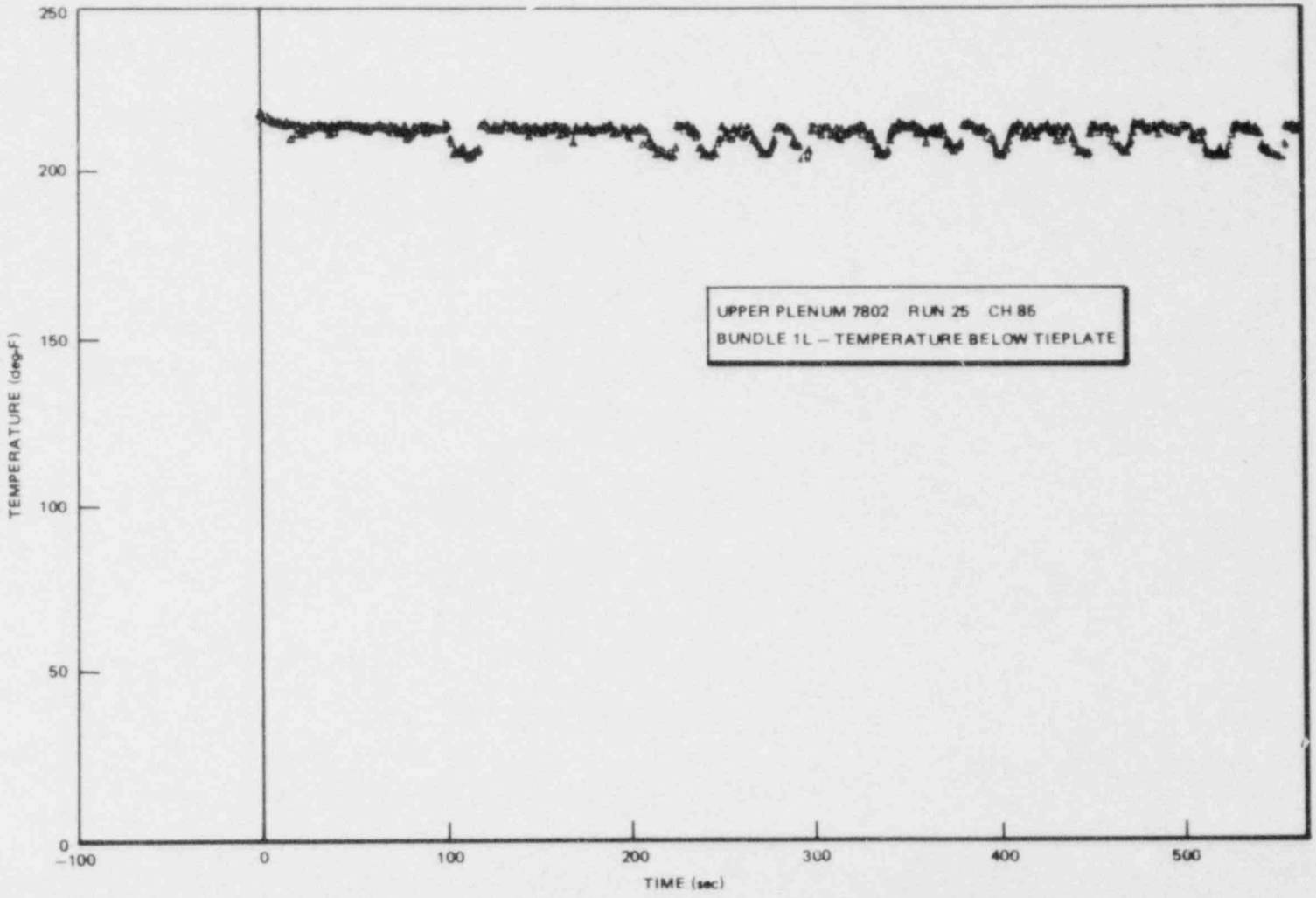

Figure B-14. Intermittent Tieplate Subcooling

values (i.e., more subcooling) were required for CCFL breakdown than were needed during lower header operation. CCFL breakdown could be accomplished from the upper header for "C" values up to 1.16 and spray temperatures up to 112°F.

The deterioration in breakdown effectiveness relative to lower header results seems largely due to the increased distance between the point of core-spray injection and the CCFL restriction (the fuel-bundle tieplate). The increased distance made the propagation of cold-spray water to the peripheral (and to a lesser extent the central) bundle tieplates more difficult. Consequently, less subcooling reached these regions than was achieved with lower header operation.

Figure B-15 displays the overall results of the CCFL breakdown experiments using the RCS configuration on the upper header. The trend of shorter breakdown time with increasing spray flow rate and decreasing temperature (i.e., lower "C" values) is again observed with this core-spray configuration. Again, for some conditions, intermittent CCFL breakdown did occur, although continuous breakdown capable of draining the upper plenum was not maintained. Figure B-16 displays intermittent CCFL breakdown as indicated by subcooled tieplate temperature excursions.

B-5.4.2 Core Radial Steam Profile

Additional tests were performed with a flatter radial distribution of bundle steam flux (refer to Section B-1). This change increased the steaming rate of the peripheral bundles by approximately 30 percent and the second row of bundles by approximately 10 percent. The steam flux split among the remaining bundles was little changed, although the magnitudes of the individual fluxes were reduced to compensate for the increased peripheral flow (i.e., total steam flow remained constant).

The effect of this change on the upper-plenum phenomena was significant. Figure B-17 demonstrates the reduction in breakdown effectiveness caused by the increased peripheral steam flux.

In lower header tests, the breakdown transition zone ("C" value range between successive breakdown and no-breakdown conditions) shifts from a mean value of approximately 1.4 to 1.0 when the steam profile is changed to increase the peripheral steam flux. The increased peripheral steam flow requires greater preferential cooling in the periphery to force breakdown of the CCFL phenomena.

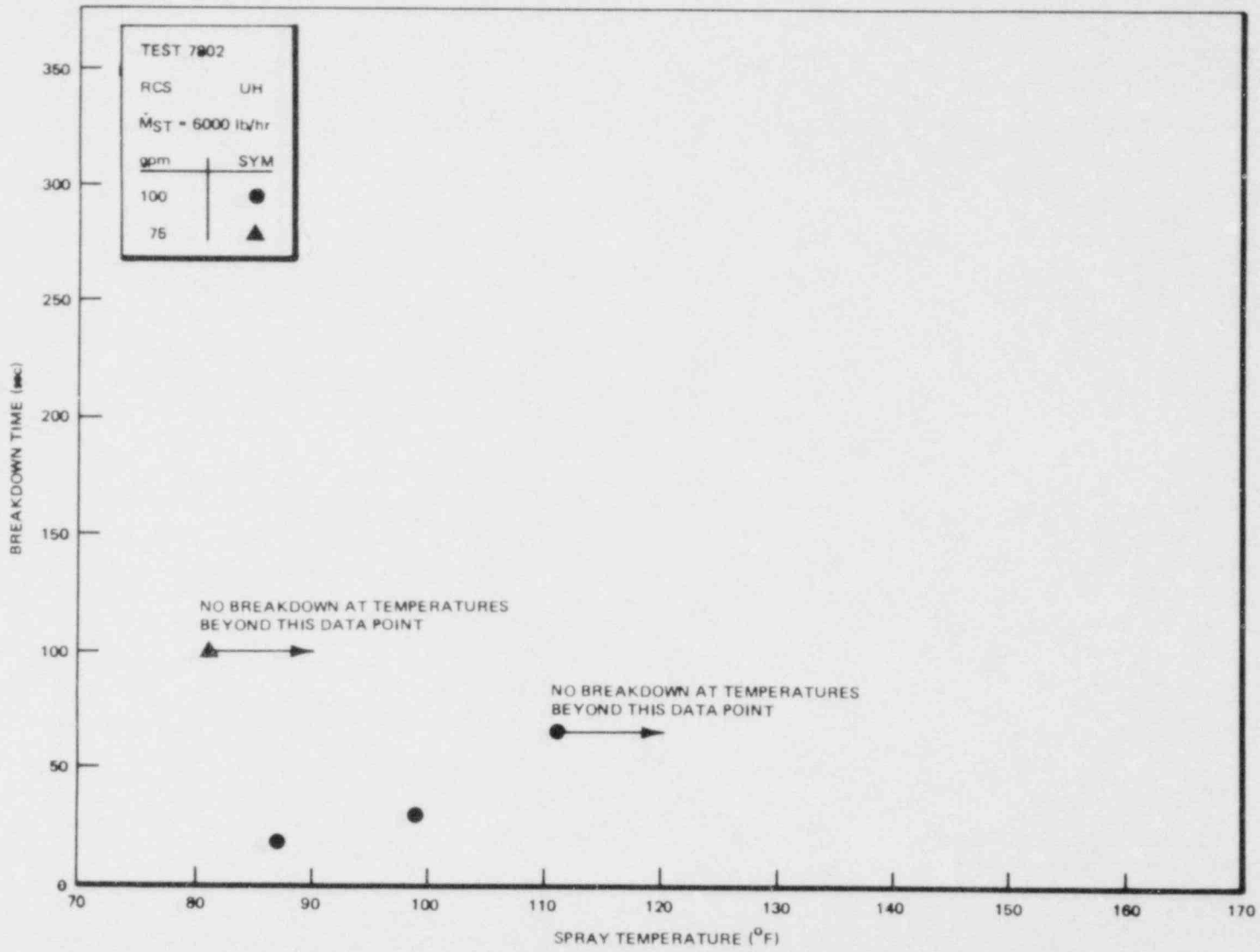

Figure B-15. Breakdown Time vs. Spray Temperature + RCS UH

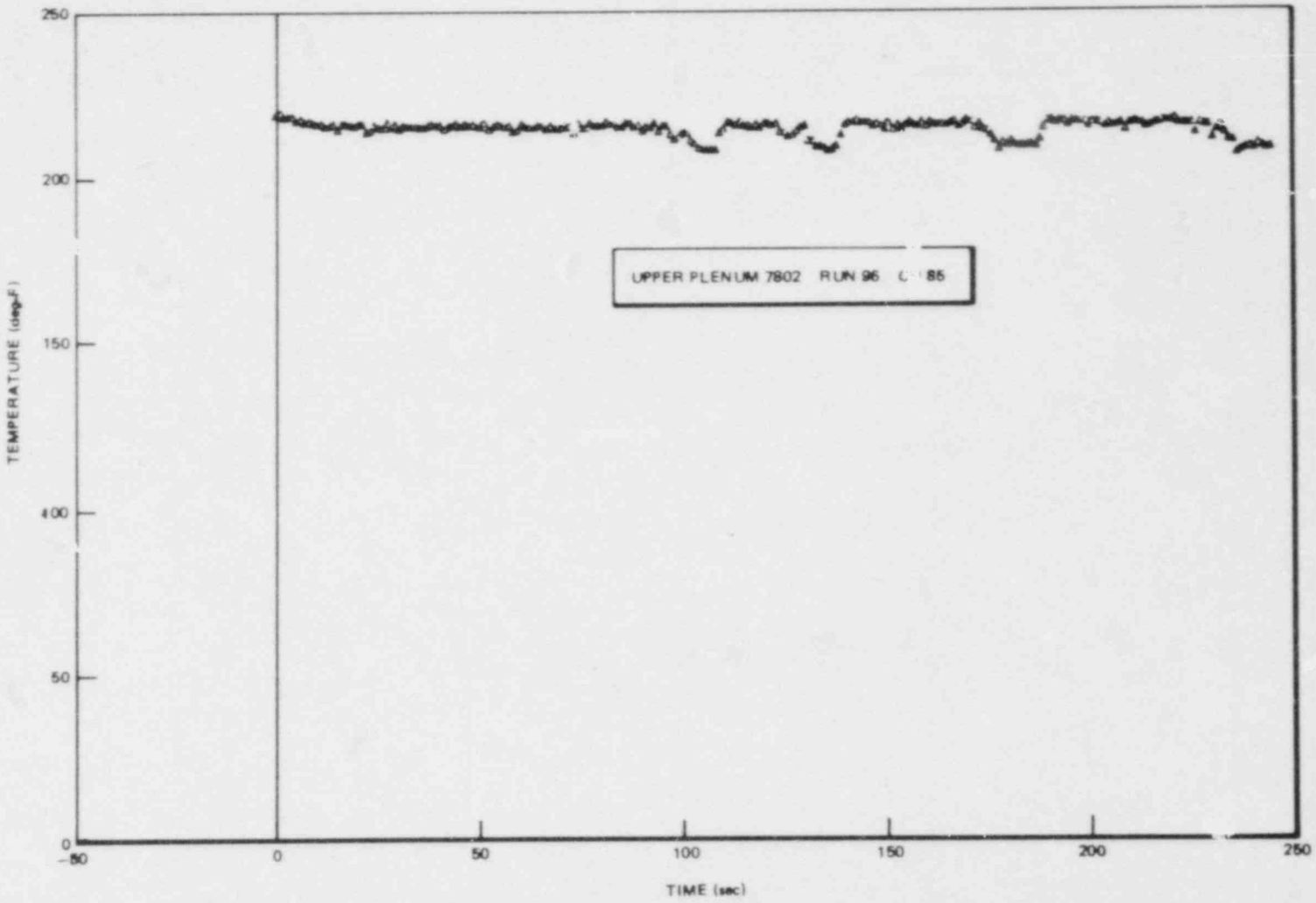

Figure B-16. Intermittent Tieplate Subcooling - RCS UH

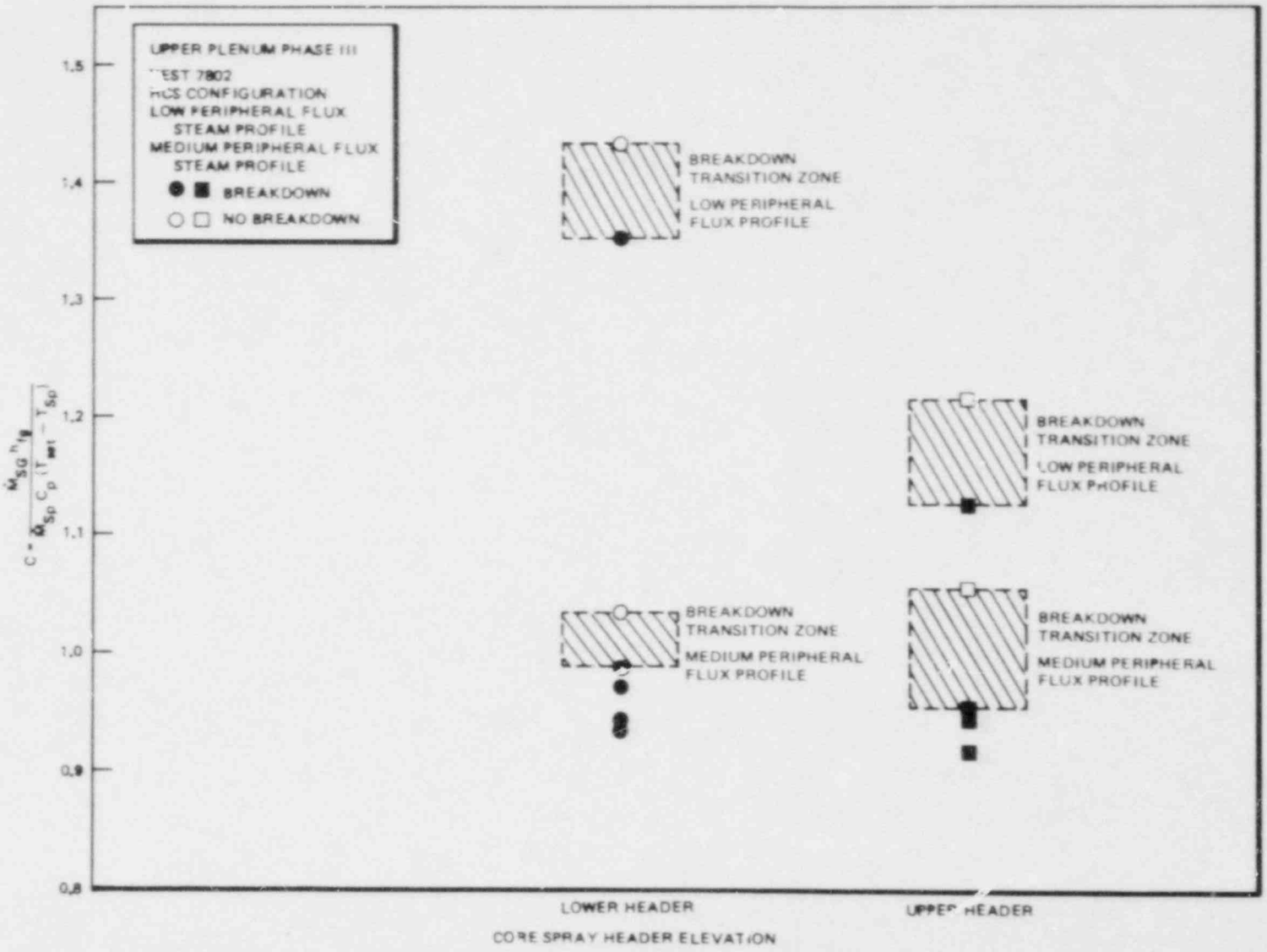

Figure B-17. Shift of Breakdown Transition Zone Caused by Radial Steam Profile

Consequently, greater overall subcooling (lower "C" values) is required to achieve breakdown. A similar trend is noticed in upper header tests in which the mean value of the breakdown transition zone shifts from approximately 1.17 to 1.0 when the peripheral steam flux is increased. As with the lower header tests, the mean "C" value of 1.0 indicates that CCFL breakdown will occur when the spray subcooling is adequate to subcool the upper plenum on a single-node energy balance basis.

Altering the steam profile to increase peripheral steam flow increases the magnitude and range of upper-plenum subcooling. Figure B-18a displays the approximate temperature zones existing in the upper plenum just as the first tieplate was subcooled. Relative to tests with less peripheral steam flux, the magnitude of subcooling in the two subcooled zones is increased while the range of the saturated zone is decreased. Figure B-18b displays the approximate upper-plenum temperature zones, at the time of first tieplate subcooling, for a low-peripheral flux case at comparable conditions. Comparison of Figures B-18a and B-18b reveals the increased upper-plenum subcooling required for breakdown with the medium peripheral flux steam profile.

Two items appear to contribute to the increase in upper-plenum subcooling. First, the increase in peripheral steam flow makes CCFL breakdown in the peripheral bundles more difficult by requiring greater peripheral subcooling. This increase in required subcooling results in longer breakdown times for a given spray temperature. Because peripheral breakdown takes longer to occur, more cold-spray water is free to accumulate in the periphery and migrate to other upper-plenum regions instead of draining through broken-down peripheral bundles. Consequently, the increased difficulty in achieving breakdown in the peripheral bundles allowed more subcooled spray to enter and remain in the upper plenum. Second, the cooler spray temperatures required for breakdown (compared to the low peripheral flux cases) increased the subcooled input to the upper plenum.

Visual observation of the upper-plenum mixture confirmed the increased upper-plenum subcooling. During tests of the RCS configuration with the low peripheral flux profile, a region of solid liquid water (subcooled region) was observed above the peripheral fuel bundles (Window 4 of Figure B-19) while the remainder of the upper plenum remained largely voided. However, when the radial steam profile was changed to increase the peripheral flux, Windows 1, 2, and 4 revealed low-void regions (indicating subcooled temperatures). Window 3 and a portion of Window 4 remained largely voided, suggesting a condensation zone separating the saturated mixture from the subcooled liquid above.

RCS-UPPER HEADER
MEDIUM PERIPHERAL FLUX PROFILE
TEST 7802
RUN NO. 134

VERTICAL TEMPERATURE ARRAY

LOC. (in.)	PERIPHERY	CENTR	APEX
62.3	0.	0.	209.0
56.3	0.	211.2	210.3
50.3	0.	125.4*	211.7
40.5	0.	207.7	211.7
36.3	0.	207.5	211.8
32.1	209.5	0.	0.
32.0	0.	208.3	212.3
29.6	209.0	0.	0.
27.8	0.	207.0	212.5
27.1	209.5	0.	0.
23.6	205.2	0.	0.
21.4	0.	206.8	212.8
20.1	199.8	0.	0.
16.0	202.5	0.	0.
15.0	0.	205.2	214.5
13.5	200.8	0.	0.
11.0	199.8	0.	0.
10.8	0.	209.5	215.5
8.5	201.8	0.	0.
6.5	0.	209.7	215.3
6.0	202.2	0.	0.

NUMERICAL VALUE (°F)

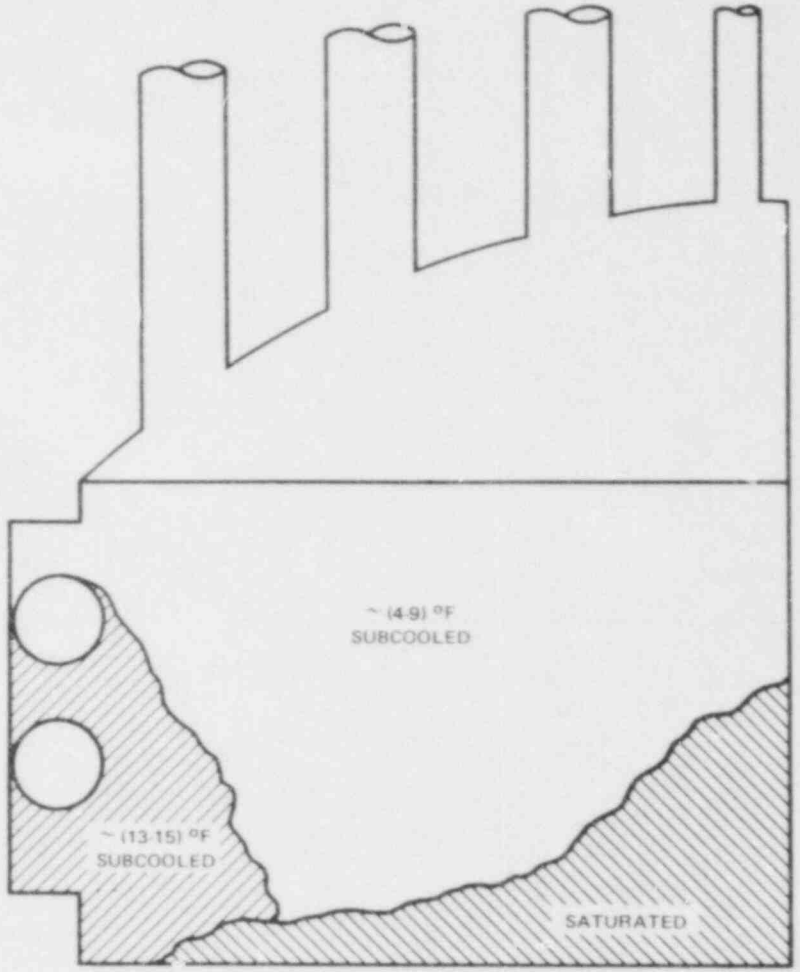

APPROXIMATE TEMPERATURE ZONES

*FAULTY THERMOCOUPLE

Figure B-18a. Upper-Plenum Temperature Distribution - RCS UH, Medium Peripheral Flux Profile

RCS-UPPER HEADER
LOW PERIPHERAL FLUX PROFILE
TEST 7802
RUN NO. 95

VERTICAL TEMPERATURE ARRAY

LOC. (in.)	PERIPHERY	CENTR	APEX
62.3	0.	0.	212.7
56.3	0.	213.5	214.2
50.3	0.	195.5	214.2
40.5	0.	212.7	214.5
36.3	0.	212.0	214.5
32.1	214.2	0.	0.
32.0	0.	209.7	214.3
29.6	214.5	0.	0.
27.8	0.	210.5	214.7
27.1	214.0	0.	0.
23.8	209.0	0.	0.
21.4	0.	210.5	215.2
20.1	199.2	0.	0.
16.0	204.8	0.	0.
15.0	0.	211.8	215.2
13.5	206.8	0.	0.
11.0	206.5	0.	0
10.8	0.	213.8	215.5
8.5	206.0	0.	0.
6.5	0.	213.5	215.5
6.0	208.7	0.	0.

NUMERICAL VALUE (°F)

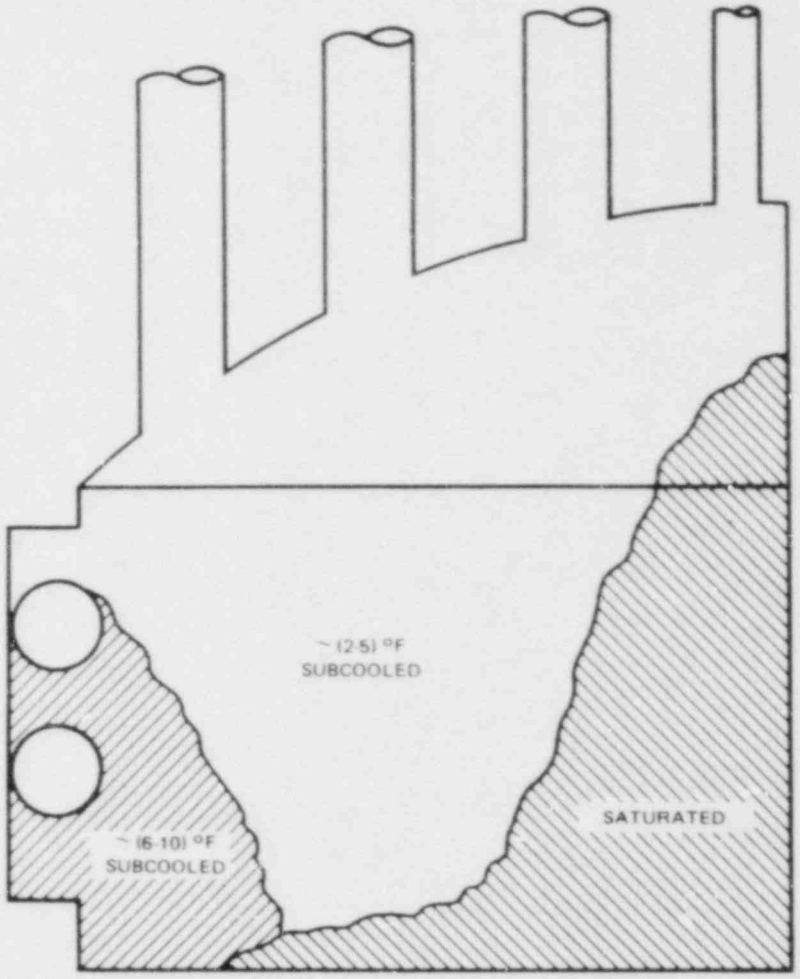

APPROXIMATE TEMPERATURE ZONES

Figure B-18b. Upper-Plenum Temperature Distribution - RCS UH, Lower Peripheral Flux Profile

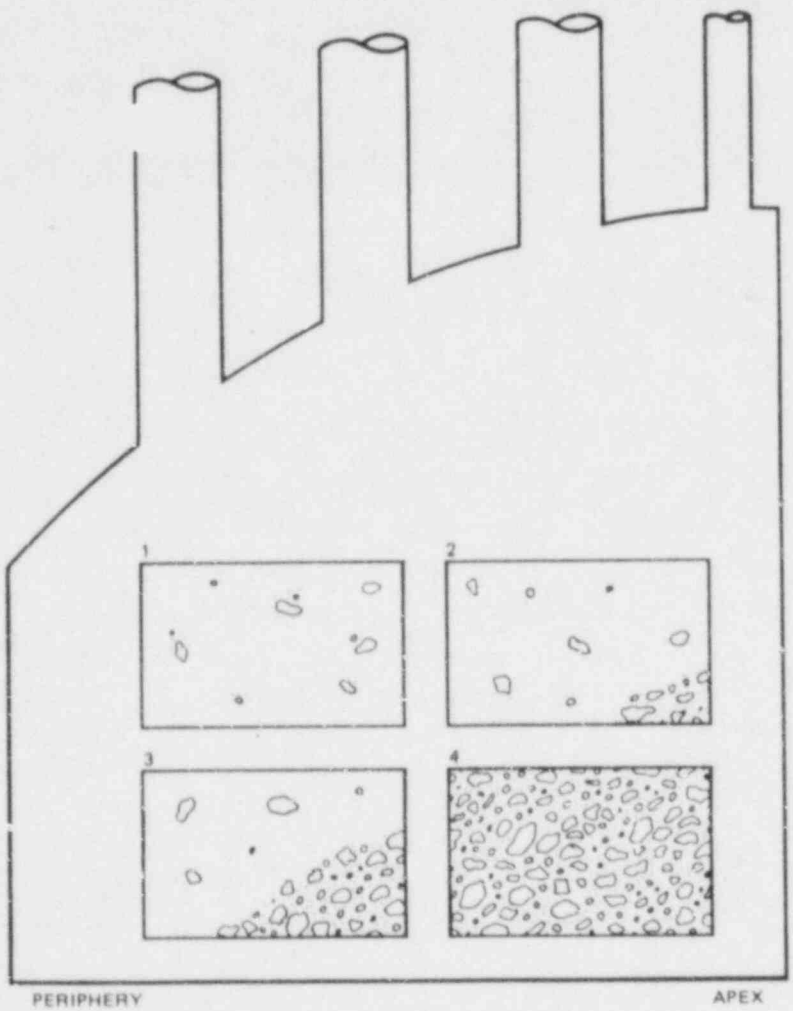

Figure B-19. Visually Observed Subcooled Regions

As a consequence of the increased upper-plenum subcooling, a greater differential fluid head was established across the upper plenum than observed in cases with lower peripheral steam flow. Figure B-20 displays the differential pressure (in-H_2O) across the upper plenum as a function of time, where time zero was the time at which cold-spray injection began. CCFL breakdown was not achieved in the test displayed in Figure B-20; therefore, the upper-plenum differential never decreased. As time increased, the differential pressure increased to a mean value of approximately 40 inches of water, which was maintained throughout the remainder of the experiment. In a corresponding no-breakdown case with the low peripheral flux steam profile, the mean upper-plenum differential pressure increased only slightly to a value of approximately 25 inches of water.

As observed in RCS tests with the low peripheral flux steam profile, intermittent CCFL breakdown could occur in one or both of the peripheral bundles without draining the upper plenum. In those cases, although the available subcooling was not adequate to sustain subcooled breakdown, local accumulation of subcooled water in the periphery would periodically reach a level adequate to achieve intervals of subcooled breakdown.

Figures B-21 and B-22 display the overall results of lower and upper header operation of the RCS configuration.

B-6. CONCLUSIONS

Test results have shown that mixed-net upper-plenum subcooling is a bounding condition for upper tieplate CCFL breakdown in a typical BWR upper plenum. In general, breakdown of the CCFL phenomena could be achieved without net upper-plenum subcooling through favorable enthalpy distributions induced by the three-dimensional characteristics of the upper plenum. Both the ECC injection location (above the core periphery) and the radial core steam profile (lower steaming rates in the peripheral fuel channels) contributed to preferential subcooling above the core periphery and local peripheral CCFL breakdown.

On a more fundamental basis, the upper-plenum mixing/CCFL breakdown phenomena were found to be influenced by variation in the following parameters:

a. core radial steam profile,

b. core spray flow rate,

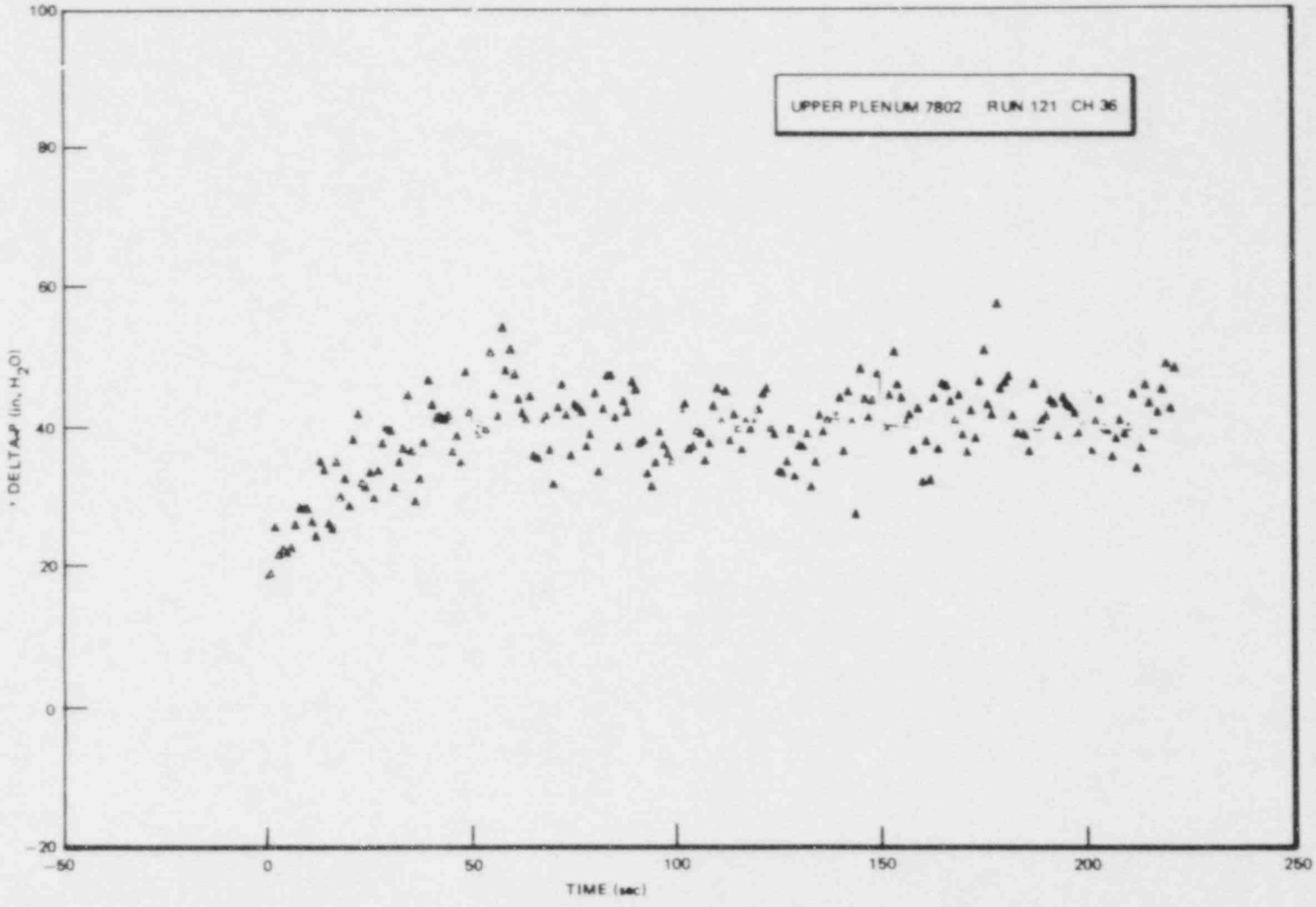

Figure B-20. Upper Plenum Differential Fluid Head

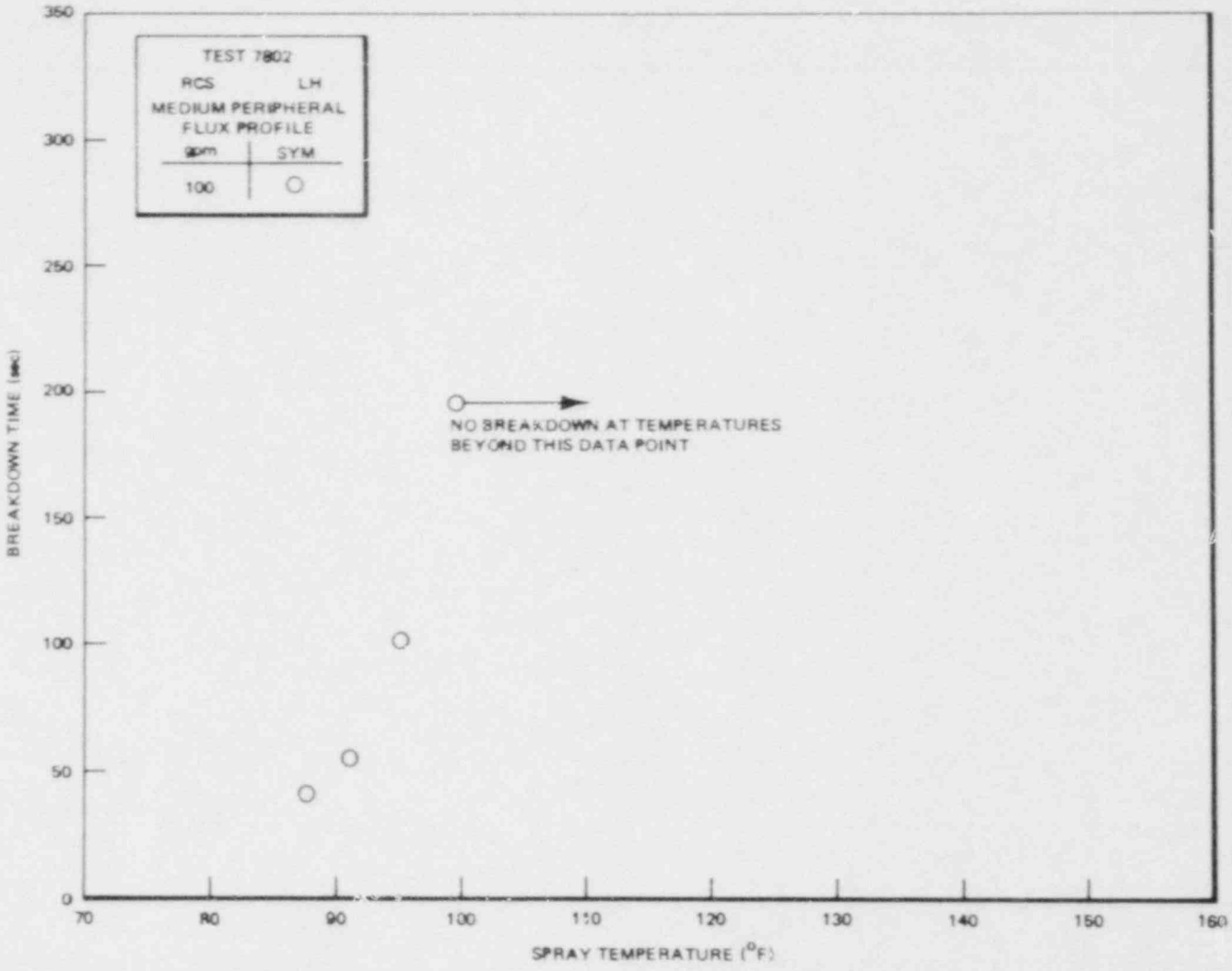

Figure B-21. Breakdown Time vs. Spray Temperature - RCS LH

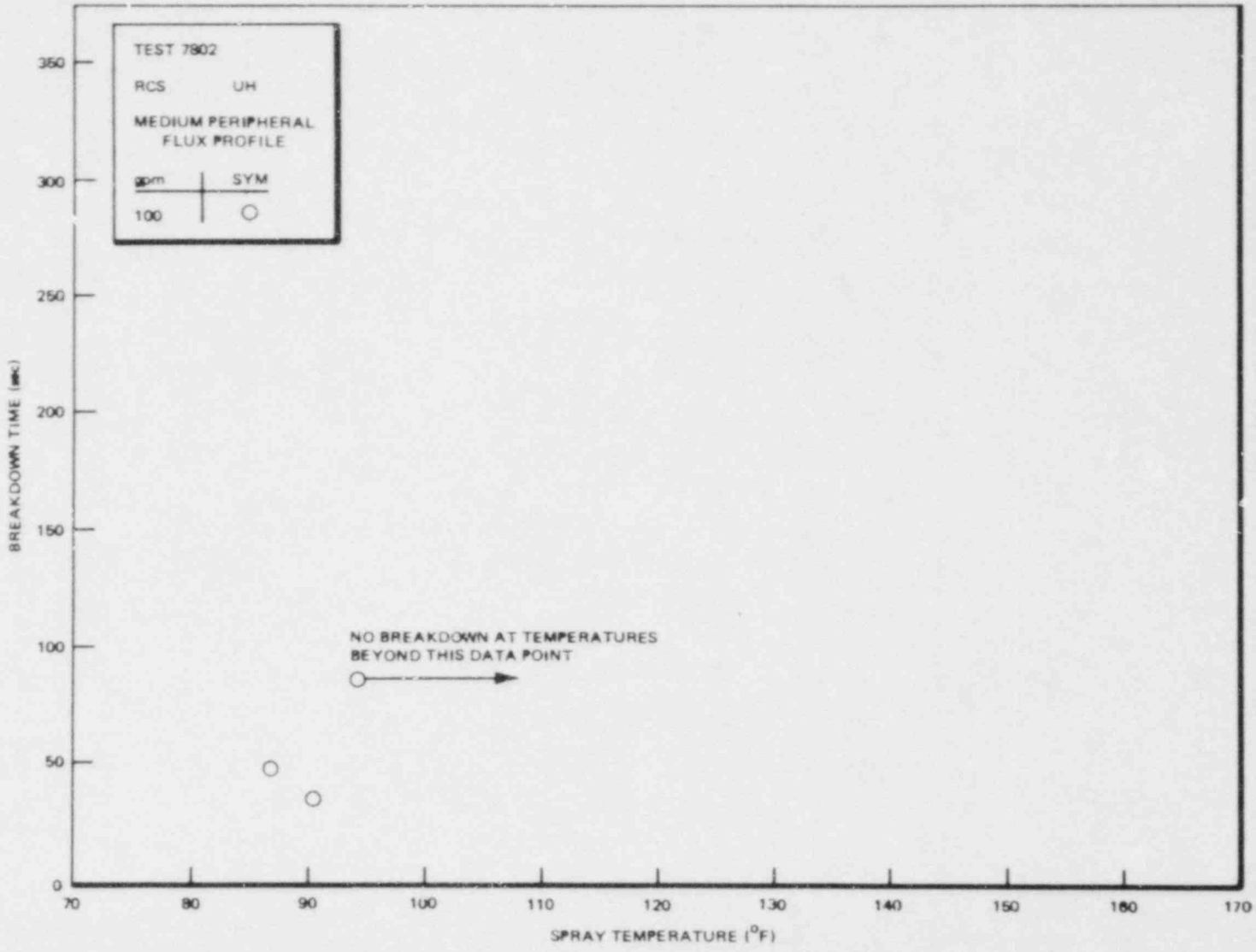

Figure B-22. Breakdown Time vs. Spray Temperature - RCS UH

c. core spray header elevation, and

d. initial upper-plenum two-phase volume (as observed in preliminary sector tests - see Section B-7).

B-7. PRELIMINARY SECTOR TESTS

Upper-plenum mixing tests were conducted with a preliminary configuration of the 16° test facility to obtain initial mixing information. Consistent with the exploratory nature of the tests, the BWR simulation characteristics of the test section were less precise than required in the final facility configuration. Figure B-23 depicts the major differences between the preliminary facility configuration and the final test configuration, specifically:

a. simulation of upper-plenum dome shape and multiple standpipe flow paths in the final configuration (the preliminary configuration utilized a flat dome and one standpipe);

b. accurate simulation of the upper-plenum shroud shape adjacent to the core-spray spargers in the final configuration (see Figure B-23); and

c. simulation of the top of the core with prototypical tieplates and foreshortened fuel bundles in the final configuration (the preliminary configuration used an orifice simulation of the upper tieplates).

The core-spray configuration utilized in the preliminary mixing tests differed from the regular core-spray configuration used in the final tests in the nozzle types and nozzle aimings (see Table B-3). The peripheral nozzle types used in the preliminary test (Spraco 3101) provided somewhat more dispersed spray patterns than the open pipe elbows used in the regular core-spray configuration.

A core-radial steam profile similar to medium peripheral flux profile was used in the preliminary tests.

The preliminary mixing tests addressed the effects of: (a) the initial two-phase mass in the test section, and (b) the core-spray flow rate on the mixing phenomena.

The two major conclusions reached in the preliminary mixing tests were that: (a) the initial volume of saturated two-phase mixture in the upper plenum affected the ease at which CCFL breakdown could be achieved (i.e., as the initial saturated volume was increased, greater spray subcooling was required to break

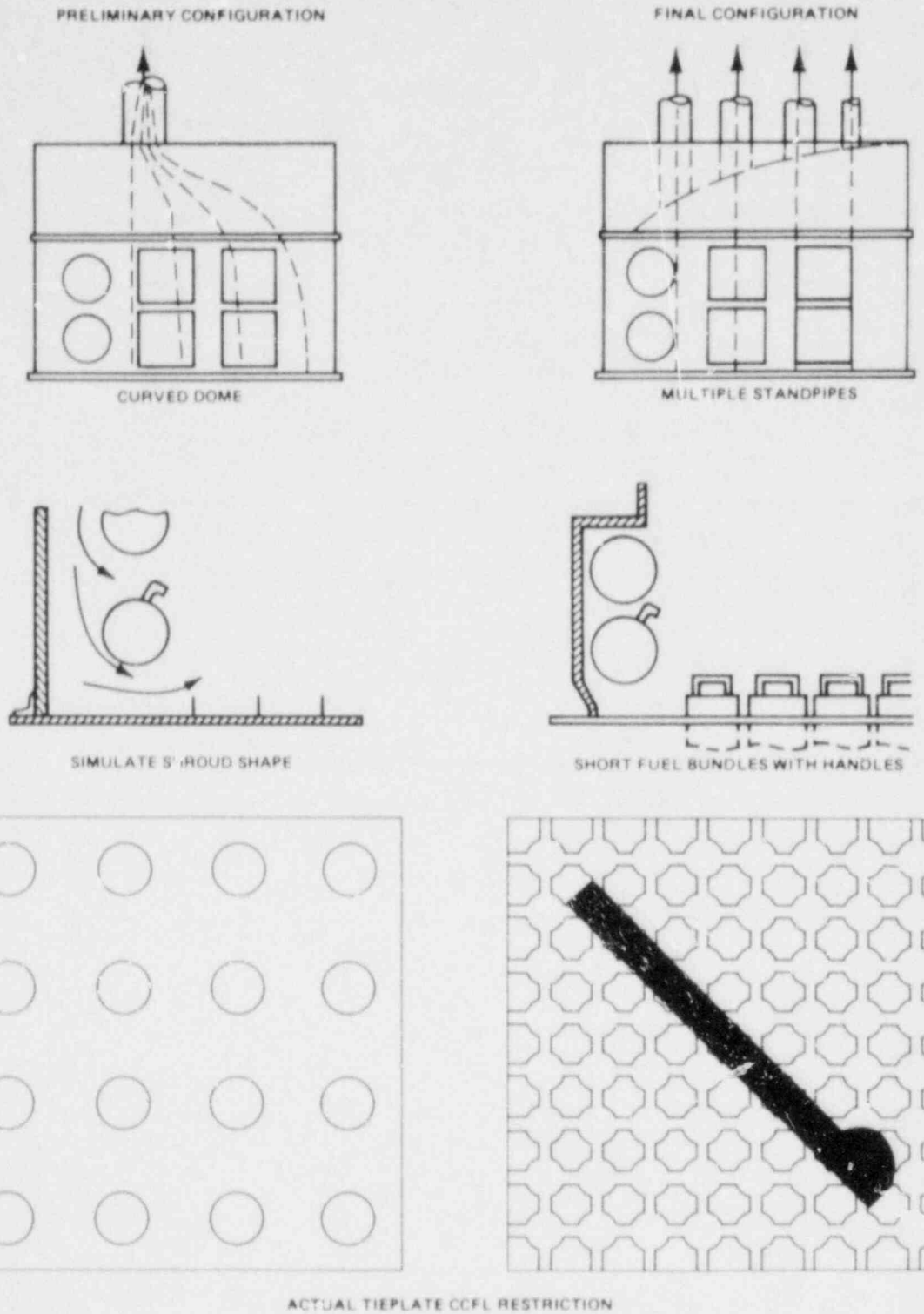

Figure B-23. Preliminary and Final Facility Configurations

Table B-3

CORE SPRAY DATA (PRELIMINARY CONFIGURATION)

Core Spray Configuration	Location 1	Location 2	Location 3
RCS LH	Spraco 3101/-47°	3/4 in. O.E./-14°	Spraco 3101/-47°

Estimated Flow Splits
(100 gpm total spray flow)

Core Spray Configuration	Location 1 (gpm)	Location 2 (gpm)	Location 3 (gpm)
RCS LH	30	40	30

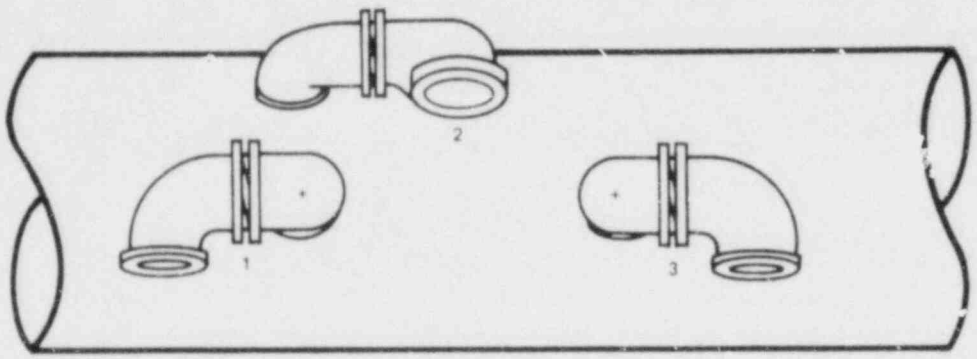

down CCFL), and (b) the core-spray system flow rate affected the steam-water mixing efficiency in the upper plenum (i.e., higher spray flow rates increased the steam-water mixing efficiency).

Figure B-24 displays these trends in terms of the condensing factor "C' and the initial two-phase mixture level in the upper plenum for spray flow rates of 83, 90, and 100 gpm. Solid symbols represent cases in which CCFL breakdown was achieved, while open symbols represent cases in which CCFL breakdown was not achieved.

As can be seen from the figure, for a given spray flow rate greater subcooling is required to induce CCFL breakdown as the initial mixture level is increased. For a given initial two-phase level, a greater fraction of spray subcooling is required for CCFL breakdown as the spray flow rate is increased.

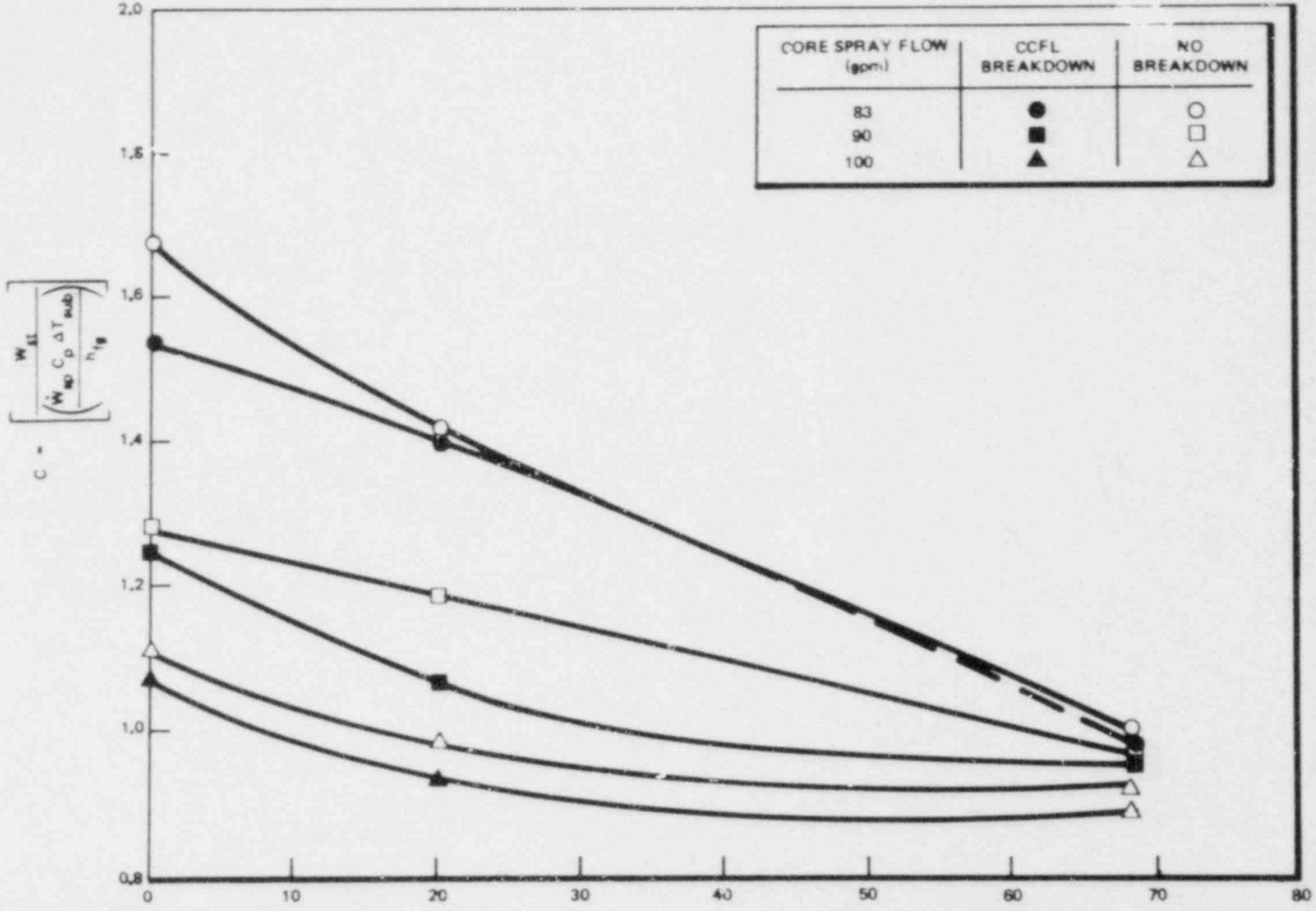

Figure B-24. Initial 2ϕ Level (in.)

The effect of the core spray configuration on the mixing phenomena (although not specifically addressed in the preliminary tests) can be inferred by comparison to results of the final test series using the medium peripheral flux core steam profile. Such a comparison shows no significant change in the mixing phenomena or CCFL breakdown performance because of minor variations in the core spray and plenum configurations utilized in the preliminary tests. Consequently, it can be concluded that minor changes to the core-spray configuration will not significantly affect the upper plenum mixing phenomena.

B-8. NOMENCLATURE

B-8.1. CONDENSING FACTOR "C"

$$\text{Condensing Factor} = \frac{\dot{M}_{steam}\, h_{fg}}{\dot{M}_{spray}\, C_p\, \Delta T_{sub}}$$

where

$$\Delta T_{sub} = T_{sat.} - T_{spray}$$

and

Terms defined as follows:

$\dot{M}_{steam}$ = Average mass flow rate of steam into the test section

h_{fg} = Latent heat of vaporization at test conditions

$\dot{M}_{spray}$ = Average mass flow rate of spray water into the test section

C_p = Specific heat of water in consistent units

T_{sat} = Saturation temperature of water at test conditions

T_{spray} = Average temperature of the spray water

B-8.2 BREAKDOWN TIME

The time in seconds at which both peripheral bundles become and remain subcooled relative to the time that the spray water temperature at the test-section inlet begins to decrease from saturated to subcooled conditions.

B-8.3 BREAKDOWN

Visually observed (and confirmed by test data) drainage of the test apparatus by subcooled core-spray injection.

B-9. INDIVIDUAL BUNDLE CCFL DATA

Table B-4

UPPER TIEPLATE FLOW AREAS

Bundle Location	Flow Area [Ft^2]
1 L, 1 R	0.07999
1 L (SB), 1 R (SB)	0.00262
2 L, 2 R	0.07999
3 L, 3 R	0.06747
4 L, 4 R	0.05404
5 L, 5 R	0.03906
6 L, 6 R	0.02756
7	0.01386
7 (SB)	0.0041

Table B-5

SATURATED CCFL DATA
[Steam Flow/Liquid Flow] (lbm/hr.)

Bundle Location	Total Core Steam Flow (lbm/hr.)				
	4000	4500	5000	5500	6000
1R	239.5/14339	269.5/10517	299.4/9571	329.4/8320	359.3/6973
1L	239.5/14554	269.5/12299	299.4/9082	329.4/8427	359.3/6766
1R(SB)*	7.9/454.1	8.9/333.1	9.8/303.1	10.8/263.5	11.8/220.9
1L(SB)*	7.9/461.0	8.9/389.6	9.8/287.7	10.8/266.9	11.8/214.3
2R	390.1/5053	438.9/3598	487.7/3756	536.5/3229	585.2/2732
2L	390.1/6915	438.3/4072	487.7/2281	536.5/1592	585.2/938
3R	426.2/1703	479.5/1125	532.8/555	586.1/297	639.3/165
3L	426.2/1664	479.5/1387	532.8/756	586.1/353	639.3/164
4R	354.9/1107	399.3/997	443.7/530	488.1/228	532.4/41
4L	354.9/1686	399.3/1520	443.7/1104	488.1/544	532.4/84
5R	277.7/604	312.4/416	347.1/217	381.8/37	416.5/39
5L	277.7/531	312.4/312	347.1/673	381.8/467	416.5/51
6R	191.1/379	214.9/316	238.8/227	262.7/134	286.6/83
6L	191.1/366	214.9/246	238.8/680	262.7/67	286.6/35
7	98.2/161.2	110.5/0	122.8/21.1	135.1/54.6	147.3/137.4
7(SB)*	29.1/21.8	32.7/0	36.3/2.9	39.9/7.4	43.6/18.6

*"Steam Box" representation of partial bundle.

B-10. AVERAGED TEST CONDITIONS

The parameters tabulated on the following pages are values averaged over the time intervals between first indication of spray temperature decrease at the test-section inlet and the end of the test run. Two time intervals are listed for the breakdown time; both are relative to the time at which the spray temperature at the test-section inlet begins to decrease. The first interval corresponds to increased peripheral drainage as indicated by the Weir tube flow-measuring elements and covers the range of time in which drainage increase is first observed in one bundle to the time at which both peripheral bundles register continuous increased flow. The second interval covers the time range in which the first tieplate subcooling is observed to the time at which both peripheral bundles become and remain subcooled, as indicated by thermocouples below the tieplates.

Table B-6

AVERAGED CONDITIONS 0.55 STEAM PROFILE

Subcooled CCFL: RCS LH

$\dot{M}_{spray}$ (lbs/hr)	$\dot{M}_{drain}$ (lbs/hr)	$\dot{M}_{steam}$ (lbs/hr)	T_{spray} (°F)	Lowest Peripheral Temperature (°F)	"C" Value	U.P. Level Increase ?	Breakdown (Visual Confirmation)	Breakdown Time (Drainage Increase/ Tieplate Subcooled) (sec)	Comments
41421	35728	6073	79.1	195, 200	1.0459	No	Yes	16-20/11-13	
48955	43006	5947	78.9	155, 208	0.8676	No	Yes	17-21/11-12	
42005	37631	5892	93.3	186, 193	1.1208	No	Yes	19-27/18-23	
-	-	-	-	-	-	-	-	-	Test Aborted
41942	37941	5930	103.7	186, 196	1.23?	No	Yes	16-20/11-20	
48079	37812	5936	104.7	190, 198	1.085	No	Yes	22-25/20-21	
-	-	-	-	-	-	-	-	-	Test Aborted
49355	36714	5944	111.8	195, 198	1.119	No	Yes	22-52/25-40	
41455	32356	5805	120.1	195, 202	1.411	No	Yes	24-164/30-172	
48278	37905	5835	121.0	195, 200	1.229	No	Yes	24-3?/24-51	
41102	38198	5891	131.3	207	1.635	No	No	24-3/120-5	
49433	39734	5917	130.4	196, 204	1.351	No	Yes	22-58/29-112	
41587	36212	6091	126.6	206	1.5795	No	No	24-?/51-?	
49749	32766	6086	125.7	195, 200	1.3111	No	Yes	19-42/19-318	
41678	35963	6057	135.7	206	1.7298	No	No	20-?/123-?	
50309	40028	6027	136.0	205[2]	1.4372	No	No	17-?/38-?	
41282	35472	5989	140.3	208[1]	1.8547	No	No	?/141-?	
50471	38051	6013	140.5	206, 207	1.5272	Yes	No	24-?/32-?	
48499	39592	6034	91.2	184, 199	0.9772	No	Yes	14-17/8-11	
41832	37617	6002	114.1	182, 200	1.381	No	Yes	19-126/25-153	
41352	34721	6002	152.0	215[1]	2.1778	Yes	No	?/?	
49735	39765	5982	150.4	206[1]	1.7699	Yes	No	?/?	

Table B-7

AVERAGED CONDITIONS 0.55 STEAM PROFILE

Subcooled CCFL: RCS UH

$\dot{M}_{spray}$ (lbs/hr)	$\dot{M}_{drain}$ (lbs/hr)	$\dot{M}_{steam}$ (lbs/hr)	T_{spray} (°F)	Lowest Peripheral Temperature (°F)	"C" Value	U.P. Level Increase ?	Breakdown (Visual) Confirmation	Breakdown Time (Drainage Increase/ Tieplate Subcooled) (sec)
Spray Distribution - - - - - - - - - - - - - - -				N/A		N/A	N/A	N/A
37439	34003	5948	88.9	204, 214	1.2215	Constant	?	25-?/39-?
49909	37344	5949	89.7	172, 179	0.9250	No	Yes	16-22/13-18
37273	34599	5953	100.7	206, 215	1.3508	Yes	No	25-?/103?
50053	38292	5975	101.2	190, 191	1.021	No	Yes	19-22/15-29
37406	34700	5992	111.9	212, 214	1.5042	Yes	No	26-?/?
50251	38354	5979	111.7	192, 192	1.122	No	Yes	22-30/22-66
37406	33509	5997	120.4	214, 215	1.6382	Yes	No	?/?
49641	38940	5951	119.3	205, 208	1.2127	Yes	No	?/?
38040	37600	5935	84.0	190, 179	1.161	Yes	Yes	18/72-100
Spray Distribution - - - - - - - - - - - - - - -				N/A		N/A	N/A	N/A
37713	32550	5956	131.4	215, 217	1.8030	Yes	No	?/?
50402	37071	5964	130.8	207, 210	1.3441	Yes	No	130-210/?
37375	31111	5966	140.9	216, 216	2.0525	Yes	No	?/?
50014	37056	6024	140.7	208, 214	1.5412	Yes	No	?/?
-	-	-	-	186, 187	-	No	Yes	66-?/57-67
36558	38999	4999	110.9	182, 179	1.3005	No	Yes	22-84/72-82
37039	38382	5015	121.5	191, 193	1.4260	No	Yes	24-?/184-225
49257	41359	4949	130.9	196, 198	1.1760	No	Yes	17-25/14-54
49785	40933	4996	139.8	207, 214	1.2978	Constant	?	17-?/27-?
37064	28737	5991	148.7	215, 216	2.3361	Yes	No	?/?
49431	37101	5961	148.3	811, 215	1.7282	Yes	No	?/?

Table B-8

AVERAGED CONDITIONS 0.67 STEAM PROFILE

Subcooled CCFL: RCS LH

$\dot{M}_{spray}$ (lbs/hr)	$\dot{M}_{drain}$ (lbs/hr)	$\dot{M}_{steam}$ (lbs/hr)	T_{spray} (°F)	Lowest Peripheral Temperature (°F)	"C" Value	U.P. Level Increase ?	Breakdown (Visual) Confirmation)	Breakdown Time (Drainage Increase/ Tieplate Subcooled) (sec)
50277	40458	6016	103.3	202, 202	1.0323	Yes	No	29-?/?
49457	37815	5973	114.6	201, 202	1.1450	Yes	No	?/?
49217	36980	5978	87.5	144, 154	0.9288	No	Yes	23-28/24-41
50203	41072	5977	90.9	154, 176	0.9328	No	Yes	28-47/44-55
49456	38107	5922	95.3	179, 190	0.9643	No	Yes	28-53/87-101
50322	37310	5938	99.5	188, 192	0.9847	No	Yes	40-123/177-194
50212	43419	5059	123.3	195, 198	1.0637	No	Yes	179-230/252-260
41736	33024	5968	107.4	199, 211	1.2798	Yes	No	?/?
41436	35675	5477	113.6	205, 213	1.2472	Yes	No	?/?
41753	33706	5927	113.0	202, 209	1.3164	Yes	No	?/?
50269	41024	5502	112.5	193, 201	1.0184	Constant	?	28-?/?-?
49260	40618	5491	119.3	210, 204	1.0964	Yes (slightly)	No	39-?/?-?
41437	38602	5100	122.0	212, 213	1.2789	Yes	No	?/?
41243	31478	5516	122.8	208, 216	1.3863	Yes	No	?/?
50293	46204	4982	129.0	205, 210	1.1129	Yes	No	36-?/?-?
42060	29309	4989	131.5	212, 214	1.3696	Yes	No	?/?

Table B-9

AVERAGED CONDITIONS 0.67 STEAM PROFILE

Subcooled CCFL: RCS UH

$\dot{M}_{spray}$ (lbs/hr)	$\dot{M}_{drain}$ (lbs/hr)	$\dot{M}_{steam}$ (lbs/hr)	T_{spray} (°F)	Lowest Peripheral Temperature (°F)	"C" Value	U.P. Level Increase ?	Breakdown (Visual Confirmation)	Breakdown Time (Drainage Increase/ Tieplate Subcooled) (sec)
50092	36087	5998	106.3	203, 203	1.0498	Yes	No	?/?
49943	36047	6027	116.5	202, 204	1.0551	Yes	No	?/?
49809	35535	6032	86.4	164, 163	0.9165	No	Yes	30-52/24-48
50007	36217	6037	90.4	167, 166	0.9367	No	Yes	38-40/33-35
30305	36821	5977	94.3	171, 172	0.9448	No	Yes	43-49/47-85
37835	38275	4996	90.5	174, 164	1.0298	No	Yes	162-199/155-169
49884	41495	5025	119.2	201, 212	1.0053	Increased slightly	?	41-?/?
37103	32282	5533	77.6	204, 205	1.0441	Yes	No	?/?
38059	28634	6018	81.9	203, 204	1.1309	Yes	No	?/?
37854	33178	5542	89.1	210, 213	1.1060	Yes	No	?/?
37415	37386	4963	100.1	211, 213	1.1110	Yes	No	?/?
49593	38184	5544	117.2	203, 205	1.0838	Yes	No	?/?
50816	33412	5516	212.0	203, 205	1.0865	Yes	No	?/?
49866	43120	4997	130.0	207, 213	1.1322	Yes	No	?/?

APPENDIX C

LIQUID INVENTORY MEASUREMENT TECHNIQUES

C-1. INTRODUCTION

During 1977 and 1978, Creare, Inc., was contracted to investigate, develop, test, and evaluate general techniques to measure liquid inventory in two-phase regions. These techniques are of particular interest in designing measurement systems for test facilities, such as the Lynn Steam Sector Test Facility (SSTF), which are designed to study core-spray distribution, counter-current flow limiting (CCFL) in parallel coolant channels, and upper-plenum fluid mixing. Creare constructed a facility, described in Section C-2, to provide for testing different liquid measurement systems for application in upper-plenum, bypass, lower-plenum, and channel-box regions.

The program assessed various liquid inventory measurement systems including differential pressure transducers, coupled conductivity probes, and a buoyant float device specially developed at Creare. The instrument principles, operating features, and installed locations are described in Section C-3. Details of the design considerations and electronic components required for the buoyant float and coupled conductivity probe devices are presented in Sections C-5 and C-6, respectively. Single and four-channel tests (Section C-4) were performed to proof-test these instruments. Transient depressurizations from initial pressure up to 120 psia were run, with saturated water in the lower plenum and bypass region. The parameters of initial plenum water level, bypass region inventory, vessel pressure injection flow rate, and channel-box steam were studied.

C-2. TEST FACILITY

C-2.1 VESSEL

The basic 150-psia test vessel consisted of three four-foot-long, flanged spool pieces constructed from 18 in. standard-wall steel pipe. The assembly is shown in Figure C-1. The lower plenum and upper plenum spool pieces had only the instrument penetrations (discussed in Section C-3). The middle spool piece had four observation ports of clear Lexan to permit visualization into the channel-box region.

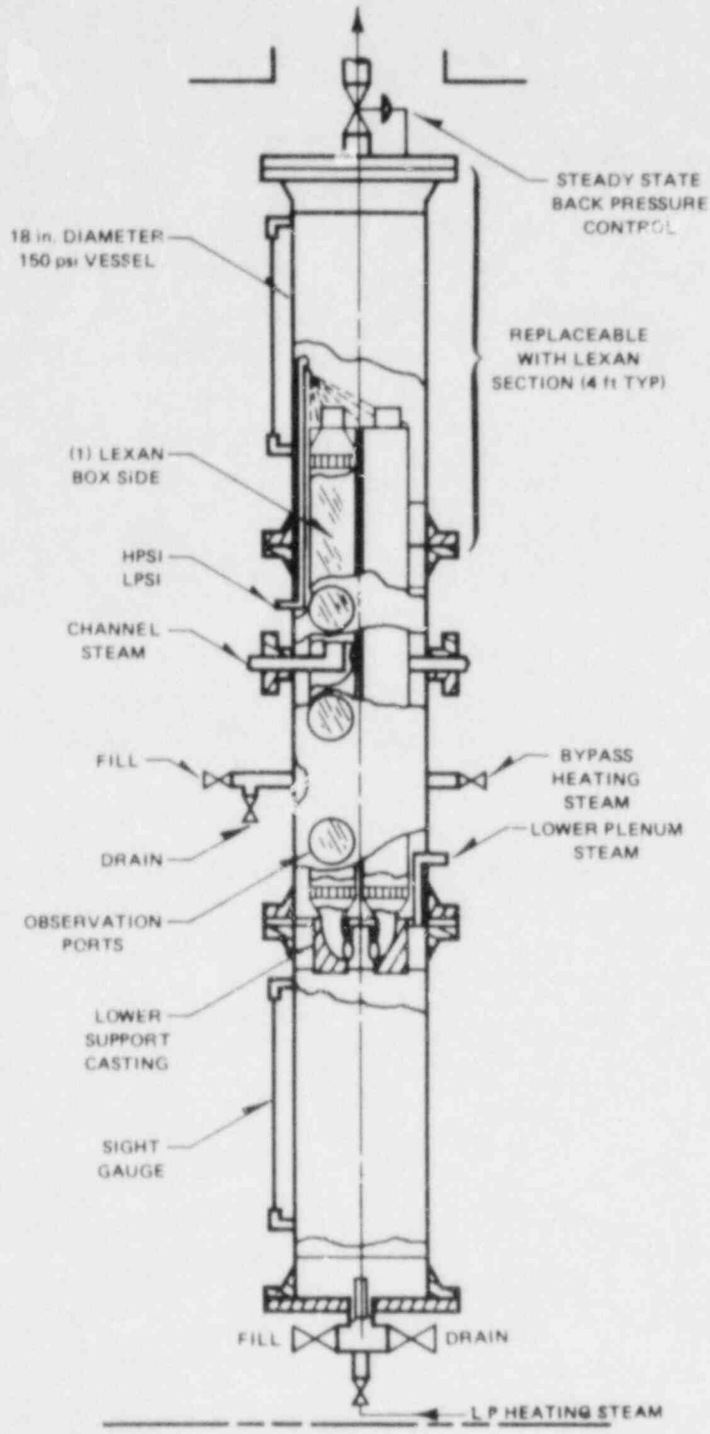

Figure C-1. Sketch of Flooding and Instrumentation Test Vessel

The Lexan viewing ports were replaced by metal flanges for tests at pressures greater than atmospheric. Other penetrations in the middle spool piece included four lower-plenum and four channel-box steam inlets for external steam supply. Two other penetrations were provided, one for the core-spray supply line leading to the nozzle, which directed ECC flow downward onto the channel boxes, and another for filling and draining the bypass region.

Liquid was drained through the bottom flange of the vessel. Steam was exhausted through a 2-in. ID pipe in the top flange of the vessel. A feedback control valve was used on the steam exhaust to control initial pressures in the transient tests. Steam-bleed lines were provided for heating of the lower plenum and bypass region liquid to saturation in the transient tests.

C-2.2 CHANNEL BOXES

The 5-ft.-long channel box consisted of the upper tieplate (recessed 3.19 inches from the top of the channel box), an 8x8 array of 64 simulated fuel rods 1 foot in length (with spacer) attached to the upper tieplate, a 30-in. open length in which the channel-box steam injector was located, 64 simulated fuel rods 1 foot in length (with spacer) attached to the lower tieplate casting, and the lower tieplate casting. The channel-box assembly was mounted on the lower core support plate and casting.

The channel-box steam injector penetrated one side of the channel box horizontally to the center of the channel. The steam distributor pipe was 2-in. Schedule 40 (capped) with 68 holes 0.209 inch in diameter arrayed in four vertical rows over a length of 16 inches (referred to as the original Creare injector).

When a single channel was tested, the other channels were eliminated as flow paths by blocking off the flow distributor orifices. When all four channels were tested, the distributor orifices remained unblocked. The 1-ft. lengths of simulated fuel rods were not included in the other three channel boxes. Instead, the fuel-rod mounting holes in the tieplates were blocked with screws, leaving the correct open area unblocked.

C-2.3 STEAM SUPPLY

Steam was supplied from a 150-psia boiler. The maximum steam flow from this boiler in the tests was 7200 lbm/hr, given the pressure-drop characteristics of the test facility.

C-2.4 COOLANT SUPPLY

ECC was drawn from a 2000-gallon water tank. The coolant could be preheated between 85°F and 212°F. Flow rates up to 20 gpm were tested.

C-3. INSTRUMENTATION

Instrumentation for this facility consisted of orifice plates with flange taps and a manometer for measuring steam flows, a rotameter for the ECC flow, thermocouples, an absolute pressure transducer, several differential pressure transducers, a coupled conductivity probe, and the specially developed buoyant float device. The locations of the instruments are sketched in Figure C-2. The maximum and minimum measured ranges for the instruments used to measure liquid inventory are shown in Table C-1. The types of instruments used and their calibration procedures are discussed below.

C-3.1 DIFFERENTIAL PRESSURES ($\Delta P1$-$\Delta P4$)

Differential pressure measurements were made for upper and lower plenum filling, channel box, and lower tieplate Δp, although not all measurements shown were made in every test. The instruments used in differential pressure measurements were Celesco P6603M1 transducers with a range of 5 to 10 psid. The operating temperature of the instruments is between 32 and 500°F; zero shift compensation and span compensation are 0.25 percent of full-scale output/100°F.

The Celesco ΔP transducers were mounted on the vessel as shown in Figure C-2. The line lengths for each leg of the transducer were made equal by coiling the lower leg of each instrument. In order to prevent a zero shift from gradual collection of condensate in the vertical leg of each transducer during a test, the vertical legs were filled with water between tests. The horizontal leg of each transducer was drained between tests. During the transient test program Creare also experimented with filling both legs of the transducer with cold water to minimize flashing in the lines. It was necessary to electronically filter the differential pressure transducer outputs during steady tests with cold ECC and during transient tests in order to eliminate large oscillations which obscured the traces. These oscillations were probably due to condensation in the vessel. The schedule of changes made to the transducers is shown in Table C-2.

C-3.2 BUOYANT FLOAT

A buoyant float device was developed and constructed at Creare. Details of the float are shown in Figure C-3. The mounting location is shown in Figure C-2. The

Table C-1

LIQUID LEVEL INSTRUMENT RANGES

Instrument	Location	Minimum* Indication (in)	Maximum* Indication (in)
ΔP1	Lower Plenum	6.25	42.25
Coupled Conductivity Probe	Upper Plenum	- 8.75	25.25
Buoyant Float	Upper Plenum	-33	27
ΔP4 (Single Channel)	Upper Plenum	- 6.75	29.25
ΔP4 (Four Channels)	Upper Plenum (Alternate Location in Figure C-6)	-34	29.25

*Lower-plenum measurements relative to bottom of vessel. Upper-plenum measurements relative to top of channel box.

Table C-2

TRANSDUCER HISTORY

Test# / Transducer	B1-B100	B101-B110	B111-B169	T1-T13	T4-1 T4-9
ΔP1	Calibrated, Coolant in Vertical Leg	---	Recalibrated, Filtered to 0.2 Hz	Recalibrated	Coolant in Horizontal Leg
ΔP2	Calibrated, Coolant in Vertical Leg	---	Recalibrated	Moved to ΔP4	---
ΔP3	Calibrated, Coolant in Vertical Leg	---	Recalibrated, Filtered to 3 Hz	Recalibrated	---
ΔP4	Calibrated, Coolant in Vertical Leg	Removed	---	Recalibrated, Filtered to 0.33 Hz, Coolant in Horizontal Leg	Recalibrated, Lower Leg Moved to Alternate Position (Figure C-2)

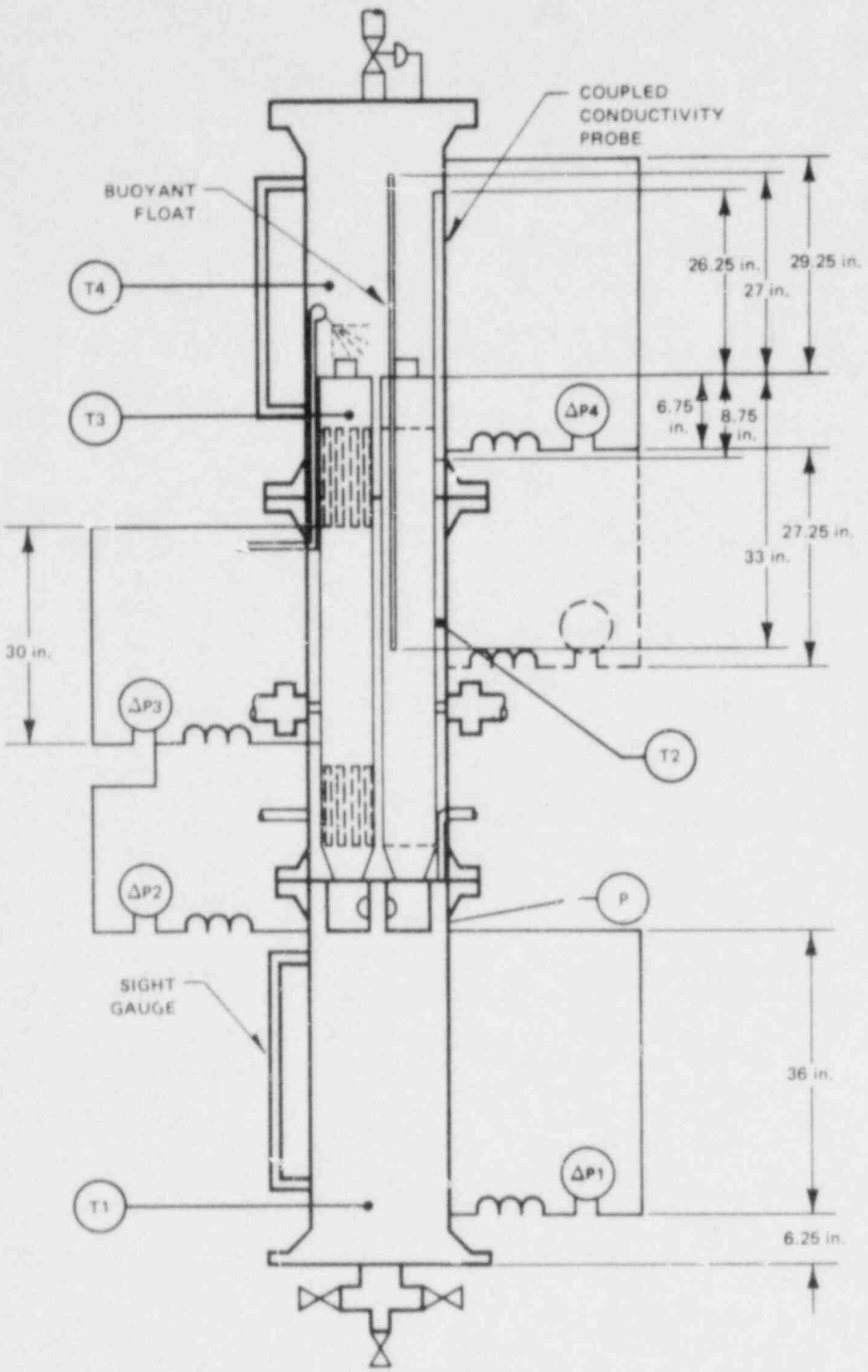

Figure C-2. Sketch of Instrumentation Locations in Test Vessel

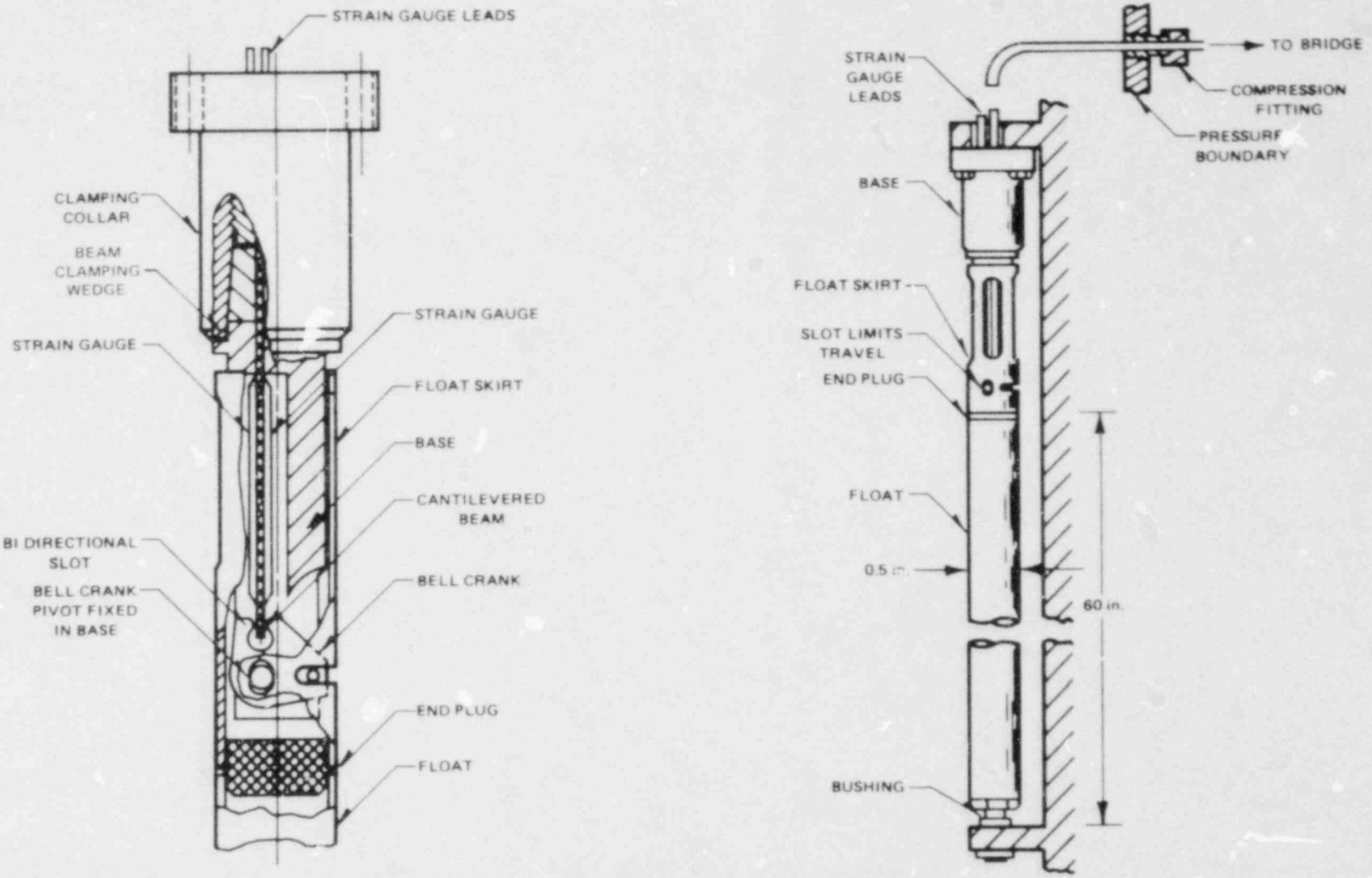

Figure C-3. Sketch of Byoyant Float Instrument Mechanism and Construction

operating principle of this device is that the float--in this case a 5-ft.-long tube 0.5 inch in diameter--will experience a buoyant force proportional to the weight of the water it displaces when it is submerged. This buoyant force is independent of the two-phase height of a steam/water mixture. In the Creare device, the axial buoyant force on the float displaces the float, and its motion is transmitted to a bell crank. The bell crank pivots and converts the translation of the float to a rotary motion which in turn stresses a cantilevered beam. The beam assembly has sealed strain gauges mounted on both sides to minimize thermal effects. Thus, the buoyant force on the float is transduced into an electrical output from the strain gauges. Detailed design considerations for this device and the circuit diagrams for the strain gauge output amplifiers are included in Section C-5.

The buoyant float device was first checked out in a bubbly air/water mixture in a facility consisting of a 60-in. tall glass vessel 6 inches in diameter and an air sparger at the bottom end of this vessel. Figure C-4 illustrates the output of the buoyant float in a bubbly air/water mixture. Air was bubbled into the bottom of the vessel at a rate which brought the two-phase height to 36 inches (or void fraction of 50 percent). The effect of filtering the output under the same two-phase conditions is shown. The strain gauge amplifier electronics had a design frequency response of 16 Hz. Oscillations of ±25 percent of the indicated level are observed (Figure C-4a), although the average output is close to the true collapsed level. Filtered to 1.6 Hz, the oscillations become smaller (Figure C-4b), and filtered to 0.5 Hz the amount of oscillation is less than ±10 percent of the collapsed level (Figure C-4c). The 0.5 Hz filter was subsequently used in the testing.

The sensitivity of the buoyant float to changes in temperature was also investigated. The strain gauge transducing element was subjected to a sudden ΔT of 80°F by immersion in alternating water baths of 60°F and 140°F water. The results are shown in Figure C-5. The change in temperature from 60 to 140°F caused a momentary zero shift of a maximum of 0.1v out of a full-scale output of 1.9v, or about 5 percent.* The shift occurred for a period of about 2 seconds, after which time the output returned to the original zero. Reversing the procedure and going from the 140 to 60°F bath reversed the direction of the zero shift, but it was again the same magnitude and duration.

*If the output is unfiltered (design response of 16 Hz), an initial spike of greater magnitude is seen for about 0.2 second before the zero shift falls to a level like that observed in Figure C-5.

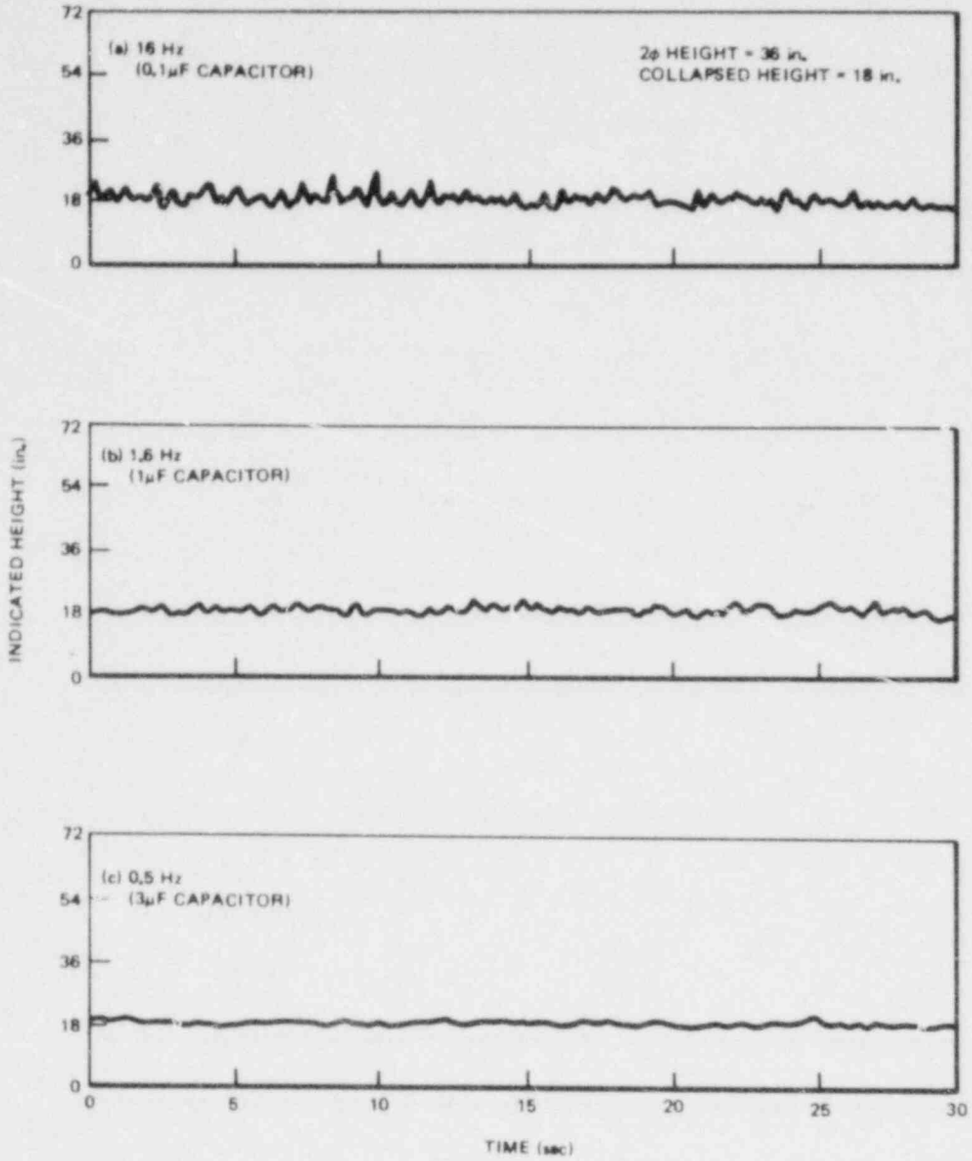

Figure C-4. Sample Output of Bucyant Float in Bubbly Air/Water Mixture (with Various Filters)

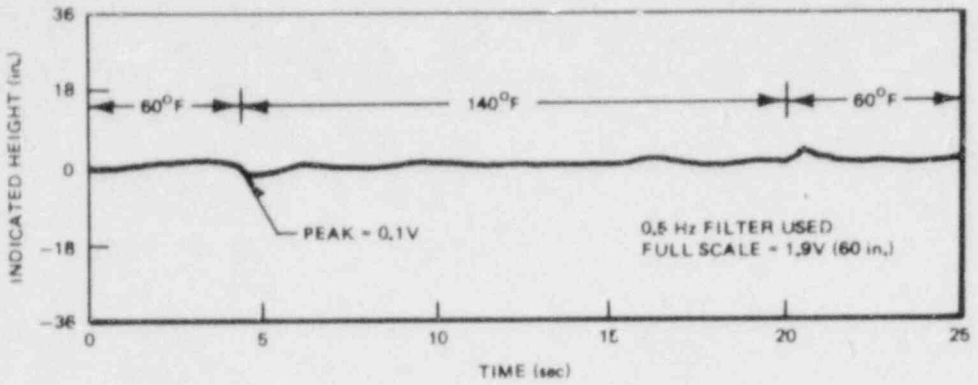

Figure C-5. Thermal Sensitivity of Buoyant Float Instrument

The buoyant float was calibrated by filling and draining the test vessel. Figure C-6a shows that the response of the buoyant float to steady filling (dashed line) was very close to the calculated slope based on the filling rate but was not perfectly linear. During these calibration procedures it was discovered that the buoyant float did not always return to its original zero in quiescent filling and draining of the vessel. This is illustrated in Figure C-6b.

The amount of this zero shift was typically ±20 percent of the full-scale output, although sometimes less. Tapping lightly on the probe or the test vessel caused the probe to return to its original zero. If the probe mounting was vibrated during filling and draining calibrations, the response was as shown by the solid line in Figure C-6b, the output returned to its original zero without any trouble upon draining. The conclusion was that the buoyant float was subject to stick-slip (friction) in its linkages, although a specific linkage was not identifiable without dismantling the device. It was decided to proceed with testing and rely on the steam/water interactions in the upper plenum to supply the agitation to overcome the stick-slip problem. This testing is discussed in Section C-4. The unit was then removed to further assess the stick-slip problem.

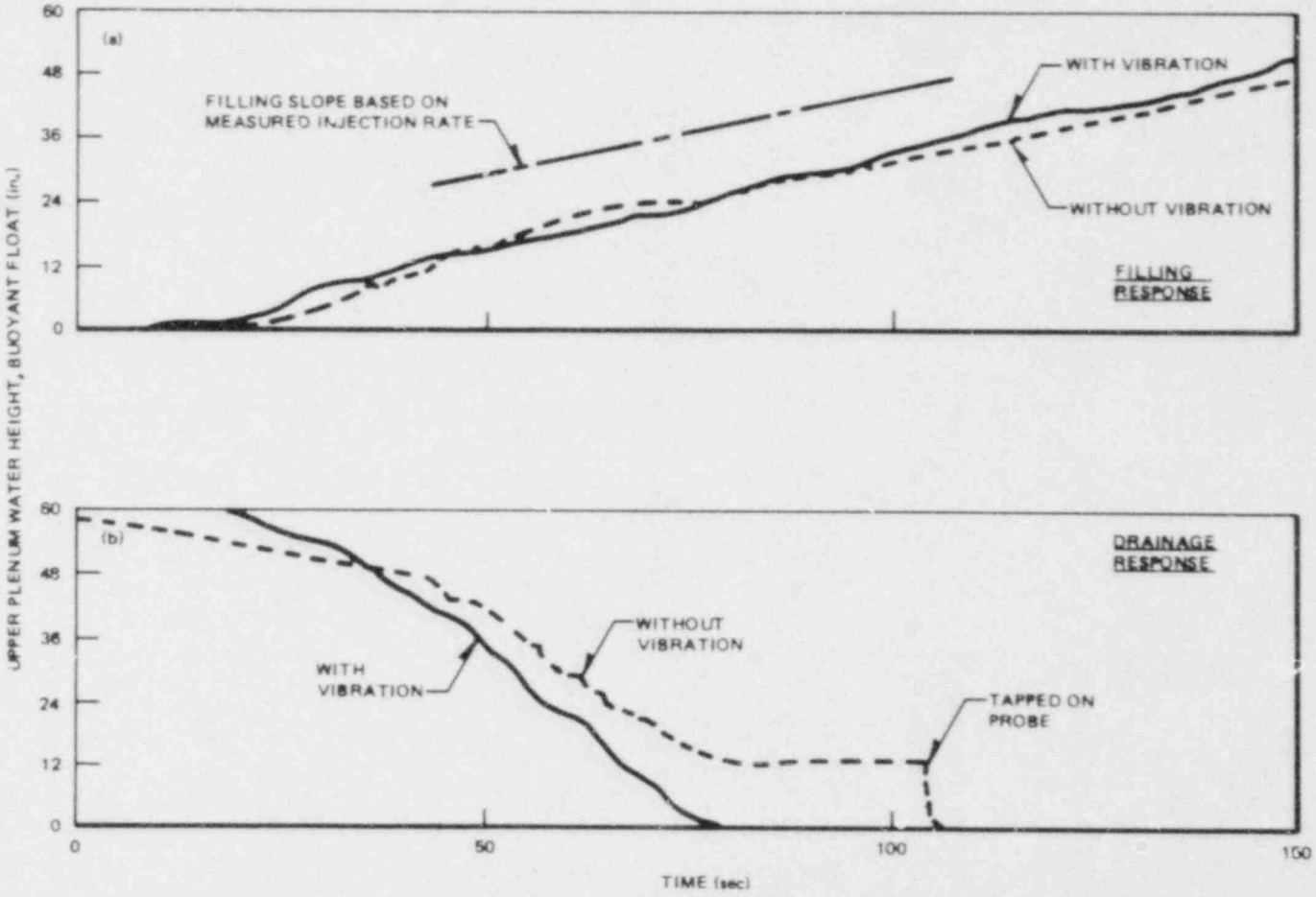

Figure C-6. Sample Traces of Buoyant Float Output in Single-Phase Filling and Draining

The first step in tracking down the sticking problem was to reassemble the instrument on a laboratory bench, using a hanging weight to simulate the float. This permitted visualization of the mechanism in operation. Diagnostic testing showed that the interface between the beam and the bell crank was the major source of friction and sticking. Several attempts were made to reduce friction at this point of contact (by applying oil and polishing the jaws of the bell crank); however, these efforts were not entirely satisfactory.

After these attempts, it was decided to adopt an alternate design, the intent of which was to reduce the potential for friction as much as possible. The device was redesigned to mount the float perpendicular to the beam, thus eliminating the pivots and the jaw of the bell crank as points of friction. The new design adopted is illustrated in Figure C-7. The mounting of the float at right angles to the beam is evident. Circular collars on the float position the float relative to the beam and limit the travel of the float to the range of operation. A Teflon bushing has been used to help minimize friction between the float and the float guide, and the fit in this region is relatively loose.

The modified instrument was tested in single and two-phase air/water mixtures in a transparent calibration vessel where the two-phase mixture conditions could be controlled. This calibration vessel is sketched in Figure C-8. It had a water inlet, a drain, and provisions for bubbling air into the water near the lower end of the vessel. The vessel was 6 inches in diameter and 66 inches tall.

C-3.2.1 Single-Phase Response

Typical response of the instrument in a simple filling and draining of this vessel with water alone is shown in Figure C-9. At a constant water inflow rate, the response was very linear with time (Figure C-9a). Contrast this with the comparatively shaky response of the earlier design during filling (Figure C-6a). In addition, the modified probe returned to its zero position without mechanical help during the draining, which the earlier design did not (Figure C-6b). Comparison with the proven conductivity probe measurement technique in Figure C-9b shows that the buoyant float responds at the right time, follows the conductivity probe well when filling and draining, and returns to zero properly.

C-3.2.2 Two-Phase Response

The steady two-phase response of the modified instrument was tested by filling the glass vessel to a given initial water level and then bubbling controlled amounts of

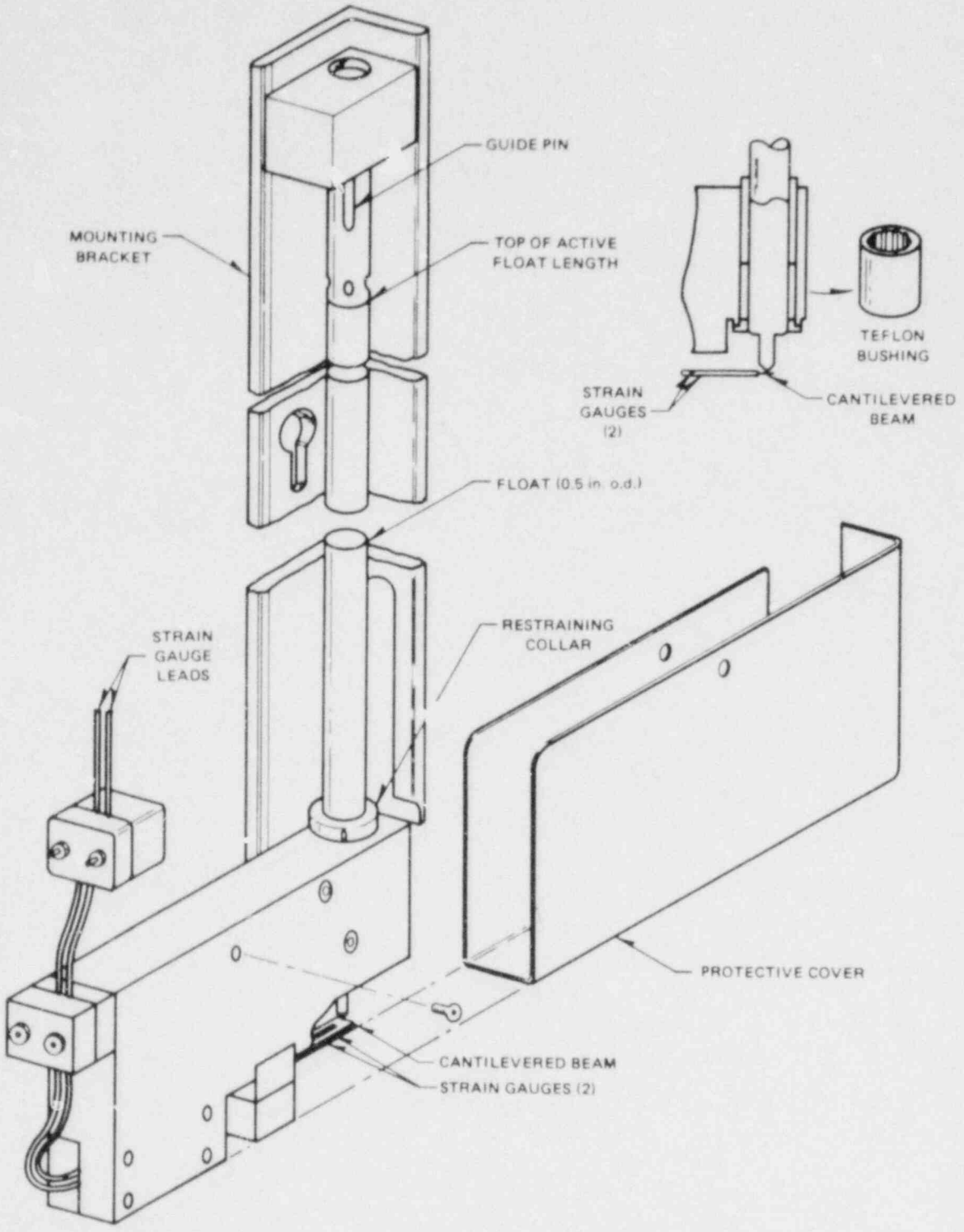

Figure C-7. Sketch of Modified Buoyant Float Instrument Construction

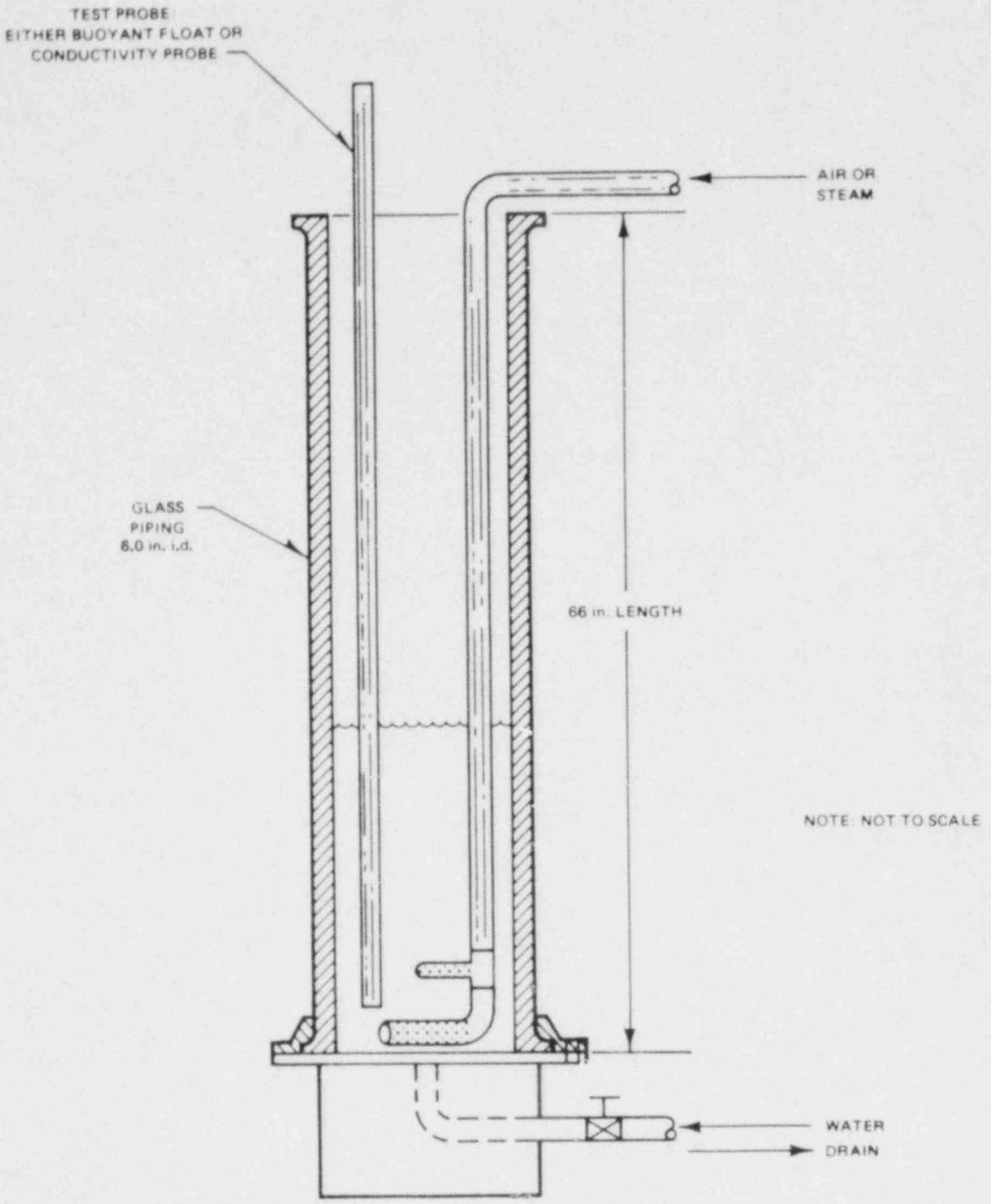

Figure C-8. Sketch of Two-Phase Mixture Calibration Vessel

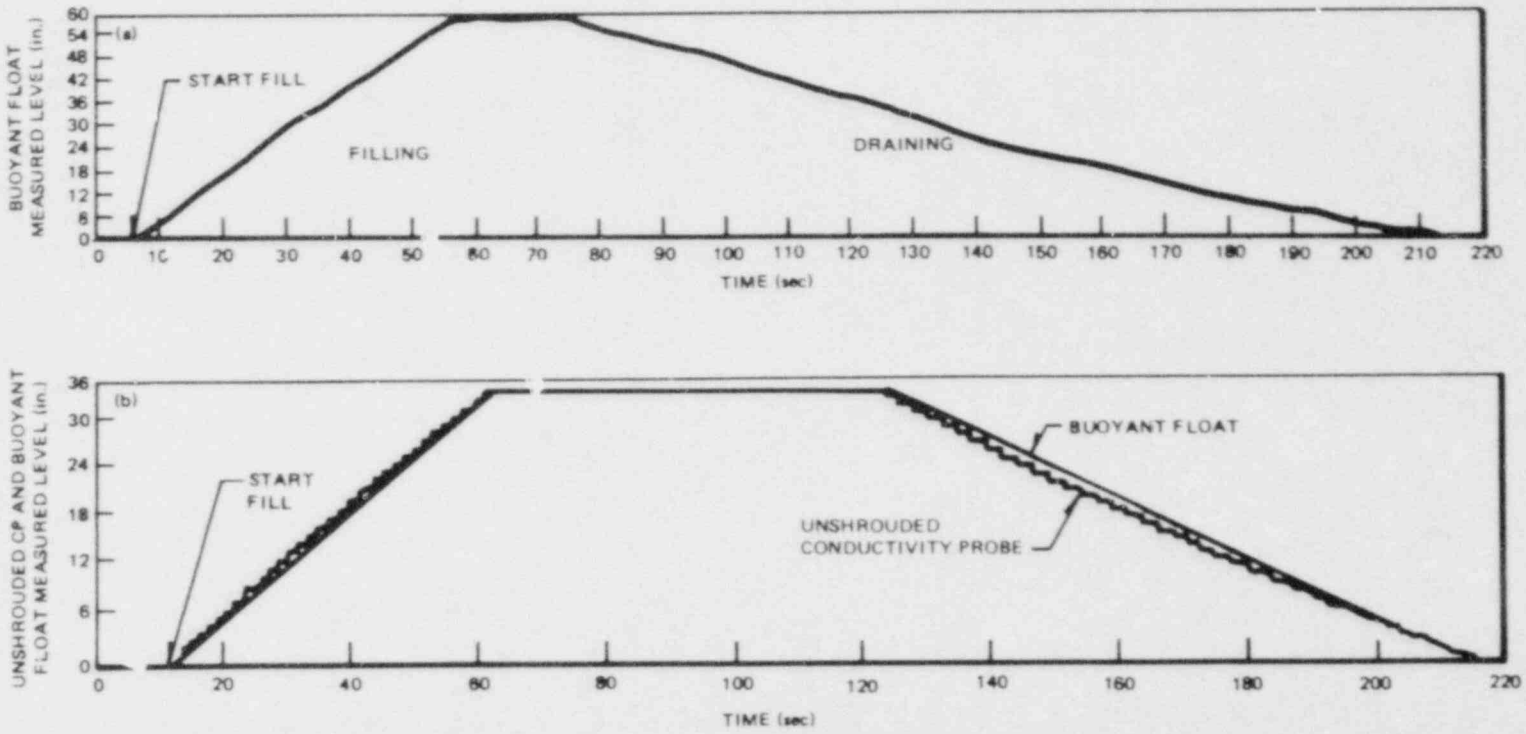

Figure C-9. Single-Phase Response of Modified Buoyant Float Instrument

air through the water to achieve desired two-phase mixture heights. Sample records from this type of test are shown in Figure C-10. The collapsed (initial) water level was 24 inches for this case.

As the amount of air bubbled through, the liquid was increased so that the void fraction increased from 0 to 50 percent; the mean collapsed level recorded by the probe decreased to about 75 percent of the true collapsed level. Oscillations about this mean level also increased with void fraction. For example, they were ±1 inch at α=0.20 and ±4 inches at α=0.50. Note that the peak values measured by the buoyant float were within two inches of the collapsed level at all void fractions. The results from tests with collapsed levels of 12, 24, and 36 inches are summarized in Figure C-11. The same trends with increasing void fraction as discussed above are seen.

To demonstrate that the buoyant float worked under transient conditions similar to those expected in the upper plenum in core-spray tests, additional tests were performed in the following manner (see Figure C-12): starting from a given initial water level, a constant flow of air was bubbled into the vessel to generate a two-phase mixture; then water was injected at a constant rate until the mixture height reached some new level. The air was then turned off and the final collapsed level observed directly. The traces in Figure C-12 show that the mean reading from the probe dropped slightly as air was turned on, increased as expected during water injection, and rose slightly when the air was turned off. The collapsed level measured by the float after the air was turned off agreed with the level measured with a ruler. The apparent sudden rise in level indicated by the probe when the air was turned off or slight drop when the air was turned on is due to the same cause as the mean level measuring low at larger void fractions (Figure C-11) as discussed above. The slight drop in mean indicated level when the gas flow was turned on was very similar to the initial drop seen in transient steam/water tests reported in Subsection C-4.2. Except for slightly low mean values, the instrument is otherwise seen to respond to transients without sticking or additional complications.

C-3.3 COUPLED CONDUCTIVITY PROBE

The coupled conductivity probe device and shroud were also designed and built at Creare. The conductivity probes consist of silvered-copper wire inserted in threaded Teflon screws and beaded with silver solder (see Figure C-13). These probes are arranged vertically on a stalk at 1-in. spacing. When an individual

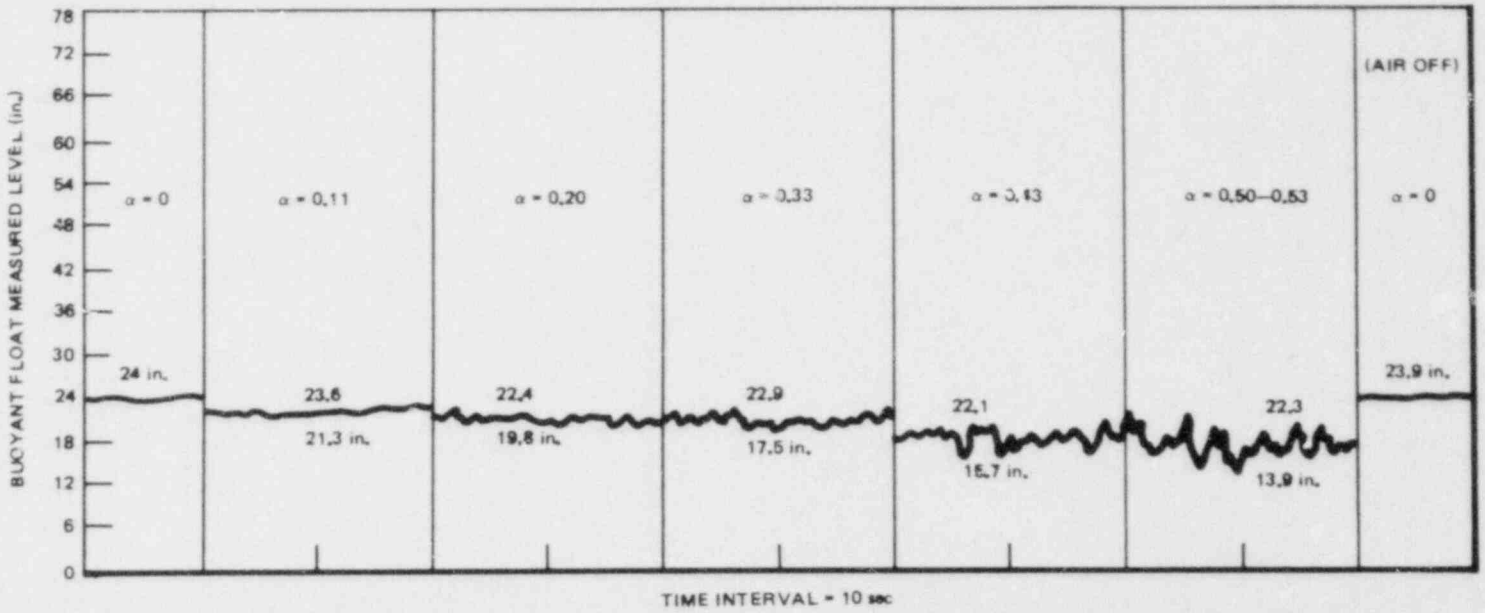

Figure C-10. Sample Traces of Modified Buoyant Float Response for 24-in. Collapsed Level

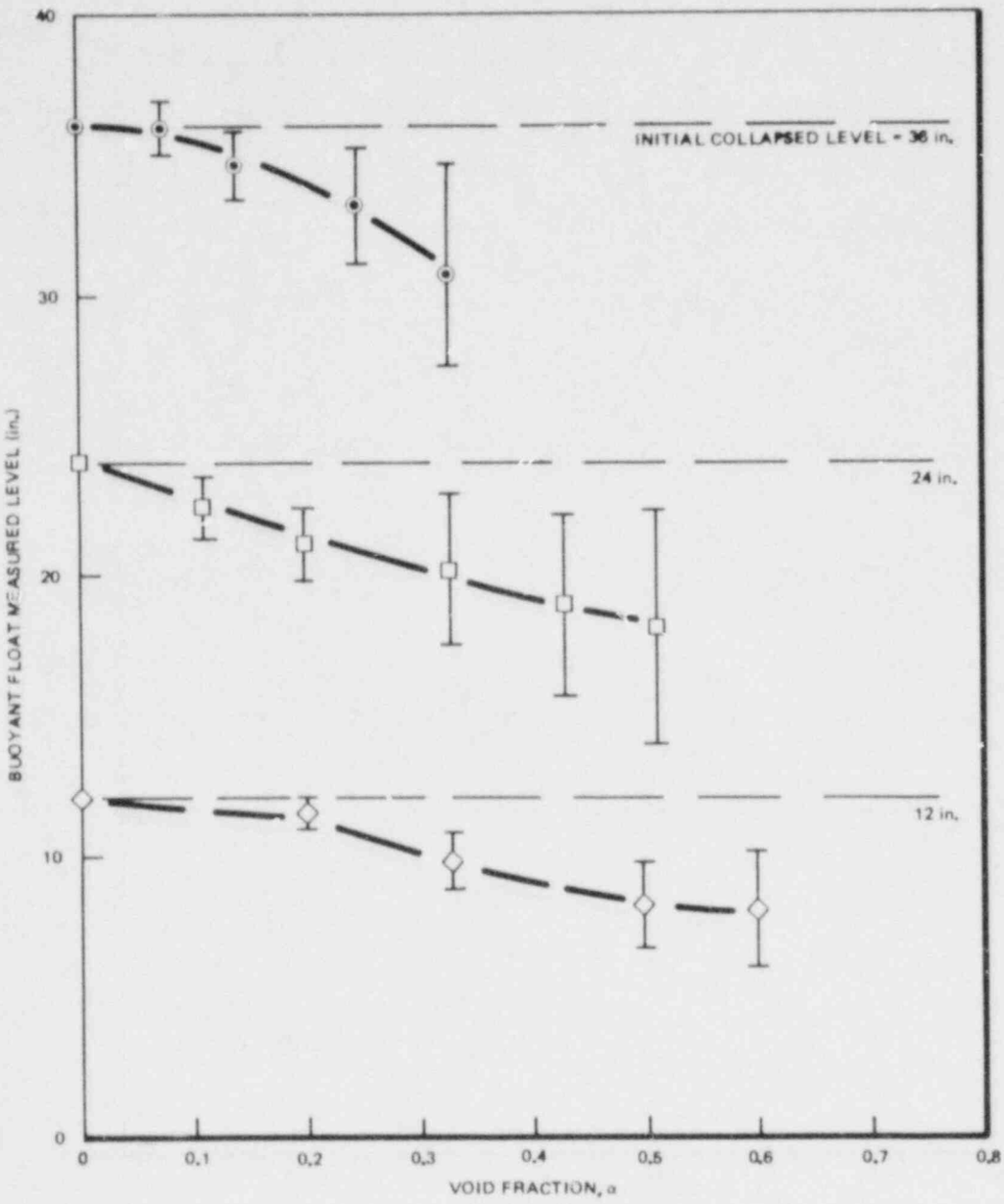

Figure C-11. Summary of Modified Buoyant Float Response at Various Collapsed Levels

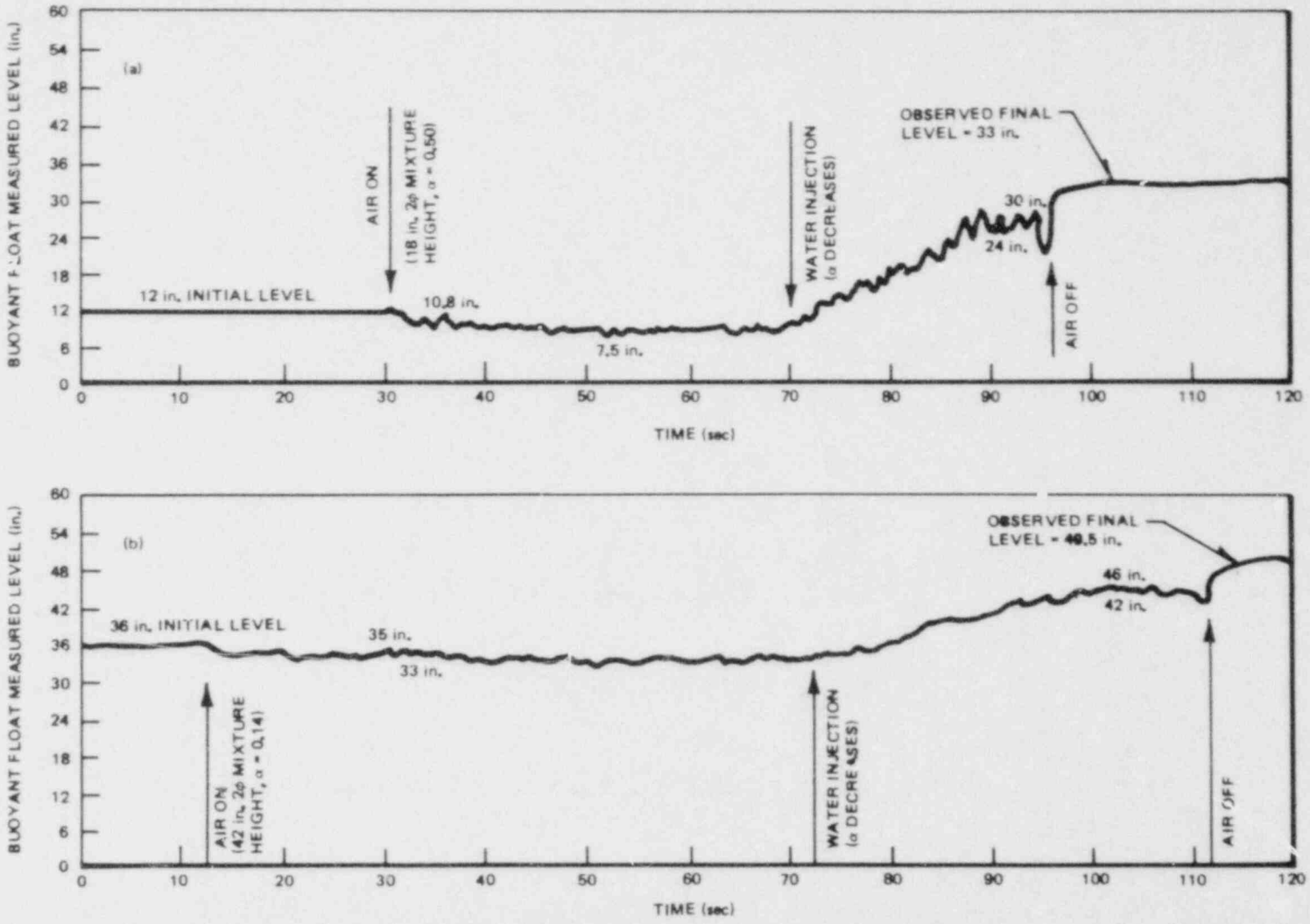

Figure C-12. Sample Traces of Modified Buoyant Float Response under Transient Two-Phase Conditions

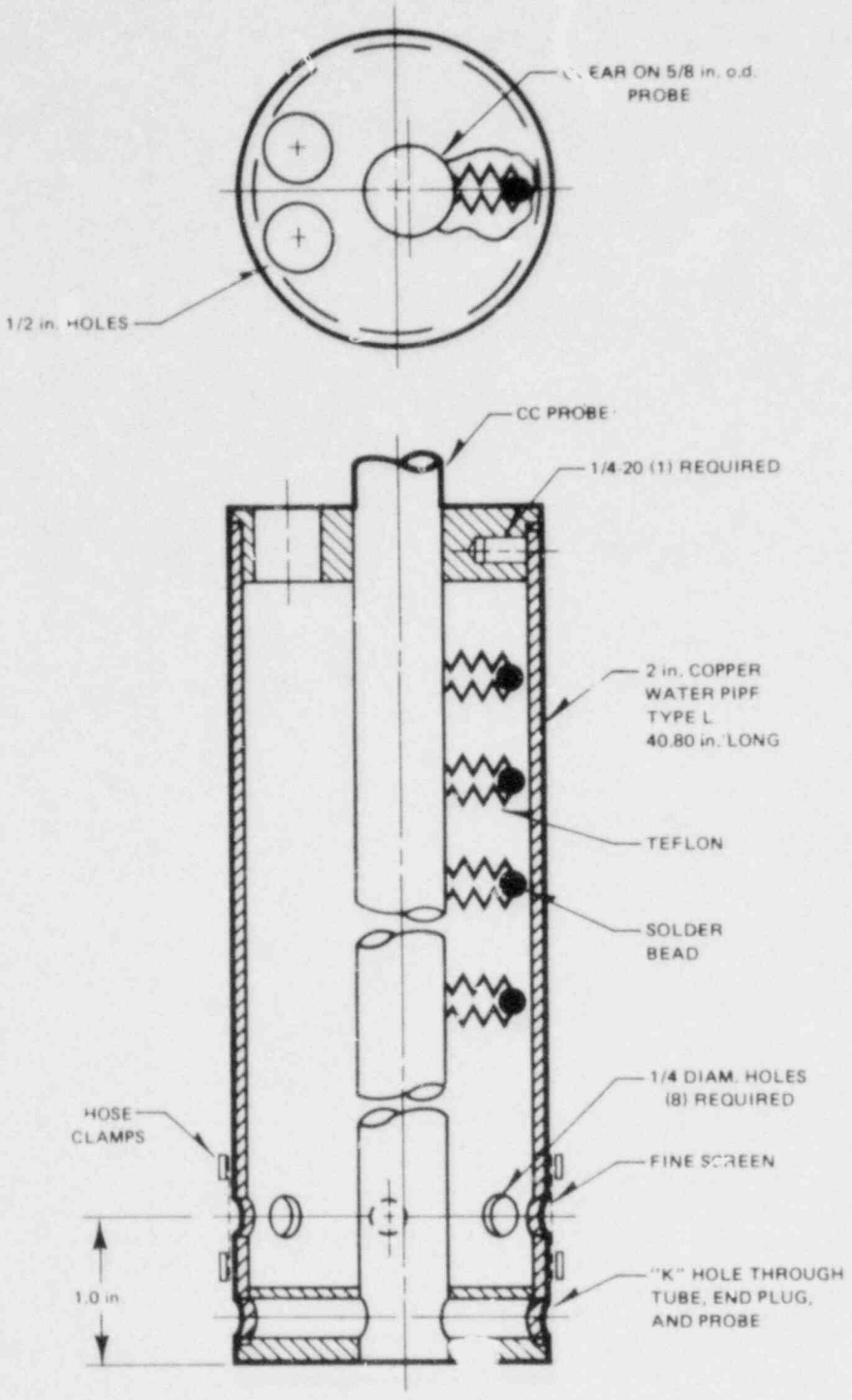

Figure C-13. Sketch of Shrouded Coupled Conductivity Probe Instrument

probe is submerged, the electrical resistance between it and the ground (usually the test vessel) is decreased. The change in resistance is sensed by the electronics, and a fixed voltage is output for each submerged probe. The output of all triggered probes is summed to give an indication of the water level with time.

Preliminary work indicated that an unshrouded conductivity probe device tended to indicate the two-phase mixture height in a bubbly air/water mixture but did not measure the collapsed level.

A shroud of the design shown in Figure C-13 was added to this probe to permit measurement of collapsed liquid level in steady-state tests. The work in a bubbly air/water mixture showed that shrouding the probe with a tube having fine-mesh screened holes at the bottom (to hinder gas bubbles from entering the shroud tube) allowed the probe to measure the collapsed level of a steam/water mixture surrounding the tube.

The coupled conductivity probes have shown no thermal or other zero shift effects with temperature. The device was also calibrated by filling and draining the vessel, and the output was very repeatable. Further information on coupled conductivity probe systems is contained in Section C-6.

C-3.4 SAMPLE OUTPUT

Sample instrument traces from a simple filling of the vessel at 20 gpm are shown in Figure C-14 (the bypass region was initially full). The figure shows that the lower-plenum, channel-box, and upper-plenum differential transducers register filling in the succession and at the timing as they should (Figure C-14a). The buoyant float output shows filling above the top of the channel box beginning at the same time as indicated by the upper plenum Δp trace (Figure C-14b). Likewise, the coupled conductivity probe also indicates filling of the upper plenum beginning at the same time. The triggering of individual conductivity probes gives the stepwise appearance in the latter trace. The performance of these instruments during actual tests is described in Section C-4. Particular attention is paid to the effect of flashing on these measurements in the transient tests because all three devices perform very well under steady conditions.

C-4. INSTRUMENTATION PROOF TESTS

The program also proof-tested liquid inventory measurement instrumentation. Specifically, a shrouded conductivity probe system, a buoyant float device, and a

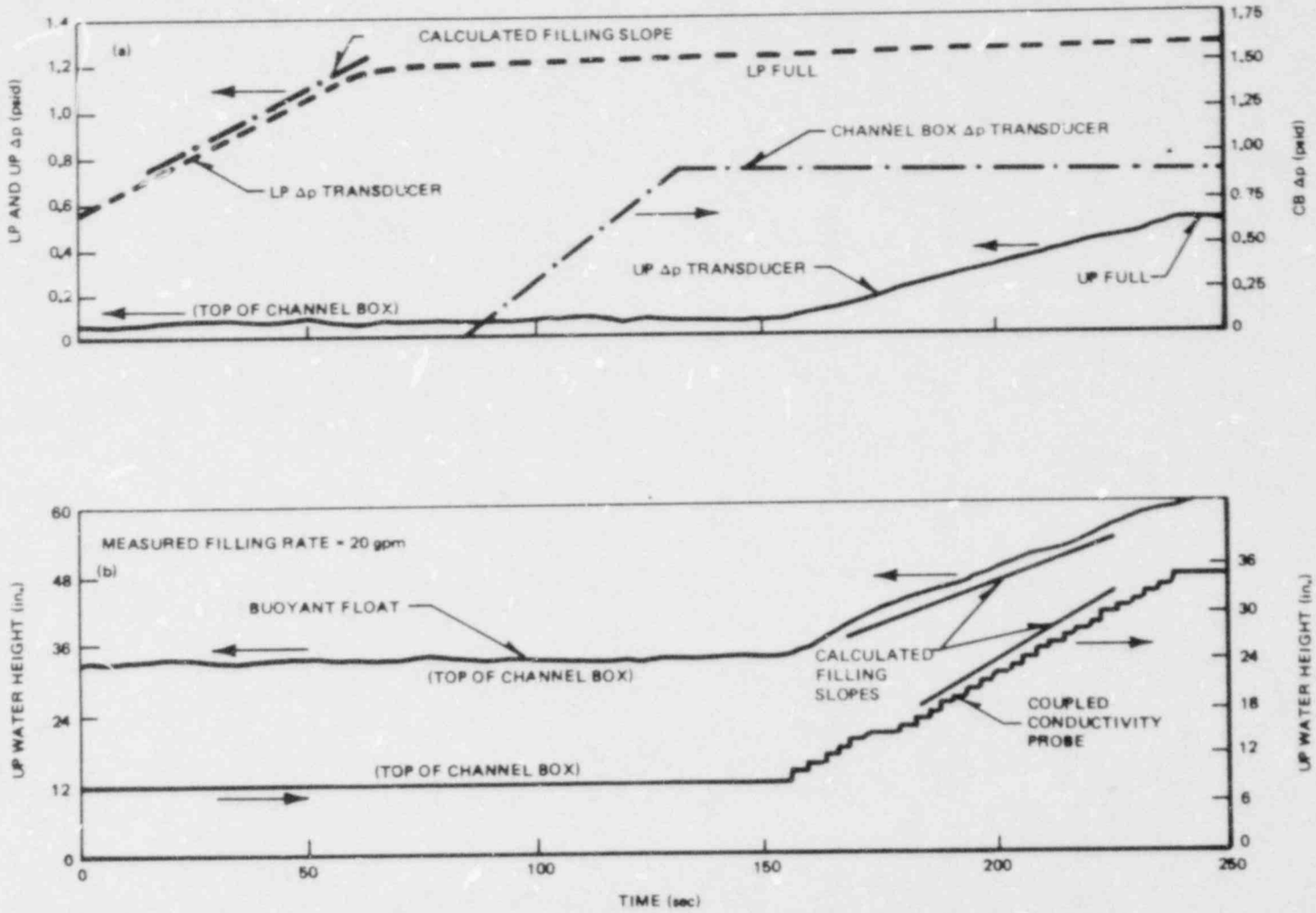

Figure C-14. Sample Output of Vessel Instrumentation in Single-Phase Filling

differential pressure transducer were studied under steady and transient test conditions. Then the instruments were installed in the upper plenum of the flooding test vessel, located as shown in Figure C-2. The steady-state tests in this vessel consisted of controlling the level of a two-phase bubbly steam/water mixture in the upper plenum and comparing the outputs from the instruments. The transient tests consisted of depressurizing the test vessel (from pressures up to 120 psia) with known levels of saturated liquid in the lower plenum and bypass region. These tests thus include the effect of flashing on the instrumentation response. The parameters of initial plenum water level, liquid injection flow rate, and channel-box steam were also scoped with four channels.

C-4.1 STEADY STATE

The initial type of steady-state test of the instrumentation involved setting a channel-box steam upflow large enough to completely limit 8 gpm of 85°F water and controlling the two-phase mixture in the upper plenum at various levels. The two-phase level was visually observed using the upper-plenum sight gauge (see Figure C-1), and the level was controlled using the bypass region drain.

The results are shown in Figure C-15. From an initial sight gauge level of 16 inches, the two-phase level was successfully dropped to 10 inches and 4 inches above the top of the channel box. Figures C-15a, b, and c compare the response of the shrouded conductivity probe, the differential pressure transducer, and the buoyant float, respectively. The indicated levels for all three instruments agree well with each other, although the indicated values are an inch or so higher than the sight gauge levels. It may be seen that the instruments respond well to changes in the upper-plenum level.

Experiments with an unshrouded conductivity probe were run in the calibration vessel sketched in Figure C-8. An initial collapsed level ranging from 6 to 24 inches was established and then air or steam bubbled into the vessel to generate mixtures of various heights. Figure C-16 shows sample traces for various mixture heights with a collapsed water level of 12 inches. The probe output is compared with visual estimates of the two-phase level for various levels. The visual measurements of the level typically spanned a couple inches as the level moved up and down somewhat, with motion of the level greater at larger void fraction. The probe output also oscillated, indicating a mean two-phase level generally in agreement with visual estimate, although slightly higher (probably because of splashing).

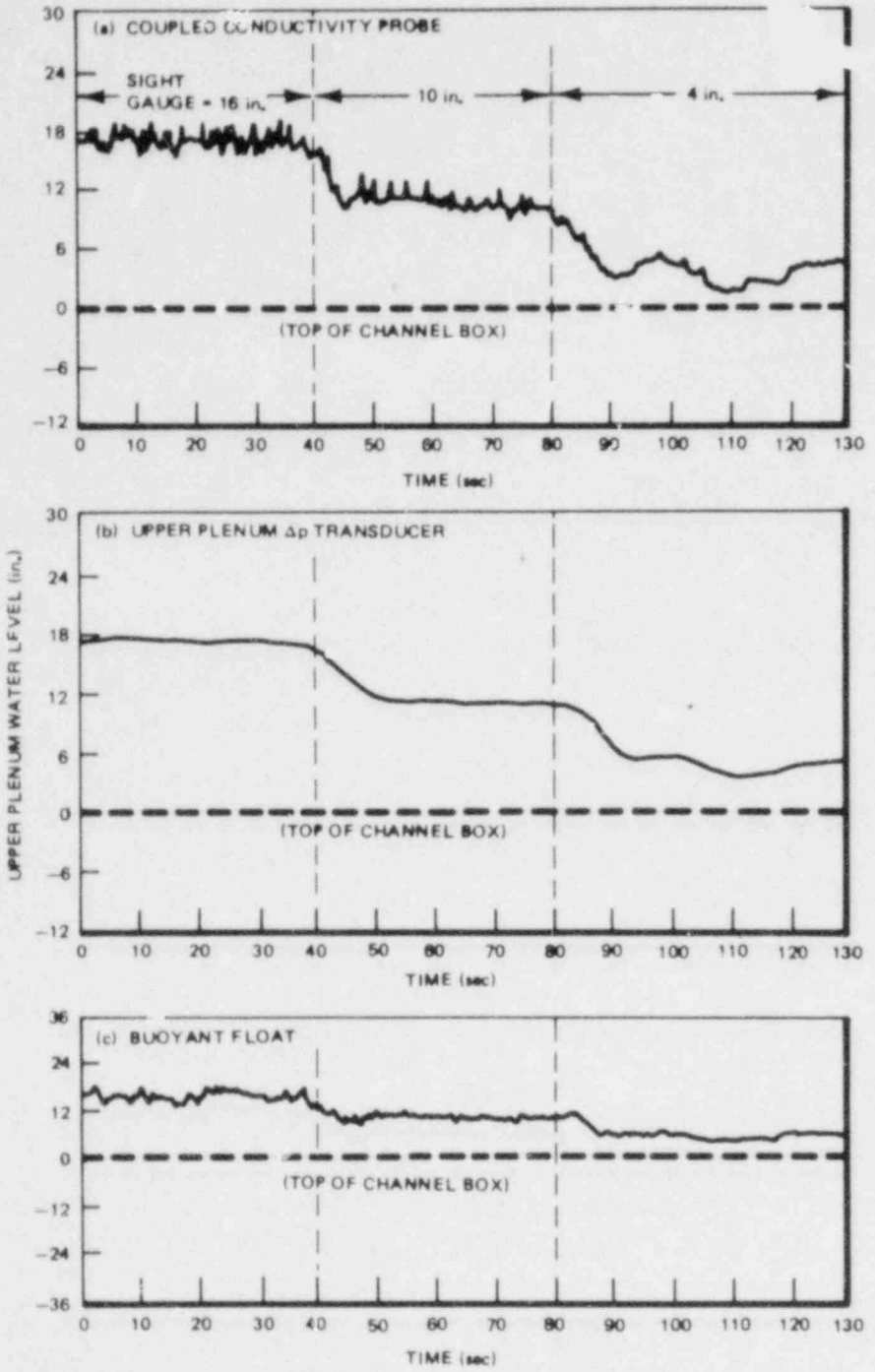

Figure C-15. Liquid Inventory Instrument Response to Steady, Bubbly Steam/Water Mixture Level

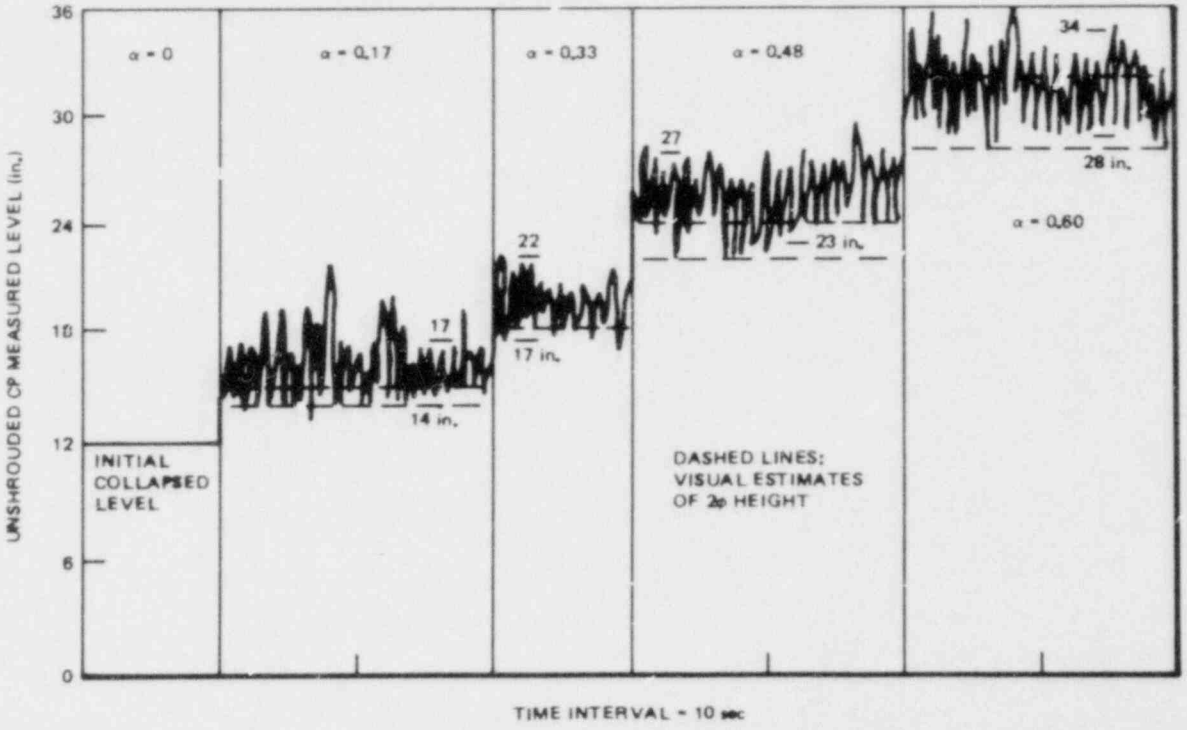

Figure C-16. Sample Traces of Unshrouded Conductivity Probe Response in Steam/Water Mixtures

Figure C-17 summarizes measurements for 6-, 12-, 18-, and 24-in. collapsed levels with various void fractions (two-phase mixture heights). Within experimental repeatability, response of the unshrouded probe in air/water and steam/water mixtures was the same, and mean level indications agreed well with visual observations.

In another test, the upper-plenum water level was initially at the top of the channel box, and the upper plenum was allowed to fill, with the 18-gpm injection flow completely limited by steam upflow. The instrument responses in this test are shown in Figure C-18, where the conductivity probe trace is linear in filling. The buoyant float reading actually decreases in the first few seconds, recovers, and then increases nearly linearly at the correct slope. The initial decrease is probably due to the injected spray wetting the float. This effect is also seen in the transient tests and is discussed in more detail later. After the initial decrease, the buoyant float response in filling of the upper plenum compares well with conductivity probe.

Once the upper plenum was full, the mixture level was decreased by reducing the steam upflow. When the steam is turned off, the upper-plenum level returns to the top of the channel box, as indicated by the conductivity probe. The original buoyant float, however, continues to indicate a level about 12 inches above the top of the channel box.

In summary, then, under steady-state, two-phase mixture conditions, the conductivity probe, buoyant float, and upper-plenum differential transducer responded well, and all three measurements agreed. In a quasi-steady two-phase filling and draining, the instruments also responded well, except for a noticeable sticking of the original buoyant float in the draining mode, which was later corrected, as discussed in Section C-3.

C-4.2 TRANSIENTS

The transient tests differed from the steady tests in that the overall system behavior was less controlled, primarily because of the effects of flashing of saturated lower plenum and bypass region liquid during depressurization. In each of the transient tests, lower-plenum steam was supplied from flashing of the lower-plenum liquid. A nominal initial plenum volume of 13.6 gallons of saturated liquid was used; the initial volume was visually verified using the

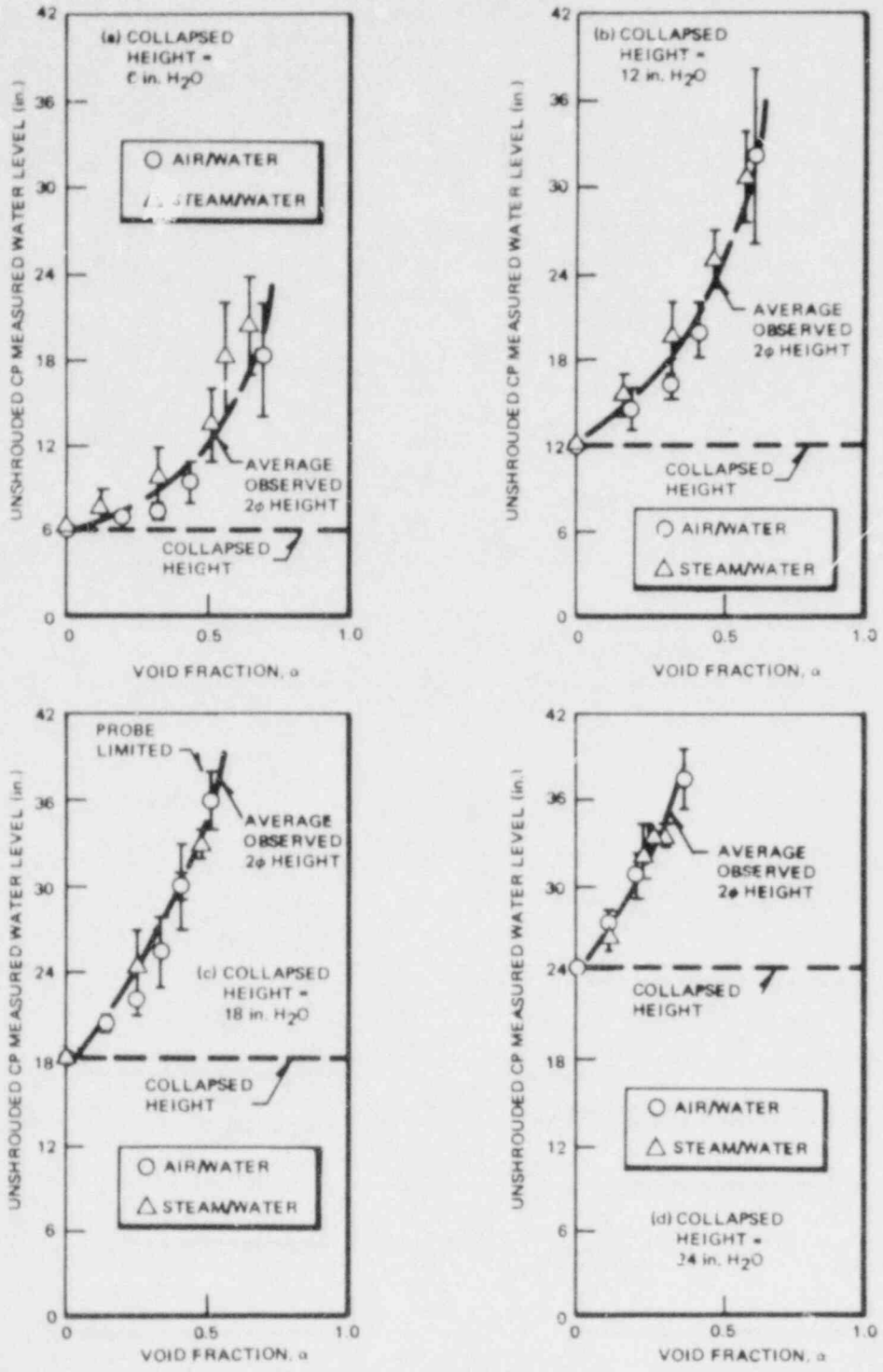

Figure C-17. Summary of Unshrouded Conductivity Probe Response in Air/Water and Steam/Water Mixtures

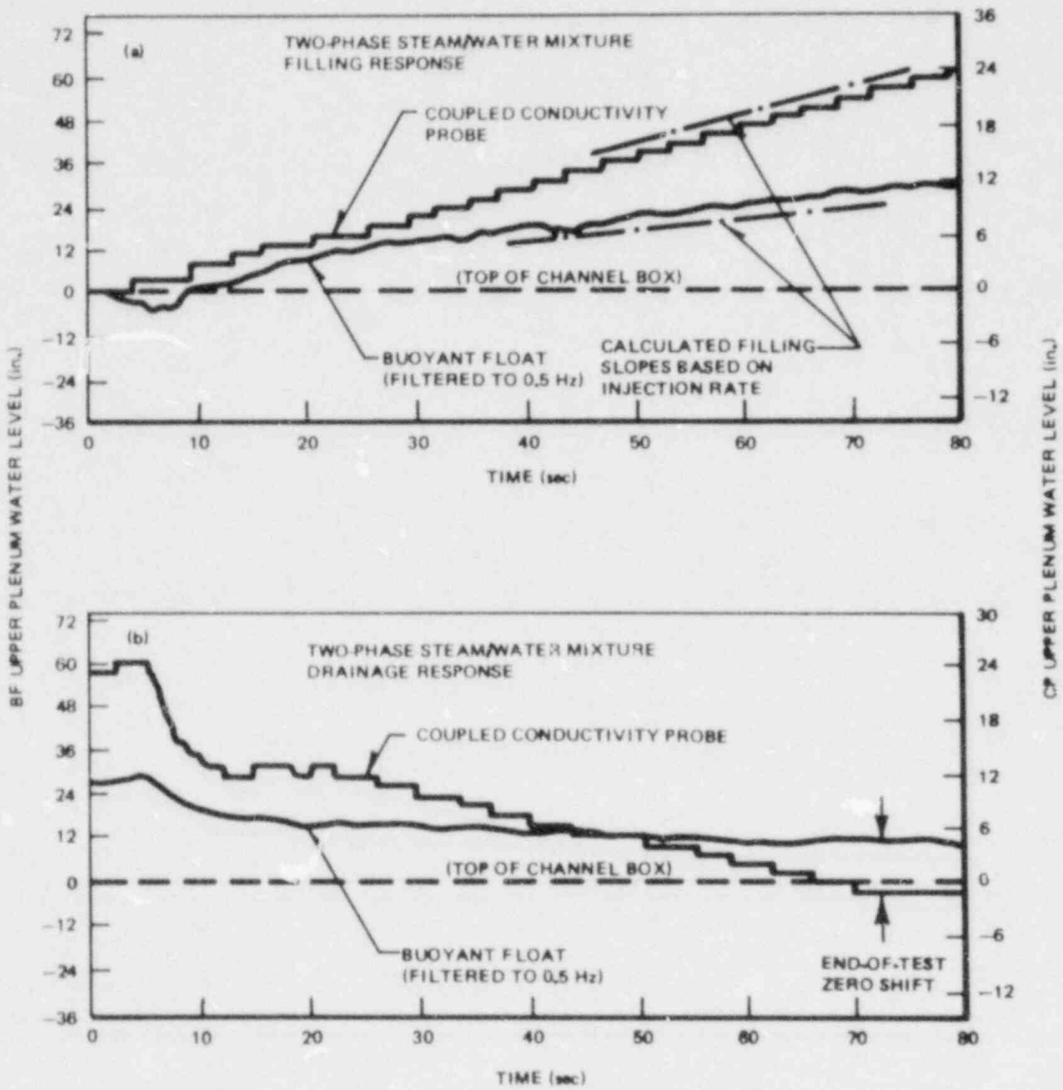

Figure C-18. Conductivity Probe and Buoyant Float Response to Filling and Draining Upper Plenum with Bubbly Steam/Water Mixture

lower-plenum sight gauge. In a few single-channel tests, channel-box steam was also input. Most of the tests were performed with the bypass region initially full of saturated water. The flashing of water in this region was also evident in these tests. The transient test matrix and data plots are included in Section C-7. The instrument response during these tests is summarized below.

C-4.3 COUPLED CONDUCTIVITY PROBE

In the transient tests, comparison of the upper-plenum pressure transducer and the shrouded coupled conductivity probe responses shows that during depressurization the coupled conductivity probe consistently gives a higher indicated water level than the pressure transducer. (Further, the indicated conductivity probe level is generally greater than the level observed with the upper-plenum sight gauge.) As the end of the depressurization is approached, the readings of the two instruments agree closely. This effect was demonstrated in Tests T-2 and T-3, for example. The difference between the two indications is probably due to flashing of the liquid in the shroud surrounding the coupled conductivity probe. As the liquid in the shroud flashes and swells, the two-phase mixture, confined to the tube, could wet most of the probes. As the flashing diminishes, both instruments begin to agree as they do in steady-state tests.

C-4.4 BUOYANT FLOAT

The principle of buoyant float has been proven in both steady-state and transient tests. As shown in the single- and two-phase filling tests of Figures C-6 and C-18, the original buoyant float exhibited some sticking (stick-slip friction) in its mechanism, in view of the fact that it did not return to its original zero upon draining unless tapped or vibrated. This sticking was also observed in some of the transient tests, during refill of the bypass region, as in Tests T4-2 and T4-7, for example. Redesign of the buoyant float instrument eliminated problems of stick-slip friction associated with the linkages in the initial design as discussed in Section C-3. The new design, in which the float was mounted perpendicular to the balance beam/strain gauge assembly, showed no difficulty in returning to its zero position. The response of the probe was such that the mean indicated level decreased to about 75 percent of the true collapsed level as a two-phase mixture covered the length of the float. This bias was because of the weight of water adhering to the surface of the float during repeated splashing.

The buoyant float exhibited a decrease in indicated level during the depressurization period. A qualitative correlation is that in tests where a large amount of

liquid was present in the upper plenum because of flashing effects (Tests T-2 and T-3, for example), the buoyant float indicated the largest initial decrease. In tests where a small amount of flashing occurred or a smaller amount of liquid was present in the upper plenum (Test T-11, for example), the buoyant float indicated a smaller initial decrease. In a depressurization with no water in the vessel, the buoyant float showed no decrease at all.

It was postulated that the observed decrease in the buoyant float indication is due to wetting of the upper portion of the float, above the level of the two-phase mixture. If we consider that liquid droplets or a film of liquid settle on the length of the probe above the two-phase mixture level, the weight of the liquid drops or a thick film represents a potential downward force negating part of the buoyant (upward) force on the float. As long as flashing entrains liquid into the upper plenum or injection spray is present, it is conceivable that any liquid which wets the buoyant float and runs off is continually replaced by more liquid.

The maximum buoyant force from the float (when it is completely submerged) is 8 ounches. We have observed what happens when a stream of liquid is squirted directly onto the initially dry float, near the top, and allowed to run off. In this crude test, a 5-percent decrease in the zero level was seen. This is less than the typical 20-percent decreases in indicated level early in Tests T-2 and T-3; however, the probe may not have been as fully wetted in the crude tests as during flashing and spray injection in the transient tests.

Given the hypothesis that liquid wetting the length of the buoyant float is responsible for the indicated level decreases observed, the effect should last as long as flashing is occurring (i.e., during the depressurization), and the greater the exposed length of the float above the two-phase mixture level, the greater the indicated decrement should be (assuming no additional liquid is supplied). In regard to the former, the buoyant float responds reasonably well after the period of depressurization has ended. In regard to the latter, Test T-8 shows that without injection of liquid the indicated decrement continues to increase as long as flashing is occurring. In tests like T-3 and T-9, with 8- and 20-gpm injection, this effect may have been offset by the added liquid mass.

In the four-channel Tests T4-2 and T4-7 where flashing does not deliver a two-phase mixture into the upper plenum for a prolonged period (the mixture spills into the plenum instead), the buoyant float agrees well with the upper-plenum pressure transucer.

To test the possible effect of liquid clinging to the probe, water was intentionally dribbled down the length of the probe by gently pouring it onto the float near its uppermost end. This was done crudely by using a syringe to squirt liquid onto the probe. As Figure C-19a shows, with most of the length of the probe exposed and able to be wetted, a deflection equivalent to -3 inches of measured collapsed level was obtained. Introducing water over shorter exposed lengths of the float gave smaller indicated decrements (Figures C-19b and C-19c). This is consistent with the observed trend toward smaller mean indication with increasing void fraction (or wetted length). Thus it is concluded that the process of splashing and churning (when the two-phase mixture covers the probe) wets the float in the mixture region, leading to the slightly larger decrements in mean value observed under certain conditions (Figure C-11).

One way to minimize the effect of water clinging to the float is to make the float larger in diameter. Wetting is related to surface area, while the buoyant force is proportional to the volume of the float; doubling the size of the float will cut the wetting effect in half.

Another way to correct the buoyant float (BF) output for splashing can be accomplished by using an unshrouded conductivity probe (CP) in conjunction with the buoyant float. As shown previously, the unshrouded conductivity probe indicates the local height of a two-phase mixture. The output of both instruments therefore can be used to estimate the local void fraction, and the buoyant float measurement of the collapsed level then can be corrected based on this estimate. A sample of this technique is discussed below.

Starting with a collapsed level of 12 inches of water in the calibration vessel, mixtures of various heights were generated and both the buoyant float and conductivity probe measurements made at the same time. The open circles and open triangles in Figure C-20 show the results for the conductivity probe and the buoyant float, respectively. The conductivity probe measures the approximate two-phase mixture height. The mean value of the buoyant float measurement is slightly less than the collapsed level as α increases, as has been discussed above.

The void fraction can be estimated by taking

$$\alpha \approx \frac{\text{(Mean CP Indication)} - \text{(Mean BF Indication)}}{\text{(Mean CP Indication)}}$$

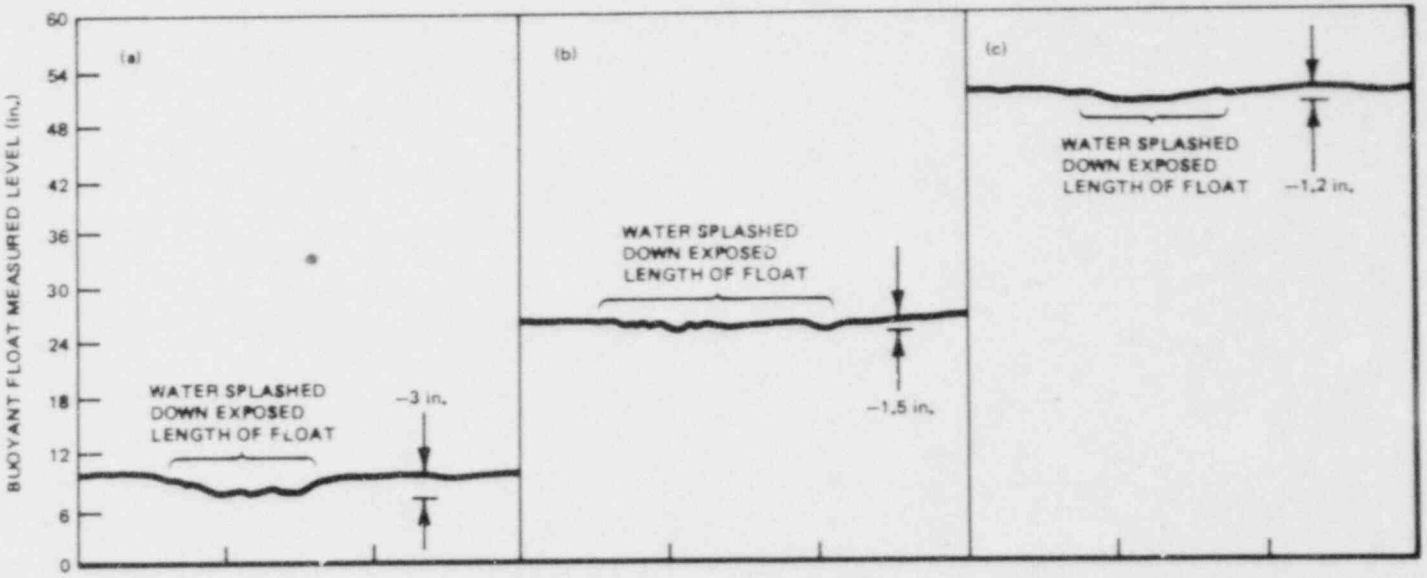

Figure C-19. Effect of Wetting on Buoyant Float Response

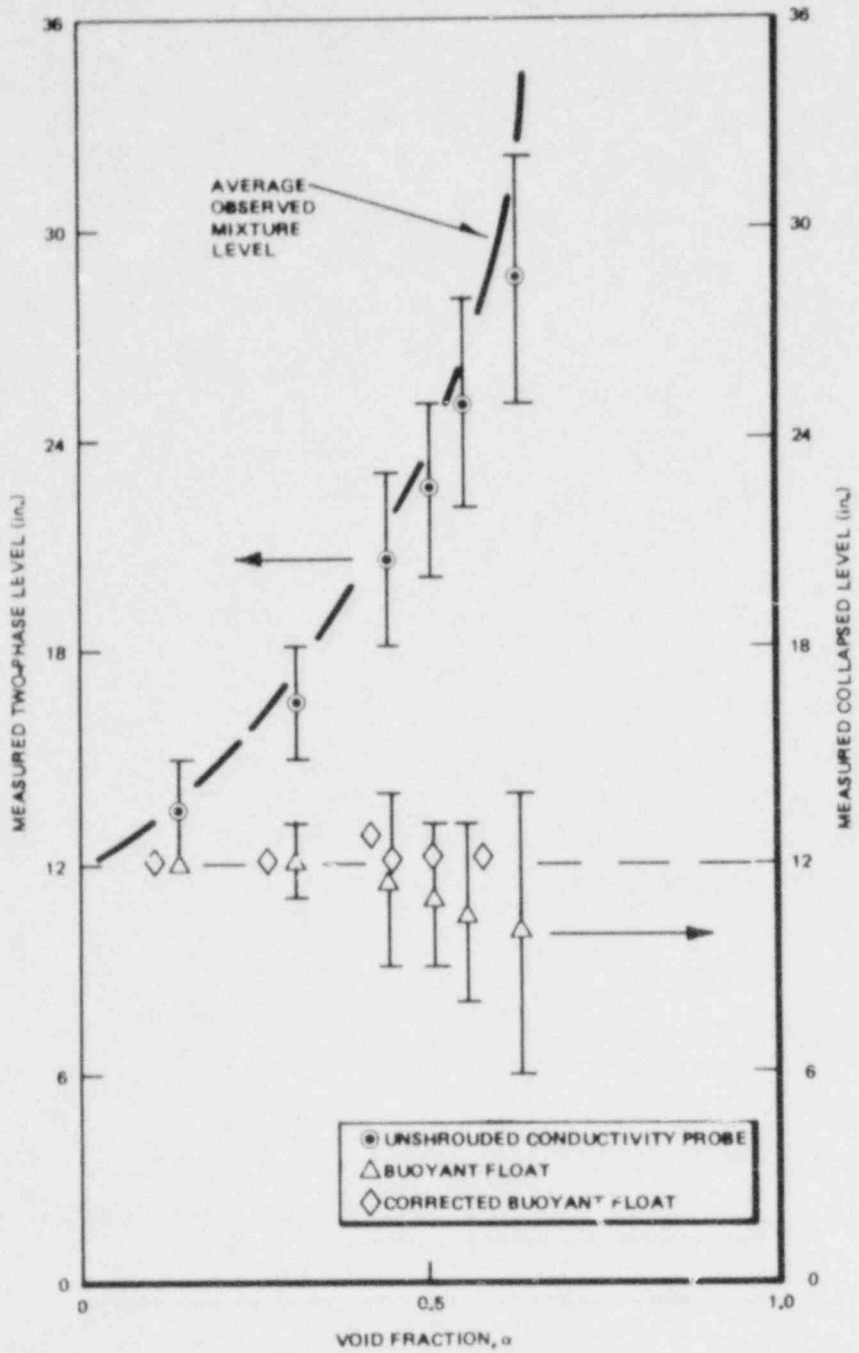

Figure C-20. Correction of Buoyant Float Output Using Buoyant Float and Coupled Conductivity Probe Together

For example, for the largest two-phase height data point of Figure C-20,

$$\alpha = \frac{28.5 \text{ in.} - 10 \text{ in.}}{28.5 \text{ in.}} = 0.65$$

This value is calculated from the outputs of the two instruments. The α values of the ordinate of Figure C-20 for the open symbols were measured from visual observations through the glass vessel.

Based on the buoyant float measured response in the calibration vessel (open triangles in Figure C-19), one can determine an algorithm for a correction for factor as a function of α which multiplies the mean indicated collapsed level to better approximate the true collapsed level. For the data in Figure C-19, we have used the algorithm*

$$BF_{corr} = \gamma \cdot BF_{indicated}$$

where

$$\gamma = \begin{cases} 1 \text{ for } 0 < \alpha < 0.3 \\ 0.6\alpha + 0.82 \text{ for } \alpha > 0.3 \end{cases}$$

For the case of the largest two-phase height data point, then, we have α=0.65 estimated above and γ=1.21 for the correction from the equation above, so the corrected measurement is 1.21x10 inches or 12.1 inches. The void fraction based on the corrected collapsed level is then

$$\alpha_C = \frac{28.5 \text{ in.} - 12.1 \text{ in.}}{28.5 \text{ in.}} = 0.58$$

which is slightly lower than the value α= 0.63 based on visual observations (because the mean value from the conductivity probe is slightly low). The corrected collapsed levels are plotted as the solid triangles in Figure C-20 against the void fraction based on the corrected collapsed level. It is seen that this technique of using both instruments in conjunction can lead to reasonable calculations of the true collapsed level (or liquid mass) at higher void fractions.

*The buoyant float data have shown that the same correction factor may be applied at a given α independent of the collapsed liquid level (Figure C-11).

C-4.5 PRESSURE TRANSDUCERS

In the transient tests it was observed that if the pressure transducer output were filtered and if the pressure lines were filled with subcooled liquid, the channel box and upper and lower plenum pressure transducers performed well. The purpose of the filtering was to diminish the effect of any oscillations caused by condensation. The purpose of filling the pressure lines with subcooled liquid was to prevent flashing in those lines.

C-5 BUOYANT FLOAT DESIGN CONSIDERATIONS AND ELECTRONICS SCHEMATICS

This section details the design considerations employed in the conceptualization and execution of the buoyant float probe built and tested by Creare. Included are the schematics for signal conditioning electronics and readout interface definition.

C-5.1 INTRODUCTION

The need addressed by this probe development effort is that of measuring time-varying liquid mass inventory in the various volumetric nodes of a vessel under nonuniform two-phase flow conditions.

The measurement environment is steam and water under both steady and transient conditions at pressures from 150 psia to atmospheric and temperatures at the corresponding saturation values.

Because of accessability limitations internal to the vessel, any instrument addressing this measurement need must combine with the requisite accuracy a high degree of reliability and durability for all in-vessel components.

C-5.2 CONCEPT OF THE BUOYANT FLOAT PROBE

This probe falls in the conceptual class of instruments driven by the vertically integrated mass of the fluid environment under the influence of a gravitational field - that is, the static pressure differential between the bottom and the top of the environment. It is therefore conceptually identical to a differential pressure transducer. In fact, the buoyant float probe is simply a differential pressure transducer with a very thick diaphragm or piston.

The top-to-bottom static pressure differential in a fluid cell caused by the fluid's weight may be expressed as:

$$\Delta P = g \int_{T}^{B} \rho(z)da \qquad \text{(C-1)}$$

Similarly, the buoyant force exerted on a body immersed in the environment (and extending over its full vertical length) may be expressed as the weight of fluid displaced by the body:

$$F_B = g \int_{T}^{B} \rho(z)A(z)da \qquad \text{(C-2)}$$

where A(z) is the horizontal cross-sectional area of the body as a function of elevation. For A(z) = const. = $\pi D^2/4$; i.e., a closed tubular vertical axis body of Diameter D, Equation C-2 reduces to Equation C-1. The buoyant force is equivalent to the differential pressure acting on the end caps of the tubular float, analogous to the diaphragm of a standard differential pressure transducer.

The buoyant float probe is therefore a differential pressure transducer which eliminates the one significant drawback of a conventional ΔP cell for this application: flashing in the fluid signal lines during depressurization transients.

In inferring a collapsed liquid level from a ΔP (or force) measurement, both a ΔP cell and the buoyant float probe neglect the weight of the steam, the density of which is two to three orders of magnitude below that of the liquid phase. Further, application of both devices assumes no horizontal pressure gradients over the cross section of the region of measurement applicability.

Both types of device allow the force arising from fluid differential pressure, or weight, to act against a grounded spring element and transduce the deflection of that element into a convenient signal for readout. As with many ΔP cells, the buoyant float probe accomplishes this by means of strain gauges affixed to the spring element.

A force balance on the buoyant float probe sums the probe weight, the weight of displaced fluid, and the viscous drag of any liquid moving vertically in the

vicinity of the float surface. This last term is unique to the buoyant float and is a disadvantage in its variability, although its magnitude is minor. Any liquid splashed on the float surface in a nominally gas-phased region will drain down the surface, its weight added to that of the probe. Conversely, net liquid phase upward motion during the level swell associated with a blowdown transient will add a viscous drag to the buoyant float. It should be noted that the significance of this effect relative to the buoyant float decreases as 1/D as float diameter is increased.

C-5.3 CONCEPT EXECUTION

The design of the buoyant float probe was influenced by the initial choice of geometric constraints perhaps more strongly than by any other single factor. This choice followed from the three potential application zones for the instrument: the upper plenum/clearance region, the lower plenum, and the channel box. The channel box was seen as the geometrically most demanding zone because instrument blockage and CCF characteristics could not be atypical of those of the channel interrals without risk of influencing test results. Float diameter was therefore chosen at 0.50 inch to closely replicate a fuel rod. The probe could then literally hide a simulated fuel rod bundle.

Float wall thickness was set at 20 Ga (0.0355 inch) on the bases of adequate pressurization capability (internal and external), robustness for mishandling, ready availability, and light weight. The 60-in.-long float, built and tested in the Creare facility, weighed 1.0 pound with end plugs. Type 304 stainless steel was employed throughout (excepting the spring element) for its general corrosion resistance.

The second major constraint on the design of the instrument was the limited availability of appropriate strain gauges for sensing spring element deflection. Given the high environmental temperatures and the desirability of eliminating coolant lines to the instrument, weldable strain gauges were deemed a necessity for reliable bonding. Also, since any scheme enclosing the strain gauges in a dry, sealed enclosure makes the apparent float force a function of environmental pressure, it was desirable to employ hermetically sealed strain gauges exposed to the environment.

The gauges chosen for this application from the limited selection meeting the specification requirements were AILTECH Type 128 SGs. These employ nichrome Alloy

filaments sheathed in 321 SS outer tubes packed tightly with magnesium oxide powder. To the length of the outer tube is welded a flat strip flange, which in turn is welded to the straining element. Strain of the flange and sheath is transmitted to the filament by the packed MgO powder via shear stress while electrical isolation of the filament is maintained. The thermal coefficient of resistivity of the filament is adjusted by heat treatment to cancel the apparent strain caused by differential thermal expansion of the specimen and the filament over the temperature range of interest, in this case ambient to 365°F.

The geometry of the gauges dictated that the spring element be flat strip stock, and a cantilever beam arrangement was selected for its symmetry, linearity, and ease of manufacture. One strain gauge was affixed to each side of the beam and wired to a Wheatstone Bridge with two active arms, providing an additional margin of temperature compensation for both gauges and leads as well as doubling sensitivity. Also, the mounting symmetry with respect to heat transfer and the use of thin beam and gauge materials with low-heat capacity and high diffusivity were deemed desirable to minimize temperature differences between the two gauge filaments during transients in ambient temperature. The design therefore addressed thermal stability criteria in both the steady and transient modes of operation.

The bridge output is amplified and filtered to remove vibrational signals from the lightly damped spring/mass mechanical system, as indicated in the attached schematic Figure C-21 and the accompanying Table C-3. Amplification was selected on the basis of strain range for a 60-in. float and the visicorder galvanometer sensitivity.

The float and spring element may be tailored easily to alternate applications with differing range and sensitivity requirements in two-phase zones where liquid mass measurement is the objective. The strain gauges on the existing prototype are usable to 650°F, and replacement with platinum-tungsten alloy filament gauges can extend the range to 950°F or 1200°F.

C-6 DESCRIPTION OF CREARE'S COUPLED CONDUCTIVITY PROBE SYSTEMS

The purpose of this section is to provide a brief description of the coupled conductivity probe system developed at Creare and tested as a two-phase level and liquid mass measuring means.

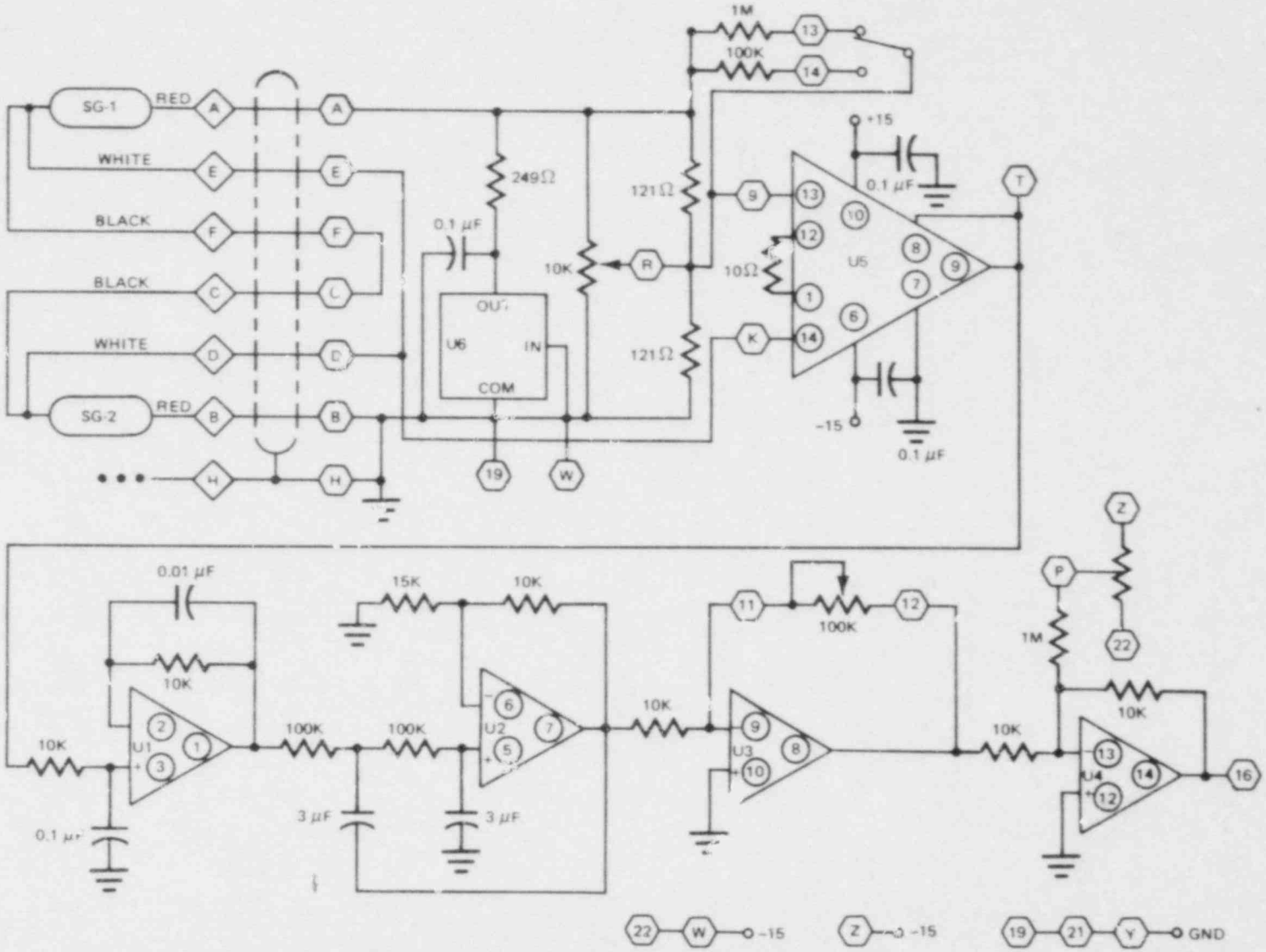

Figure C-21. Strain Gauge Bridge Amplifier Schematic

Table C-3

NOTES FOR SGBA ELECTRONICS

SG-1 = AILTECH Type 128

SG-2 = AILTECH Type 128

◇ - Represents male/female Amphenol Hexagon Connectors

⬡ - Represents finger connections on Vector #3662 board

○ - Represents IC pin numbers

U_{1-4} = TL 084 OPAMPS (Texas Instruments)

U_5 = B.B. 3626 Instrumentation AMP (Burr-Brown)

U_6 = µA 7806 UC Voltage Regulator (Fairchild)

All resistors 1%

OPAMP power +15 (pin 4) and -15 (pin 11) bypassed by .1µF capacitors.

Power supply bypassing was with 6.8µF capacitors.

All potentiometers are 10-turn precision types.

The 3µF capacitors (2) control the bandwidth of the amplifier.

A shrouded version of the coupled conductivity probe system, designed to measure collapsed liquid level, was described in Section C-3. The basic system, designed to measure the transient water level in a certain volume, is described herein. This system consists of a series of sensing elements and triggering circuitry which responds in an on-off fashion and combines the individual signals to produce a single output to a data recorder. This output is directly proportional to the number of probes wetted. This system involves four principal elements:

a. A series of conductivity probes consisting of a ground bar and numerous exposed electrical contacts separated from the ground bar by about 1/2 inch of nonwetting insulating material (Teflon).

b. Circuitry which sensed whether the conductivity between any probe and ground is greater than or less than a predetermined value.

c. Circuitry which provides a known, fixed voltage level to a summing circuit if the conductivity at any probe is greater than the predetermined triggering value.

d. Circuitry which sums the voltage level of each probe circuit and outputs the total voltage to a suitable recording device.

Because the conductivity of water is a function of temperature and concentration of dissolved salts and other materials, a device whose output is proportional to the conductivity of water was unacceptable for the desired purposes. Thus, our system was designed to electronically replicate mechanical on-off circuitry; if the conductivity at a given probe is greater than a predetermined value, a known, fixed voltage, independent of the conductivity at this probe, is added to the output signal. Because under normal conditions the conductivities of water and steam are sufficiently different, this system can be made extremely reliable and fast-responding. However, in certain high-grade reactor experiments utilizing high-pressure steam and very pure water, the difference in conductivities between the liquid and vapor phase may need to be examined before utilizing this system. This has not been done, but for all the applications in which this system has been employed to date, the relative conductivities have been sufficiently different to achieve excellent performance.

A circuit diagram, the power supply system, and three of the array of conductivity probes are shown in Figure C-22.

Table C-4 lists several of the components utilized in the present Creare system. Alternate components accomplishing essentially the same function should certainly be acceptable.

Operating experience has shown that the individual probes need to be reconditioned after about six months of moderate to heavy use. The reason for this is that, depending upon whether the probes are at a positive or negative voltage with respect to ground, electrolytic corrosion or the plating out of electrolytic salts on individual probes occurs and prevents them from responding. Another user's experience will depend upon the materials chosen for the probes and the purity of the water.

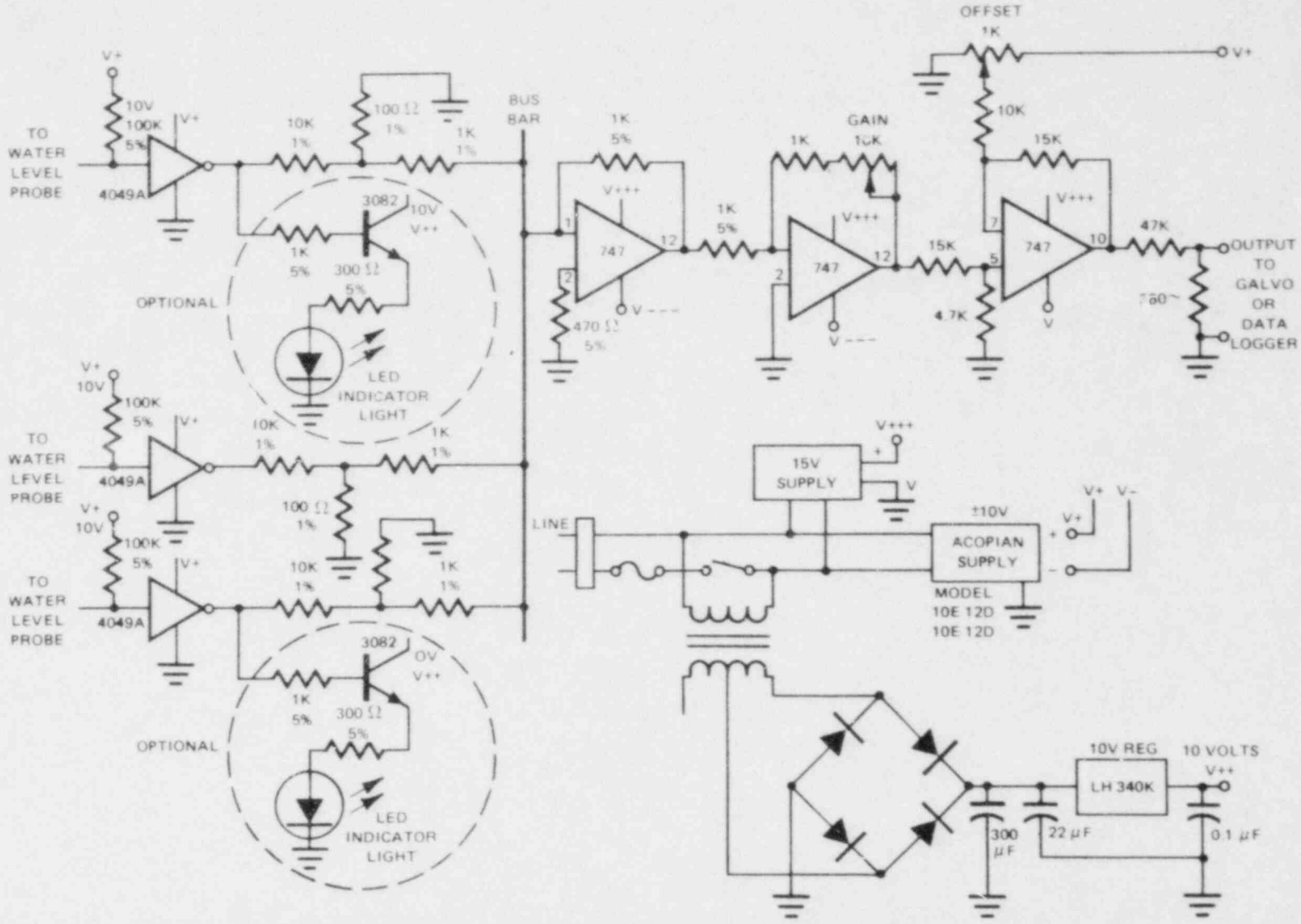

Figure C-22. Coupled Conductivity Probe Amplifier Schematic

Table C-4

CREARE WATER LEVEL ELECTRONICS—
GUIDE TO SOME OF THE COMPONENTS

4049A	Solid State Scientific #SCL 4049AE (6 CMOS Hex Inverting Buffers per Plastic Dip)
*3082	Linear Transistor Arrays RCA Part No. CA3082
742	Fairchild Operation Amp. #747 HC
Potentiometer	10KΩ AB #NP103U
	1KΩ AB #NP102U
*LED Light	Chicago Miniature #CM4-23

*Optional

C-7 TRANSIENT TEST MATRIX AND DATA PLOTS

The transient test matrix is presented below, in Table C-5, followed by transient test data Figures C-23 through C-40.

Table C-5

TRANSIENT TEST MATRIX

Test #	Injection Location	Nominal Initial Test Pressure (PSIA)	Initial Plenum Water Height (in)	Bypass Region	Q_f (gpm)	T_f (°F)
Single						
T-2	None	55	13.5	Filled	8	91
T-3	None	95	13.5	Filled	8	85
T-4	None	120	13.5	Filled	8	91
T-5	None	95	0	Filled	8	89
T-6[a]	None	95	0	Filled	8	86
T-7	None	95	13.5	Empty	8	88
T-8	None	95	13.5	Filled	0	88
T-9	None	95	13.5	Filled	20	85
T-10	None	95	37.5	Filled	8	90
T-11[b]	None	95	13.5	Filled	8	85
T-12	Channel (WgCB=0.25 lbm/sec	55	13.5	Filled	8	89
T-13	Channel (WgCB=0.29 lbm/sec)	55	13.5	Filled	8	88
Four						
T4-1	None	55	13.5	Filled	20	89
T4-2	None	95	13.5	Filled	20	91
R4-3	None	95	37.5	Filled	20	93
R4-4	None	95	0	Filled	20	92
T4-5	None	95	13.5	Filled	0	92
T4-6	None	95	13.5	Filled	8	85
T4-7	None	120	13.5	Filled	20	88
T4-8[c]	None	55	13.5	Filled	20	86
T4-9[d]	None	120	13.5	Filled	20	89

[a] Repeat of Test T-5 (identical results not shown).
[b] Slow depressurization.
[c] Like T4-1 except fuel rod mounting holes plugged (identical results not shown).
[d] Like T4-6 except fuel rod mounting holes plugged (identical results not shown).

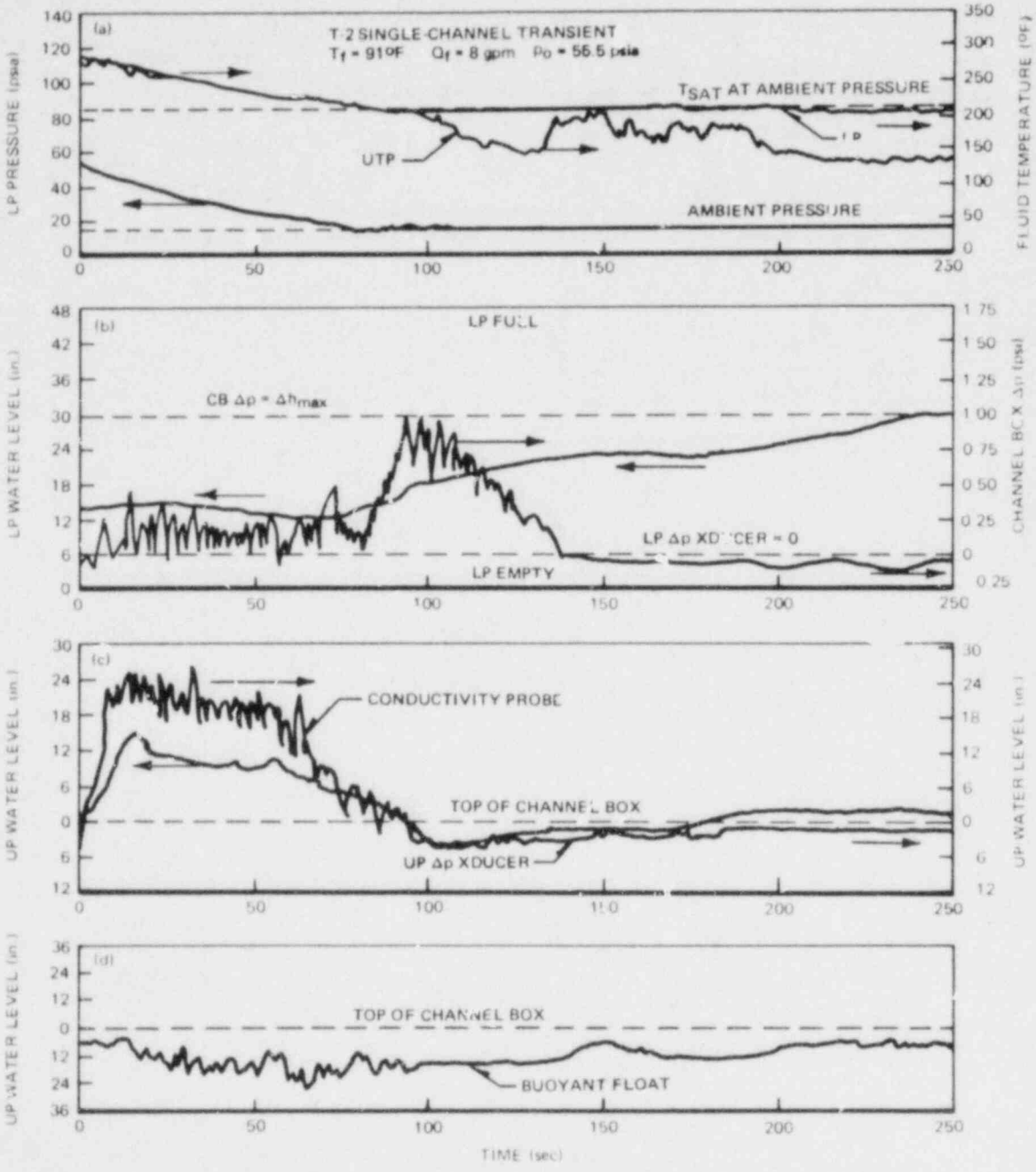

Figure C-23. Single-Channel Transient with 55 psia Initial Pressure

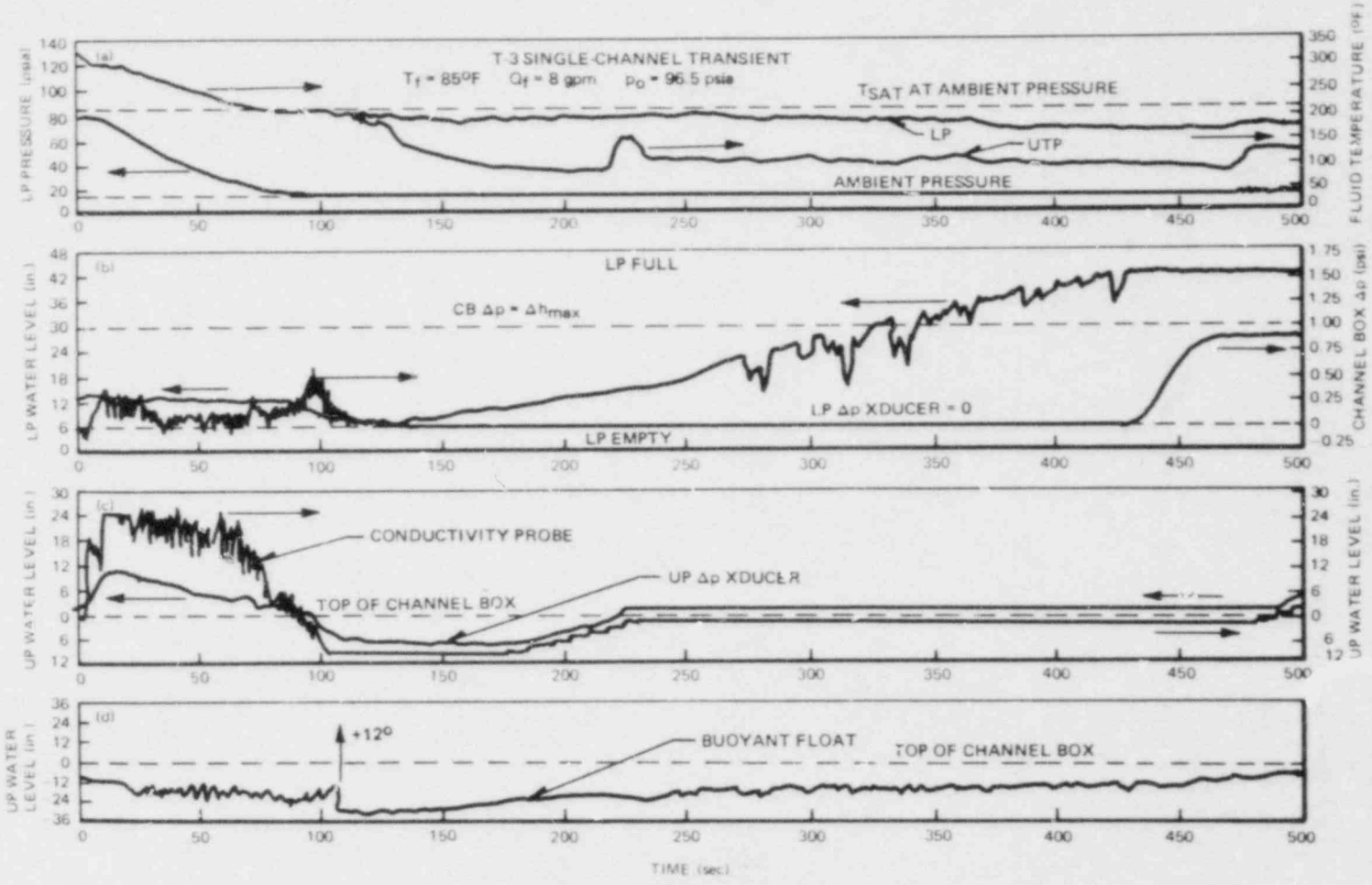

Figure C-24. Single-Channel Transient with 95 psia Initial Pressure

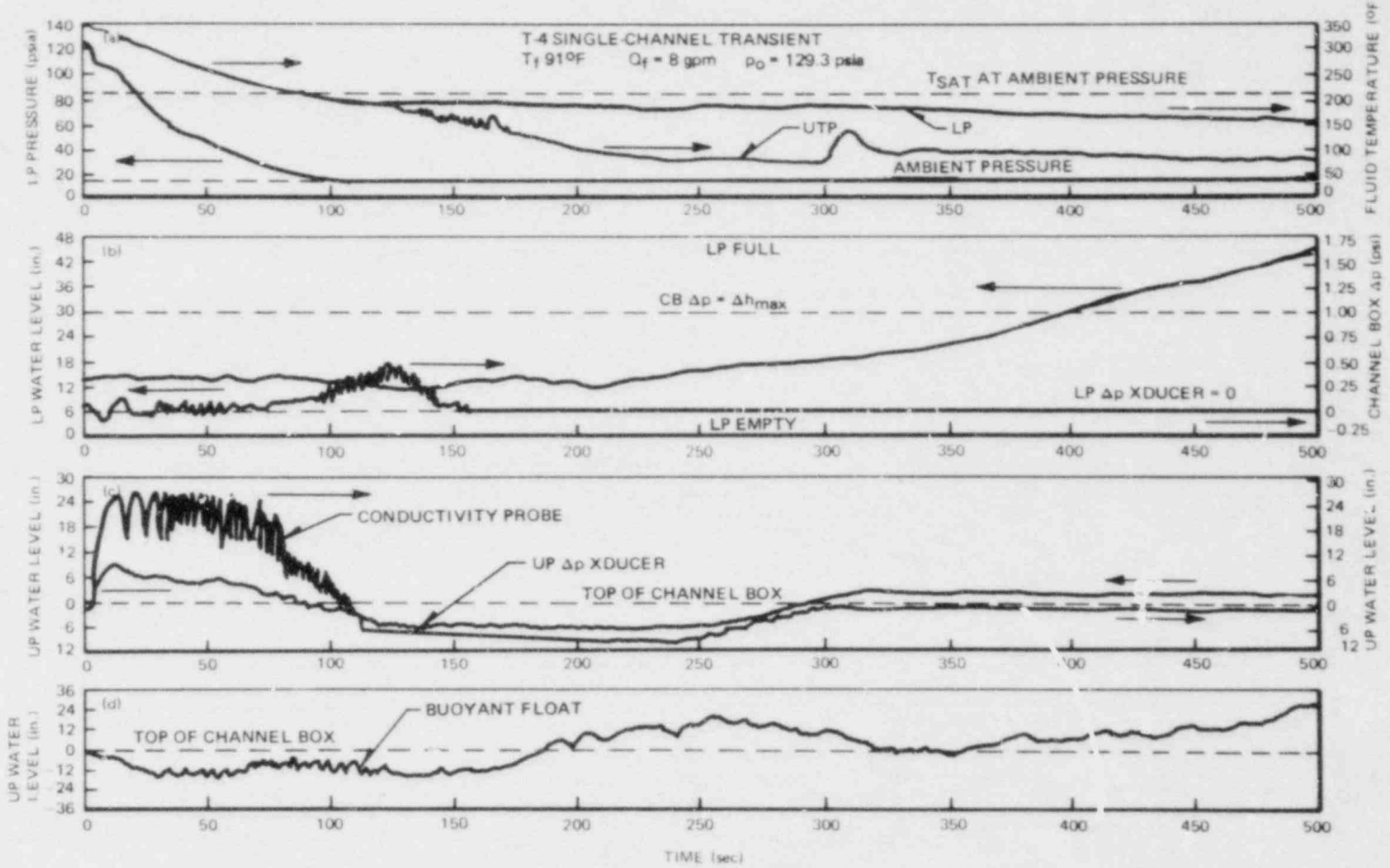

Figure C-25. Single-Channel Transient with 120 psia Initial Pressure

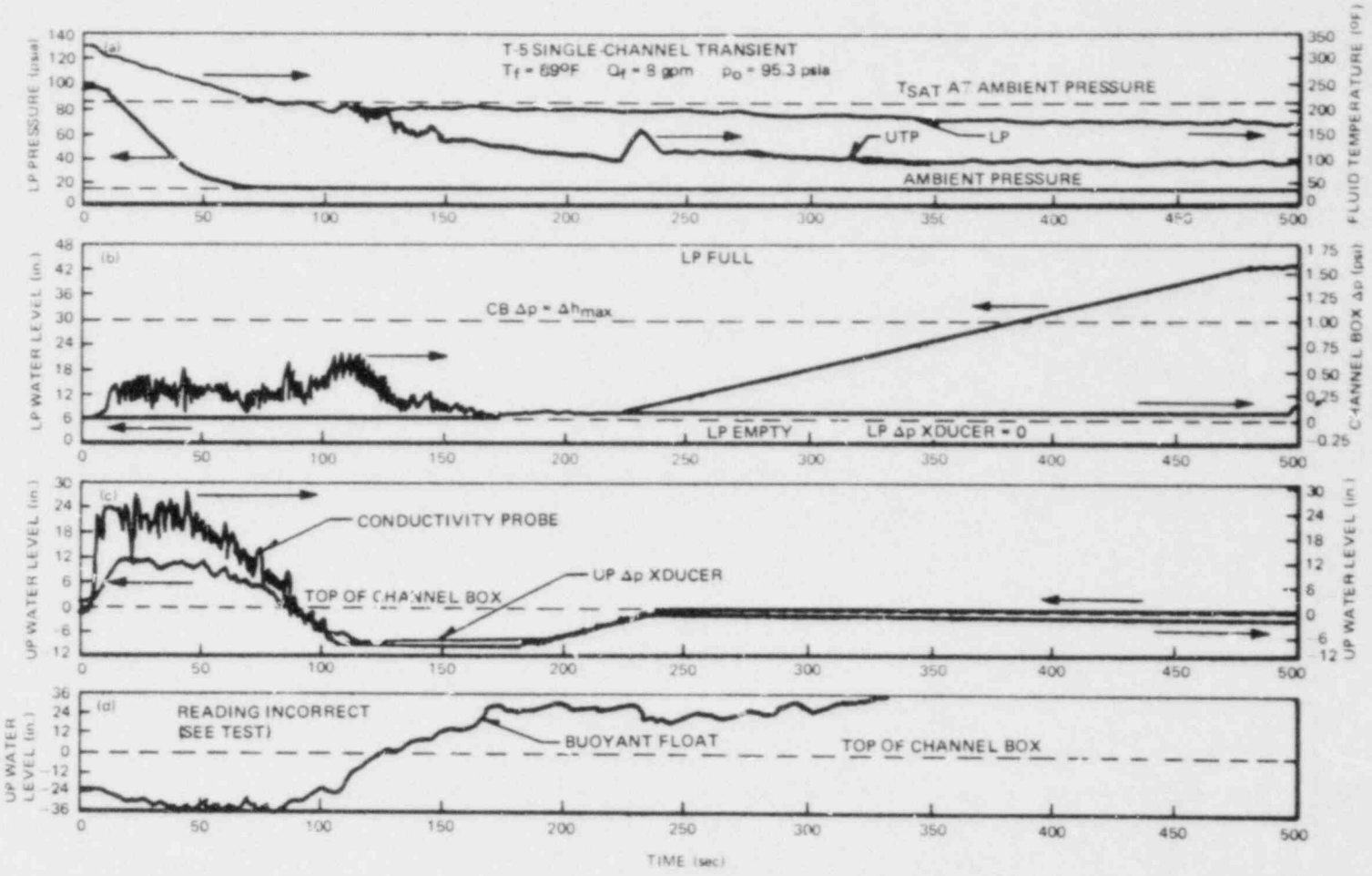

Figure C-26. Single-Channel Transient with Initially Empty Lower Plenum (95 psia Initial Pressure)

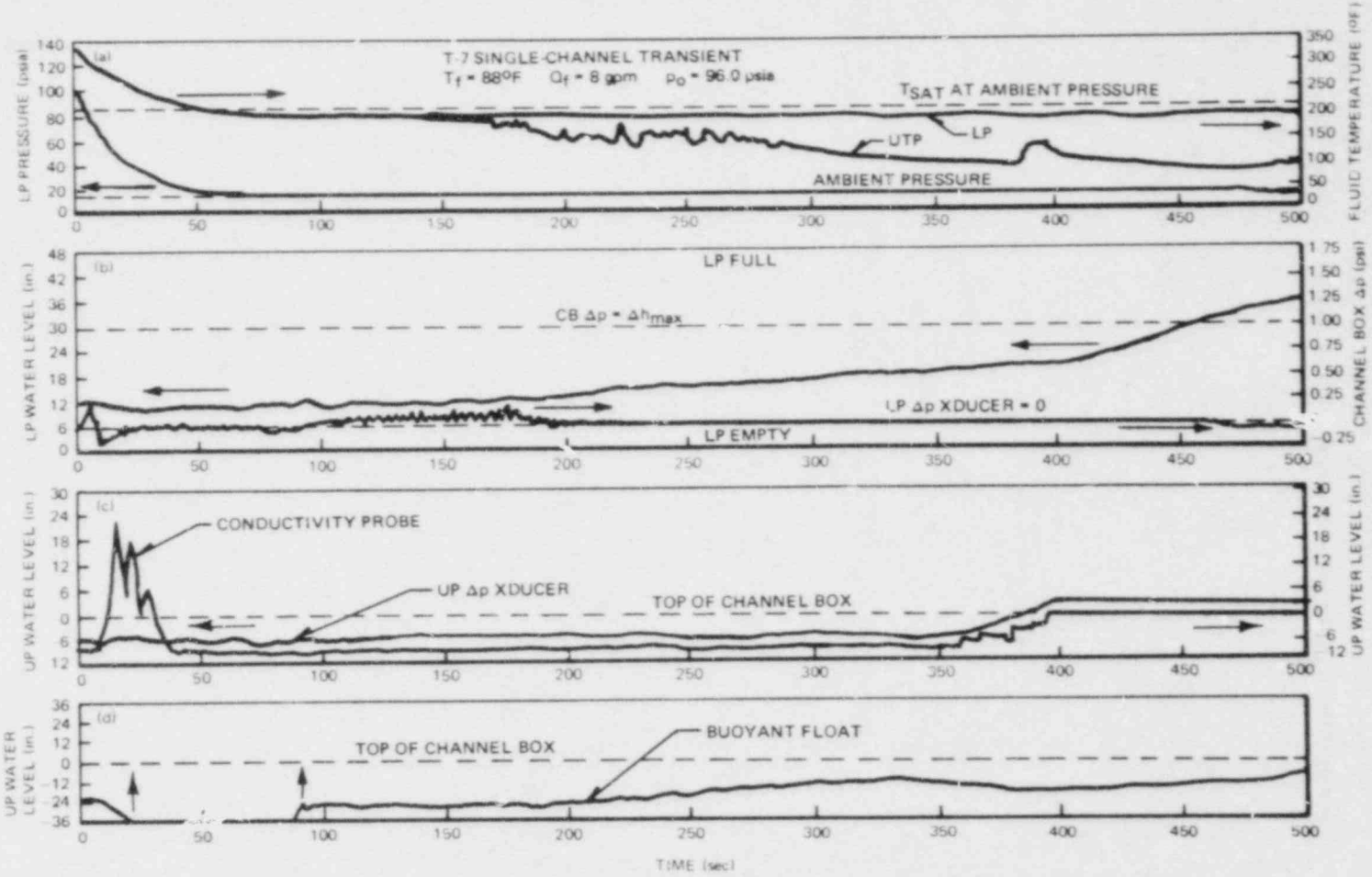

Figure C-27. Single-Channel Transient with Initial Plenum Water Height of 13.5 in. (95 psia Initial Pressure)

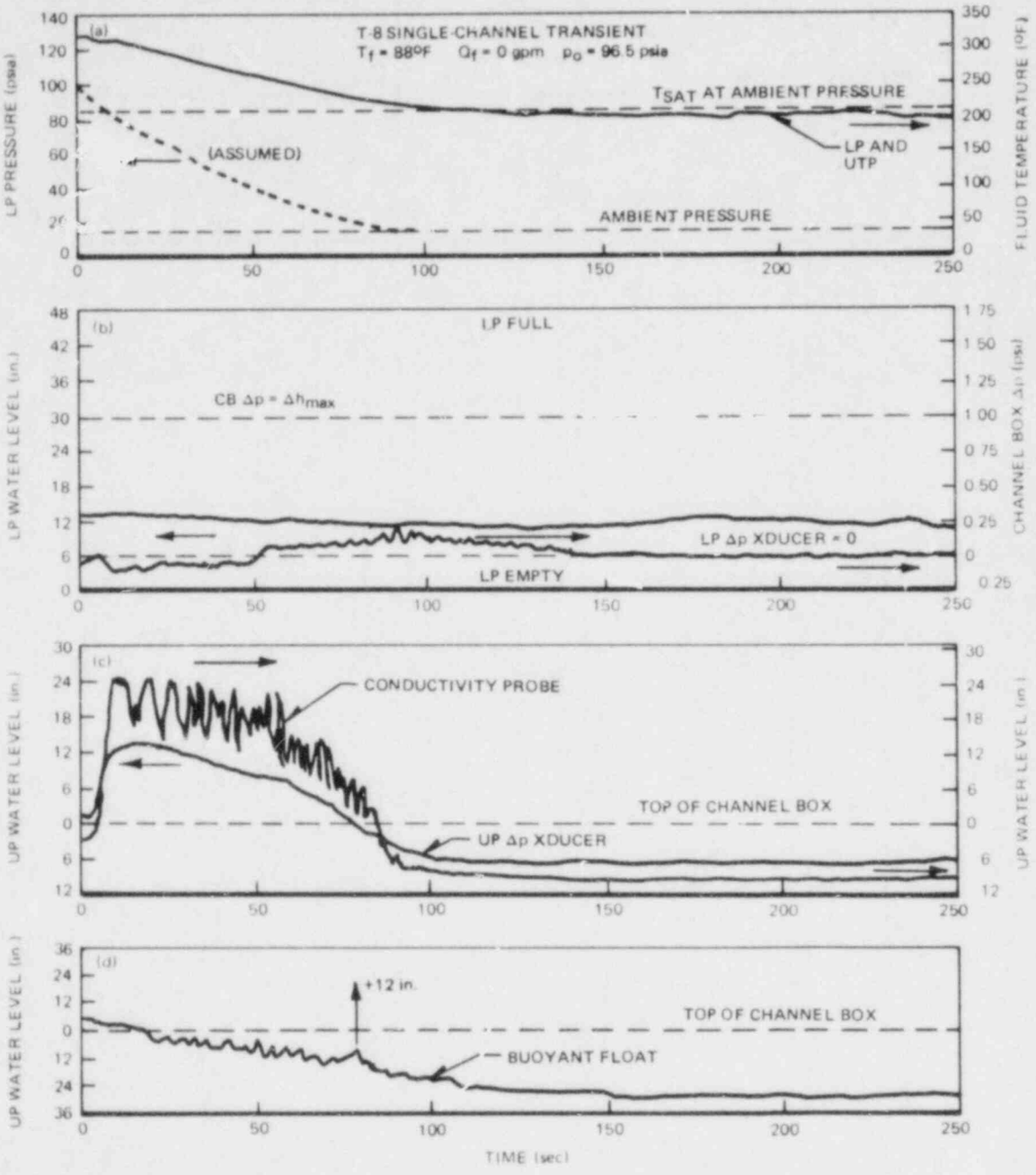

Figure C-28. Single-Channel Transient without Spray Injection (95 psia Initial Pressure)

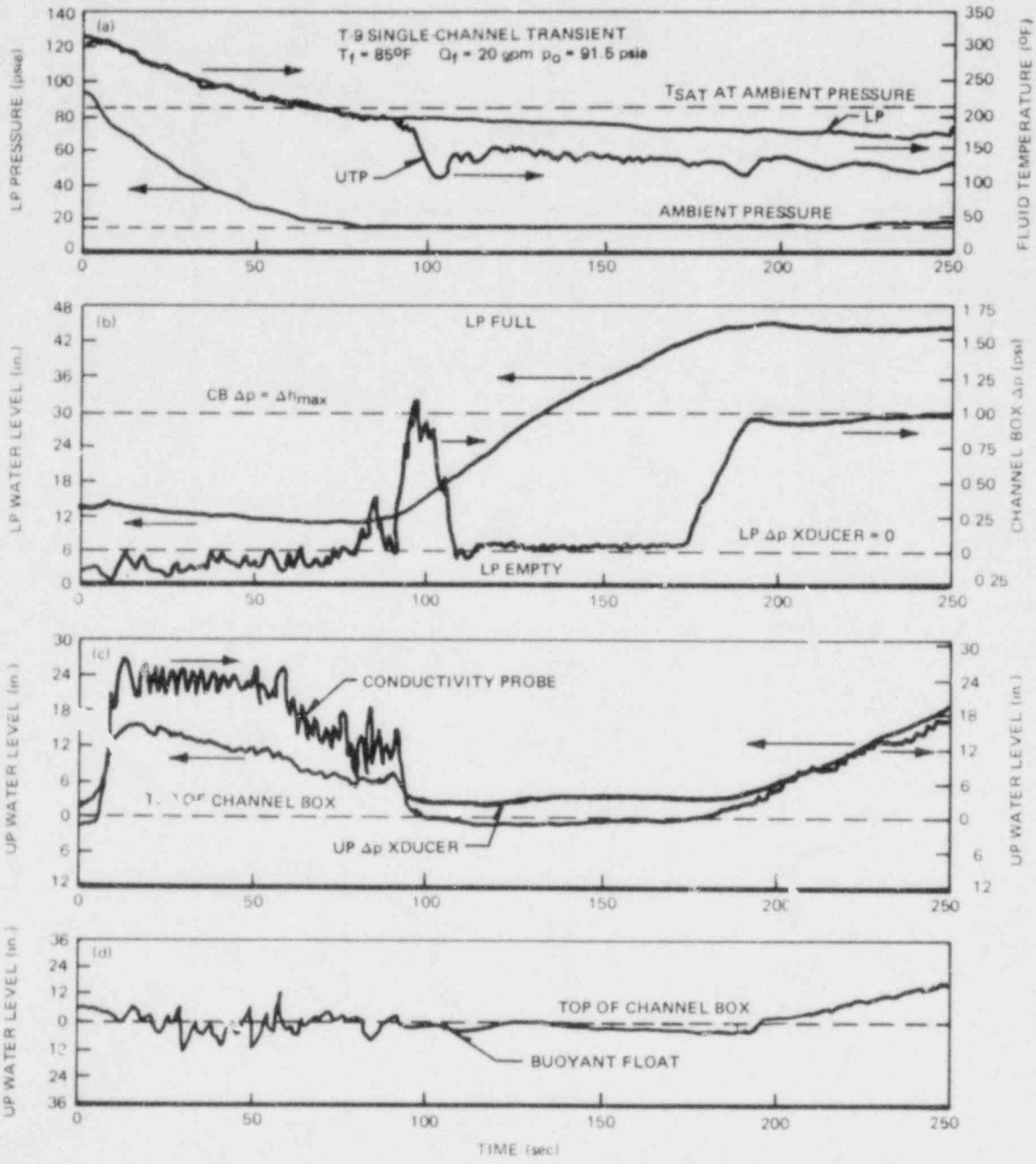

Figure C-29. Single-Channel Transient with 20 gpm Injection (95 psia Initial Pressure)

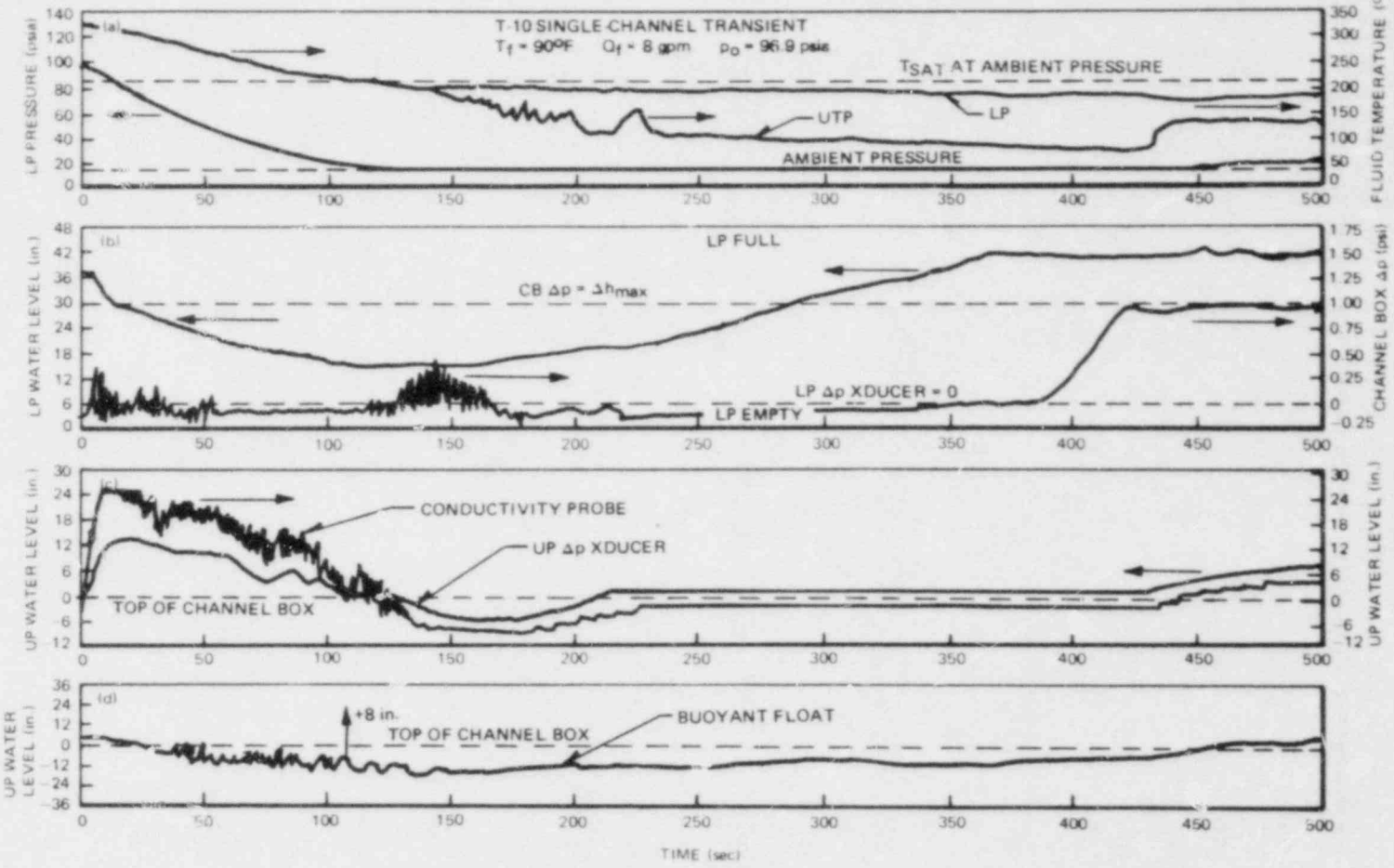

Figure C-30. Single-Channel Transient with Increased Initial Inventory (95 psia Initial Pressure)

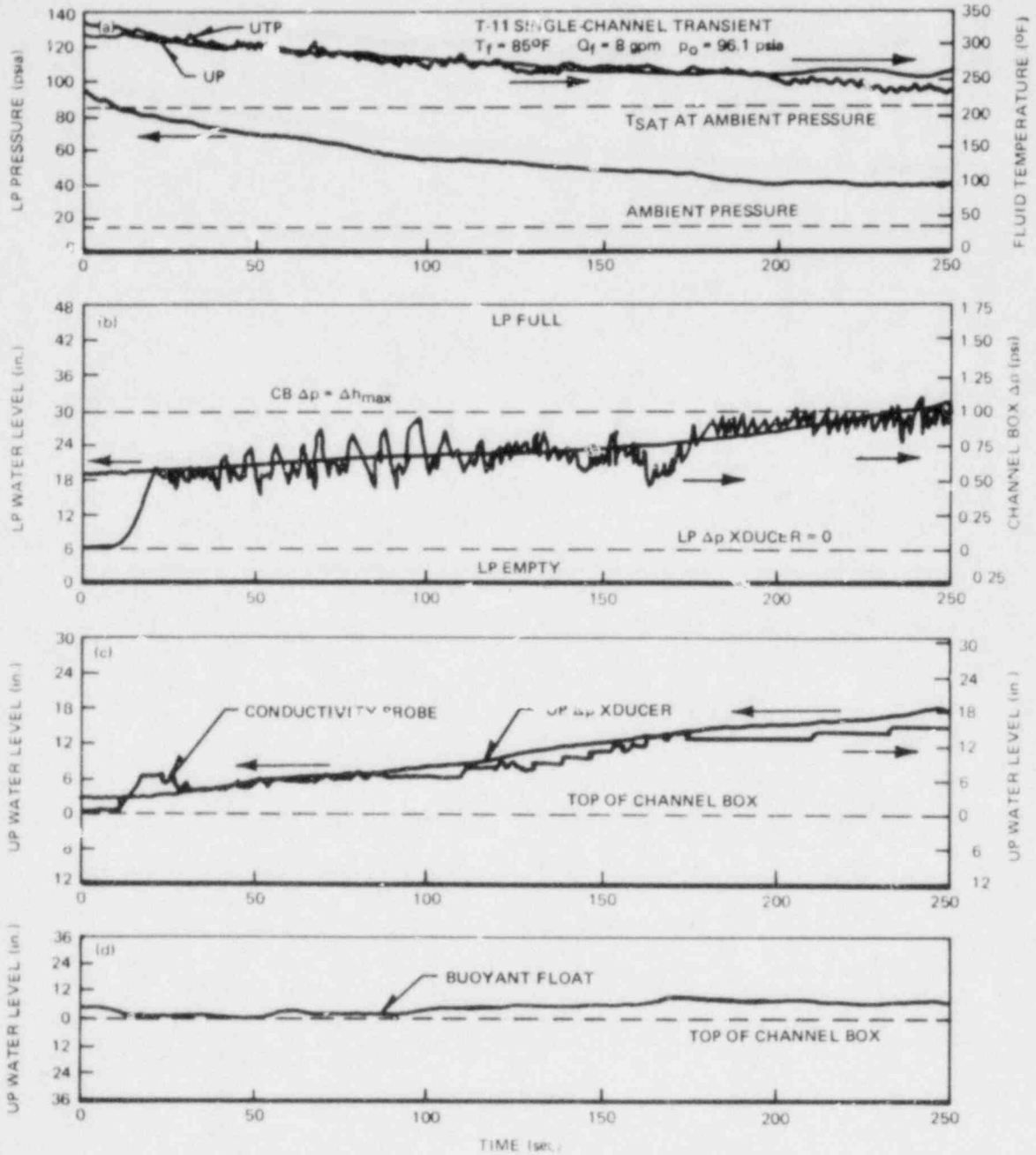

Figure C-31. Single-Channel Transient with Slow Depressurization from 95 psia Initial Pressure

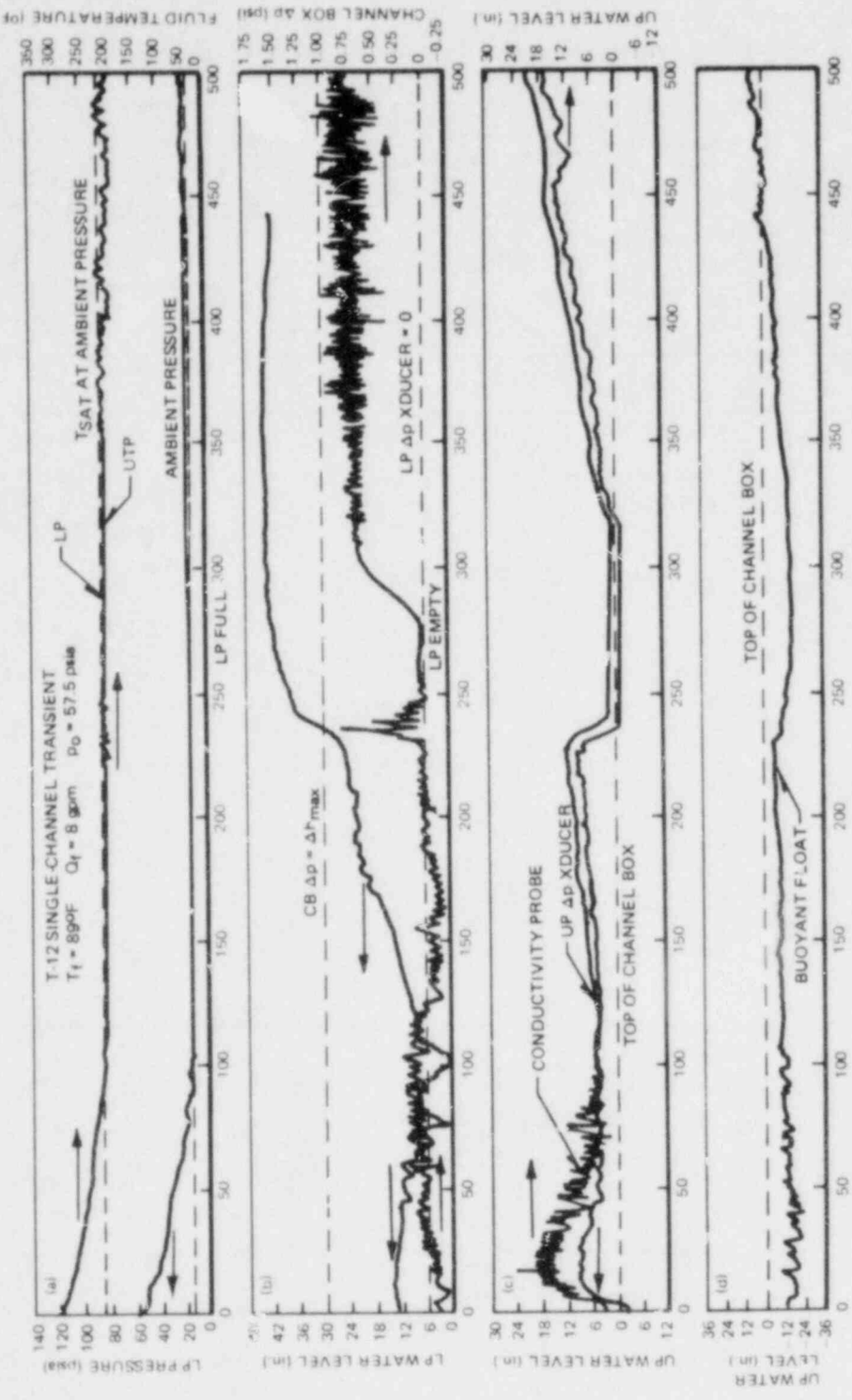

Figure C-32. Single-Channel Transient with 55 psia Initial Pressure

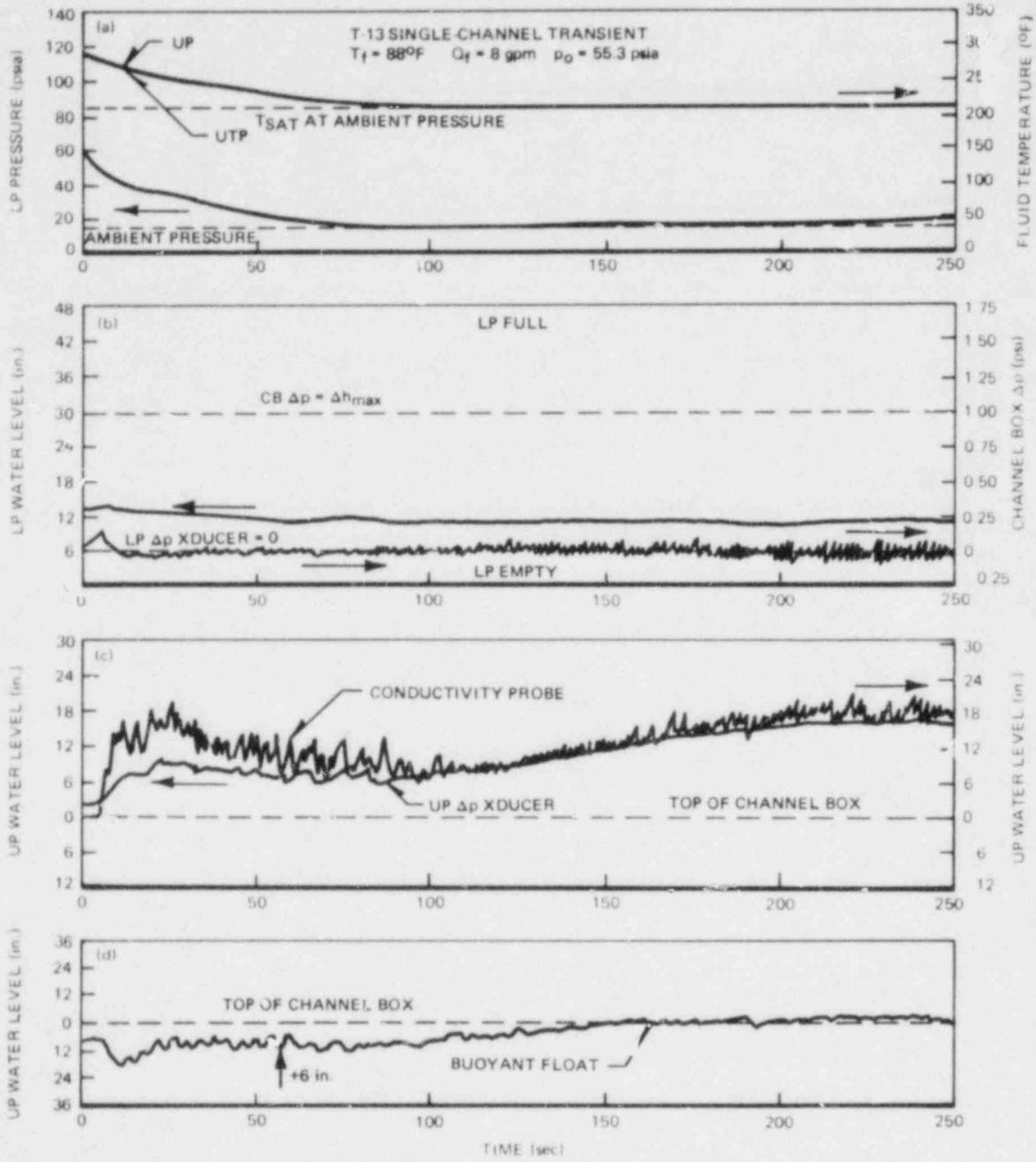

Figure C-33. Single-Channel Transient with Channel Box Steam (95 psia Initial Pressure)

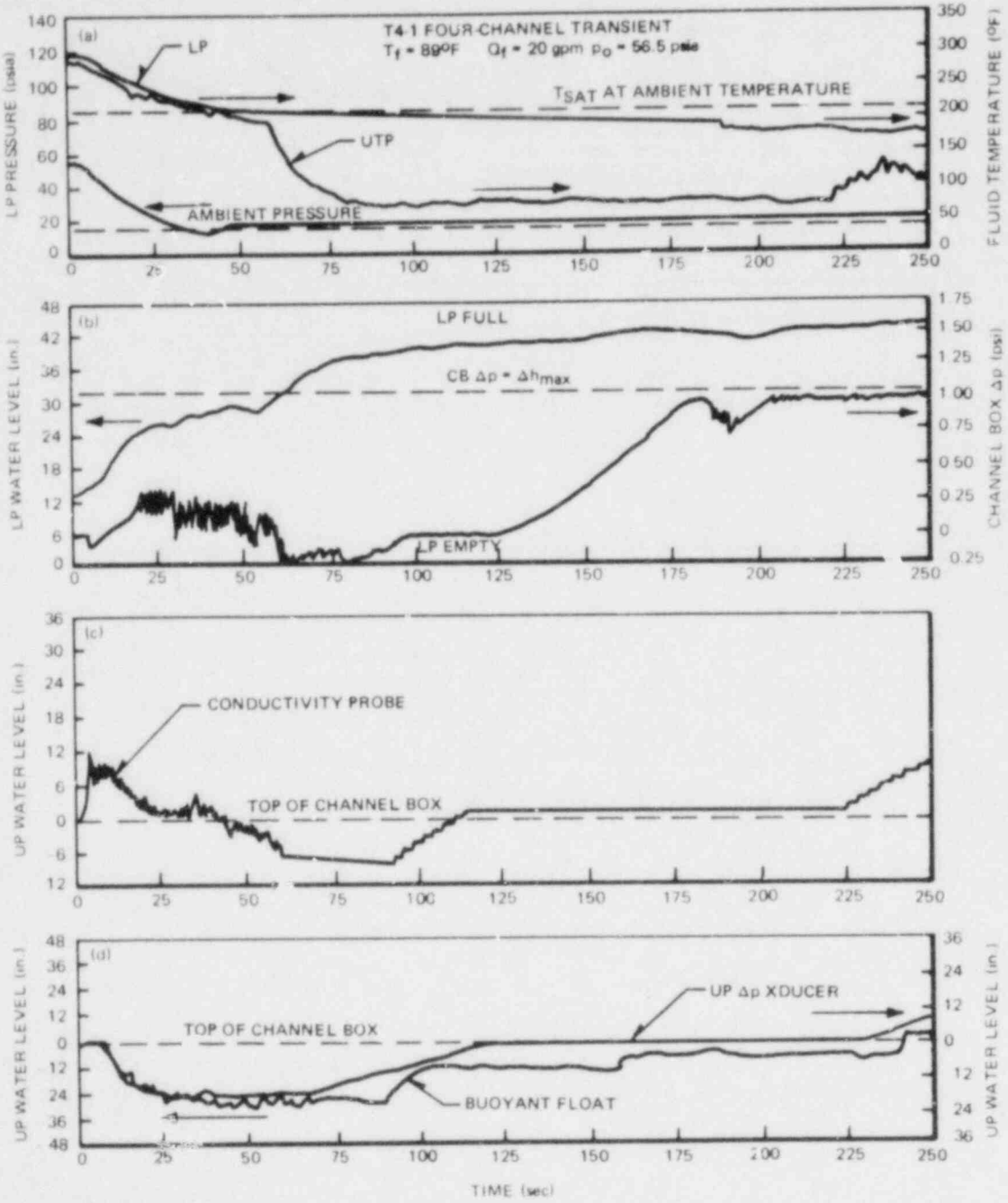

Figure C-34. Four-Channel Transient with 55 psia Initial Pressure

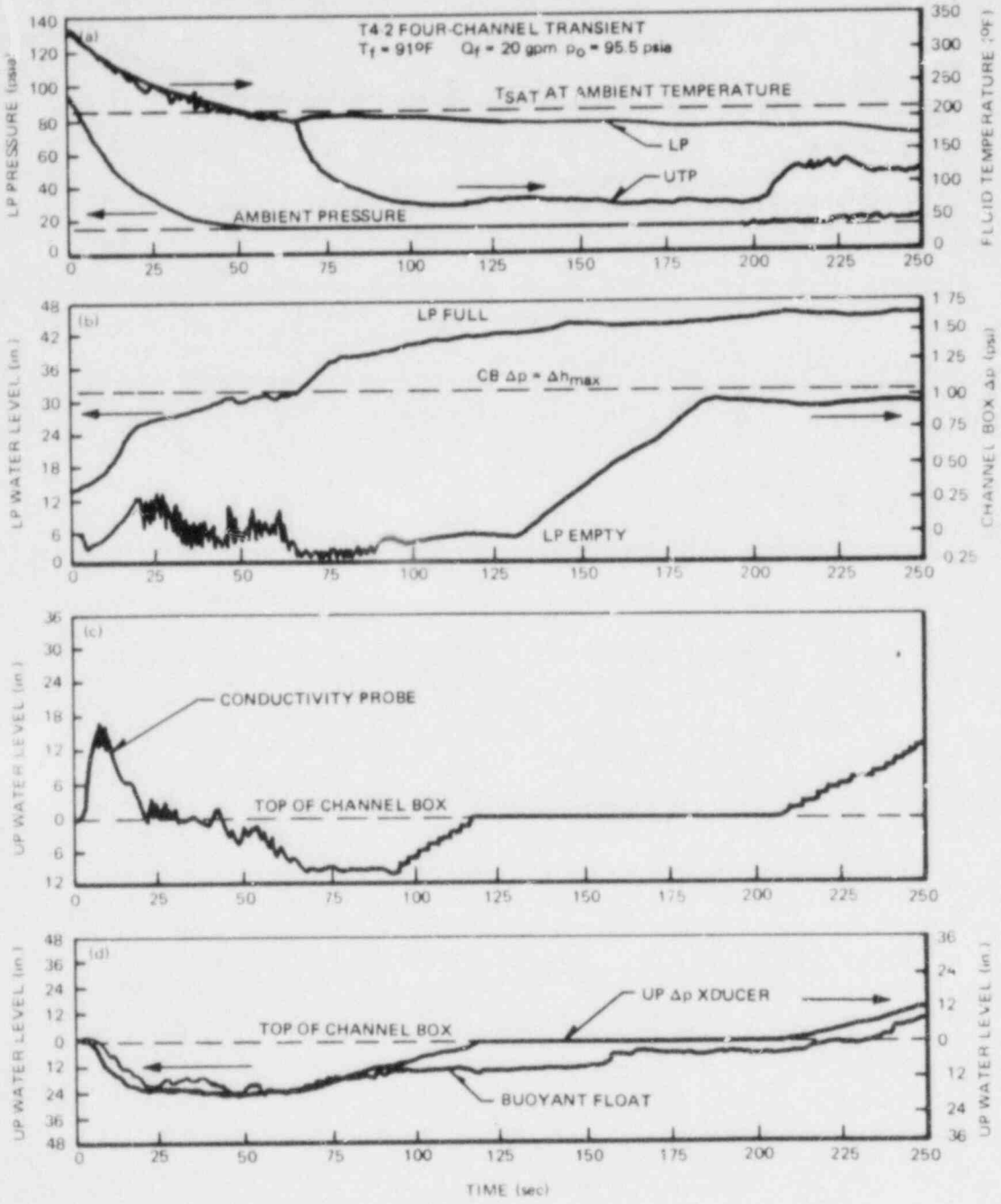

Figure C-35. Four-Channel Transient with 95 psia Initial Pressure

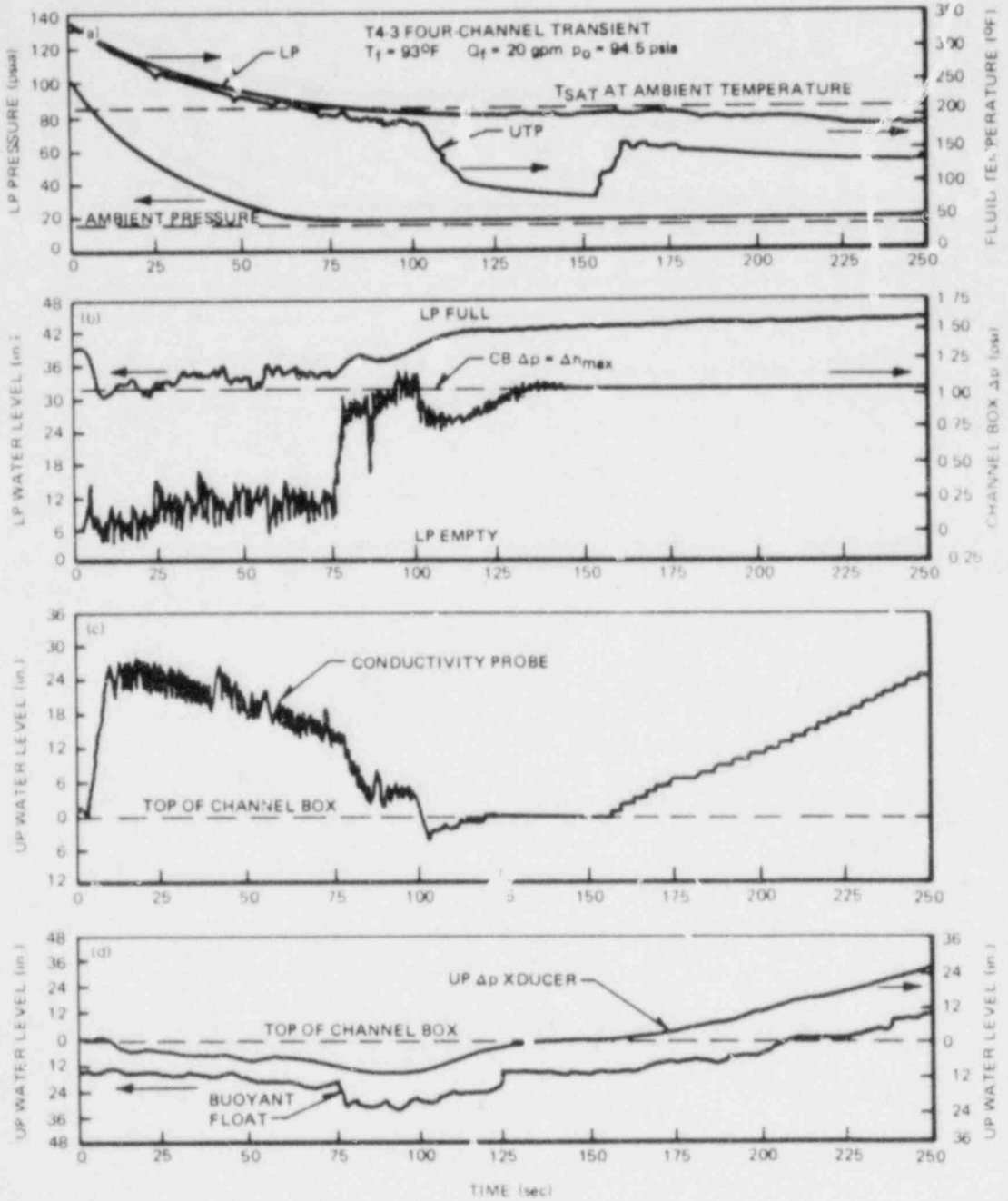

Figure C-36. Four-Channel Transient with Initial Plenum Water Height of 37.5 in. (95 psia Initial Pressure)

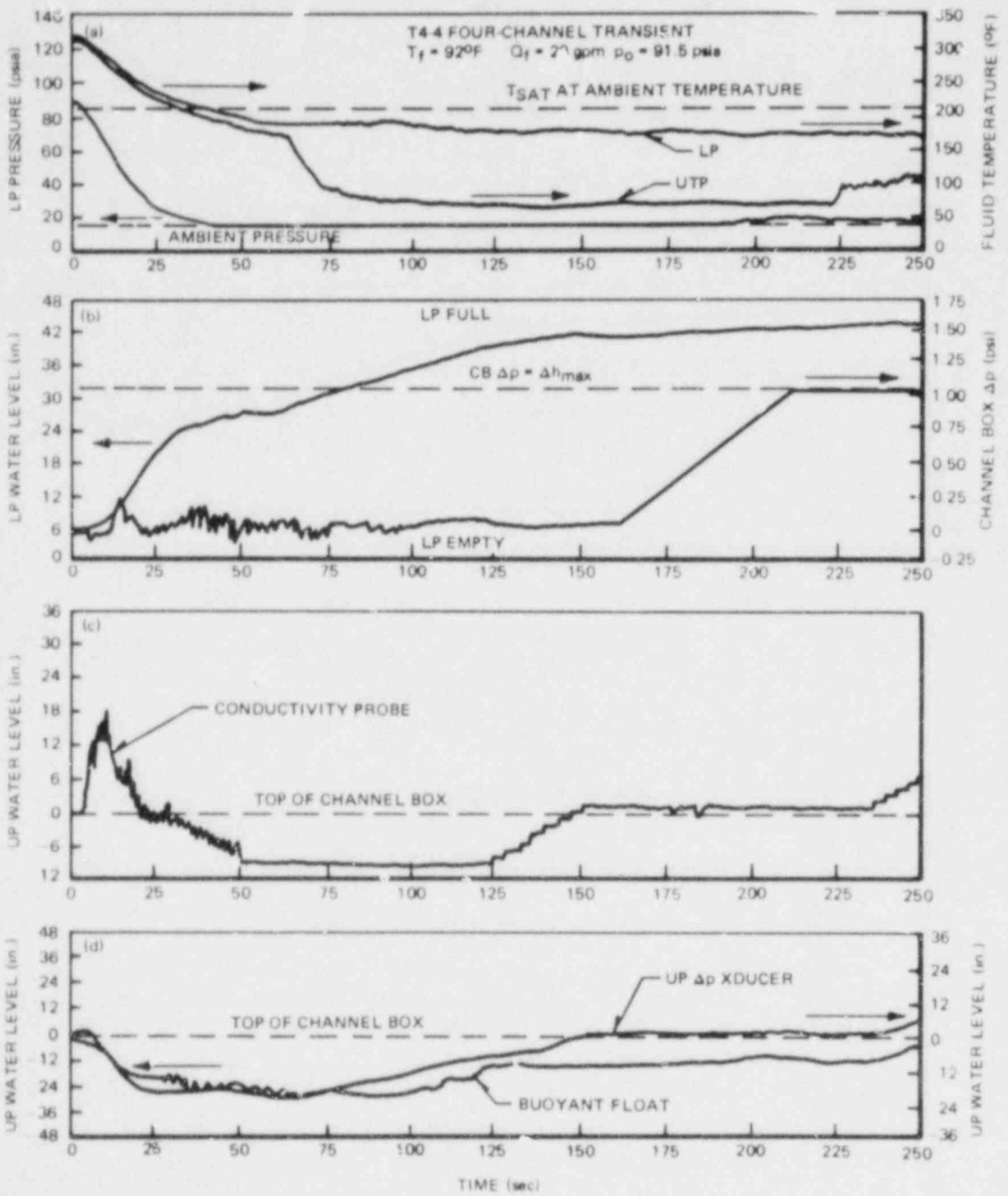

Figure C-37. Four-Channel Transient with Initially Empty Plenum (95 psia Initial Pressure)

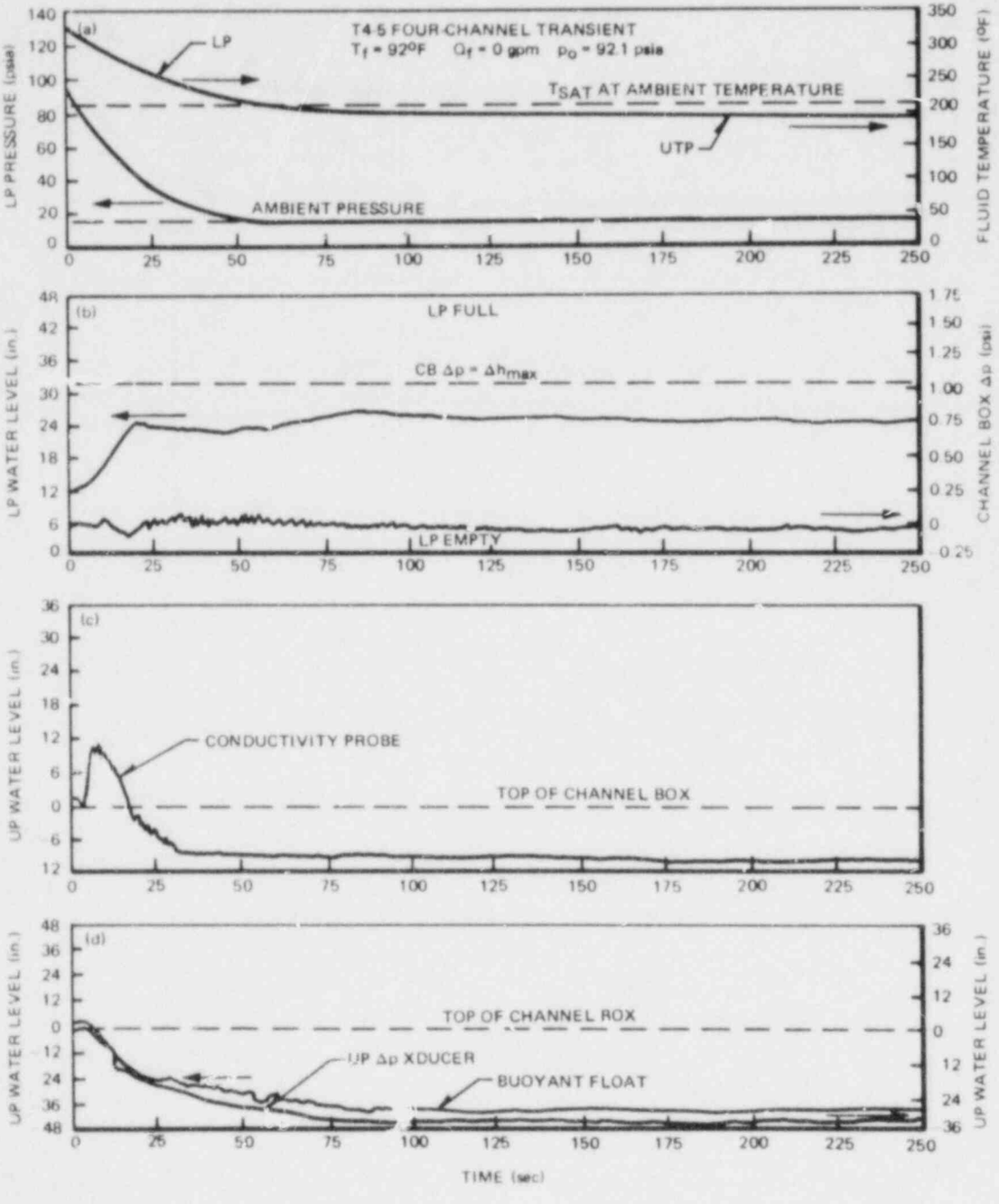

Figure C-38. Four-Channel Transient with Initial Plenum Water Level of 13.5 in. (95 psia Pressure, Zero Liquid Injection)

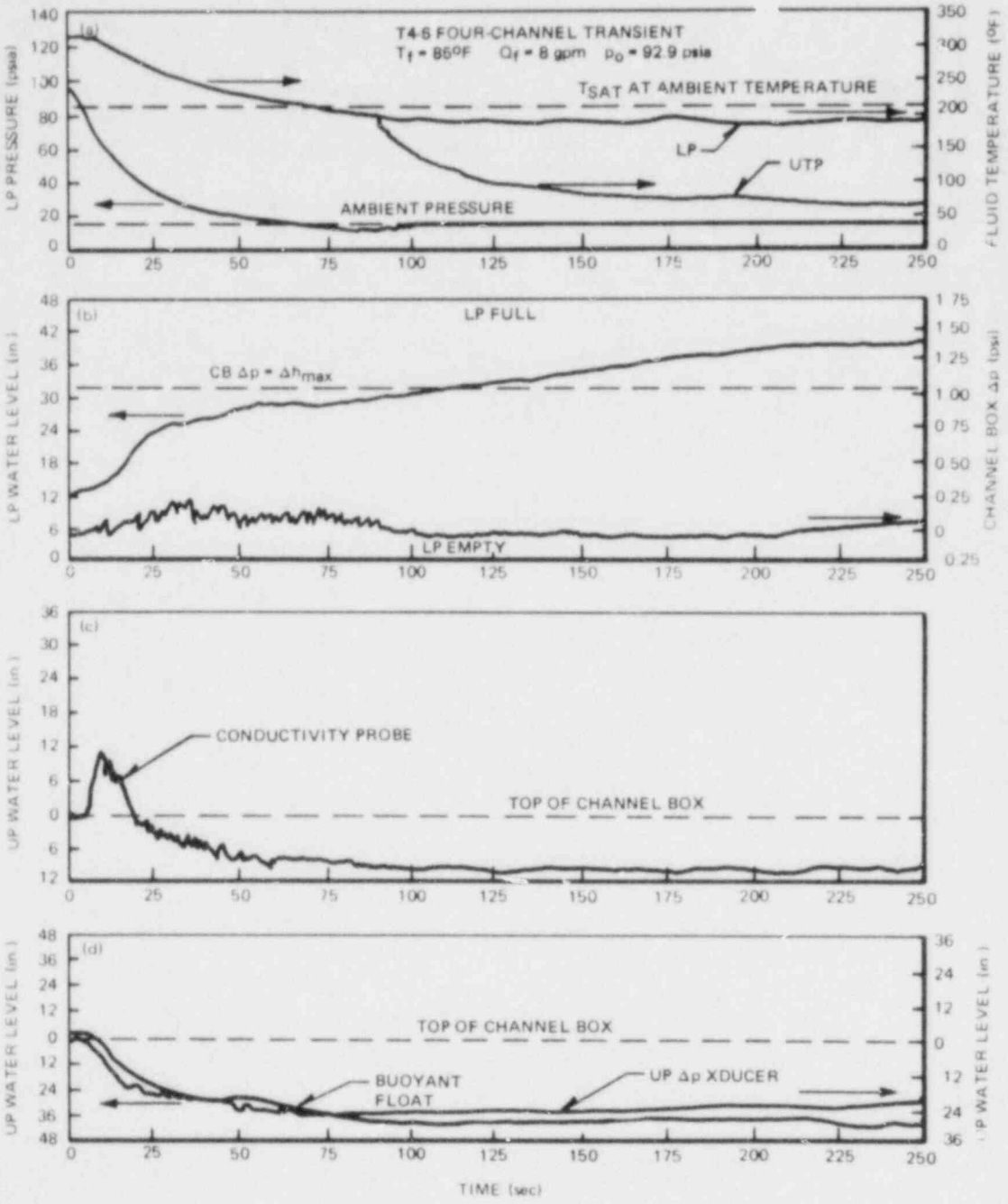

Figure C-39. Four-Channel Transient with Initial Plenum Water Height of 13.5 in. (95 psia Pressure, 8 gpm Liquid Injection)

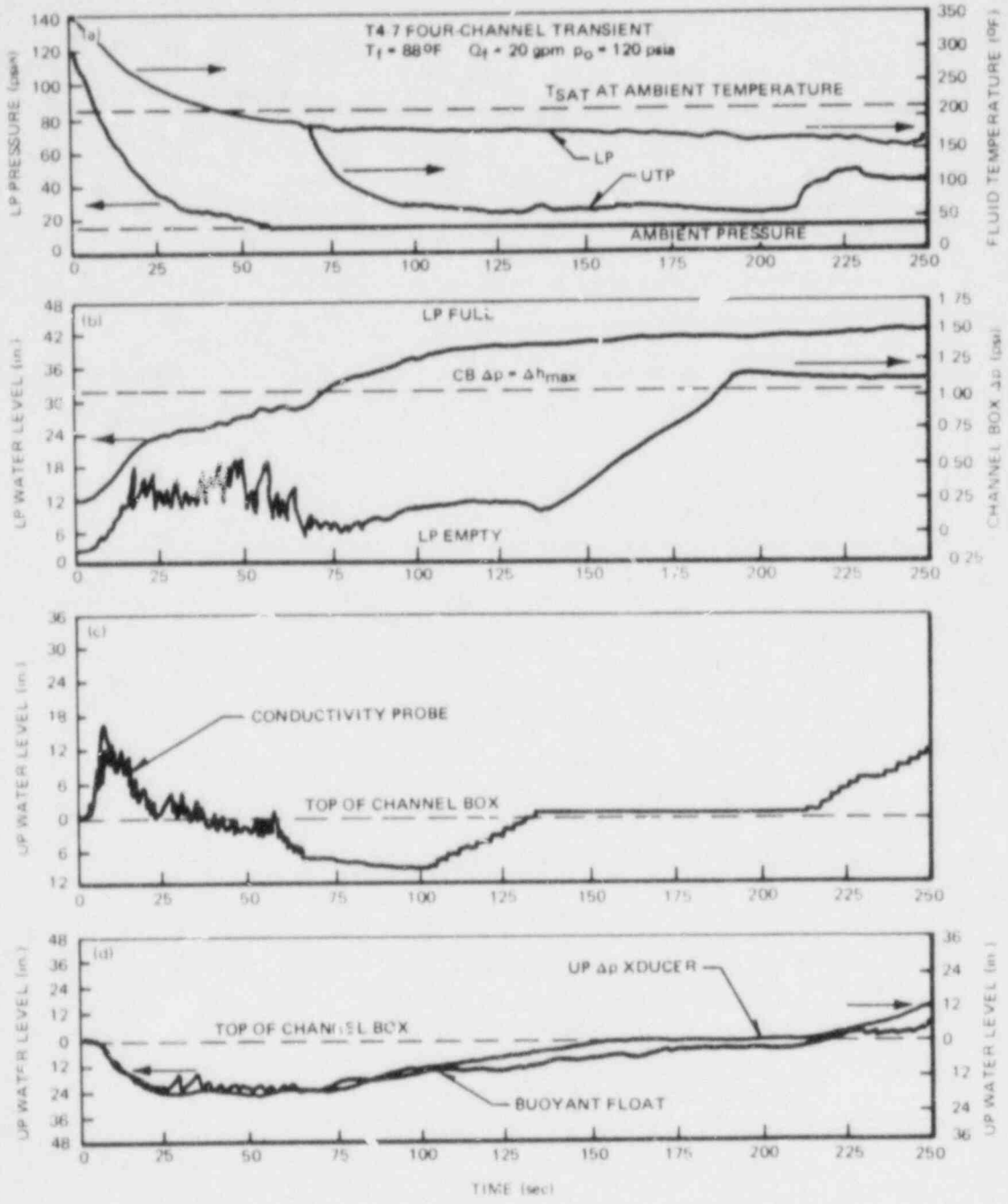

Figure C-40. Four-Channel Transient with 120 psia Initial Pressure

Appendix D

STEAM INJECTOR PERFORMANCE EVALUATION

D-1. INTRODUCTION

As part of the development of the Lynn Steam Sector Test Facility (SSTF) design, Creare, Inc. was contracted to study the counter-current flow-limiting (CCFL) performance of BWR fuel-bundle simulation using steam injection within the bundles to simulate the vaporization that would occur because of the heated fuel rods under postulated loss of coolant accident conditions (LOCA). Two different steam injector designs were developed by GE and Creare. A third design was suggested by Hitachi, Ltd. of Japan. This appendix includes the results of CCFL evaluations for all three injector designs.

D-2. TEST FACILITY

The facility used has capabilities for a broad range of studies. Here the features relevant to the CCFL studies in a single channel box are summarized. Test procedures are also described.

D-2.1 VESSEL AND INSTRUMENTATION

The vessel and associated measurement locations are sketched in Figure D-1. The vessel consists of three spool pieces 18 inches inside diameter (ID) and four feet in length which form the lower plenum, bypass region, and upper-plenum volumes. Four BWP fuel channels are located in the bypass region spool piece, although in these CCFL tests only a single channel was tested. The three remaining channels were scaled by blind-flanging the lower-core support castings. The two small drain holes in the lower tieplate casting of the test channel were also plugged. As shown in Figure D-2, the test channel included a steam-flow distributor, upper and lower tieplates, and upper and lower simulated fuel rod sections one foot long. (For certain tests reported here, the upper rods were removed.) The injector design pictured in Figure D-2b is the Hitachi design. The original and modified Creare designs are sketched in Figure D-3.

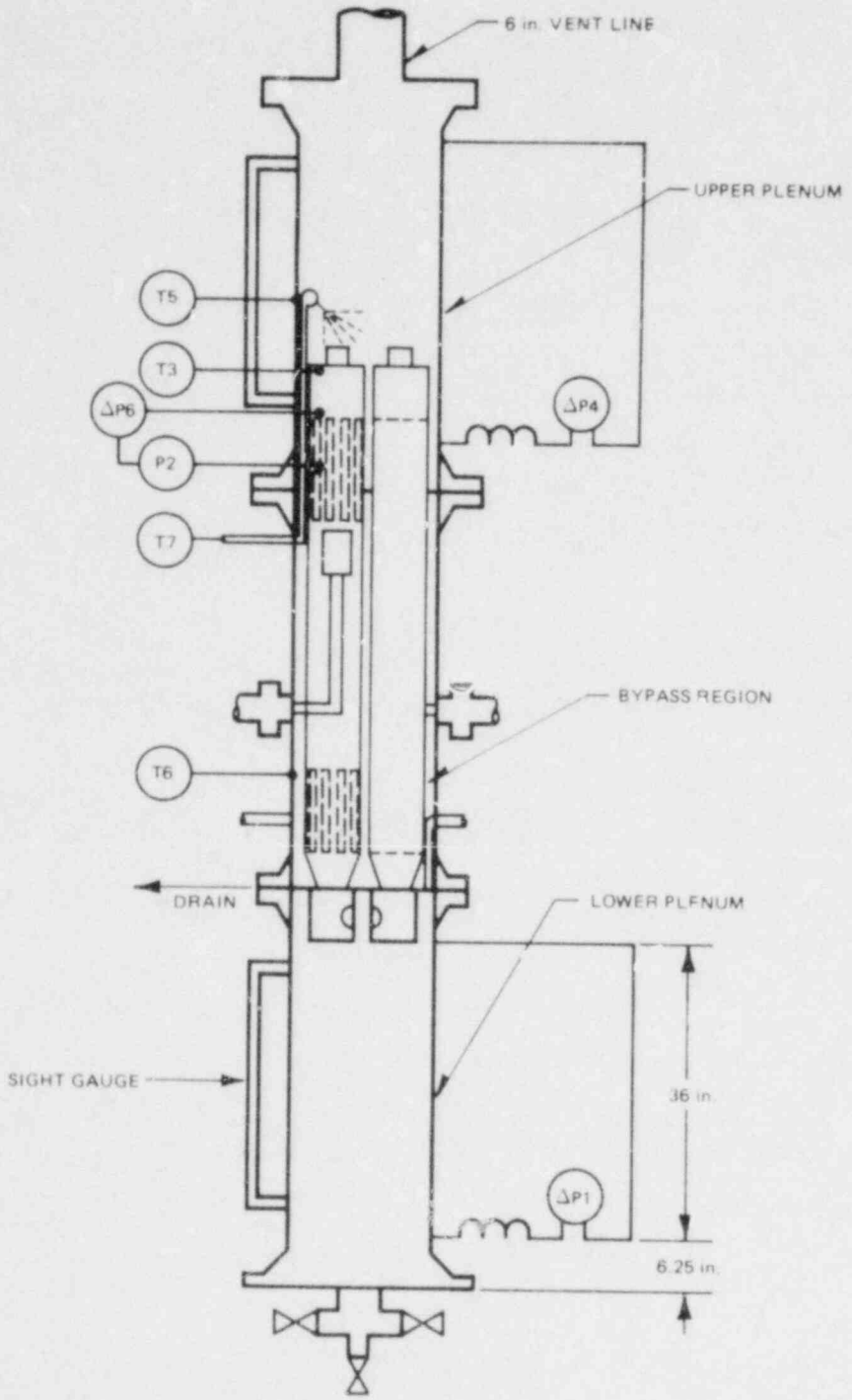

Figure D-1. Test Vessel and Instrumentation

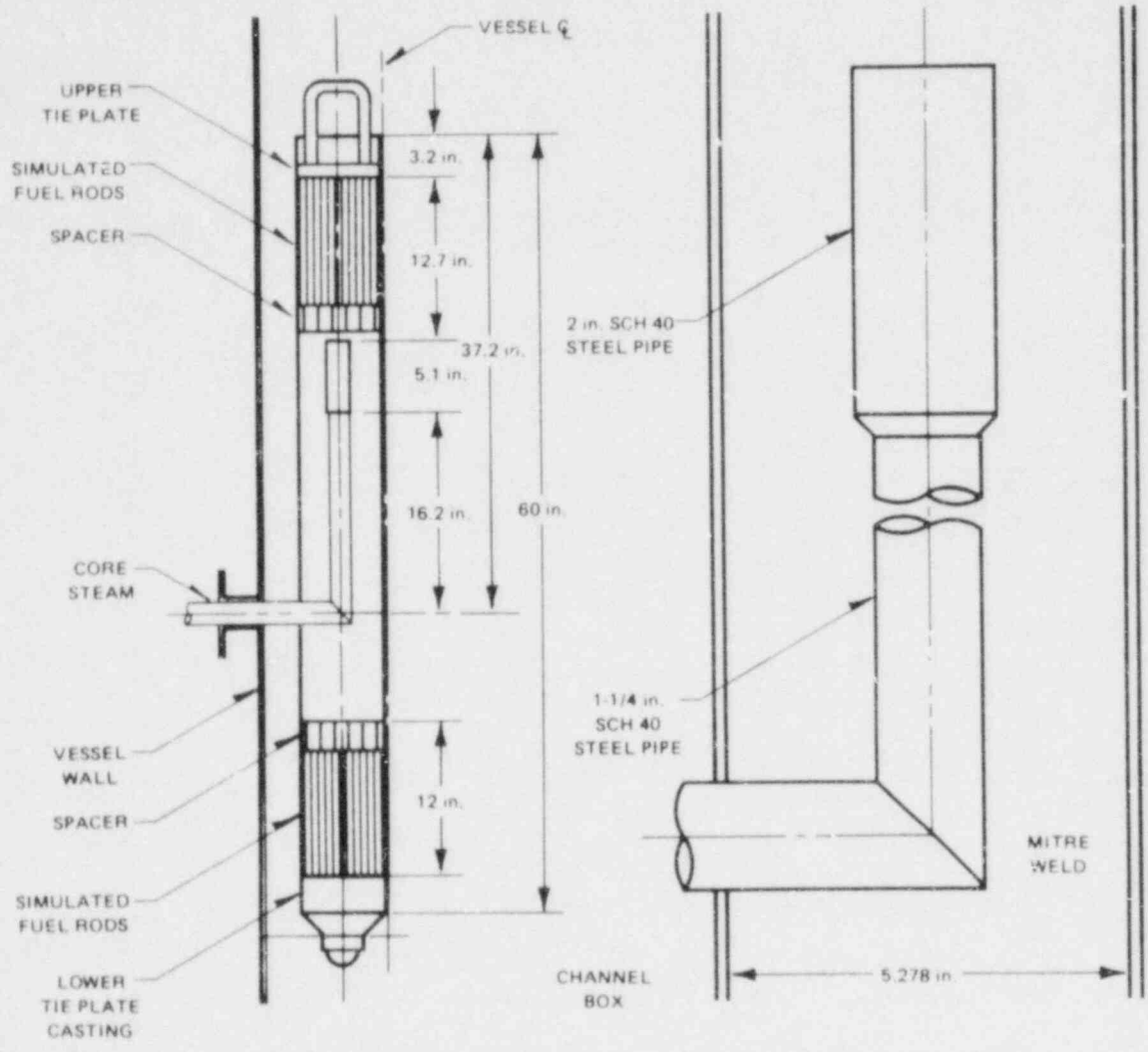

Figure D-2. Hitachi Steam Injector Design and Location

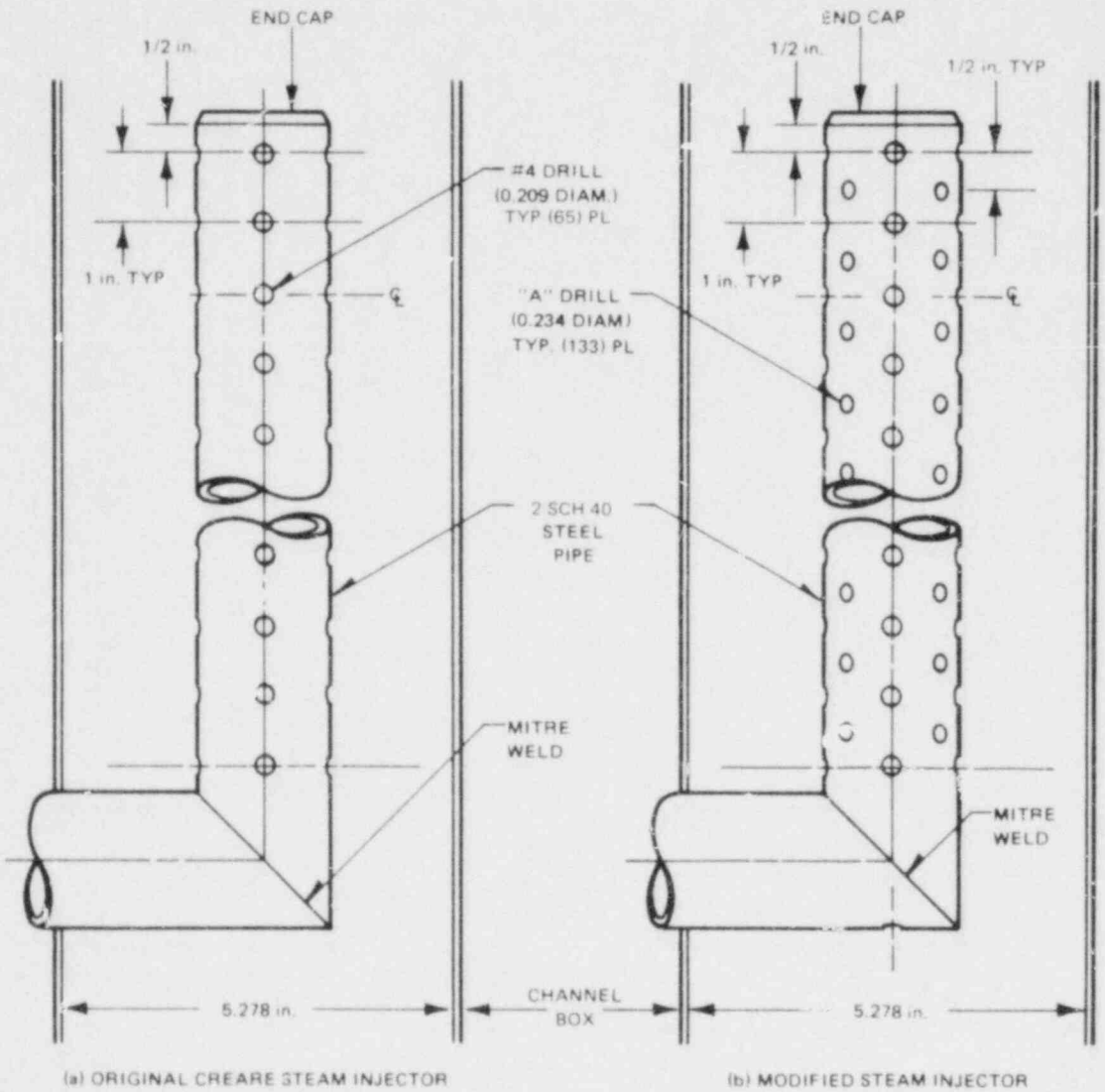

Figure D-3. Original and Modified Steam Injector Designs

The steam exhaust from the upper plenum of the vessel was a 6-in. ID pipe. The large exhaust pipe kept the backpressure in the vessel (caused by the single-phase pressure dropout) to a low value. Pressure remained less than 14.8 psia.

D-2.2 INSTRUMENTATION

Absolute pressure P2 was included just below the upper tieplate and was used in determining the steam density for momentum flux calculations. The differential pressure ΔP1 measured the lower-plenum filling, differential pressure transducer ΔP6 measured the pressure drop across the upper tieplate, and ΔP4 the upper-plenum water level. Thermocouple T3 measured the fluid temperature above the upper tieplate, and T5 and T6 the temperature of the liquid near the top and the bottom of the bypass region.

D-2.3 TEST PROCEDURES

In these tests, a measured steam upflow was first established. Then a specified core-spray flow was introduced in the test facility via a spray nozzle located in the upper plenum. The tests began with the bypass region initially full of saturated water. The injected flow could both penetrate the upper tieplate and fill the upper-plenum region by liquid hold-up in CCFL. The water level in the upper plenum was allowed to build up to a level four inches above the top of the channel box (as measured by a sight gauge) where this level was then maintained by manually draining the bypass region. Liquid penetrating the upper tieplate flowed through the channel box and collected in the lower plenum. The transient liquid level in the lower plenum was measured by ΔP1 (with the sight gauge as a double-check) for 60 to 180 seconds after the 4-in. upper-plenum level was attained.

D-3. CCFL PENETRATION DATA

All penetration data are plotted in terms of a steam-flow coordinate

$$j^*_{gCB} D^{1/2} = \frac{W_{gCB}}{A \rho_g^{1/2} [g \Delta \rho]^{1/2}} \qquad \text{(D-1)}$$

and a water delivery coordinate

$$j^*_{fd}{}^{D^{1/2}} = \frac{W_{fd}}{A\rho_f{}^{1/2}\,[g\Delta\rho]^{1/2}} \qquad \text{(D-2)}$$

where A=12.69 in^2 is the measured open area at the upper tieplate. See Section D-7 for a discussion of experimental and geometric uncertainties. Penetration data are tabulated in Section D-6.

The penetration data for the original and modified steam injectors are shown in Figures D-4 and D-5, respectively. Data at injection rates of 8 and 16 gpm are shown for the original injector; data at 4.1, 8, and 16 gpm are shown for the modified injector. After the point where limiting begins, delivery data overlay very well at each injection rate. The steam flow at which complete delivery occurs (i.e., no limiting) with 4.1 gpm injection in Figure D-4 is slightly higher than expected, based upon the 8 and 16 gpm partially-limited data.

The original and modified steam injector data are compared at 8 and 16 gpm in Figures D-6 and D-7. At delivery rates less than 50 percent of the injected flow rate, there appears to be no difference because of the modified injector. At delivery greater than 50 percent of the injected flow rate it appears that a steam flow about 5 percent higher is needed to produce a given rate of delivery with the modified injector. The effect of modifying the injector on penetration is therefore seen to be small.

Penetration data for saturated ECC at atmospheric pressure at injection flow rates of 4.1, 8.0, and 16.3 gpm were obtained with the Hitachi injector. A corresponding set of data was obtained with the same injector but without the simulated rods at the upper tieplate.

Penetration data for the Hitachi injector with the simulated rods are displayed in Figure D-8. For the purposes of discussion, if we consider the 16.3-gpm data as representative of the basic flooding curve in these tests, it is seen that the 8-gpm data are in close agreement. At 8 gpm, complete delivery occurs at a steam flux which may be slightly higher (about 5-10%) than expected, but agreement at $J^*_{gCB}{}^{1/2} > 0.25$ is excellent. The 4.1-gpm data deviate significantly from the 16.3-gpm data. Complete delivery is seen to continue up to a steam flux of

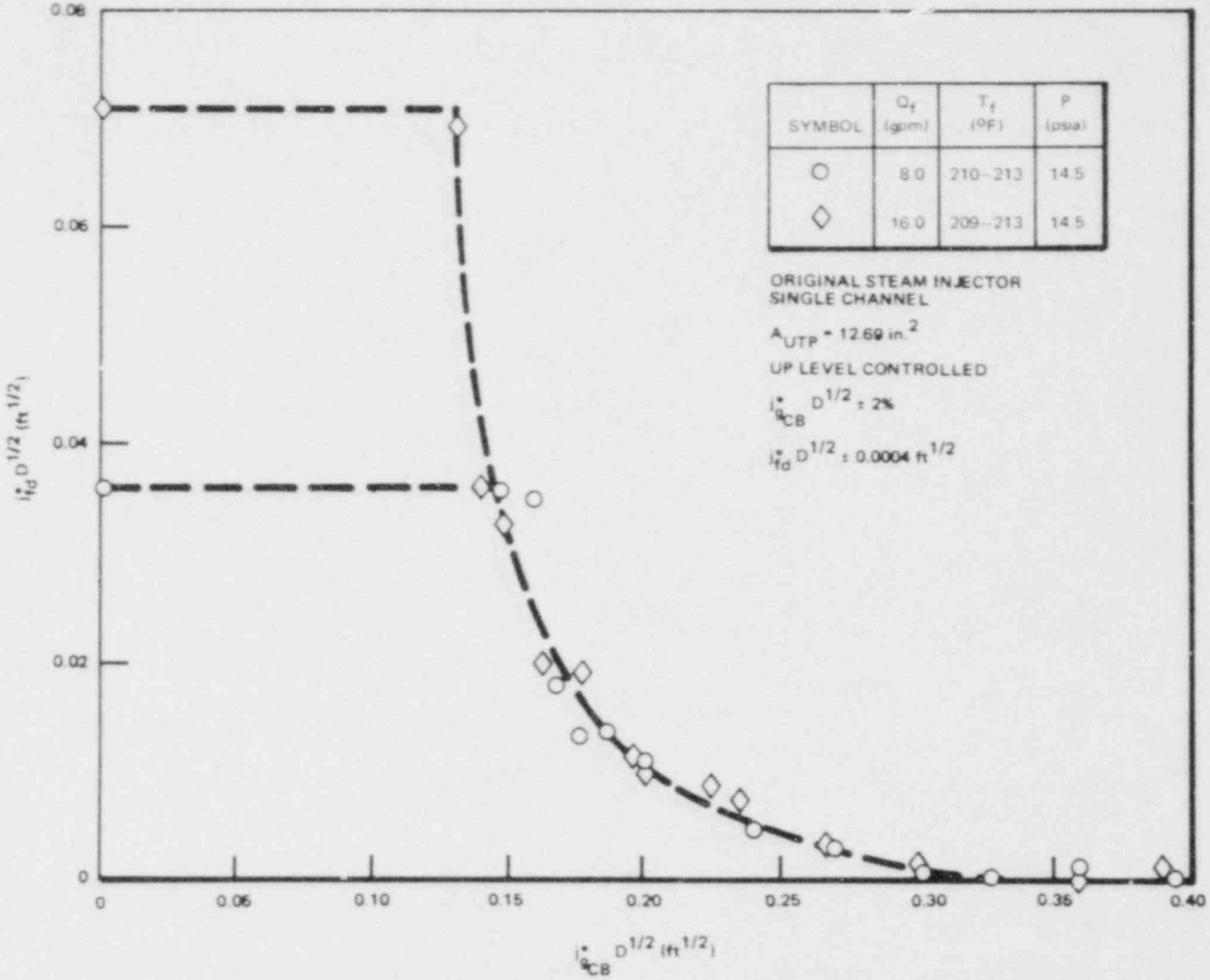

Figure D-4. Original Steam Injector CCFL Data

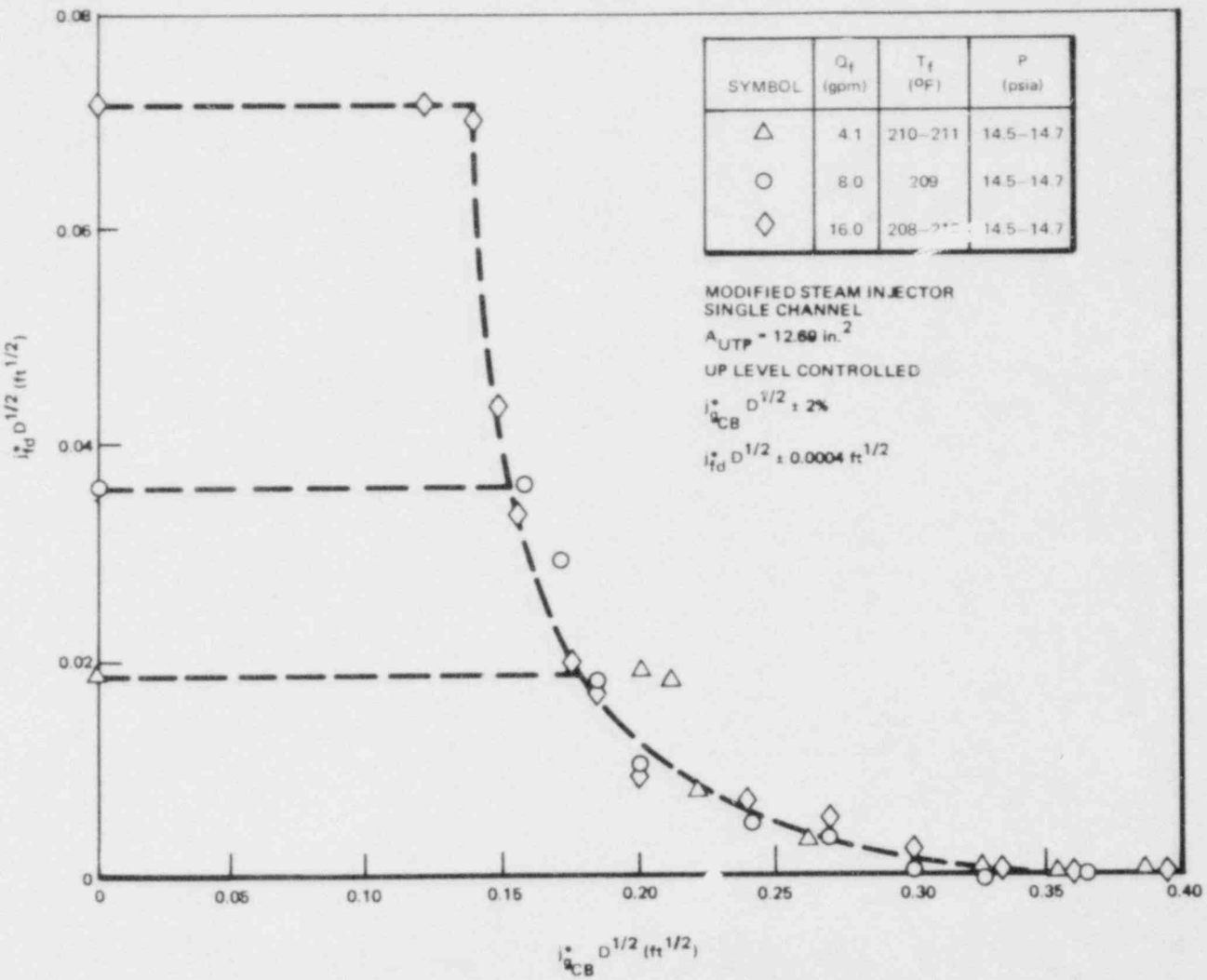

Figure D-5. Modified Steam Injector CCFL Data

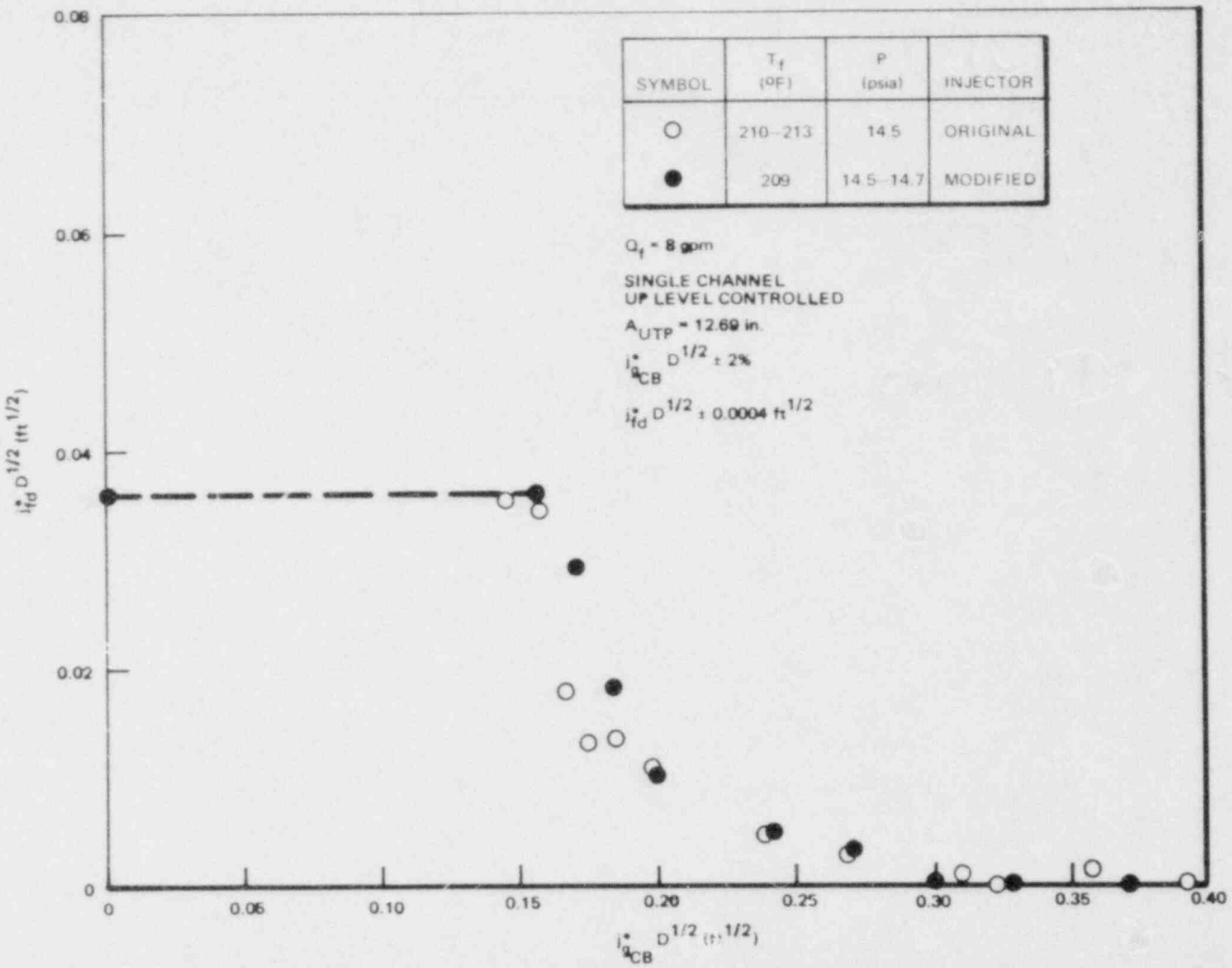

Figure D-6. Comparison of Original and Modified Steam Injector CCFL Data at 8 gpm

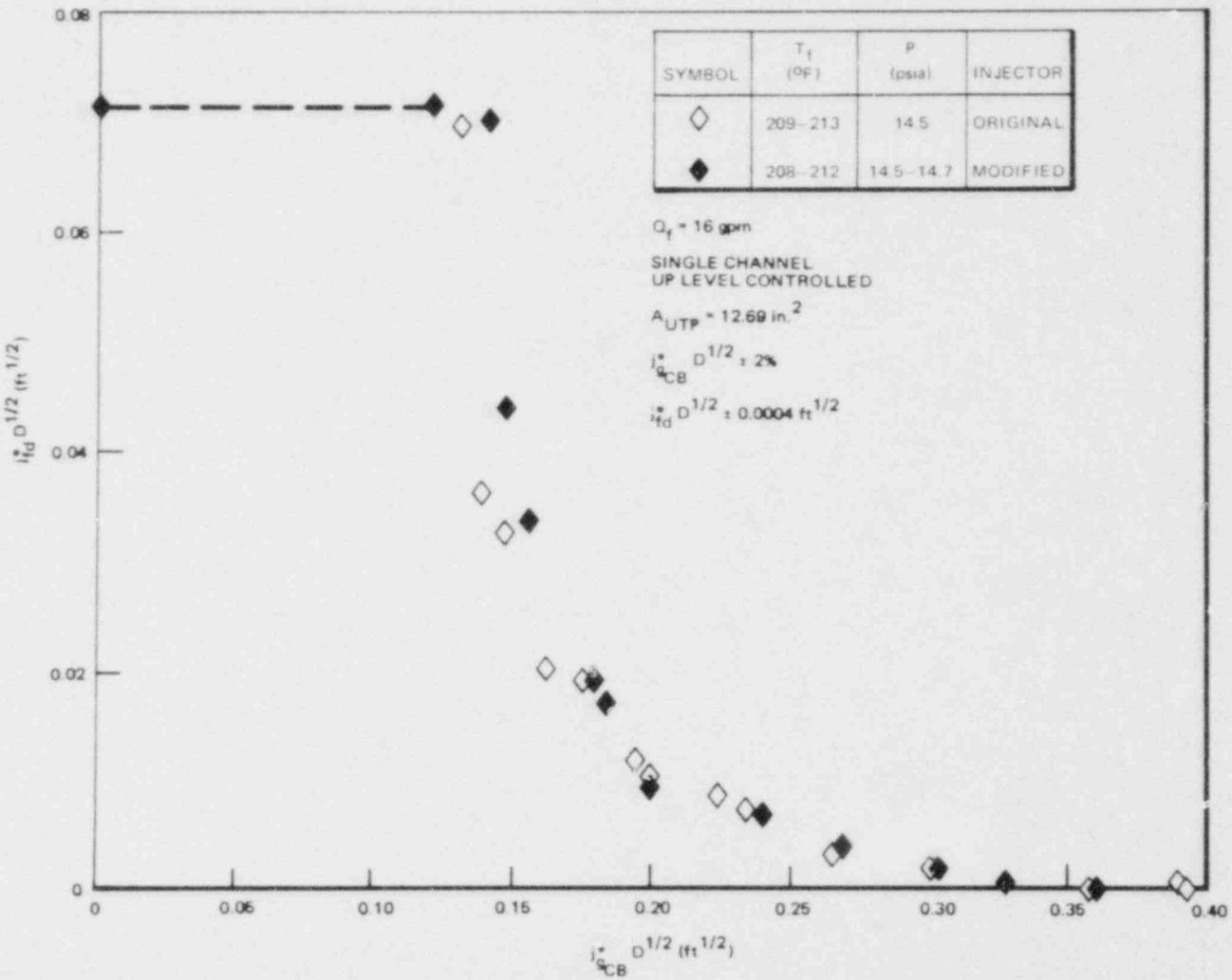

Figure D-7. Comparison of Original and Modified Steam Injector CCFL Data at 16 gpm

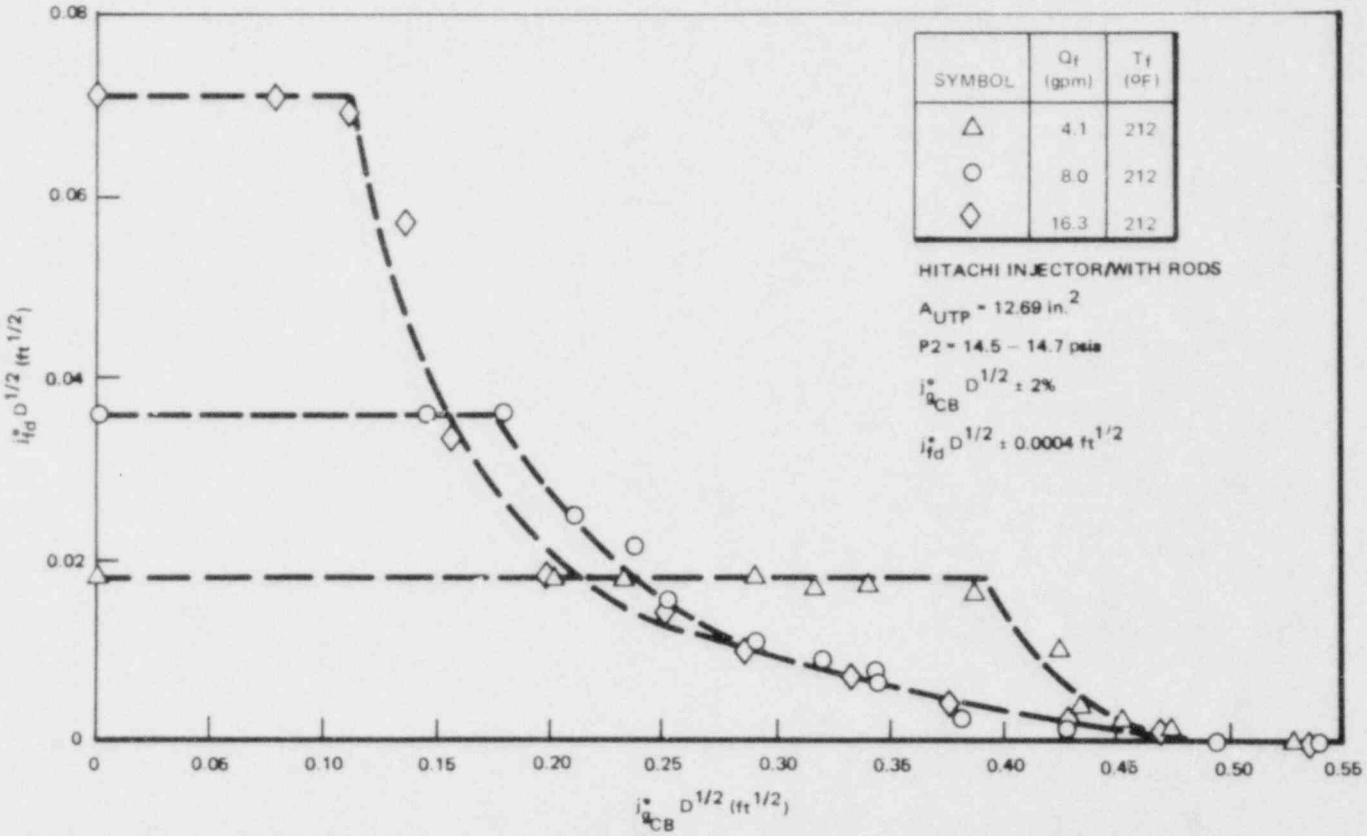

Figure D-8. CCFL Data for Hitachi Injector with Rods

approximately $j^*_{gCB}D^{1/2}=0.40$ (much higher than expected) although above $j^*_{gCB}D^{1/2}=0.45$ good agreement (complete bypass) is obtained. These data thus exhibit a flow-rate effect at low-flow rate, which is a tendency to allow complete delivery at higher steam flows than expected. The effect is small at 8 gpm but quite noticeable at 4.1 gpm. This behavior is believed to be related to the initial test conditions as discussed below.

The corresponding results without the simulated rod sections are shown in Figure D-9. These data also demonstrate a flow-rate effect similar to data with the rods; however, the effect at 4.1 gpm is even more dramatic than with the rods. Nearly complete delivery is obtained at very high steam flows, even greater than those in Figure D-8. Further differences are also noted. Figure D-10 directly compares the results with and without the rods at 8-gpm injection and illustrates these differences. First, whereas with simulated rods it was possible to obtain complete bypass at $j^*_{gCB}D^{1/2}=0.45$ to 0.50, without the simulated rods a small amount of delivery occurs even at higher steam fluxes. Further, a great deal of scatter in the range $j^*_{gCB}D^{1/2} > 0.35$ is seen in the data obtained without rods. The delivery at high steam flows is confirmed by sight-gauge observations and was a factor-of-10 greater than a small measured amount of leakage (less than 0.1 gpm). The simulated rods apparently help to reduce stochastic effects (such as asymmetries in the steam or water flows) which affect the penetration behavior.

Figures D-11 and D-12 compare the Hitachi steam injector results to the modified Creare injector results. Figure D-11 includes the Hitachi injector data with the simulated rods. Penetration is greater, and complete limiting occurs at a higher steam flow with the Hitachi injector. Figure D-12 shows that delivery is also greater for the Hitachi design even without the simulated rods. Note that with the modified Creare design, the steam flow for complete delivery at 4 gpm is somewhat higher than expected. This feature appears to have been exaggerated by the Hitachi injector design.

To investigate this apparent flow-rate effect, additional experiments were performed in which the injection flow was initially 8 gpm, but was reduced to 4 gpm during the tests when the liquid in the upper plenum reached the 4-in. controlled level. Using this test procedure, the results (solid symbols) agree with 8 gpm results as shown in Figure D-13. We conclude that the behavior with 4 gpm

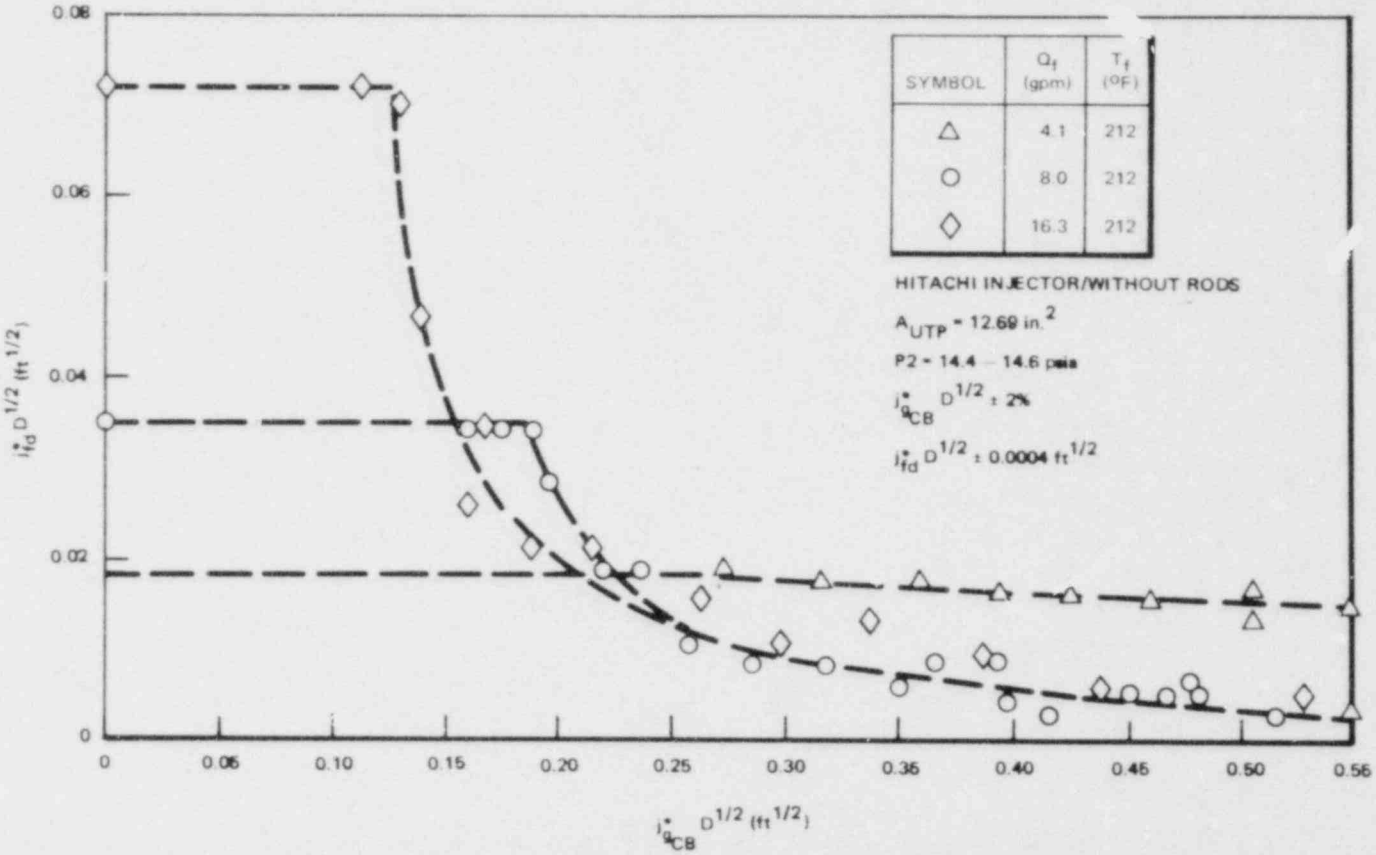

Figure D-9. CCFL Data for Hitachi Inejctor without Rods

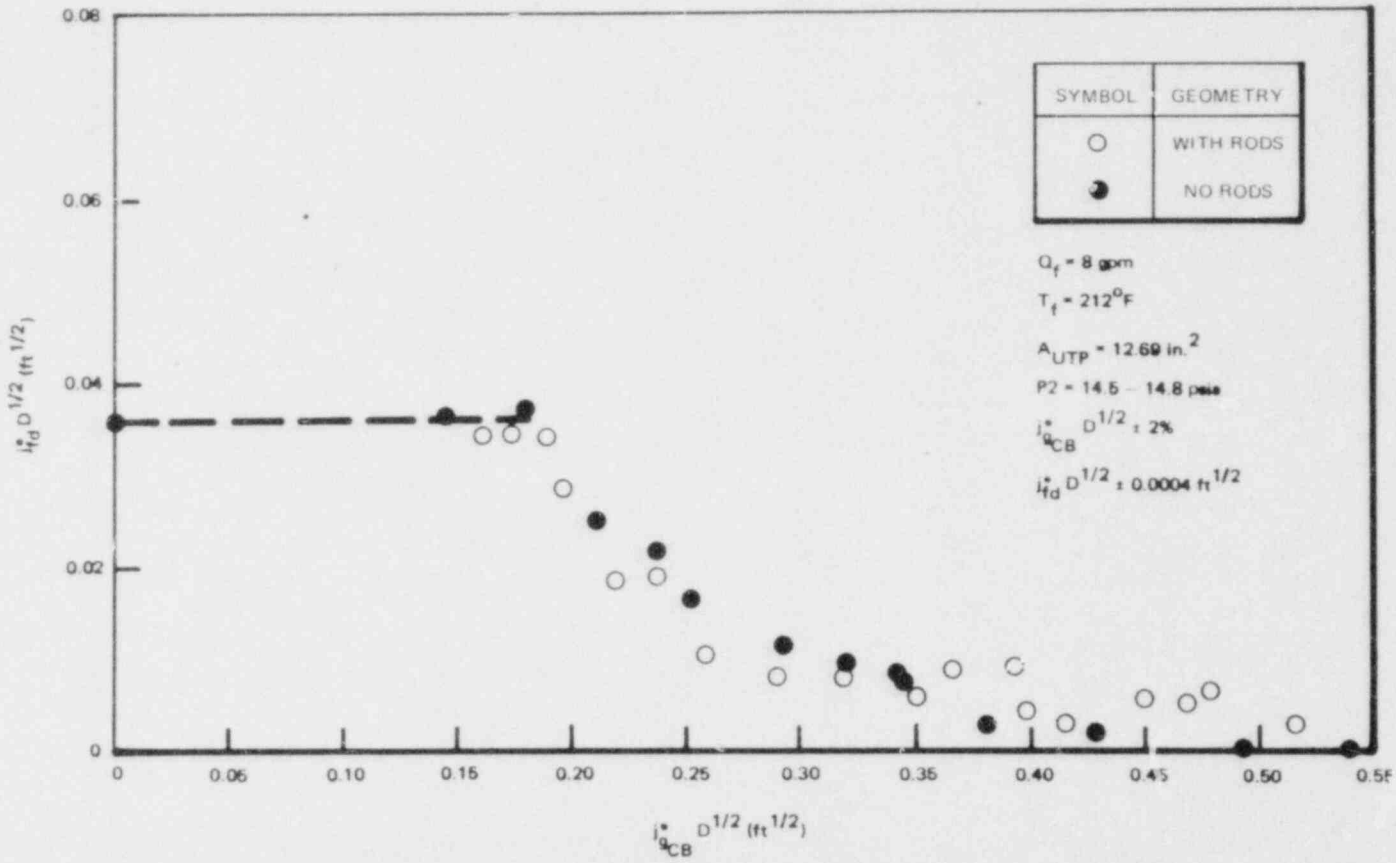

Figure D-10. Comparison of Hitachi Injector CCFL Data with and without Rods

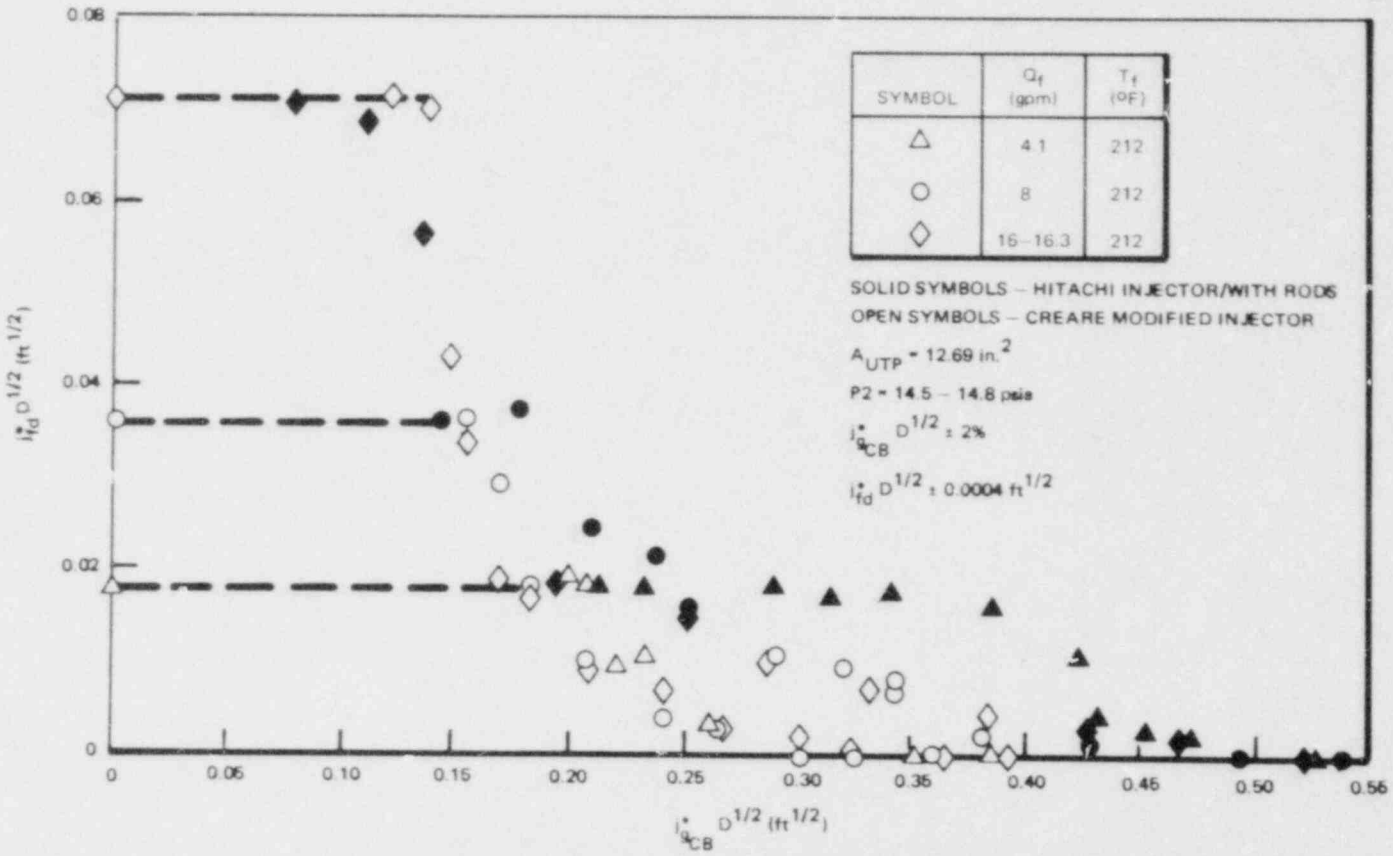

Figure D-11. Comparison of CCFL Data for Hitachi (with Rods) and Modified Creare Injectors

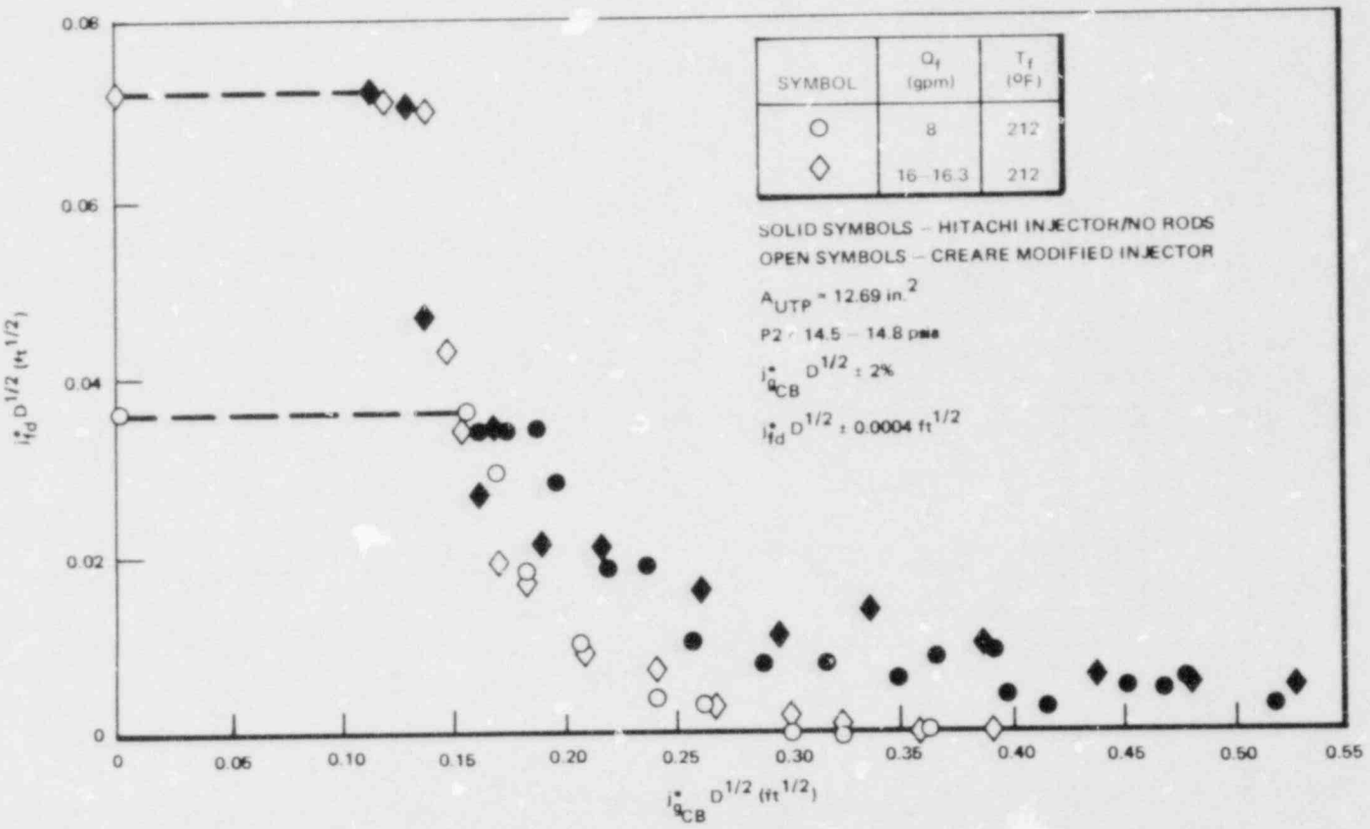

Figure D-12. Comparison of CCFL Data for Hitachi (without Rods) and Modified Creare Injectors

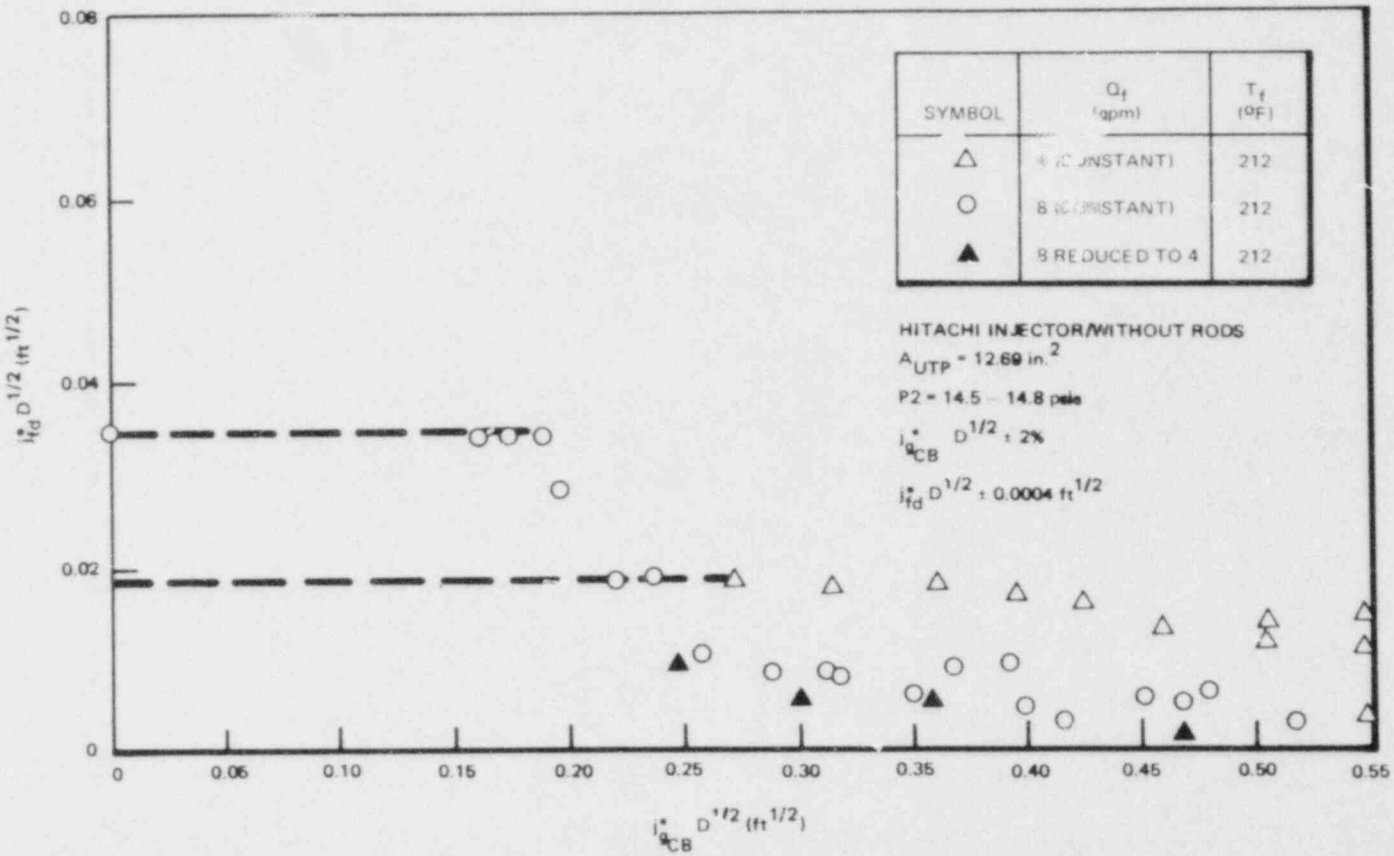

Figure D-13. Effect of Initial Injection Flow Rate with Hitachi Injector

is related to the test procedures, specifically the starting conditions where water overflows the top of the channel box as if it were a weir. At a low-flow rate or low height of liquid in the upper plenum, the liquid is able to enter the channel box more easily than at a higher liquid flow rate. We believe that the Hitachi injector allows water to flow in near the periphery of the channel despite a steam upflow concentrated near the center. The critical flow rate, where limiting versus nearly complete delivery is observed at $j^*_{gCB}D^{1/2}=0.35$, is about 5 gpm as shown in Figure D-14. These tests thus indicate that in our facility the starting test conditions are important at low-water flow rates with the Hitachi injector.

D-4. CCFL PRESSURE DROP DATA

The pressure-drop measurements across the simulated fuel rods in the upper end of the channel box (ΔP5) and across the upper tieplate (ΔP6) were of interest in the recent experiments. Figure D-15 presents representative pressure-drop measurements in the test with the modified steam injector. Similar results were obtained with the other injectors. Mean pressure drop data are tabulated in Section D-8.

For each water injection rate, data are shown for a steam flow just slightly greater than the steam flow at which complete delivery occurs and also for a steam flow very near to completely limiting. Little difference is seen in the pressure traces at each injection flow across the range of limiting steam flows. At steam flows equal to and below those at which complete delivery of injected water occurs, the pressure oscillations are negligible (not shown), increasing suddenly as limiting begins (Figures D-15a, D-15c, and D-15e). Figures D-15c and D-15d show that, at a nominal injection flow of 8 gpm, ΔP6 is very small, oscillating from 0 to 0.15 psid with a mean of 0.075 psid.* The ΔP5 measurement oscillates from approximately 0.03 to -0.20 psid, with a mean value therefore of 0.05 psid. The peak and the mean measurements at each water flow rate are very similar for ΔP6; there is a small decrease in peak values for ΔP5 for 16-gpm injection. The frequencies of the oscillations are about 5 Hz for ΔP5 and about 3 Hz for ΔP6.

*The accuracy of the pressure transducers used in these measurements is ±0.05 psid.

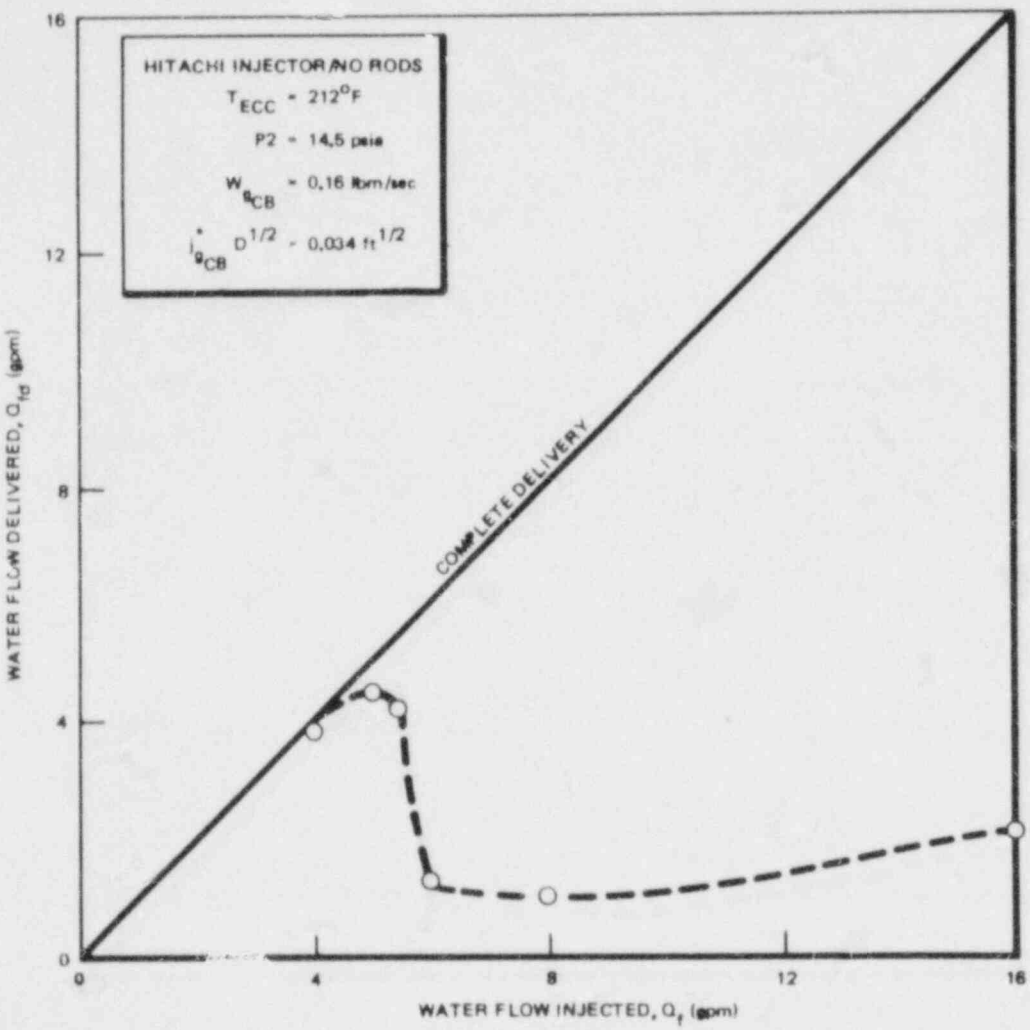

Figure D-14. Effect of Water Flow Rate on Limiting with Hitachi Injector

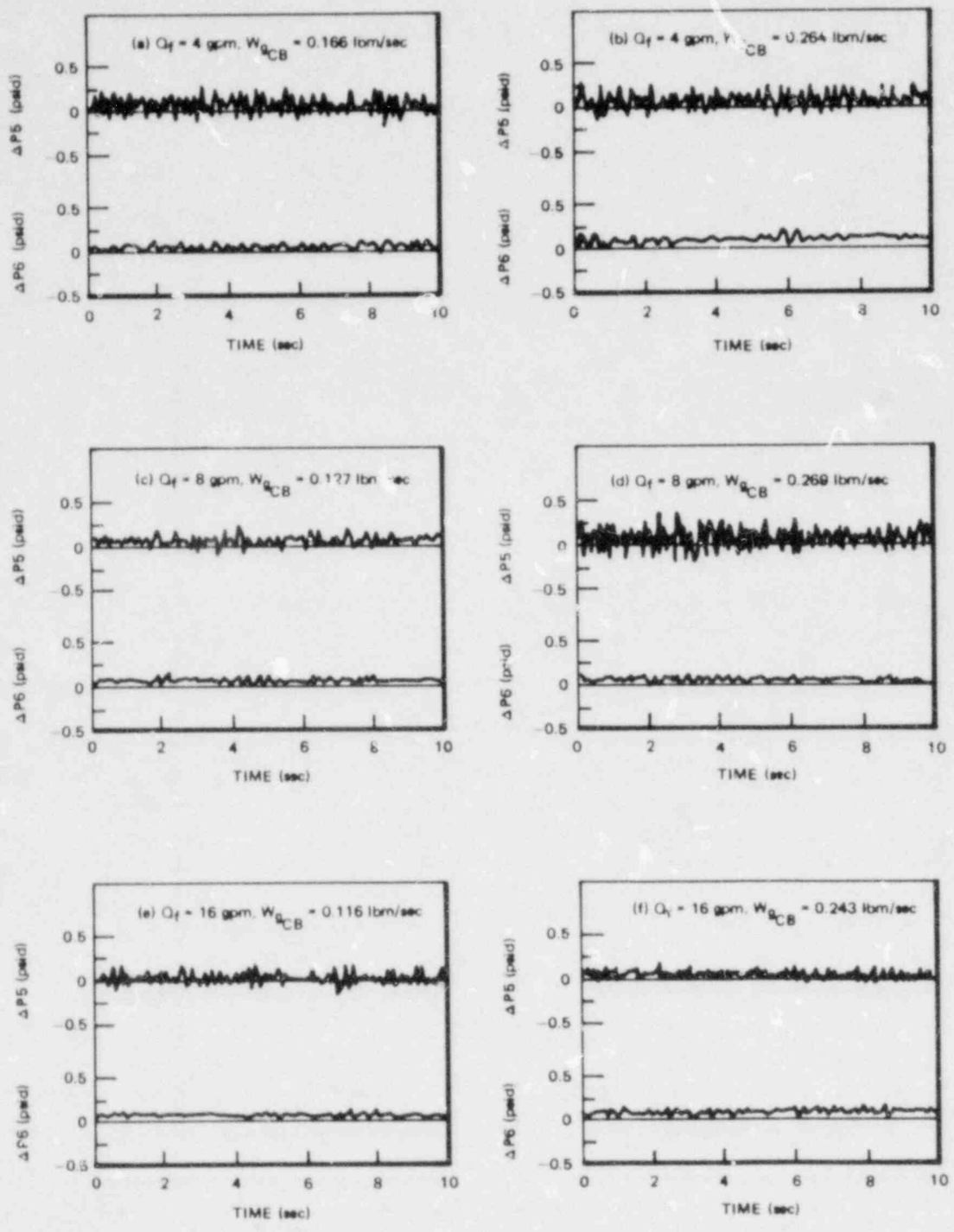

Figure D-15. Sample Traces of Differential Pressure Measurements in CCFL

It is noted that the mean pressure drops do not increase significantly with a factor-of-two change in the steam upflow across the range of limiting steam flows. This could be because the magnitude of the pressure oscillations relative to the mean makes the mean values of the pressure drops difficult to determine accurately; however, no significant increase in the mean values is detected.

D-5. CCFL TEMPERATURE MEASUREMENTS

Sample temperature measurements at 4- and 16-gpm injection are listed in Table D-5 in order of increasing steam flow. These temperature measurements were made with fluid thermocouples located as shown in Figure D-1. Data from the remainder of the tests are listed in Section D-8.

Thermocouples T3 and T4, measuring temperatures above the upper tieplate and in the upper plenum, fall into the range 211 ± 3°F which is the same as the injected water temperature (and saturation temperature) given the ±3°F accuracy of the thermocouples.

Thermocouples T5 and T6 measure the temperatures at the top and bottom of the bypass region. T5 measurements are also in the range 211 ± 3°F. T6 may show a trend of being 1-3°F hotter than T5. If a 2°F heatup of water flowing through the bypass region is assumed, it may be calculated from an energy balance that a maximum of 0.001 lbm/sec. of channel-box steam could be condensed (via heat transfer across the channel-box walls to bypass region liquid) with 4 gpm flowing through the bypass region (i.e., nearly complete limiting), and up to 0.004 lbm/sec could be condensed with 16 gpm flowing through the bypass region. This represents about 0.5 percent and 2 percent of the channel-box steam flow, respectively. One would thus expect to see a trend of approximately 2 percent greater steam flow to limit 4- and 16-gpm injection flows to low delivery rates if significant heat transfer were occurring. There is no discernible trend (see Figure D-5) in the penetration data for these data between 0.5- and 3.0-gpm delivery, which further indicates that bypass-region heat transfer has a negligible effect.

D-6. CCFL PENETRATION DATA

In this section the CCFL penetration data for all three injectors are tabulated. Each test has been assigned a code number, and listed for each test are this number, the injected water temperature, the spray mass flow rate, the measured channel-box pressure, and the steam and water delivery in terms of the dimensional correlating variables. The measured upper tieplate area is $A=12.69$ in.^{2}.

Table D-5

THERMOCOUPLE MEASUREMENTS DURING
CCFL WITH A MODIFIED STEAM INJECTOR

Test #	Q_f (gpm)	W_{gCb} (lbm/sec)	T3 (°F)	T4 (°F)	T5 (°F)	T6 (°F)
E-23	4	0.149	210	208	208	209
E-29	4	0.158	211	213	---	209
E-25	4	0.166	212	211	211	211
E-24	4	0.174	212	210	210	212
E-26	4	0.196	214	213	214	214
E-27	4	0.243	213	212	211	213
E-28	4	0.264	212	209	209	211
E-30	4	0.289	210	210	208	212
E-1	16	0.110	215	213	213	216
E-6	16	0.104	211	210	209	211
E-7	16	0.116	213	211	212	214
E-8	16	0.127	212	210	210	212
E-9	16	0.137	212	211	211	214
E-2	16	0.156	213	212	212	213
E-10	16	0.180	211	211	210	213
E-11	16	0.201	211	209	210	212
E-3	16	0.226	214	212	213	214
E-12	16	0.243	211	209	209	211
E-4	16	0.269	214	212	212	212

Table D-6

ORIGINAL CREARE STEAM INJECTOR

Test #	T_f (°F)	W_{fin} (lbm/s)	P (psia)	W_{gCB} (lbm/s)	W_{fLP} (lbm/s)	$J^*_{gCB}(D)0.5$ (ft 0.5)	$J^*_{fd}D0.5$ (ft 0.5)
C-1	211	2.133	14.5	0.108	0.984	0.146	0.032
C-2	211	2.133	14.5	0.153	0.324	0.207	0.01
C-3	209	2.135	14.5	0.223	0.061	0.3	0.002
C-4	212	2.133	14.5	0.289	0.031	0.39	0.001
C-5	212	2.133	14.5	0.265	0.018	0.358	0
C-6	212	2.133	14.5	0.198	0.114	0.267	0.003
C-7	211	2.133	14.5	0.13	0.573	0.176	0.019
C-8	212	2.133	14.5	0.166	0.259	0.223	0.008
C-9	212	2.133	14.5	0.173	0.222	0.234	0.007
C-10	212	2.133	14.5	0.145	0.345	0.195	0.011
C-11	213	2.132	14.5	0.12	0.606	0.162	0.02
C-13	212	2.133	14.5	0.096	2.077	0.129	0.069
C-14	215	2.13	14.5	0.102	1.087	0.138	0.036
C-20	212	1.066	14.5	0.328	0.028	0.443	0
C-21	210	1.067	14.5	0.177	0.14	0.238	0.004
C-22	212	1.066	14.5	0.137	0.395	0.185	0.013
C-23	210	1.067	14.5	0.146	0.324	0.197	0.01
C-24	210	1.067	14.5	0.198	0.086	0.267	0.002
C-25	211	1.066	14.5	0.223	0.041	0.3	0.001
C-26	210	1.067	14.5	0.242	0.028	0.327	0
C-27	210	1.067	14.5	0.265	0.046	0.358	0.001
C-28	213	1.066	14.5	0.289	0.021	0.39	0
C-29	211	1.066	14.5	0.308	0.028	0.416	0
C-30	210	1.067	14.5	0.117	1.045	0.157	0.034
C-31	210	1.067	14.5	0.129	0.401	0.174	0.013
C-32	212	1.066	14.5	0.123	0.536	0.166	0.017
C-19	212	1.066	14.5	0.107	1.066	0.145	0.035

Table D-7

MODIFIED STEAM INJECTOR

Test #	T_f (°F)	W_{fin} (lbm/s)	P (psia)	W_{gCB} (lbm/s)	W_{fLP} (lbm/s)	$J^*_{gCB}(D)0.5$ (ft 0.5)	$J^*_{fD}0.5$ (ft 0.5)
E-1	210	2.134	14.5	0.11	1.306	0.148	0.043
E-2	209	2.135	14.5	0.155	0.28	0.209	0.009
E-3	210	2.134	14.6	0.226	0.068	0.302	0.002
E-4	209	2.135	14.6	0.269	0.021	0.36	0
E-5	210	2.134	14.5	0.09	2.134	0.121	0.071
E-6	209	2.135	14.5	0.104	2.11	0.139	0.07
E-7	209	2.135	14.5	0.116	1.022	0.156	0.034
E-8	212	2.133	14.6	0.127	0.571	0.17	0.019
E-9	208	2.136	14.5	0.137	0.518	0.184	0.017
E-10	208	2.136	14.5	0.179	0.221	0.241	0.007
E-11	210	2.134	14.6	0.2	0.116	0.268	0.003
E-12	210	2.134	14.6	0.243	0.036	0.325	0.001
E-13	209	2.135	14.6	0.293	0.025	0.392	0
E-14	209	1.067	14.6	0.269	0	0.36	0
E-15	209	1.067	14.6	0.243	0	0.326	0
E-16	209	1.067	14.6	0.226	0.028	0.302	0
E-17	209	1.067	14.6	0.2	0.093	0.269	0.003
E-18	209	1.067	14.6	0.179	0.145	0.241	0.004
E-19	209	1.067	14.6	0.155	0.307	0.208	0.01
E-20	209	1.067	14.6	0.127	0.874	0.17	0.029
E-21	209	1.067	14.5	0.116	1.081	0.156	0.036
E-22	209	1.067	14.5	0.137	0.556	0.184	0.018
E-23	210	0.547	14.5	0.148	0.573	0.2	0.019
E-24	211	0.546	14.6	0.173	0.241	0.233	0.008
E-25	210	0.547	14.6	0.165	0.237	0.221	0.007
E-26	210	0.547	14.6	0.195	0.105	0.261	0.003
E-27	210	0.547	14.6	0.243	0.033	0.325	0.001
E-28	210	0.547	14.6	0.264	0.005	0.353	0
E-29	210	0.547	14.5	0.157	0.552	0.211	0.018
E-30	210	0.547	14.6	0.289	0	0.387	0

Table D-8

CCFL PENETRATION DATA FOR HITACHI INJECTOR (WITH RODS)

Test #	T_f (°F)	W_{fin} (lbm/s)	P_2 (psia)	W_{gCB} (lbm/s)	W_{fLP} (lbm/s)	$J^*_{gCB}D^{1/2}$ (ft)	$J^*_{fd}D^{1/2}$ (ft)
I- 1	212	1.066	14.7	0.157	0.735	0.21	0.0246
I- 2	212	1.066	14.6	0.170	0.637	0.238	0.0213
I- 3	212	1.066	14.5	0.187	0.637	0.238	0.0213
I- 4	212	1.066	14.5	0.217	0.322	0.292	0.0107
I- 5	212	1.066	14.5	0.239	0.266	0.321	0.0089
I- 6	212	1.066	14.5	0.256	0.234	0.344	0.0078
I- 7	212	1.066	14.5	0.318	0.046	0.429	0.0015
I- 8	212	1.066	14.5	0.132	1.097	0.179	0.0366
I- 9	212	1.066	14.5	0.283	0.066	0.381	0.0022
I- 10	212	1.066	14.5	0.401	0	0.54	0
I- 11	212	1.066	14.5	0.366	0	0.494	0
I- 12	212	1.066	14.5	0.257	0.201	0.345	0.0067
I- 13	212	1.066	14.5	0.109	1.066	0.146	0.0356
I- 14	212	0.546	14.5	0.215	0.546	0.291	0.0182
I- 15	212	0.546	14.5	0.234	0.499	0.316	0.0167
I- 16	212	0.546	14.5	0.253	0.515	0.341	0.0172
I- 17	212	0.546	14.5	0.287	0.483	0.387	0.0161
I- 18	212	0.546	14.5	0.335	0.078	0.452	0.0026
I- 19	212	0.546	14.5	0.351	0.062	0.473	0.002
I- 20	212	0.546	14.5	0.396	0	0.534	0
I- 21	212	0.546	14.5	0.321	0.125	0.433	0.0041
I- 22	212	0.546	14.5	0.315	0.311	0.425	0.0104

Table D-8 (Continued)

CCFL PENETRATION DATA FOR HITACHI INJECTOR (WITH RODS)

Test #	T_f (°F)	W_{fin} (lbm/s)	P2 (psia)	W_{gCB} (lcm/s)	W_{fLP} (lbm/s)	$J^*_{gCB} D^{1/2}$ (ft)	$J^*_{fd} D^{1/2}$ (ft)
I- 23	212	0.546	14.5	0.174	0.53	0.235	0.0177
I- 24	212	0.546	14.5	0.149	0.546	0.201	0.0182
I- 25	212	2.173	14.7	0.147	0.551	0.197	0.0184
I- 26	212	2.173	14.6	0.214	0.301	0.287	0.01
I- 27	212	2.173	14.5	0.188	0.434	0.252	0.0145
I- 28	212	2.173	14.5	0.247	0.217	0.332	0.0072
I- 29	212	2.173	14.5	0.286	0.133	0.385	0.0044
I- 30	212	2.173	14.5	0.318	0.066	0.429	0.0022
I- 31	212	2.173	14.5	0.349	0.05	0.47	0.0016
I- 32	212	2.173	14.5	0.394	0	0.533	0
I- 33	212	2.173	14.5	0.082	2.066	0.111	0.069
I- 34	212	2.173	14.5	0.116	1.002	0.157	0.0335
I- 35	212	2.173	14.5	0.101	1.693	0.136	0.0566
I- 36	212	2.173	14.5	0.058	2.106	0.079	0.0704

Table D-9

CCFL PENETRATION DATA FOR HITACHI INJECTOR (WITHOUT RODS)

Test #	T_f (°F)	W_{fin} (lbm/s)	P2 (psia)	W_{gCB} (lbm/s)	W_{fLP} (lbm/s)	$J^*_{gCB}D^{1/2}$ (ft)	$J^*_{fd}D^{1/2}$ (ft)
H- 32	212	1.053	14.5	0.237	0.233	0.319	0.0077
H- 33	212	1.053	14.5	0.259	0.167	0.35	0.0056
H- 34	212	1.053	14.5	0.212	0.231	0.287	0.0077
H- 35	212	1.053	14.5	0.191	0.305	0.258	0.0102
H- 36	212	1.053	14.5	0.176	0.557	0.237	0.0186
H- 37	212	1.053	14.5	0.163	0.549	0.22	0.0183
H- 38	212	1.053	14.5	0.145	0.847	0.196	0.0283
H- 39	212	1.053	14.5	0.13	1.019	0.175	0.034
H- 40	212	1.053	14.5	0.12	1.026	0.161	0.0343
H- 41	212	1.053	14.5	0.272	0.251	0.367	0.0084
H- 42	212	1.053	14.5	0.308	0.079	0.416	0.0026
H- 43	212	1.053	14.5	0.291	0.265	0.393	0.0088
H- 44	212	1.053	14.5	0.334	0.151	0.451	0.005
H- 45	212	1.053	14.5	0.355	0.185	0.478	0.0061
H- 46	212	1.053	14.5	0.303	0.079	0.515	0.0026
H- 47	212	1.053	14.5	0.419	0.125	0.565	0.0041
H- 48	212	1.053	14.5	0.438	0.053	0.59	0.0017
H- 49	212	1.053	14.5	0.296	0.119	0.398	0.004
H- 50	212	1.053	14.4	0.347	0.145	0.468	0.0048
H- 51	212	1.053	14.5	0.14	1.019	0.109	0.034
H- 61	212	2.173	14.6	0.221	0.314	0.297	0.0105
H- 62	212	2.173	14.6	0.195	0.462	0.262	0.0154

Table D-9 (Continued)

CCFL PENETRATION DATA FOR HITACHI INJECTOR (WITHOUT PODS)

Test #	T_f (°F)	W_{fin} (lbm/s)	P2 (psia)	W_{gCB} (lbm/s)	W_{fLP} (lbm/s)	$J^*_{gCB}D^{1/2}$ (ft)	$J^*_{fd}D^{1/2}$ (ft)
H- 63	212	2.173	14.5	0.16	0.627	0.215	0.0209
H- 64	212	2.173	14.5	0.12	0.770	0.161	0.036
H- 65	212	2.173	14.5	0.103	1.391	0.138	0.0465
H- 66	212	2.173	14.5	0.084	2.159	0.113	0.0722
H- 67	212	2.173	14.5	0.096	2.106	0.13	0.0704
H- 68	212	2.173	14.6	0.252	0.397	0.338	0.0132
H- 69	212	2.173	14.5	0.29	0.281	0.389	0.0094
H- 70	212	2.173	14.5	0.325	0.182	0.438	0.0061
H- 71	212	2.173	14.5	0.357	0.0165	0.48	0.0055
H- 72	212	2.173	14.5	0.392	0.147	0.527	0.0049
H- 73	212	2.173	14.5	0.437	0.098	0.588	0.0032
H- 74	212	2.173	14.5	0.14	0.627	0.188	0.0209
H- 75	212	2.173	14.5	0.125	1.027	0.169	0.0343
H- 80	212	0.546	14.5	0.202	0.546	0.273	0.0182
H- 81	212	0.546	14.5	0.234	0.515	0.315	0.0172
H- 82	212	0.546	14.5	0.267	0.53	0.36	0.0177
H- 83	212	0.546	14.5	0.293	0.483	0.395	0.0161
H- 84	212	0.546	14.5	0.314	0.467	0.424	0.0156
H- 85	212	0.546	14.5	0.34	0.453	0.459	0.0151
H- 86	212	0.546	14.5	0.374	0.343	0.505	0.0114
H- 87	212	0.546	14.5	0.405	0.093	0.547	0.0031
H- 88	212	0.546	14.4	0.422	0.297	0.569	0.0099
H- 89	212	0.546	14.4	0.451	0.171	0.609	0.0057

Table D-9 (Continued)

CCFL PENETRATION DATA FOR HITACHI INJECTOR (WITHOUT RODS)

Test #	T_f (°F)	W_{fin} (lbm/s)	P2 (psia)	W_{gCB} (lbm/s)	W_{fLP} (lbm/s)	$J^*_{gCB}D^{1/2}$ (ft)	$J^*_{fd}D^{1/2}$ (ft)
H- 90	212	0.546	14.4	0.404	0.311	0.545	0.0104
H- 91	212	0.546	14.5	0.374	0.406	0.505	0.0135
H- 99	212	0.546	14.6	0.407	0.437	0.546	0.0146
H- 100	212	0.546	14.5	0.458	0.437	0.618	0.0146
H- 101	212	0.546	14.4	0.458	0.421	0.619	0.014
H- 102	212	0.546	14.3	0.458	0.421	0.619	0.014
H- 103	212	0.546	14.5	0.561	0.082	0.756	0.0027
H- 98	212	1.053+ 0.546	14.5	0.267	0.155	0.359	0.0052
H- 104	212	1.053+ 0.546	14.6	0.35	0.[illegible]	0.469	0.0015
H- 105	212	1.053+ 0.546	14.5	0.225	0.155	0.302	0.0052
H- 106	212	1.053+ 0.546	14.5	0.185	0.281	0.248	0.0094

D-7. UNCERTAINTY ESTIMATES

It is important to examine the overall uncerainty in the measurement being made both from the standpoint of understanding the uncertainty bands on the data and in order to indicate where improvements to individual measurements will decrease uncertainty. We have used the technique of Kline and McClintock to estimate the overall uncertainty in the calculated quantity.

$$j^*_{gCB}D^{1/2} = \frac{W_{gCB}}{A\rho_g^{1/2}[g\Delta\rho]} \tag{D-3}$$

This technique yields an expression for the uncertainty written in terms of individual uncertainties:

$$\left(\frac{\Delta j^*_{gCB}D^{1/2}}{j^*_{gCB}D^{1/2}}\right) = \left\{\left(\frac{\Delta W_{gCB}}{W_{gCB}}\right)^2 + \left(\frac{\Delta A}{A}\right)^2 + \left(\frac{1}{2}\frac{\Delta\rho_g}{\rho_g}\right)^2 + \left(\frac{1}{2}\frac{\Delta g}{g}\right)^2 + \left(\frac{1}{2}\frac{\Delta(\Delta\rho)}{\Delta\rho}\right)^2\right\}^{1/2} \tag{D-4}$$

Some of the individual uncertainties such as $\Delta g/g$ and $\Delta(\Delta\rho)/\Delta\rho$ are known to be negligible compared with other uncertainties. The others are discussed in turn below.

D-7.1 STEAM DENSITY

The uncertainty in ρ_g is determined by the uncertainty in the channel-box pressure measurement and any superheat of the steam flow. The uncertainty in the pressure measurement is ±0.2 psi. The possible superheat of the steam was measured at about 4°F (steam temperature 216°F). Both these measurements translate to an uncertainty of approximately 2 percent or $\Delta\rho_g/\rho_g = 0.02$ at ambient pressure.

D-7.2 UPPER TIEPLATE OPEN AREA

The open area at the upper tieplate, $A\text{-}A_{UTP}$, was directly measured in the channel used for these experiments. Three features differentiate the Creare channel from a BWR channel: (a) our channel box is not a "regulation" GE BWR channel box but was fabricated in New England; (b) one side of the channel was cut away so that a Lexan viewing window (and later a metal replacement) could be installed; and (c) the nuts

used to hold the simulated fuel rods at the tieplate are just slightly larger than the upper tieplate bosses. The latter is not felt to be significant because there is only the infinitesimally thin plane where the bosses and the nuts meet that could be restricted by the nuts.

Two separate measurements were made: first, the open area of the channel box itself; second, the solid cross-sectional area of the upper tieplate. The difference between these gave the open area at the upper tieplate. A micrometer was used to measure the channel-box flow area. Three measurements were made across each pair of sides, at the corner radii, and for the area of the window cutout (because the Lexan window or metal plate was attached to the outside of the channel box). The open area of the channel box plus the cut-out section area were calculated to be 28.69 $in.^2$

The solid cross-sectional area of the upper tieplate was measured using a volumetric displacement method. The procedure used was to suspend the upper tieplate assembly from the arm of a mill in the shop, submerge the assembly to the level of the bottom of the tieplate in a container of water with an overflow drain (i.e., position the bottom of the tieplate at the overflow level), then raise the bed of the mill 0.400 ± 0.001 inches and collect the water subsequently displaced. This displaced water was at room temperature (70°F), having been left in the container overnight. The weight of water displaced was measured at 104.7 ± 0.5 grams in four separate measurements. This volume of liquid over the linear displacement gives a solid cross-sectional area of 16.00 $in.^2$ for the upper tieplate.

Subtracting the solid cross-sectional area of the upper tieplate from the open area of the channel box gives an open area of 12.69 ± 0.1 $in.^2$ The uncertainty in the flow area at the upper tieplate is therefore about 1 percent or $\Delta A/A=0.01$.

D.7-3 STEAM FLOW

It is possible to construct an expression similar to that of Equation D-4 which estimates the uncertainty in the steam flow measurement, given the uncertainty in the orifice plate size, the absolute upstream pressure at the orifice, and the orifice differential pressure. A maximum uncertainty of 2 percent or $\Delta W_{gCB}/W_{gCB} = 0.02$ is estimated.

Another consideration in determining the steam flow uncertainty is the possible condensation of steam between the measurement station and the upper tieplate. The most likely location for heat transfer and hence condensation of the steam is

between the interior of the channel box and the bypass region (which carries the bypass through-flow).

Energy balance calculations (and convective heat transfer calculations) give estimates of approximately 0.5 - 2 percent of the steam possibly condensed; however, it was concluded by comparing penetration data at 4- and 16-gpm penetration rates that heat transfer to the bypass region has a negligible effect.

D-7.4 TOTAL UNCERTAINTY

Combining the individual uncertainties from the above in Equation D-4 gives a calculated maximum uncertainty of $\Delta j^*_{gCB} D^{1/2} / j^*_{gCB} D^{1/2} = 0.024$. In a similar manner, the uncertainty in j^*_{fd} may be determined as $j^*_{fd} D^{1/2} = \pm 0.0004\ ft^{1/2}$ given the uncertainty in calculating the filling rate (0.08 gpm). The percentage uncertainty $\Delta j^*_{fd} D^{1/2} / j^*_{fd} D^{1/2}$ will depend upon $j^*_{fd} D^{1/2}$ measured.

D-8. MEAN PRESSURE DROP AND TEMPERATURE DATA

In this section the mean pressure drop and temperature data for all three injectors are tabulated in Tables D-10 through D-13. The code number for each test is listed along with mean values of ΔP5, ΔP6, T3, T4, T5, and T6, as defined in Figure D-1.

Table D-10

ORIGINAL CREARE STEAM INJECTOR

Test #	Mean Delta P5 (psid)	Mean Delta P6 (psid)	T3 (Deg F)	T4 (Deg F)	T5 (Deg F)	T6 (Deg F)
C-1	0.125	0.06	212	211	209	---
C-2	0.09	0.06	207	202	206	206
C-3	0.11	0.03	202	206	199	203
C-4	0.04	0.03	210	209	209	209
C-5	0.02	0.05	209	---	208	208
C-6	0.025	0.12	210	---	208	209
C-7	0.05	0.06	210	209	209	209
C-8	0.03	0.105	214	212	212	214
C-9	0.08	0.075	217	215	212	215
C-10	0.06	0.05	215	213	212	214
C-11	0.01	0.07	216	215	212	213
C-13	0.06	0.03	209	208	208	209
C-14	0.03	0.08	214	209	210	211
C-20	0.08	0.11	211	204	211	202
C-21	-0.04	0.17	218	217	216	217
C-22	0.07	0.045	218	216	214	204
C-23	0.05	0.06	215	199	199	196
C-24	-0.03	0.08	213	---	212	212
C-25	-0.05	0.06	211	---	210	209
C-26	0.2	0.02	223	---	219	220
C-27	0.03	0.1	219	216	216	218
C-28	0.06	0.11	219	217	217	218
C-29	0.035	0.08	217	216	216	216
C-30	0.04	0.06	215	210	215	213
C-31	0.06	0.07	216	214	213	213
C-32	0.035	0.085	216	214	213	213
C-19	0.05	0.04	221	218	219	217

Table D-11

MODIFIED STEAM INJECTOR

Test #	Mean Delta P5 (psid)	Mean Delta P6 (psid)	T3 (Deg F)	T4 (Deg F)	T5 (Deg F)	T6 (Deg F)
E-1	0.04	0.05	214	212	212	215
E-2	0.025	0.075	213	211	211	213
E-3	0.04	0.075	214	212	212	214
E-4	0.025	0.14	213	211	211	212
E-5	0	0.02	207	209	203	---
E-6	0.05	0.04	211	210	209	211
E-7	0.03	0.06	212	210	211	214
E-8	0.025	0.1	211	209	210	212
E-9	0.03	0.05	212	211	211	213
E-10	0.04	0.06	211	210	209	212
E-11	0.025	0.08	211	209	209	212
E-12	0.06	0.08	210	209	208	211
E-13	0.075	0.04	---	---	---	---
E-14	0.03	0	206	205	208	209
E-15	0.06	0.06	208	208	---	210
E-16	0.016	0.11	209	208	206	209
E-17	0.05	0.08	208	207	207	210
E-18	0.05	0.05	209	210	207	209
E-19	0.05	0.07	208	207	206	209
E-20	0.06	0.07	210	208	207	210
E-21	0.05	0	209	209	206	210
E-22	0.06	0.04	210	208	208	211
E-23	0.04	0.03	210	208	207	209
E-24	0.08	0.04	212	210	210	211
E-25	0.05	0.06	211	210	210	211
E-26	0	0.08	213	212	214	213
E-27	0.05	0.07	212	212	210	212
E-28	0.04	0.1	211	209	208	210
E-29	0.07	0.06	211	212	---	209
E-30	0.06	0.09	210	210	208	212

Table D-12

PRESSURE DROP AND TEMPERATURE DATA FOR HITACHI INJECTOR (WITHOUT RODS)

Test #	Mean ΔP6 (psid)	T3 (°F)	T5 (°F)	T6 (°F)
H-32	0	214	209	213
H-33	0.016	219	210	212
H-34	0	219	211	213
H-35	0.008	219	210	212
H-36	0.008	219	209	208
H-37	0.008	219	208	205
H-38	0.008	219	208	205
H-39	0	219	210	208
H-40	0	219	206	202
H-41	0.025	219	211	211
H-42	0.016	220	210	210
H-43	0.016	219	211	212
H-44	0.016	220	212	213
H-45	-0.017	219	211	213
H-46	0	219	211	212
H-47	0.008	219	211	211
H-48	0.016	220	211	213
H-49	0.008	219	210	210
H-50	0.016	219	211	211
H-51	0.008	220	208	210
H-61	-0.026	220	208	207
H-62	-0.042	223	213	214
H-63	-0.009	220	211	212
H-64	0.008	220	212	213
H-65	-0.017	220	209	212
H-66	0.008	221	210	209
H-67	0	219	210	211
H-68	-0.009	220	211	211
H-69	0.008	221	212	212
H-70	0.016	220	212	213
H-71	0.016	221	213	217
H-72	0.016	220	212	213
H-73	0.016	220	214	215
H-74	0	221	212	213

Table D-12

PRESSURE DROP AND TEMPERATURE DATA FOR HITACHI INJECTOR
(WITHOUT RODS) (Continued)

Test #	Mean $\Delta P6$ (psid)	T^3 (°F)	T^5 (°F)	T^6 (°F)
H-75	0.008	220	212	214
H-80	0	219	207	201
H-81	-0.009	217	204	204
H-82	0	218	206	205
H-83	0.008	218	207	205
H-84	0.008	218	206	204
H-85	0.008	218	208	206
H-86	0.016	218	210	207
H-87	0.016	219	210	208
H-88	0.016	218	210	207
H-89	0.016	218	210	210
H-90	0.016	218	210	210
H-91	0.016	218	---	211
H-99	0.016	220	---	182
H-100	0.016	221	---	186
H-101	0.016	220	---	196
H-102	0.016	220	---	207
H 103	0	220	---	209
H-99	0.033	220	198	191
H-104	-0.017	220	---	212
H-105	-0.009	221	---	214
H-106	0	220	---	213

Table D-13

PRESSURE DROP AND TEMPERATURE DATA FOR HITACHI INJECTOR (WITH RODS)

Test #	Mean ΔP6 (psid)	T3 (°F)	T5 (°F)	T6 (°F)
I-1	0.066	220	211	211
I-2	0	220	212	210
I-3	0.016	220	212	210
I-4	0	220	211	210
I-5	0	220	213	212
I-6	0	221	213	212
I-7	0.083	221	212	212
I-8	0.008	219	211	208
I-9	0.1	221	212	213
I-10	0.1	221	213	211
I-11	0.083	221	213	212
I-12	0.033	221	213	212
I-13	0.008	220	212	211
I-14	0.016	216	206	105
I-15	0.016	218	211	192
I-16	0.025	217	211	206
I-17	0.033	219	212	204
I-18	0.041	221	211	205
I-19	0	221	213	206
I-20	0.083	221	213	210
I-21	0.066	221	212	205
I-22	0.075	220	213	207
I-23	0.016	220	211	209
I-24	0.016	221	211	211
I-25	0.033	222	213	213
I-26	0.008	222	213	213
I-27	0.008	222	213	213
I-28	0.083	222	213	212
I-29	0.25	222	212	212
I-30	0.066	222	212	212
I-31	0.083	222	212	212
I-32	0.133	222	210	210
I-33	0.008	222	213	212
I-34	0.008	222	213	211
I-35	0.008	222	213	212
I-36	0.008	221	212	212

Appendix E

LEXAN BUNDLE MOCKUP EVALUATIONS

E-1. INTRODUCTION

As part of the development of the Lynn Steam Sector Test Facility (SSTF) design, General Electric performed a series of flow visualization and performance evaluation tests during 1978 with a Lexan prototype of the Lynn mock fuel bundle. This appendix describes the test bundle and summarizes the results of the tests.

E-2. TEST DESCRIPTION

The clear Lexan plastic test bundle was built as a prototype based on the conceptual design of the Lynn SSTF bundle and was installed in a test loop as shown in Figure E-1. Photographs of the Lexan bundle are shown in Figures E-2a through E-2d, and the lower plenum region is shown in Figure E-3. The configuration shown in these figures is the one used for the initial flow visualization tests described in Subsection E-3.1 with the four plastic air spargers located as shown in Figure E-4.

E-3. TEST RESULTS

Several different groups of tests were performed to meet various objectives. The results of these tests are described in this section.

E-3.1 Initial Flow Visualization Tests

Single-phase water tests and air/water tests were performed with the Lexan test section. The results of each of these tests are discussed in the following paragraphs.

E-3.1.1 Single Phase Water Tests. Two methods of water injection were used for the single phase water tests: (a) water entered the prototype by building up in the upper plenum and then spilling over the top of the bundle, and (b) a hose was inserted into the outer tube of the weir assembly so that the water was injected directly into the weir measuring device. The first configuration represents the prototypical situation, while the second configuration provides a means for

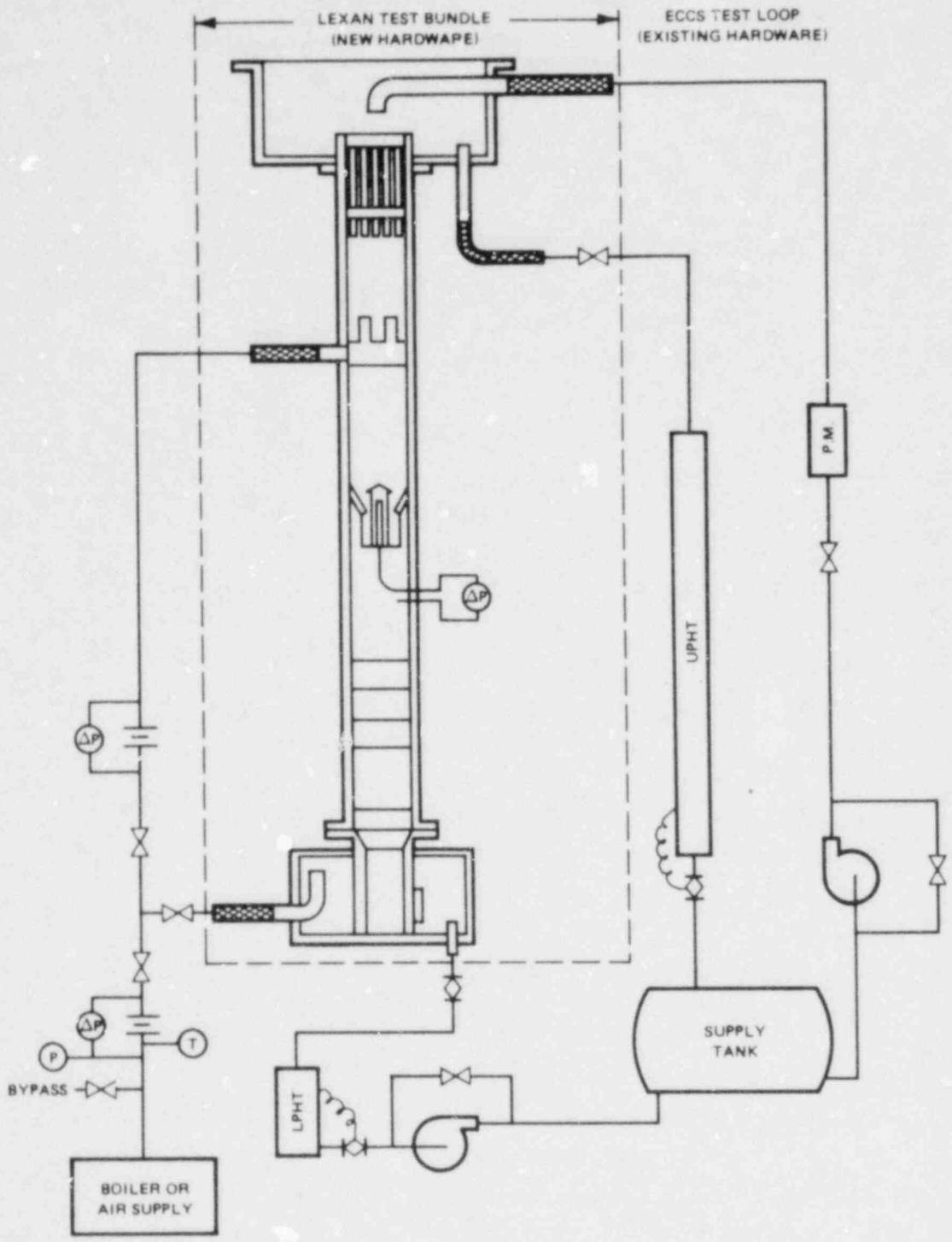

Figure E-1. Lexan Bundle Test Loop

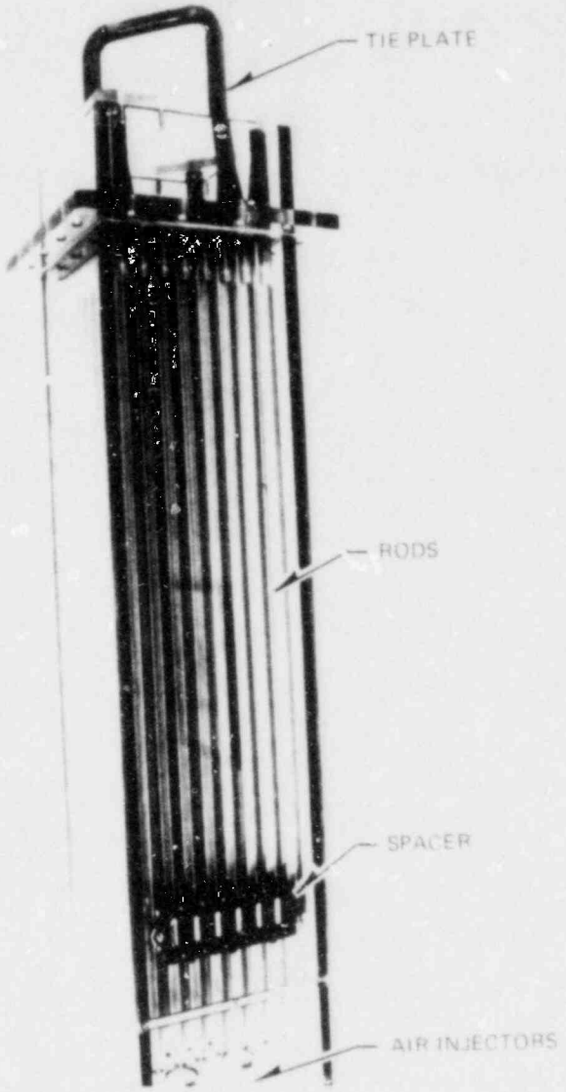

Figure E-2a. Lexan Bundle

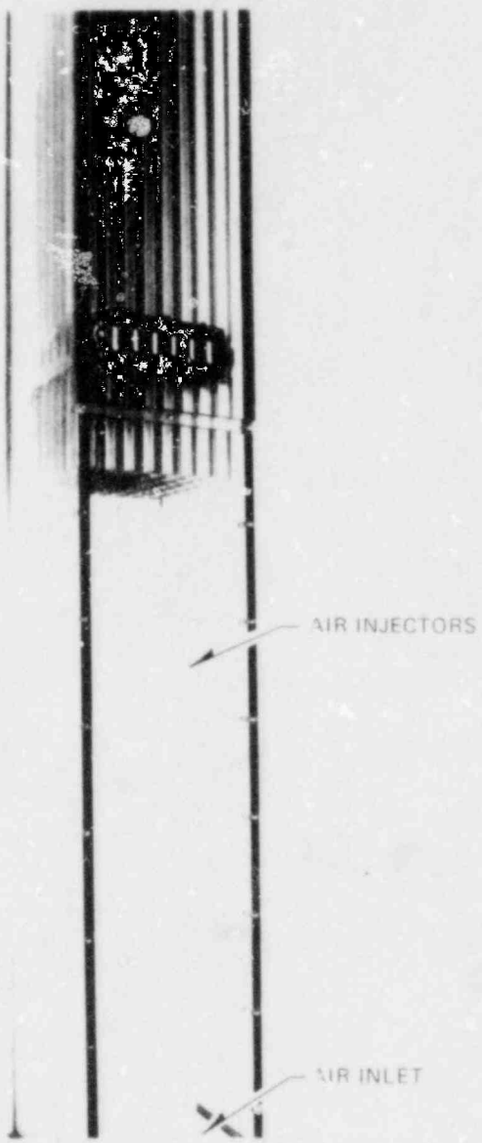

Figure E-2b. Lexan Bundle

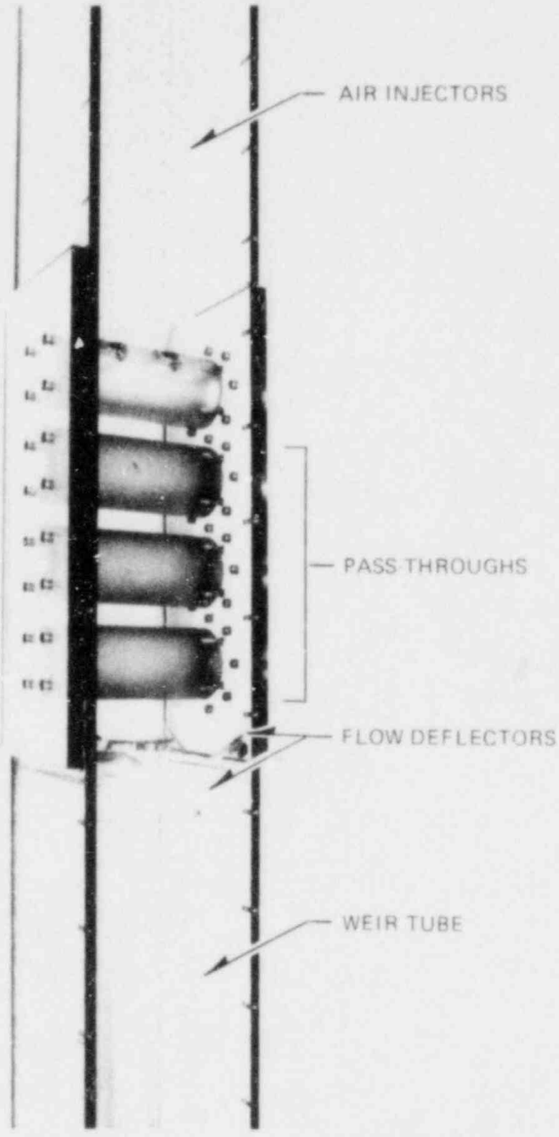

Figure E-2c. Lexan Bundle

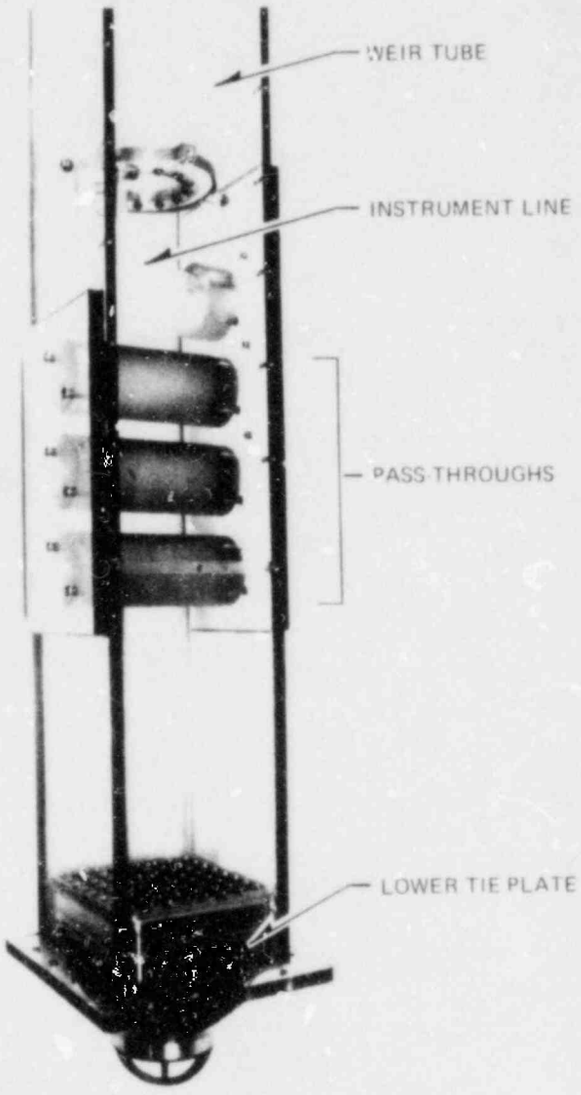

Figure E-2d. Lexan Bundle

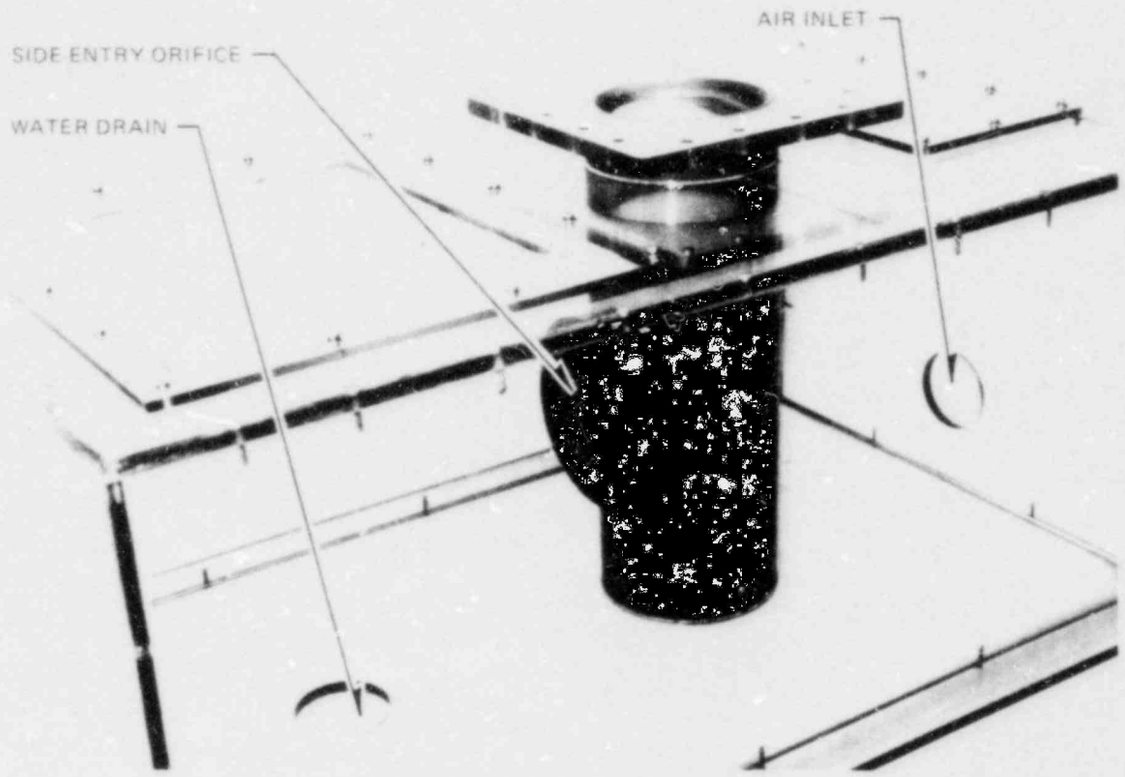

Figure E-3. Lower Plenum

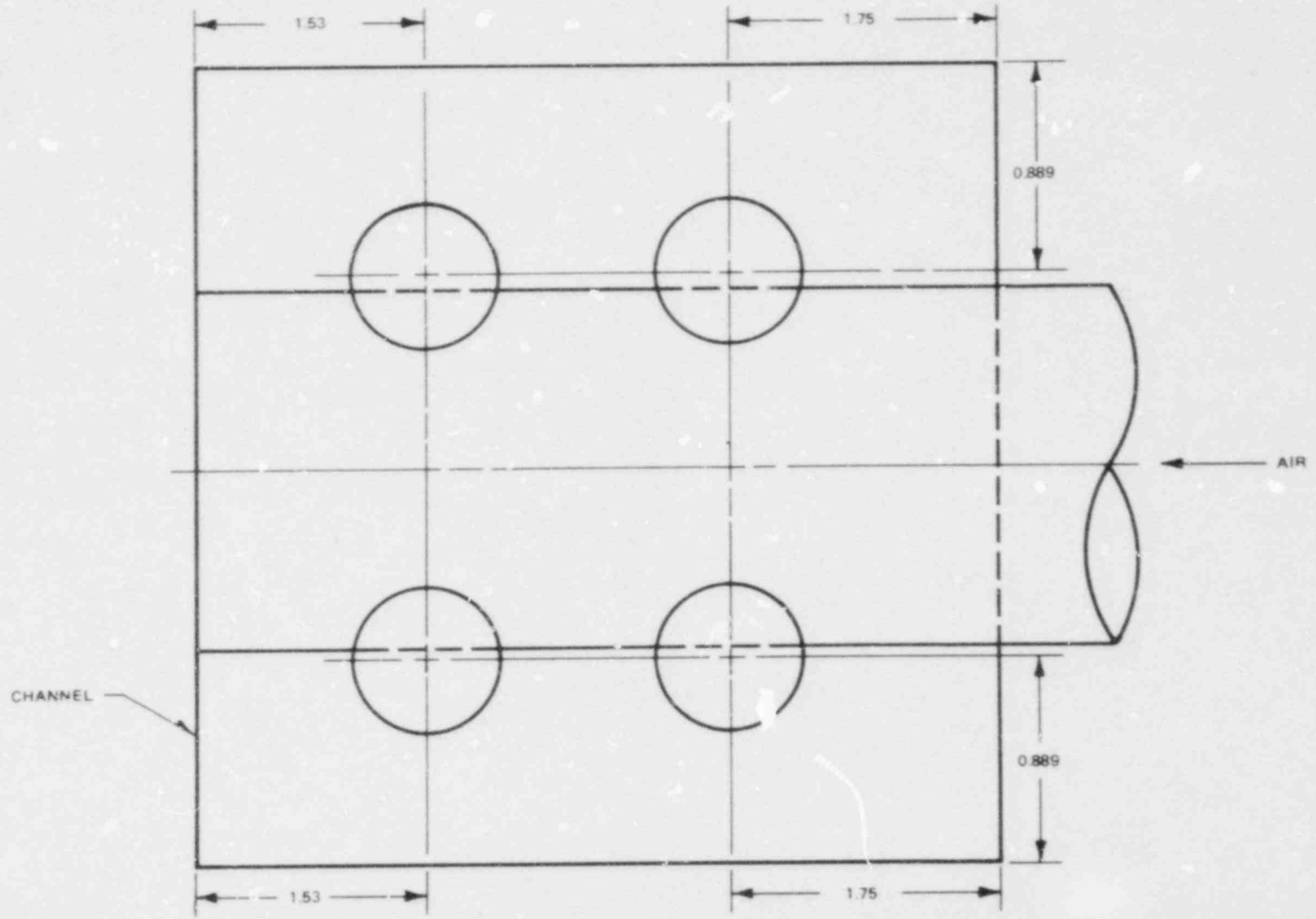

Figure E-4. Location of Air Spargers

determining how much water splashed through the weir assembly during the prototypical tests without being measured. The head of water in the weir was determined by visually measuring the water level in the weir annulus with a scale. Although the water in the weir annulus contained a small amount of entrained air, the scale readings provide a useful indication of the weir performance.

The results of the single-phase tests are plotted vs. the scale ΔP in Figure E-5, where the darkened symbols are the data for the direct injection tests. During the prototypical tests, some water was observed splashing into the center tube, thus bypassing the weir tube measurement. The data of Figure E-5 confirm this observation because the direct injection tests consistently result in a higher ΔP for a given flow rate. Referring to Figure E-5, the amount of splashing is seen to vary from approximately 20 percent of the injected flow at the low flows (<2500 lbm/hr) to 10-12 percent at the higher flows. The final single-phase test performed was to determine the weir performance with a high flow rate of approximately 30 gpm. The measured weir ΔP (~19 inches) did not exceed the height of the weir slot, but the high flow caused such an agitated flow pattern that a considerable amount of water was observed to splash into the center weir tube.

Two ideal head-flow curves for the weir tube are also shown in Figure E-5. The expression for these curves, which was derived from Bernoulli's equation, is written as

$$\dot{M}_{WEIR} = 2/3\, d_1\, \rho\, C_D \sqrt{2g}\, (h)^{3/2} + \beta\, [2/3\, (d_2 - d_1)\, \rho\, C_D \sqrt{2g}\, (h - h_1)^{3/2}] \qquad \text{(E-1)}$$

Discharge coefficients of 0.5 and 1.0 were assumed to generate the curves shown in Figure E-5. It is evident from Figure E-5 that the data follow the trend of the ideal curves and that with the proper discharge coefficient, Equation (E-1) can be used to determine the flow rate from the measured head in the weir tube.

where

$\dot{M}_{WEIR}$ = water flow, lbm/sec

d_1 = width of narrow slot, ft.

d_2 = width of wide slot, ft.

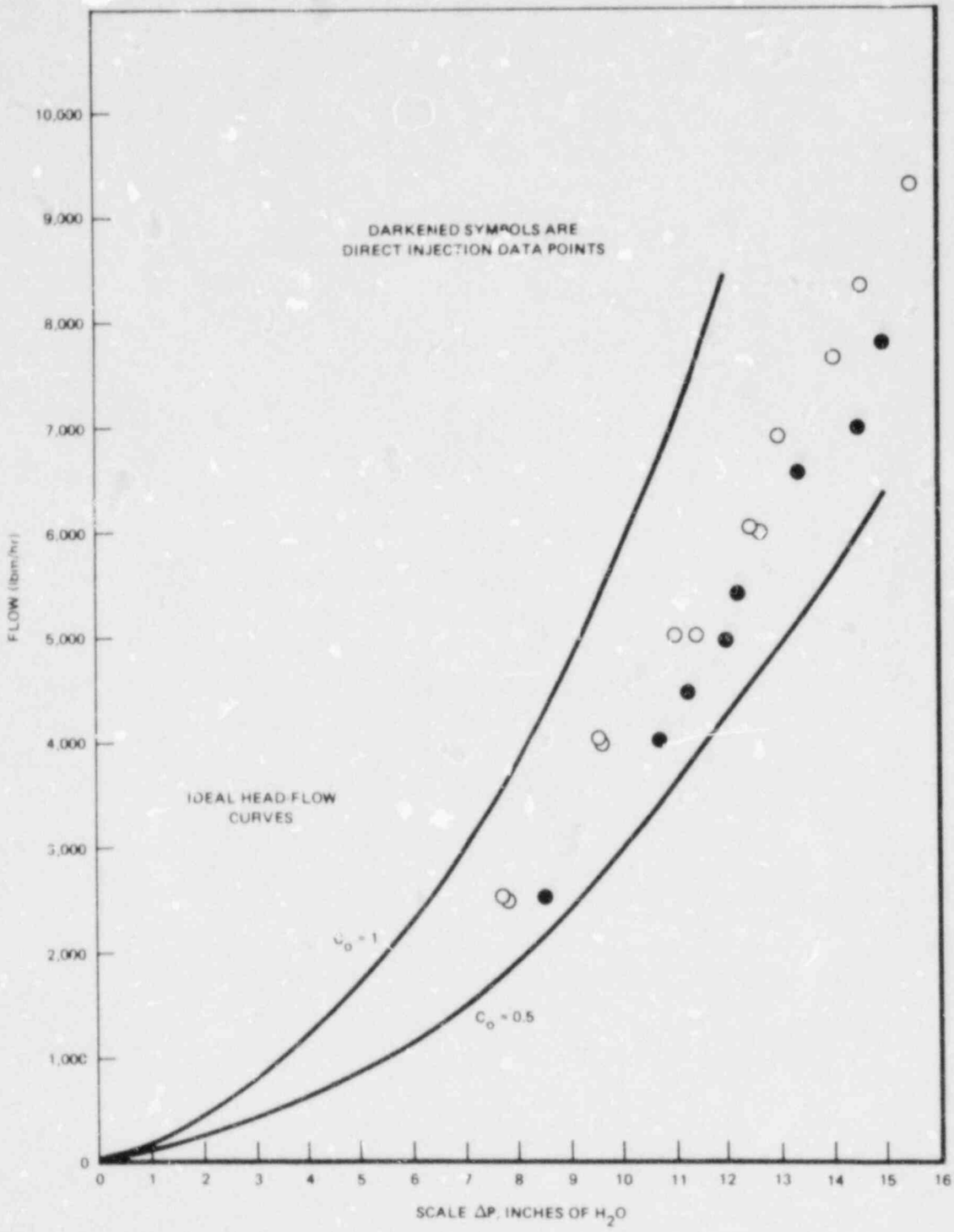

Figure E-5. Weir Tube Calibration

ρ = density of water, lbm/ft^3

C_D = slot discharge coefficient

g = acceleration of gravity, ft/sec^2

h = head of water in weir, ft.

h_1 = height at which slot width increased from d_1 to d_2, ft.

$\beta = 0$ for $h \leq h_1$

$\beta = 1$ for $h > h_1$

Air/water CCFL tests were conducted by injecting air into the lower plenum or into the mock fuel bundle via the bundle air injectors. For these tests, the simulated lower fuel support was fitted with a 2.5-in. diameter orifice. Thus, for lower plenum air injection, the flow area used in reducing the data was the area of the lower orifice, while for bundle air injection the flow area was that of the upper tieplate. The data are plotted in the Modified Wallis form in Figure E-6.

E-3.2 Lexan Bundle Redesign Tests

Based on the qualitative and visual observations of the Initial Flow Visualization Tests, efforts were made to design and test improved steam injection sparger's and to redesign the weir tube and funnels to provide better performance. Results of the Lexan Bundle Redesign Tests are discussed below.

E-3.2.1 CCFL Testing. Various vapor injectors were designed, built, and tested in the Lexan bundle in an attempt to create a uniform distribution of the vapor updrafting through the upper rod bundle/tieplate assembly. The injectors tested were:

a. The Creare Injector, consisting of an inlet base and a capped injector tube 17 inches long. The tube is 2.25 inches O.D. with 68 holes (4 rows of 17), with 0.209 inch diameter aimed at the channel walls.

b. The Modified Creare Injector, similar to the Creare Injector but with 136 holes (8 rows of 17) with 0.234 inch diameter.

c. The Porous S/S Injector, using a similar inlet base with a porous sintered stainless steel injector tube. The injector tube is 22 inches tall, 2.50 inches O.D., with 137 square inches of 20 micron porosity surface area. A cone piece caps off the injector tube.

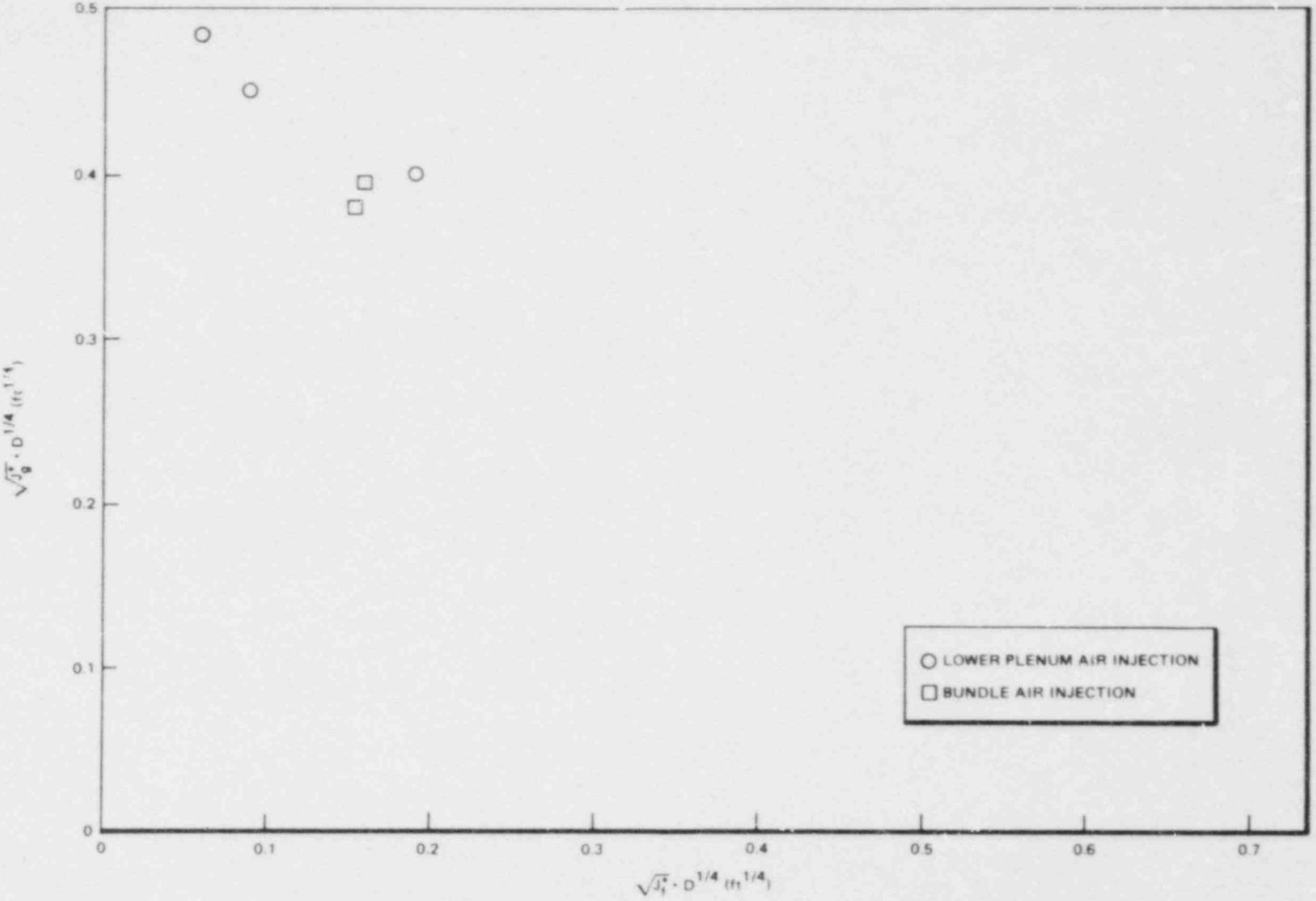

Figure E-6. CCFL Data

E-3.2.2 Air Testing. More than a hundred air tests were performed using the three injectors and various modifications to the standard hardware. Modifications to the standard hardware include: Pointed rods, pointed rods with long rods surrounding injector, no rods, the injector at the bottom of the channel, decreased size of upper plenum, no spacer on rods, corner tabs removed from top of channel, and a thin wall at the top of channel.

The use of pointed rods instead of square ended rods caused higher CCFL flows for all injectors used. Of the other hardware changes, only the "no rods" and removed corner tabs on the channel top configurations significantly changed the CCFL performance. During "no rods" testing, it appeared that the vapor updraft distribution was parabolic rather than uniform, allowing more water to drain down at the edge of the tieplate. With the corner tabs removed from the channel top, a greater amount of water downflow was achieved, suggesting that free access to the open area at the tieplate edge is an important CCFL parameter in addition to the overall tieplate open area.

E-3.2.3 Steam Testing. Nine steam tests were performed with the Porous S/S Injector and the Modified Creare Injector combined with standard hardware inside the channel. Steam testing was limited because the high temperature rapidly deteriorated the plastic test section, creating a safety hazard. Figure E-7 shows the CCFL performance for these injectors.

The Lexan Bundle CCFL data do not clearly indicate a best injector design. All performance data are fairly consistent. The Modified Creare and Porous S/S injectors were very close in performance. The Modified Creare Injector was selected as being the preferred choice because (a) no other injector tested has significantly different performance, (b) the cost is lower than Porous S/S, and (c) the Porous S/S injector has a much greater probability of plugging.

E-3.2.4 Weir Tube Testing. Modifications made to the Lexan bundle as a result of the Initial Flow Visualization Tests included the following:

a. A strainer/still tube with cover was installed between the weir tube and collector tube. Made of a 1/32 in. hole perforated S/S sheet metal, this tube maintains a steady water level for more accurate performance and prevents crud from reaching the small holes in the weir tube.

b. The weir tube was increased in height, and the open vents at the top were decreased in size to prevent water from entering the weir tubes via the vent holes. A lip on the top cover was added to prevent water from entering the weir tube via the vents at very low flows.

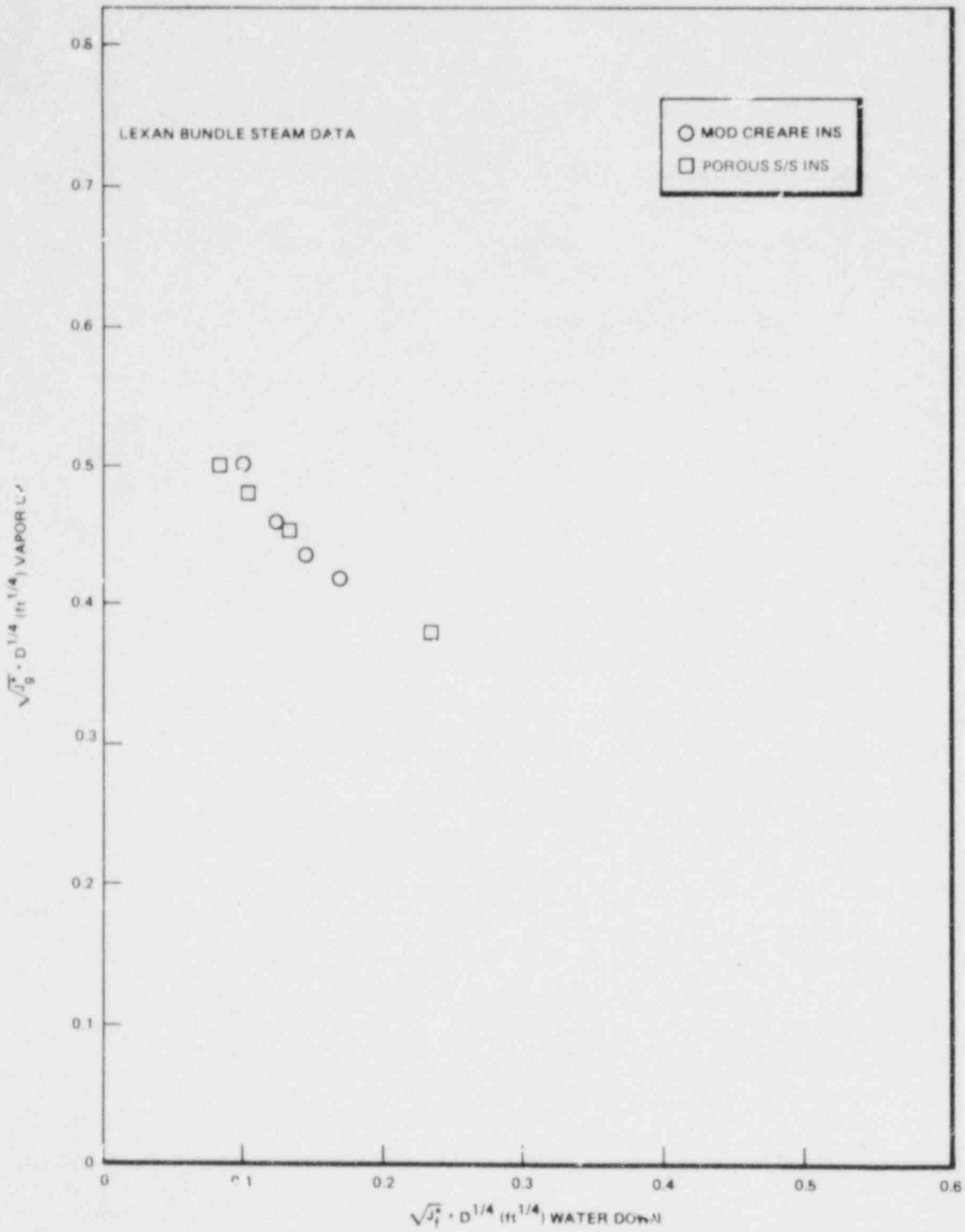

Figure E-7. CCFL Correlation

c. A hat was added to the low pressure port to prevent splashing water from affecting the pressure reading.

d. A funnel was added to the O.D. of the collector tube.

e. The upper funnel was extended inward to eliminate the flow spillage that was found to occur at the cut-out regions of the lower funnel.

f. The hole pattern used for the weir tube is summarized in Table E-1. The bottom hole was 0.8125 inch above the bottom of the weir tube.

This pattern of round holes replaced the vertical slots used in the original design (0.062-in. wide slot for the bottom 6 inches, with a 0.125-in. wide slot for the next 14 inches).

A calculation and in-place calibration were performed on the weir tube and are shown plotted in Figure E-8. The calculation and calibration agree very closely (±5%) except at flow rates below 0.7 gal/min. Below this flow the water flow through the weir tube holes is laminar, whereas the calculation uses a turbulent flow coefficient for all flow rates. The calculation used a discharge coefficient value of 0.55.

E-3.2.5 K/A^2 Testing. The hydraulic performance (K/A^2) of the Lexan Bundle was measured with air updraft. The Lexan Bundle overall channel K/A^2 was measured to be 0.122 $inch^{-4}$ over the Reynolds number range of 3×10^5 to 7×10^5 at the rod bundle.

Table E-1

WEIR TUBE HOLE PATTERN

Hole Position	Number of Holes	Diameter of Holes, in.	Distance above Bottom Hole, In.
1	1	0.125	0
2	1	0.125	0.5
3	1	0.125	1.0
4	1	0.250	1.5
5	1	0.250	2.5
6	1	0.250	3.5
7	2	0.250	4.5
8	2	0.250	5.5
9	2	0.250	6.5
10	2	0.250	7.5
11	2	0.250	8.5
12	2	0.250	9.5
13	2	0.250	10.5
14	2	0.250	11.5
15	2	0.250	12.5
16	2	0.250	13.5
17	2	0.250	14.5
18	3	0.250	15.5
19	3	0.250	16.5

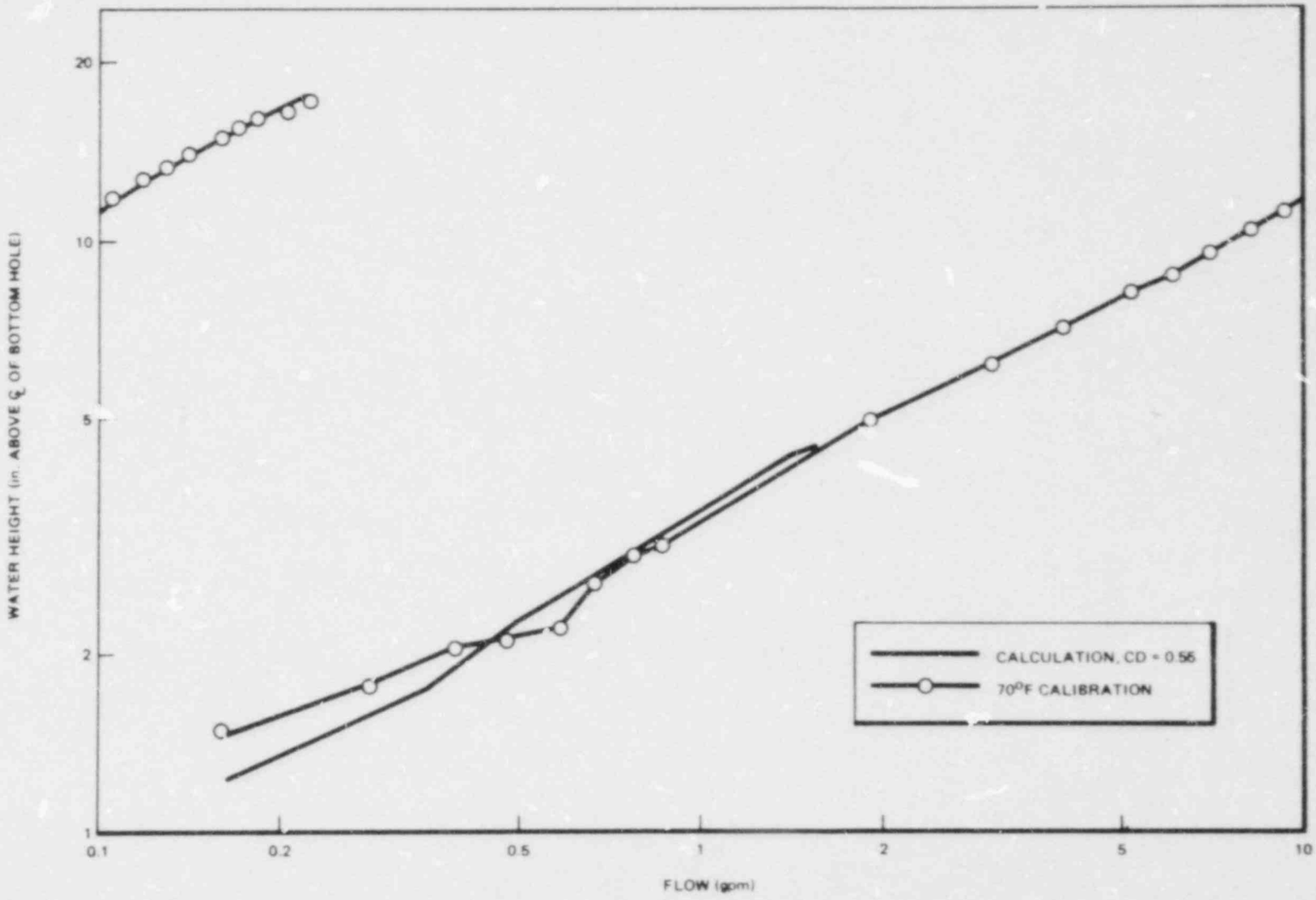

Figure E-8. Lexan Bundle Redesign Test

DISTRIBUTION

Division of Reactor Safety Research 5
U.S. Nuclear Regulatory Commission
Washington, DC 20555
Attn: W. D. Beckner

Division of Reactor Licensing
U.S. Nuclear Regulatory Commission
Washington, DC 20555
Attn: R. K. Frahm

Electric Power Research Institute
4312 Hillview Avenue
Palo Alto, CA 94303
Attn: M. Merilo

Argonne National Laboratory
9700 Cass Avenue
Argonne, IL 60439
Attn: P. Lottes
RSR Heat Transfer Coordinator

EG & G
550 Second Street
Idaho Falls, ID 83401
Attn: R. J. Dallman

Safety and Systems Analysis
Nuclear Power Generation Division
Babcock & Wilcox
P.O. Box 1260
Lynchburg, VA 24505
Attn: Dr. B. E. Bingham

Reactor Development Center
Babcock & Wilcox
P.O. Box 1260
Lynchburg, VA 24505
Attn: Mr. D. Montgomery

Safeguards Development
Pressurized Water Reactor Systems Division
P.O. Box 355
Pittsburgh, PA 15230
Attn: Dr. [illegible] E. Hochreiter

C-E Power Systems
Combustion Engineering, Inc.
1000 Prospect Hill Road
Windsor, CT 06095
Attn: Mr. J. D. Crawford

Librarian, General Atomic
P.O. Box 81608
San Diego, CA 92138

Department of Nuclear Engineering
University of California at Berkeley
Berkeley, CA 94720

Department of Nuclear Engineering
Massachusetts Institute of Technology
77 Massachusetts Avenue
Cambridge, MA 02139

Engineering Library
Stanford University Campus
Stanford, CA 94305

Los Alamos Scientific Laboratory
Los Alamos, NM 87544
Attn: C. W. Hirt, Group T-3

Environmental Protection Agency
P.O. Box 15027
Las Vegas, NV 89114

U.S. Nuclear Regulatory Commission
Reactor Analysis Section/Analysis Branch
Washington, DC 20555
Attn: W. Hodges

U.S. Nuclear Regulatory Commission
Division of System Integration
Washington, DC 20555
Attn: T. Huang

NRC FORM 335 (7-77)

U.S. NUCLEAR REGULATORY COMMISSION

BIBLIOGRAPHIC DATA SHEET

1. REPORT NUMBER (Assigned by DDC)
NUREG/CR-1846
EPRI NP-1525
GEAP-24893

4. TITLE AND SUBTITLE (Add Volume No., if appropriate)
BWR Refill/Reflood Program Task 4.4 - CCFL/Refill System Effects Tests (30° Sector) Experimental Task Plan

2. (Leave blank)

3. RECIPIENT'S ACCESSION NO.

7. AUTHOR(S)
D. G. Schumacher

5. DATE REPORT COMPLETED
MONTH: December | YEAR: 1980

9. PERFORMING ORGANIZATION NAME AND MAILING ADDRESS (Include Zip Code)
General Electric Company
175 Curtner Ave.
San Jose, CA 95125

DATE REPORT ISSUED
MONTH: July | YEAR: 1981

6. (Leave blank)

8. (Leave blank)

12. SPONSORING ORGANIZATION NAME AND MAILING ADDRESS (Include Zip Code)
Division of Accident Evaluation
Office of Nuclear Regulatory Research
U.S. Nuclear Regulatory Commission
Washington, DC 20555

10. PROJECT/TASK/WORK UNIT NO.

11. CONTRACT NO.
FIN B3012

13. TYPE OF REPORT
Technical Report

PERIOD COVERED (Inclusive dates)

15. SUPPLEMENTARY NOTES

14. (Leave blank)

16. ABSTRACT (200 words or less)

An experimental task plan for the CCFL/Refill system effects tests (30° Sector) of the BWR Refill-Reflood program is presented. The CCFL/Refill system effects tests will provide separate effect and BWR system response data from a large scale sector test facility (30° SSTF) for use in LOCA best estimate model assessment. Contained in the document is definition of: the experimental task objectives, required modification to the existing 30° SSTF, test parameters and ranges, individual test categories measurement plan approach, and data utilization.

17. KEY WORDS AND DOCUMENT ANALYSIS

17a. DESCRIPTORS

17b. IDENTIFIERS/OPEN-ENDED TERMS

18. AVAILABILITY STATEMENT
Unlimited

19. SECURITY CLASS (This report)
Unclassified

21. NO. OF PAGES

20. SECURITY CLASS (This page)
Unclassified

22. PRICE
$

120555064215 2 ANR2
US NRC
ADM DOCUMENT CONTROL DESK
PDR
C16
WASHINGTON DC 20555